ENHANCED INTERFACES AND TRAIN CATEGORIES FOR DYNAMIC COMPATIBILITY ASSESSMENT OF EUROPEAN RAILWAY BRIDGES

D4.1 – Revision of damping

DELIVERABLE INFORMATION	
Work package number:	WP4
Work package title:	Revision of damping in railway bridges
Deliverable number:	D4.1
Deliverable title:	Revision of damping
Due date of deliverable:	28-02-2025
Actual submission date of 1st version:	03-04-2025
Current version submission date:	03-04-2025
Responsible partner	UPORTO
Version:	V1
Dissemination level:	PU

PUBLICATION HISTORY

Revision	Date	Description	Responsible
V1	03-04-2025	Initial version	P. Montenegro / UPORTO

CONTRIBUTORS TO THE DELIVERABLE

Name	Institution	Role
P. Montenegro	UPORTO	Deliverable responsible
F. Pimenta	UPORTO	Contributor
A. Silva	UPORTO	Contributor
E. Laligant	AVLS	Contributor
C. Laurent	AVLS	Contributor
O. Ahmed	AVLS	Contributor
C. Dos Santos	AVLS	Contributor
P. Galvín	UdS	Contributor
A. Romero	UdS	Contributor
A. Andersson	KTH	Contributor
J. M. Goicolea	UPM	Contributor
R. Behnke	DB InfraGO	Contributor

BRIDGE AND MEASUREMENTS DATA PROVIDERS

The authors of this report would like to thank the following bridge and measurements data providers, without whom this work would not have been possible to accomplish.

Name	Institution	Country	Role
F. Durot & Q. Jungers	SNCF Réseau	France	Provided French bridge data
R. Behnke	DB InfraGO	Germany	Provided German bridge data
P. Montenegro & A. Silva	UPORTO	Portugal	Tests conduction in Portugal
H. Patrício	UIC (former IP)		Provided Portuguese bridge data
M.D. Martínez	UJI	Spain	Tests conduction in Spain
P. Galvín	UdS		
David Vargas & David Villalmanzo	ADIF		Provided Spanish bridge data
A. Andersson	KTH/Trafikverket	Sweden	Tests conduction in Sweden and provided Swedish bridge data
G. Grunert	CEN/TC250/SC1 DIBRST Group	EU	Provided informative DIBRST portal frame bridge data
I. Bucknall	CEN/TC250/SC1 DIBRST Group	UK	Provided informative NR prestressed concrete bridge data
B. Wilkinson	Network Rail		

PROJECT CONSORTIUM

Coordinator	*Universidade do Porto* *UPORTO, Portugal*	
Beneficiaries	*Kungliga Tekniska Hoegskolan* *KTH, Sweden*	
	Universidad Politecnica de Madrid *UPM, Spain*	
	Bundesanstalt für Materialforschung und -Prüfung *BAM, Germany*	
	Deutsche Bahn InfraGO AG *DB, Germany*	
	Acoustique Et Vibrations Logiciels Scientifiques *AVLS, France*	
Affiliated Partners (to UPM)	*Universitat Politecnica de Valencia* *UPV, Spain*	
	Universitat Jaume I de Castellon *UJI, Spain*	
	Universidad de Sevilla *UdS, Spain*	
	Administrador de Infraestructuras Ferroviarias *ADIF, Spain*	
Associated Partner	*University Of Huddersfield* *HUD, UK*	

Disclaimer: Views and opinions expressed are however those of the author(s) only and do not necessarily reflect those of the European Union or Europe's Rail Joint Undertaking. Neither the European Union nor the granting authority can be held responsible for them.

TABLE OF CONTENTS

LIST OF ABBREVIATIONS

3D: Three Dimensional

API: Application Programming Interface

CEN: European Committee for Standardization

COMP: Steel-Concrete Composite bridge type

D214: Special committee from ERRI that studied bridge dynamics

DIBRST: Dynamic interface between Railway Bridges and Rolling Stock (CEN group)

DOF: Degree of Freedom

Dx.y: Deliverable number y from Work Package x

EN: European Norm

ERA: European Union Agency for Railways

ERRI: European Rail Research Institute

EU: European Union

EU-Rail: Europe's Rail Joint Undertaking

FB/RC: Filler Beam and Reinforced Concrete bridge type

FEM: Finite Element Method

FFT: Fast Fourier Transform

FRF: Frequency Response Function

GEV: Generalized Extreme Value

GODLIKE: Global Optimum Determination by Linking and Interchanging Kindred Evaluators

ID: Identification

IP: Infraestruturas de Portugal

JSON: JavaScript Object Notation

LD: Logarithmic Decrement method

MCO: Multi-Criteria Optimisation method

MEMS: Micro-Electro-Mechanical Systems

MSx: Milestone number x

No.: Number

NR: Network Rail

ÖBB: Österreichische Bundesbahnen

PF: Portal Frame bridge type

PU: public deliverable

PSC: Prestressed Concrete bridge type

RMS: Root Mean Square

RP3: Report 3 (ERRI D214 Report)

SC: Sub-Committee

SEN: sensitive deliverable

SNCF: Société Nationale des Chemins de Fer Français

SSI-COV: Covariance Driven Stochastic Subspace Identification method

STL: Steel bridge type

STL/COMP: Steel and Composite bridge type

TBI: Train-Bridge-Interaction

TC: Technical Committee

URL: Uniform Resource Locator

WP: Work Package

1 INTRODUCTION

The present deliverable D4.1 is included within Work Package 4 (WP4) entitled *"Revision of damping in railway bridges"* and aims to present the final results associated with it. The estimated value of damping has a significant impact on the dynamic response of railway bridges, especially at resonance, which may strongly influence the design of new railway bridges or the evaluation of existing ones. Experimental testing conducted in previous projects, namely Shift2Rail In2Track2 (2018) and In2Track3 (2023), has shown that the damping estimated for existing bridges is often higher than the values specified in EN 1991-2 (2023), which were originally derived from studies conducted by ERRI D214 committee (ERRI D214/RP3, 1999), especially in structures where the SSI plays an important role, such as portal frame bridges. Moreover, the estimations showed a wide variety of values for the same structures, which may be related with the level of amplitude of vibration to which the bridges were subjected or to the modes considered for the damping definition. Therefore, the present document aims to provide insights about damping in railway bridges and present recommendations for more realistic values of damping to be considered in the assessment of existing and new bridges.

WP4 is divided in three tasks that can be summarized as follows:

- Task 4.1 – "*Collection of dynamic measurements carried out in European networks*", led by UdS, where all the experimental data related to bridge responses under railway traffic and forced excitation has been retrieved and incorporated into a database.

- Task 4.2 – "*Damping estimations based on dynamic responses under railway traffic and forced vibration testing*", led by AVLS, where damping coefficients for the different bridges and measurements available in the database were estimated based on two methods, which will be described later.

- Task 4.3 – "*Identification of the bridge parameters that most influence damping and reasons or damping value dispersion*", led by UPORTO, where insights about damping dispersion, justifications for lower values and recommendations for upgrading the current normative values stipulated in EN 1991-2 (2023) were discussed.

Two milestones (MS) and one deliverable (D) were defined for WP4, namely: MS12 – "Database of dynamic tests," which introduced the measurements' database; MS13 – "Damping estimation," which compiled the damping values derived from approximately 1,500 measurements conducted on around 90 bridges across five different countries; and D4.1 – "Revision of damping," which outlines the results and recommendations. Thus, the present deliverable is structured in the following chapters:

- Chapter 1 is dedicated to the introduction of the present document.

- Chapter 2 presents the format used to store the measurement files in the database developed within the project's Task 4.1, as well as the bridges involved in this work. It also gives a short presentation of the two types of tests used in this work, namely tests under railway traffic and under forced excitation performed in Sweden.

- Chapter 3 describes the damping estimation algorithms adopted in this work, more precisely in Task 4.2, namely the Multi-Criteria Optimisation (MCO) and the Covariance Driven Stochastic Subspace Identification (SSI-COV) methods for estimating damping through free decay periods after the train crossing the bridge and the method based on the least squares ratio function estimation adopted in the tests under forced excitation through actuators. This section also presents procedures to define the free decay period used as input of the methods, as well as some benchmarking tests used to compare them.

- Chapter 4 summarizes all the estimated damping coefficients calculated in Task 4.2 as function of bridge span, amplitude and bridge types. It also shows the format of the damping results obtained in each measurement previously stored in the database.

- Chapter 5 covers the analysis of all the results obtained in this WP carried out within Task 4.3, evaluates the factors that may influence damping and gives insights to the recommendations that arise from the present work and presented in the following section.

- Chapter 6 finally presents the normative recommendations which arise from the present WP.

2 MEASUREMENT DATABASE AND STUDIED BRIDGES DESCRIPTION

2.1 Initial considerations

UdS has developed a database containing a list of bridges (InBridge4EU-Database, 2024), whose structure has been detailed in Deliverable D2.1, with relevant data provided for each. The database stores measurement recordings from bridges where experimental programs have been conducted. UPORTO, KTH, UJI, UdS, DB InfraGO, and AVLS collected the experimental data and provided it to UdS, which organized the recordings and incorporated them into the database (see Figure 1a). Some of the bridges where tests were conducted are a subset of those selected for WP2, while others correspond to additional bridges.

The collection of experimental data on railway bridges includes bridges from 5 countries thanks to the assistance of national Infrastructure Managers (Portugal – Infraestruturas de Portugal, Spain – ADIF, Sweden – Trafikverket, Germany – DB InfraGo and France – SNCF) and some partners. All partners provided acceleration data in one or more locations of bridges when a train passes. This constitutes the most exploited signal for damping estimation.

The database stores the measurement data in the cases where experimental programs have been carried out on the bridges. The database contains more than 2200 measurements, of which approximately 1150 were used for damping estimation due to their higher signal quality. Some measurements were excluded as they corresponded to the same train passage but were recorded by different sensors, making separate analysis unnecessary. When recordings are available, the variable Data has the value True. A *pdf* file with a scheme of the instrumentation can be downloaded from the Experimental Section of each bridge, as well as the measurement raw data (see Figure 1b).

List of bridges

Page 1 of 29.

⬇ Download selected bridges

ID	Bridge	Name	Country	Line	Config	Deck	Support	Material	Data	Type	Info	Select
1	75205288	Bryngeån	SE	Bothnia	['Simply-supported']	Beam	['Pinned roller bearings', 'Pinned fixed bearings']	['Composite steel-concrete']	True	Dynamic	ℹ	☐
2	75205302	Faresmyren	SE	Bothnia	['Portal frame open']	Slab full	['Monolithic']	['Reinforced concrete']	True	Dynamic	ℹ	☐
3	75205304	Gideåbacka	SE	Bothnia	['Continuous']	Beam	['Pot bearings']	['Prestressed concrete']	False		ℹ	☐
4	75205305	Gideälven	SE	Bothnia	['Continuous']	Beam	['Pot bearings']	['Composite steel-concrete']	False		ℹ	☐

a)

b)

Figure 1: Structure of the database: a) general view with some bridges containing dynamic measurements and b) experimental section with the instrumentation scheme for downloading,

2.2   Data format of the measurements

Experimental data is accessible in the "*Information*" tab for each bridge, where each recording is identified by the fields *ID*, *Date*, and *Train* (see Figure 2). The variable *Train* contains the name of the train crossing the bridge when the response is measured (if available). If the variable indicates *"Forced vibration"* this means that the dynamic response of the bridge is measured under the action of an external shaker (see details of the test types ahead in Section 2.5). The information on each bridge in JSON format includes the URLs to access the experimental setup, but these URLs should be strongly avoided by web browsers, and they should be only accessed via GET methods (see *"API MATLAB"* and *"API Python"* in the *"Documentation"* tab from the InBridge4EU-Database (2024)). The experimental setup is also saved in a JSON file, whose format is explained in the same *"Documentation"* tab, namely in *"Data structure"*.

Figure 2: Experimental data of a given bridge.

Each data file contains the following information:

- Experimental Data ID;

- Bridge ID;

- Date;

- Channel labels and units;

- Sensor locations;

- Sensor directions;

- Sampling frequency;

- Recordings;

- Train type;

- Train speed;

- Circulated track name;

- Rail directions;

- Related report reference.

Experimental data can be downloaded in GNU zip (*.*gz*) compressed files. This type of file has been chosen for the high compression ratio (several easily available programs can be used to uncompress this file type). Once the *gz* file is uncompressed, the experimental data is obtained in binary files given its compact format. After uncompressed, the binary files can be read by MATLAB® (2023a) and Python® (Van Rossum and Drake, 2009) programming languages using the scripts in the database's *"Documentation"* tab, namely in *"Binary files"*.

The cloud database is accessible from external applications such as MATLAB® and Python®. To access the database from external applications authentication by the user's API token is needed. Information about the process can be found in the *"Documentation"* tab (*"API MATLAB"* and *"API Python"* links)

2.3   Data format of the results associated with damping estimation

The results should be stored in a MATLAB® file named as "*bridge_*ID*_damp.mat"*, where *"*ID*"* should be the bridge's *ID*, to be later incorporated in the online InBridge4EU-Database (2024). This file should include the following data related with the estimation of damping explained in the next chapters:

- *bridgeID*: bridge identification.
- *recordfile*: reference of the source file in the database.
- *label*: channel label that acquired the bridge response.
- *unit* (m or m/s or m/s²): unit associated with the time history.
- *span_measurement*: gives the span where measurement have been performed.
- *eurocode*: damping ratio as calculated with Eurocode formula.
- *method* (MCO, SSI_COV or modalfit): identification of the method used to estimate damping.
- *t0*: identification of the starting time of the free decay period used to estimate damping.
- *tend*: identification of the end time of the free decay period used to estimate damping.
- *fs*: sampling frequency.
- *time_vetor_decay*: time vector of the time history of the free decay period of the bridge response.
- *amplitude_vector_decay*: acceleration amplitude vector of the time history of the free decay period of the bridge response.
- *freq_mode1*: estimated frequency of the first fundamental vertical bending mode.
- *damping_mode1*: estimated damping coefficient of the first fundamental vertical bending mode.

- *amplitude_mode1*: maximum amplitude of the contribution of the first fundamental vertical bending mode in the free decay period response.
- *freq_mode2* (empty if non-existent): estimated frequency of the mode that most contribute to the response (if not the fundamental mode).
- *damping_mode2* (empty if non-existent): estimated damping coefficient of the mode that most contribute to the response (if not the fundamental mode).
- *amplitude_mode2* (empty if non-existent): maximum amplitude of the contribution of the mode that most contribute to the response in the free decay period response.

2.4 List of studied bridges

In Part 2 of the ERRI D214/RP3 (1999) report, the authors note that the available data for each bridge type was limited. In contrast, the present study, conducted within InBridge4EU, includes a significantly larger number of bridges, as shown in Table 1. Furthermore, ERRI D214/RP3 (1999) does not specify the exact number of measurements per bridge. However, in this study, the total number of valid measurements, and consequently, the estimated damping ratios, reaches approximately 1150, representing a substantial volume of processed data.

Table 1: Comparison between the bridge data used in D214 and that in InBridge4EU.

Database / Bridge type	ERRI D214/RP3	Inbridge4EU	Difference (%)
Steel	24	20	-17 %
Composite	6	18	+200 %
Prestressed concrete	9	13	+122 %
Reinforced concrete		7	
Filler beam	14	24	+71 %
Portal Frame	0	7	-
Total	53	89	+68 %

Damping estimations have been processed on the 89 bridges listed in Table 2 (FB/RC, PSC and STL/COMP stands for the Eurocode damping normative bridge types *"filler beam and reinforced concrete"*, *"prestressed concrete"* and *"steel and composite"*, respectively). A more detailed description of these bridges, including the results obtained in this work relative to the estimation of damping ratios presented later in Chapter 4, is presented in Annex A – *"Summary of damping estimation results"* and in Annex B – *"Bridge datasheets"*. Note that three of the bridges, namely Laguna Blanca, Gesällgatan North and Gesällgatan South, are included in two Eurocode families, since they are prestressed concrete bridges but present structural characteristics similar to a portal frame, with integral abutments monolithically connected to deck with backfill walls.

Table 2: List of bridges from which damping is estimated.

Bridge designation	Country	Structural type	Eurocode normative type	Span (m)
070000_205+406	France	U-shaped composite, simply supported	STL/COMP	16.80
070000_219+422	France	U-shaped composite, simply supported	STL/COMP	9.20
070000_230+956	France	U-shaped steel, simply supported	STL/COMP	6.80
070000_231+572	France	U-shaped composite, simply supported	STL/COMP	20.00

Bridge designation	Country	Structural type	Eurocode normative type	Span (m)
070000_383+560	France	Filler beam, simply supported	FB/RC	16.60
070000_384+378	France	Filler beam, simply supported	FB/RC	15.40
070000_470+164	France	Filler beam, simply supported	FB/RC	9.00
070000_484+884	France	Filler beam, simply supported	FB/RC	8.97
070000_492+208	France	Filler beam, simply supported	FB/RC	11.40
070000_496+533	France	High upper side beams composite, simply supported	STL/COMP	38.50
830000_034+307	France	Filler beam, simply supported	FB/RC	14.90
830000_036+790	France	U-shaped composite, simply supported	STL/COMP	14.00
830000_351+364	France	U-shaped composite, simply supported	STL/COMP	7.50
830000_380+357	France	U-shaped composite, simply supported	STL/COMP	11.00
830000_697+966	France	Filler beam, simply supported	FB/RC	8.86
830000_699+425	France	Filler beam, simply supported	FB/RC	14.20
830000_739+502	France	Filler beam, simply supported	FB/RC	13.80
752000_083+112	France	Filler beam, simply supported	FB/RC	20.0 + 34.4
752000_185+353	France	Filler beam, simply supported	FB/RC	27.8 + 32.0 + 29.8
752000_241+136	France	Slab, simply supported	FB/RC	17.38
752000_249+715	France	Filler beam, continuous	FB/RC	13.6 + 3.4
752000_287+961	France	Filler beam, continuous	FB/RC	7.80 + 4.2
752000_318+837	France	Filler beam, continuous	FB/RC	31.2 + 29.2 + 34.8
752000_335+986	France	Filler beam, continuous	FB/RC	11.4 + 14.5 + 11.4
590000_261+703	France	U-shaped steel, simply supported	STL/COMP	10.38
590000_235+895	France	U-shaped composite, simply supported	STL/COMP	6.40
810000_097+770	France	Upper lateral inclined girders composite, simply supported	STL/COMP	24.70
001000_186+312	France	U-shaped steel, simply supported	STL/COMP	8.00
001000_459+633	France	U-shaped composite, simply supported	STL/COMP	15.07
242000_138+166	France	Upper lateral inclined girders composite, simply supported	STL/COMP	31.50
272000_048+164	France	U-shaped composite, simply supported	STL/COMP	13.60

Bridge designation	Country	Structural type	Eurocode normative type	Span (m)
570000_041+757	France	U-shaped composite, simply supported	STL/COMP	8.16
EÜ Milde bei Beese - ID24193	Germany	Filler beam, simply supported	FB/RC	12.90
EÜ Str.Vinzelb.-Käth - ID26496	Germany	Filler beam, simply supported	FB/RC	12.86
EÜ über477 bei Kerpen - ID20726	Germany	Filler beam, simply supported	FB/RC	15.92
Nuthe Drewitz - ID23194	Germany	Filler beam, simply supported	FB/RC	17.70
Straßenunterführung - ID12391	Germany	Filler beam, simply supported	FB/RC	12.00
Ebr ü.Wenderterstraße - ID5046	Germany	Slab beam, simply supported	PSC	22.60
Hamminkelner Landstr - ID34492	Germany	Slab beam, simply supported	PSC	16.73
Friedrich Allee - ID7341	Germany	Steel trough cross-section, simply supported	STL/COMP	14.71
Augsburg - ID31962	Germany	Steel trough cross-section, simply supported	STL/COMP	20.08
BadOldesloe - ID24517	Germany	Steel hollow box with concrete slab, simply supported	STL/COMP	30.10
Bonn - ID7342	7343	Germany	Steel trough cross-section, simply supported	STL/COMP	14.37
Boppard - ID7640	Germany	Steel trough cross-section, simply supported	STL/COMP	27.30
Boppard - ID7641	Germany	Steel trough cross-section, simply supported	STL/COMP	31.80
Braunschweig - ID3648	Germany	Steel trough cross-section, simply supported	STL/COMP	35.20
Duisburg - ID15906	16955	Germany	Steel trough cross-section, simply supported	STL/COMP	30.20
Essen - ID17028	17553	Germany	Steel trough cross-section, simply supported	STL/COMP	22.70
Halle - ID11874	11875	Germany	Steel trough cross-section, simply supported	STL/COMP	28.00
HannoverLeinhausen - ID4500	Germany	Girder grid with concrete slab, simply supported	STL/COMP	21.00
Karlsruhe - ID6007	6008	Germany	Steel trough cross-section, simply supported	STL/COMP	21.00

Bridge designation	Country	Structural type	Eurocode normative type	Span (m)
Langenhorn - ID23875	Germany	Steel trough cross-section, simply supported	STL/COMP	36.30
Sehnde - ID15894 | 18019	Germany	Steel trough cross-section, simply supported	STL/COMP	20.10
95.965 - PI Braço do Cortiço	Portugal	Filler beam, simply supported	FB/RC	7.02
100.629 - PI da Cascalheira	Portugal	Filler beam, simply supported	FB/RC	10.92
282.943 - Ponte de Canelas	Portugal	Filler beam, simply supported	FB/RC	6×12.00
Sangalhos	Portugal	Portal Frame, closed	FB/RC	8.00
Pausinho	Portugal	Portal Frame, closed	FB/RC	3.25
Algodor	Spain	Filler beam, simply supported	FB/RC	10.25 + 10 + 10.25
Bracea	Spain	Girder deck, simply supported	PSC	15.25 + 15.25
Guadiana	Spain	Girder deck, simply supported	PSC	11.93 + 11.93
Jabalon	Spain	Girder deck, simply supported	PSC	24.00 + 24.00 + 24.00
Laguna Blanca	Spain	Prestressed Portal Frame, closed	FB/RC (portal frame) / PSC	8.00
Tirteafuera	Spain	Girder deck, simply supported	PSC	18.00
Arroyo Corbones: PC029_100017615	Spain	Truss, simply supported	STL/COMP	30.42
Barranco Bancal Redo: PC030_100017609	Spain	Truss, simply supported	STL/COMP	16.00
Barranco Corrimientos: PC040_100016018	Spain	Truss, simply supported	STL/COMP	21.20
Tejería Lateral: PC041_100015418	Spain	Truss, simply supported	STL/COMP	25.90
Tejería Central: PC041_100015418	Spain	Truss, simply supported	STL/COMP	41.00
Arroyo de las Piedras	Spain	Steel box with concrete slab, continuous	STL/COMP	$50.4 + 17 \times 63.5 + 44 + 35$
Casamisarro	Spain	U-Girder deck, simply supported	PSC	29.65
Banafjällsån	Sweden	Steel beam with concrete slab, simply supported	STL/COMP	42.00
Hästhovsgatan	Sweden	Slab full, simply supported	FB/RC	14.20

Bridge designation	Country	Structural type	Eurocode normative type	Span (m)
Bryngeån	Sweden	Steel beam with concrete slab, simply supported	STL/COMP	48.00
Bodavägen	Sweden	Beam, simply supported	PSC	22.00
Aspan	Sweden	Slab full, simply supported	FB/RC	24.00
Enköpingsvägen	Sweden	Beam, continuous	PSC	13.00 + 20.00 + 13.00
Fanna	Sweden	Beam, continuous	PSC	17.4 + 20.3 + 19.3
Sidensjövägen	Sweden	Slab full, continuous	FB/RC	13.00 + 17.00 + 13.00
Taxinge	Sweden	Slab full, continuous	PSC	16.10 + 22.90 + 17.60
Sveavägen	Sweden	Slab full, continuous	FB/RC	9.50 + 11.60 + 9.50
Vasavägen	Sweden	Slab full, continuous	FB/RC	8.60 + 12.50 + 8.60
Pershagen	Sweden	Slab full, continuous	FB/RC	11.00 + 18.40 + 11.00
Degermyran	Sweden	Portal Frame, open	FB/RC	8.70
Faresmyren	Sweden	Portal Frame, open	FB/RC	8.70
Gesällgatan North	Sweden	Beam, continuous abutment	FB/RC (portal frame) / PSC	30.60
Gesällgatan South	Sweden	Beam, continuous abutment	FB/RC (portal frame) / PSC	28.60
Norra Kungsvägen	Sweden	Portal Frame, open	FB/RC	15.70
Sodra Kungsvägen	Sweden	Portal Frame, open	FB/RC	15.25

2.5 Test types

2.5.1 Tests under railway traffic

Most of the measurements collected and stored in the database came from tests under railway traffic carried out by UPORTO/Infraestruturas de Portugal in Portugal, KTH/Trafikverket in Sweden, UJI/UdS/UPM/ADIF in Spain, DB InfraGO in Germany and SNCF in France. This type of tests is conducted to measure the dynamic response of the bridge in terms of accelerations caused by the passing trains. The accelerations of the bridge are recorded using accelerometers attached to the bridge deck connected to an acquisition system that gathers all the data in a computer. Different triggers may be used to ensure that the sensors record the bridge response only during the moments when the train is crossing it. As an example, in the tests performed in Portugal, four optical sensors were installed in the track sleepers, two in each track, to detect the instants when the train enters and leaves the bridge (see Andersson et al. (2021) and Silva et al. (2023) for details). Other options consist of

setting the acquisition system to start recording only after a predetermined threshold of acceleration is reached. Figure 3 depicts and example of a test setup carried out in Portugal.

a)   *b)*
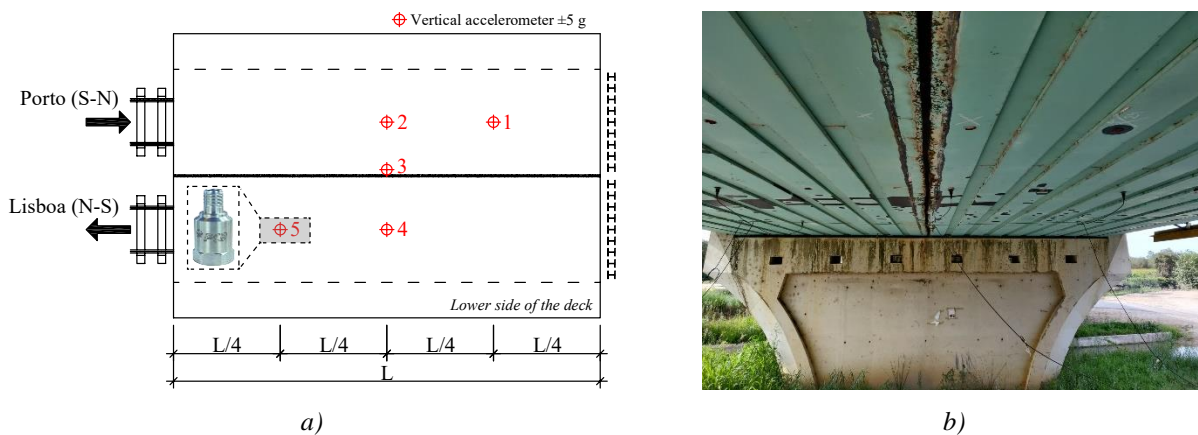
Figure 3: Test under railway traffic performed in the Canelas bridge in Portugal: a) instrumentation setup and b) accelerometers installation in the lower face of the deck.

Depending on the test, different types of accelerometers may also be used, but they should have measurements ranges compatible with the levels of vibration expected in the bridge to avoid the saturation of the sensor. Table 3 presents the basic properties of the accelerometers used in the tests conducted in each country, along with the main references that describe these tests in detail, while Figure 3 depicts examples of raw time series records obtained in the field measurements. Damping is estimated through the MCO and/or SSI-COV methods, which use the free decay vibration of each time series record as input, as explained later in Chapter 3.

Table 3: Accelerometers used in the tests carried out in the different countries.

Country	Infrastructure Manager	Entity responsible	Sensor main characteristics	Reference
Portugal	Infraestruturas de Portugal	UPORTO	PCB model 393A03 piezoelectric accelerometer Measurement range: ±5 g Sampling frequency: 2048 Hz	(Andersson et al., 2021) (Silva et al., 2023)
Sweden	Trafikverket	KTH	SiFlex-SF1500S MEMS accelerometer Measurement range: ±3 g Sampling frequency: 1200 Hz	(Andersson et al., 2021)
Spain	ADIF	UJI/UdS/ADIF	Endevco model 86 piezoelectric accelerometer Measurement range: ±0.5 g Sampling frequency: 4096 Hz	(Sánchez-Quesada et al., 2021) (Sánchez-Quesada et al., 2023)
Germany	DB InfraGO	DB InfraGO	Measurement range: ±5 g Sampling frequency: 2400 Hz	DB InFraGO Dynamic Reports
France	SNCF Réseau	AVLS	LORD MicroStrain G-Link 200 8G Measurement range: ±8 g Acquisition frequency: 4096 Hz	SNCF Réseau Dynamic Reports
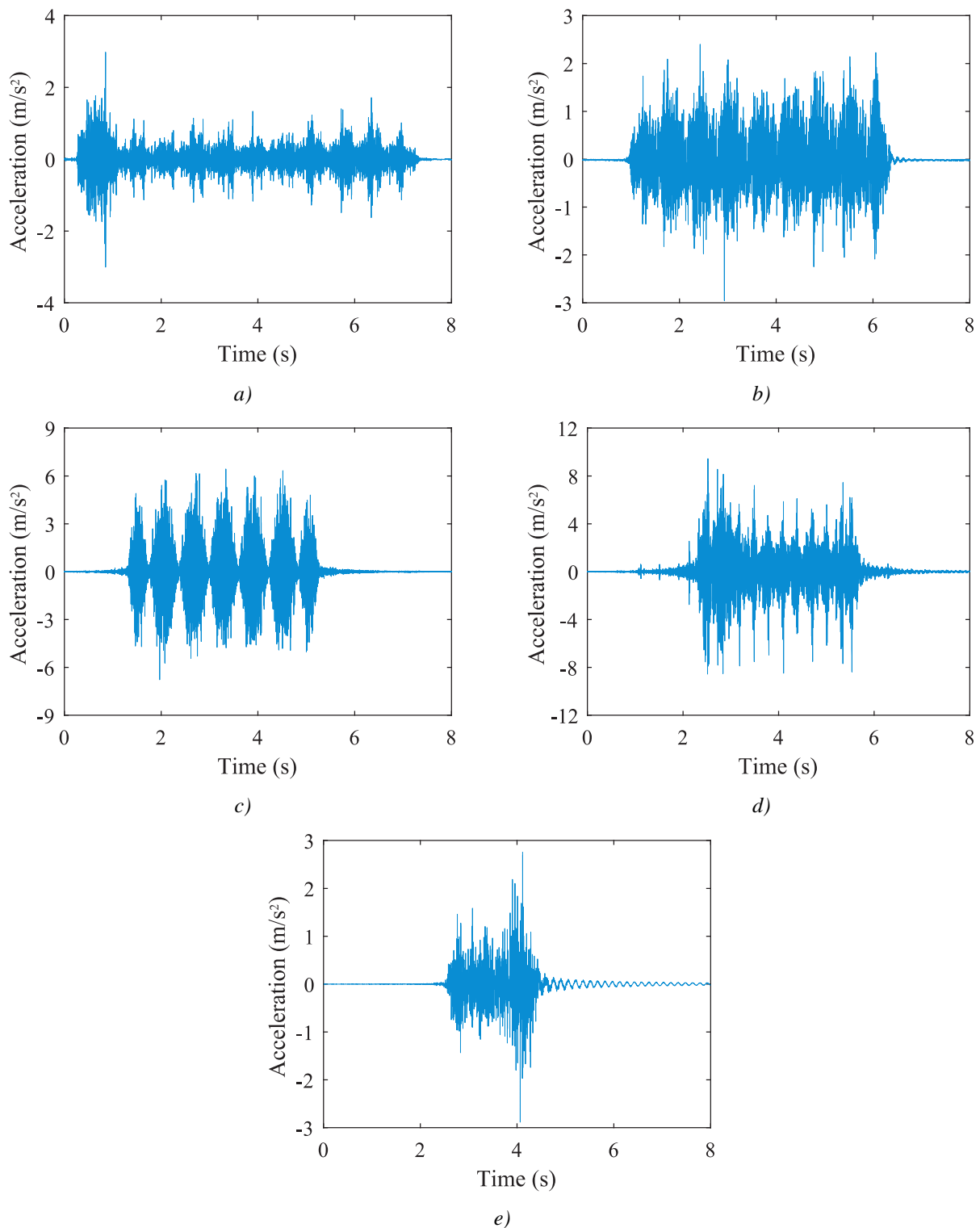
Figure 4: Examples of raw time series records: bridge a) 810000_097+770 in France, b) Hamminkelner Landstraße in Germany, c) Canelas in Portugal, d) Guadiana in Spain and e) Aspan in Sweden.

2.5.2   Tests under forced excitation

Although most of the measurements used in the present work came from tests under railway traffic, some tests under forced excitation performed in Sweden were also processed. In these tests, a load-controlled hydraulic actuator (see Figure 5) has been used to apply a constant amplitude harmonic load to the structure.

The system consists of a 50 kN MTS actuator equipped with two model 252 servo-valves, each with a capacity of 56 lpm. The actuator is connected to a stand-alone oil pump with a peak pressure of 210 bar and a flow rate of 120 lpm, powered by an integrated 40 hp diesel engine. The actuator is mounted on a 0.9×0.9 m base plate and connected to the bridge soffit by an aluminium truss. The tests are conducted under load-controlled conditions using an MTS FlexTest SE controller, and the input force is measured by a load cell located at the top of the actuator. The bridges were instrumented with uniaxial MEMS-accelerometers from Colibrys, as previously described in Table 3 (SiFlex SF1500S with a range of ±3 g and a sensitivity of 1.2 V/g). The input force and the output acceleration were recorded by a MGCPlus DAQ-system with a sample frequency of 1200 Hz and a 200 Hz Bessel LP-filter. Most of the tested bridges were subjected to forced excitation loads of 1 kN, 5 kN, 10 kN, and 20 kN for a range of frequencies (frequency sweep) to study possible amplitude-dependent nonlinearities. Thus, the tests consisted of applying a sinusoidal force with constant amplitude to the deck, sweeping through various frequencies within a given range, in order to induce the bridge to resonance states when these matched the natural frequency of any of its modes.
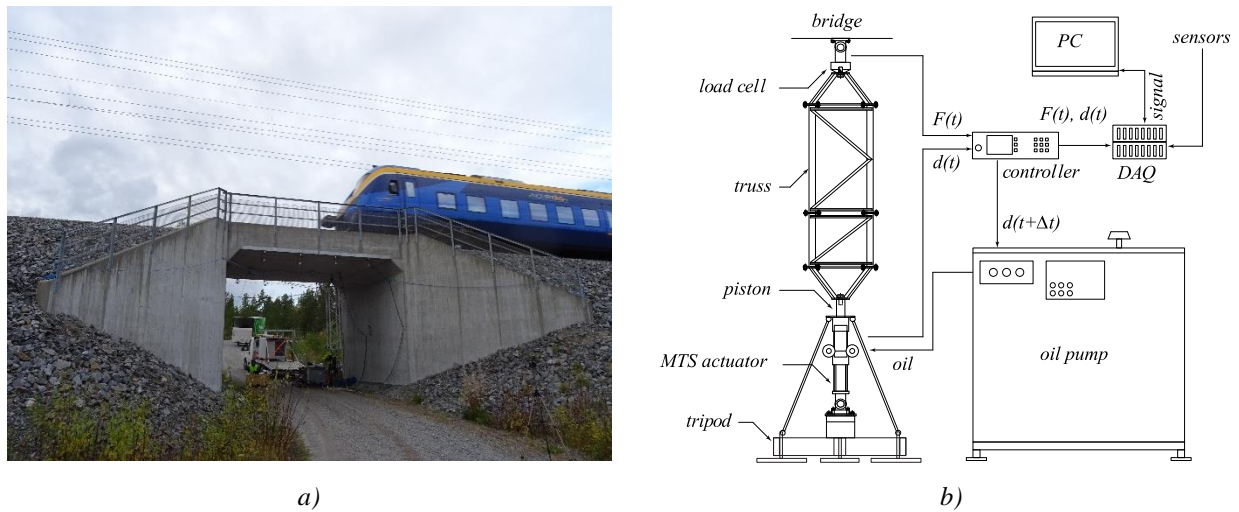
Figure 5: Load-controlled hydraulic actuator used by KTH in the tests under forced excitation: a) installation in the Degermyran portal frame bridge tests and b) schematic (Andersson et al., 2021).

The complex-valued Frequency Response Function (FRF) $\mathbf{H}(\omega)$, given in m/s^2 kN, has been calculated according to Equation (1) based on the input force $F(t)$ and output acceleration $a(t)$. Since the records obtained from these tests do not contain free decay periods as the tests under railway traffic, a different approach has been adopted to estimate damping based on the procedure described by Andersson et al. (2021) and Albright et al. (2025). This method estimates critical damping ratios for each mode using the least squares ratio function estimation formulated in detail by Ozdemir and Gumussoy (2017) and it was executed through the built-in MATLAB® (2023a) function *"modalfit"* contained in the System Identification Toolbox™.

$$\mathbf{H}(\omega) = \mathbf{A}(\omega)/\mathbf{F}(\omega) \tag{1}$$

Figure 6 depicts the typical inputs/outputs from a forced excitation test, namely input force, output acceleration and respective FRF using the Aspan bridge as an example.
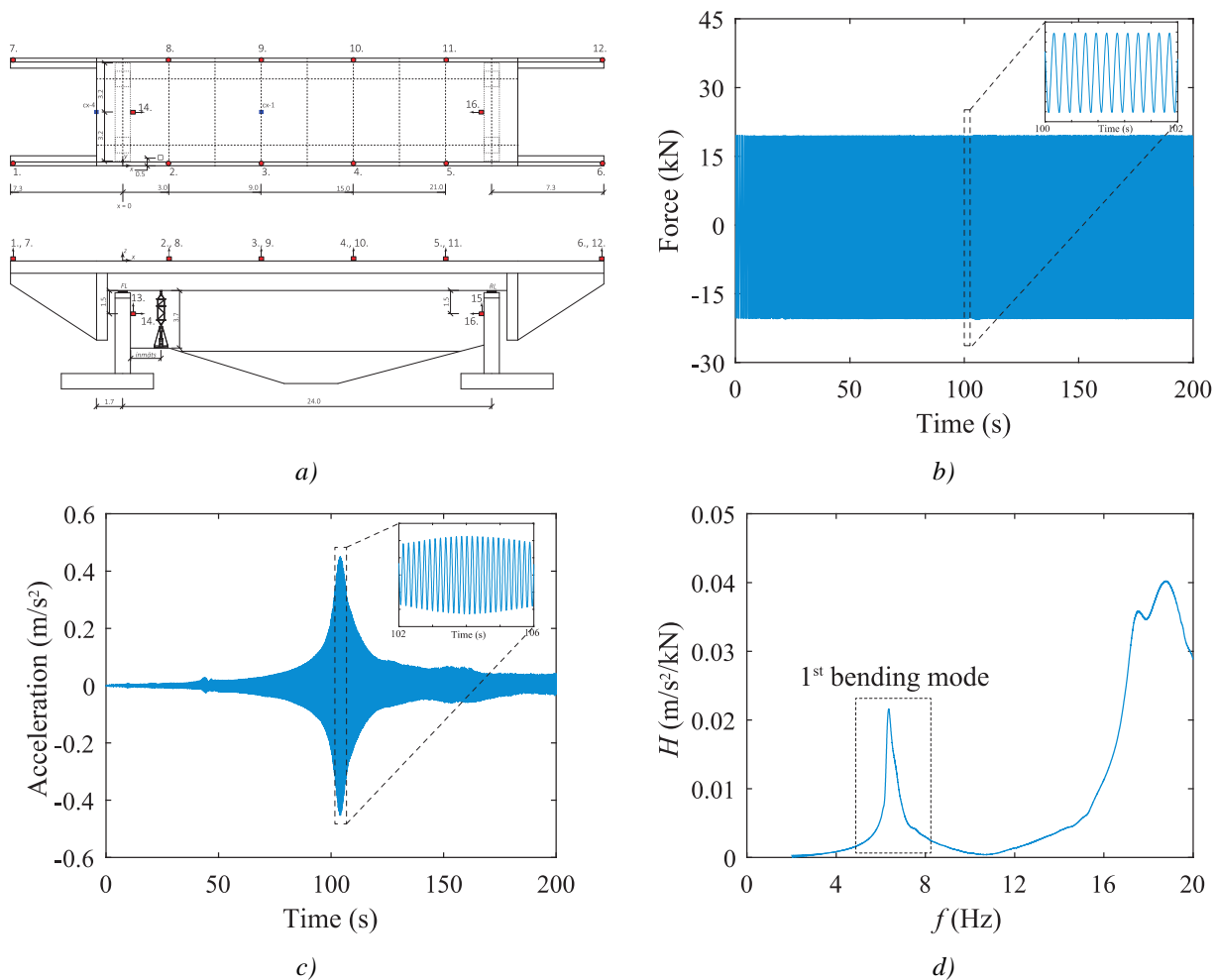
Figure 6: Typical inputs/outputs from a forced vibration test exemplified with Aspan bridge: a) instrumentation setup, b) input force of 20 kN, c) acceleration measured through accelerometer 3 and d) respective FRF.

3   DAMPING ESTIMATION METHODS

3.1   Initial considerations

Damping has been estimated, within Task 4.2, from the free decay period of the records obtained in the tests under railway traffic by AVLS and UPORTO using the MCO and SSI-COV methods, respectively. As for the calculation of the critical damping from the data obtained in the tests under forced excitation performed in Sweden, an alternative method based on the least squares ratio function estimation, included in the MATLAB® (2023a) built-in function *"modalfit"*, has been adopted. The present section begins by introducing the damping estimation methods (Section 3.2), followed by an explanation of the approach used to define the free decay period after train passage (Section 3.3). Finally, it concludes with a discussion of several benchmark tests used to compare the outputs of MCO and SSI-COV (Section 3.4). The estimated damping ratios for all bridges are presented later in Chapter 4.

3.2   Description of the damping estimation methods

3.2.1   Foreword

In the tests under railway traffic (see Section 2.5.1), damping is estimated based on the bridge's free vibration response (acceleration) after the train passage. Identifying the onset of the free response is a key

focus of this study and will be described in more detail later in Section 3.3. Naturally, the free response exhibits lower amplitudes compared to the forced regime, which can introduce bias if damping is amplitude-dependent, as is often observed. However, estimating damping while the train is still on the bridge presents a highly complex challenge and would not be feasible for the entire database. Therefore, apart from the tests under forced excitation performed in Sweden (see Section 2.5.2), all the damping estimations obtained from the tests under railway traffic were carried out based only on the free decay period of the bridge response.

For systems with linear damping, one may immediately see that the response is given by a periodic function modulated by a negative exponential, implying that the damping ratio can be directly evaluated from the free decay response through the classic Logarithmic Decrement (LD) method. These bridge's free decays measured after the train passage should only contain the contribution of a single mode, so the exponential functions can be directly fitted to the recorded time series. This classical approach, however, faces difficulties to isolate the contribution of modes with close natural frequencies. Therefore, more accurate methods should be adopted for better damping estimations in more complex systems, such as bridges. The following sections present the two main methods used in this work to estimate damping through the free decay period, namely the MCO, described in Section 3.2.2, and the SSI-COV, presented in Section 3.2.3. The method based on the least squares ratio function estimation incorporated in the MATLAB® (2023a) built-in function *"modalfit"* and used for computing damping from the tests under forced excitation is briefly introduced in Section 3.2.4.

3.2.2 *Multi-Criteria Optimisation (MCO)*

The multi-criteria optimisation method (MCO) set up by AVLS is based on the reconstruction of an analytic multi-degrees of freedom function matching the measured free response signal in both time and frequency domains. It is based on the MATLAB® multi-objective optimisation toolbox *GODLIKE* (abbreviation for Global Optimum Determination by Linking and Interchanging Kindred Evaluators) developed by (Vandekerckhove and Oldenhuis, 2009), which implements the combination of 4 metaheuristics (solving procedures) to find an optimum of a problem involving several input variables and several objective functions. The 4 metaheuristics are: Genetic Algorithm (GA), Differential Evolution (DE), Particle Swarm Optimization (PSO) and Adaptive Simulated Annealing (ASA). The multi-evaluator step aims at approaching a global minimum and it is followed by the use of a second optimisation step with the Nelder-Mead algorithm (function *"fminsearch"* from MATLAB®) in order to help converging towards a local minimum.

In the present case, the damping estimation methods assumes that the measured vibration signal (acceleration) during free-responses of the bridge can be decomposed into a sum of exponentially decaying sines according to the Equation (2). Is it then assumed that the damping model is linear viscous and the amplitude and frequency parameters are constant over the response.

$$s(t) = \sum_{i=1}^{Ndof} A_i \cdot \exp(-\omega_i \cdot \xi_i \cdot t) \cdot \sin\left(\omega_i \cdot \sqrt{1 - \xi_i^2} \cdot t + \phi_i\right) \tag{2}$$

where N_{dof} is the number of considered modes, t is time, and A_i, ω_i, ξ_i and ϕ_i are the signal amplitude, the angular frequency, the damping ratio and the phase of mode *i*, respectively. Additional variables related to the definition of the starting time of the decay and its duration do not appear in Equation (2), but are referred to as t_0 and t_{end} later in this report.

The optimisation cost function ϵ of the method evaluates the good fitting of the synthesized signal and the measured signal in both the time domain and in the frequency domain through the following equation (the cost function should tend towards zero):

$$\epsilon = h_{tmp} \cdot \frac{\int \left(s_{init}(t) - s_{calc}(t)\right)^2 dt}{\int s_{init}(t)^2 dt} + h_{fft} \cdot \frac{\int \left(p_{init}(f) - p_{calc}(f)\right)^2 df}{\int p_{init}(f)^2 df} \qquad (3)$$

in which h_{tmp} and h_{fft} are weighting factors for the time- domain and frequency-domain scores, s_{init} is the initial time-domain signal (measured), s_{calc} is the calculated time-domain signal (synthesized), p_{init} is the initial frequency-domain signal (calculated on s_{init}) and p_{calc} the calculated time-domain signal (calculated on s_{calc}).

This model allows to evaluate the superposition of several modes at once and does not require to heavily filter signals to process modes separately. Indeed, close modes can be difficult to isolate with filters and increasing the filter order can deform signals significantly. Additionally, the ability of the procedure to provide boundaries for variables helps eliminating spurious values and computing the cost function on time and frequency domains criteria also improves the ability of the method to deal with very close modes which would be more difficult to separate in only one domain.

The procedure is user-dependent for the choice of variables boundaries for each mode before running the optimisation process (boundaries for frequency, amplitude, damping and phase). To lessen user-dependence, starting time t_0 and final time t_{end} are calculated automatically according to procedure described in Sections 3.3.2 and 3.3.3, respectively, however they can be adjusted manually is the initial estimate appears irrelevant.

The optimisation tool involves generating random samples at several steps of the procedure causing a variability in the results. This is mitigated by running the procedure several times and averaging results and in the end, the user expertise is required to validate the final damping estimation.

To exemplify the method's application, Figure 7 presents the signal fitting performed by MCO for damping estimation in the Spanish bridge Tirteafuera. As a result of the algorithm, a superimposition of the original measured signal and the analytically fitted one is presented in both the time and frequency domains, while the parameters of the analytical model are obtained (shown in Table 4 for this example). The user then validates these results based on the accuracy of the fitted curves in both domains. For instance, mode 4 at 20.4 Hz is not perfectly fitted, as seen in the Fast Fourier Transform (FFT) spectrum, but since its frequency is much higher than that of the first mode and its amplitude is lower, it is not considered critical from a bridge design perspective. Finally, mode 1, with a frequency of 8.18 Hz and a damping ratio of 1.71%, is selected for damping estimation as it corresponds to the fundamental bending mode. It has the highest amplitude and, consequently, the greatest contribution to the dynamic response. In cases where the fundamental bending mode does not have the highest contribution, the properties of the mode with the most significant impact are also stored, as described in Section 2.3.

a)

b)
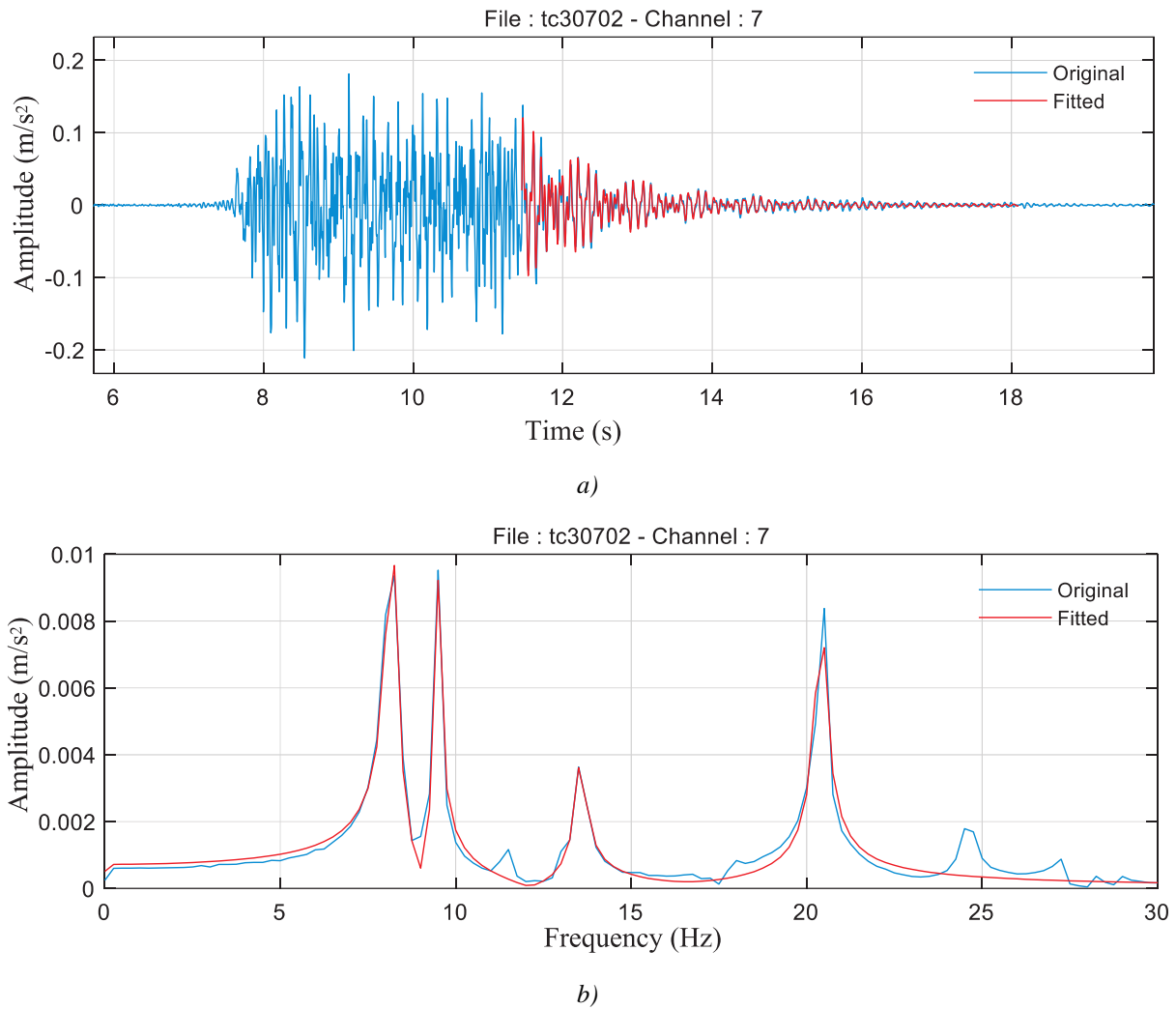
Figure 7: Signal fitting through MCO: a) time and b) frequency domains (example with the ADIF Tirteafuera bridge in Spain).

Table 4: Parameters estimated by the MCO method corresponding to the fitted analytical model (example with the ADIF Tirteafuera bridge in Spain).

Mode	Amplitude (m/s²)	Frequency (Hz)	Damping (%)
1	0.055	8.18	1.71
2	0.028	9.46	0.77
3	0.020	13.56	1.02
4	0.043	20.40	0.72

3.2.3 Covariance Driven Stochastic Subspace Identification (SSI-COV)

The Covariance Driven Stochastic Subspace Identification (SSI-COV) method, originally introduced by Peeters and De Roeck (1999) and widely used in civil engineering applications related with structural health monitoring (SHM), such as bridges (Magalhães and Cunha, 2011) or wind turbines (Pimenta et al., 2024b), has been adopted by UPORTO to estimate damping through the bridge's free decay response after the train

passage. This parametric method in the time domain tries to identify a discrete state space model from the recorded response to characterise the structure's dominated modes. This methodology is based on the identification of a state-space model of the recorded (output) response $\mathbf{y}_k$ as (Pimenta et al., 2024a)

$$\begin{aligned}\mathbf{x}_{k+1} &= \mathbf{A} \cdot \mathbf{x}_k + \mathbf{w}_k \\ \mathbf{y}_k &= \mathbf{C} \cdot \mathbf{x}_k + \mathbf{v}_k\end{aligned} \tag{4}$$

where $\mathbf{x}_k$ is the state vector, and $\mathbf{w}_k$ and $\mathbf{v}_k$ the process and measurement noise, respectively, $\mathbf{C}$ is the output matrix and where the state matrix $\mathbf{A}$ contains all the relevant dynamic information of the system (see Magalhães (2010) for details). Although initially developed for stochastic identification, this method can also be adapted to extract modal parameters from free decays, such as those observed in the bridge response after the train exits it. The observed free decays can be directly used as input of the SSI-COV method, taking the place of the correlation functions calculated from the ambient responses. With this technique, after the identification of the modal properties, it is possible to decompose the measured free decays in modal decays using the decomposition of the output correlation matrix $\mathbf{R}_y$:

$$\mathbf{R}_y(j) = \mathbf{C} \cdot \mathbf{A}^{j-1} \cdot \mathbf{G} \tag{5}$$

where $\mathbf{G}$ is the "next state-output" correlation matrix (see Magalhães (2010) for details). When the correlation matrix $\mathbf{R}_y$ is replaced by the measured free decays $\mathbf{y}_k$ and $\mathbf{A}$ substituted by its modal decomposition, the following expression is obtained:

$$\mathbf{y}_k = \mathbf{C} \cdot \mathbf{\Psi} \cdot \mathbf{\Lambda}^{k-1} \cdot \mathbf{\Psi}^{-1} \cdot \mathbf{G} \tag{6}$$

where $\mathbf{\Psi}$ contains in its columns the mode shapes, $\mathbf{\Lambda}$ is a diagonal matrix, whose elements are equal to $e^{\lambda_i \cdot \Delta t}$, Δt is the time interval between each sample and λ_i are the eigenvalues of the state-space model that are related with the natural frequencies and modal damping ratios of the tested structure. The contribution of a specific mode for the measured decays can be obtained with Eq. (6), considering in the diagonal matrix only the two eigenvalues (complex conjugate pairs) that are associated with that mode. The damping estimates of the less excited modes are expected to be less reliable. A detailed description of the theoretical background of the SSI-COV method and the definition of the contribution of each mode for the measured decay can be found in Pimenta et al. (2024a) and Magalhães (2010).

For the present work, and since damping estimation is difficult to automatize, an user-friendly SSI-COV application developed in Python® (Van Rossum and Drake, 2009) was made by UPORTO, allowing the estimation of damping ratios from free decay responses (bridge response after the train exits the bridge) in a fast way. The steps used to estimate the damping through the application can be summarized as following:

1) Upload the raw time series record measured in a test under railway traffic, including the sampling frequency to define the time vector (see Figure 8).
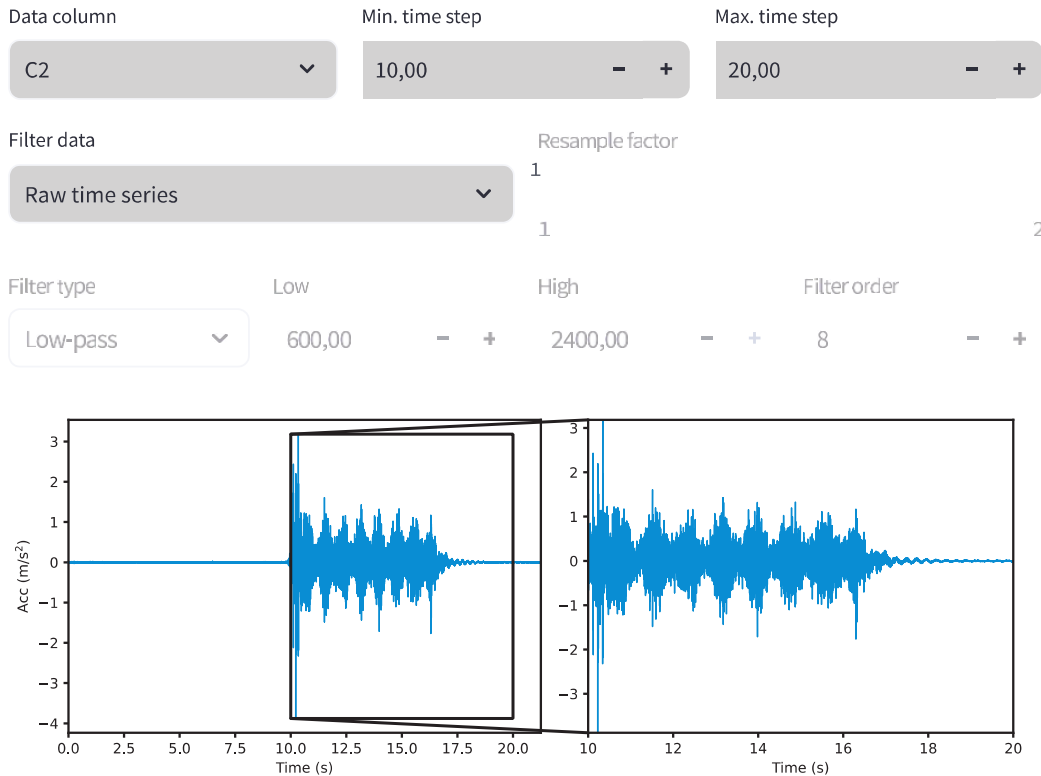
Figure 8: Step 1 – Uploading a raw time series through the SSI-COV (example with the DB InfraGO EÜ über Stöckener Straße bridge – ID4500 in Germany).

2) Filter the signal and isolate the free decay part of the time series (see Figure 9): to easily identify the free decay period, it may be helpful to filter the signal using a lower cutoff frequency, such as near the first fundamental vertical bending mode, to isolate this component. In this study, this frequency was determined in advance using dynamic reports from Infrastructure Managers or through ambient vibration tests conducted during measurements. For estimations performed using SSI-COV, the start of the free decay period was determined following the procedure outlined in Section 0, but was always manually verified by the operator. The decay length was consistently set to 10 vibration cycles, with its duration depending on the first mode frequency. Such procedure avoided the interference from cycles with very low amplitude in the damping ratio evaluation.
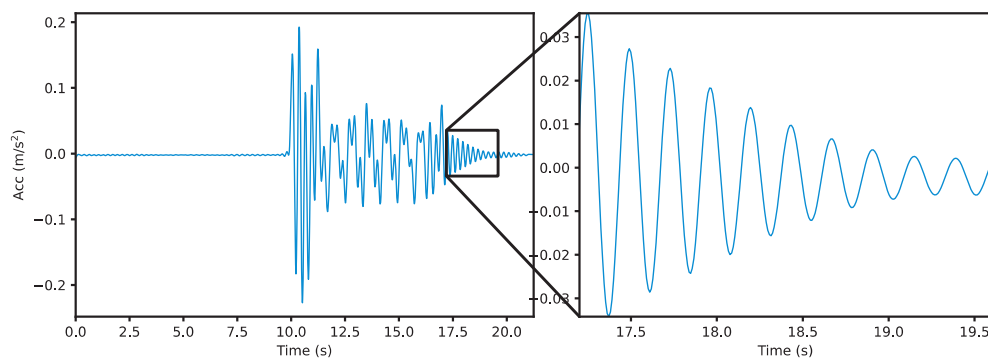
Figure 9: Step 2 – Filtering and isolating the free decay period (example with the DB InfraGO EÜ über Stöckener Straße bridge – ID4500 in Germany – for $f_1 \approx 4.2$ Hz, 10 cycles correspond to approximately 2.4 s).

3) Execute SSI-COV considering only the free decay period (see Figure 10): the application can compute not only the damping ratio ξ, but also the mode's frequency f. Naturally, it is also possible to extract the vibration (acceleration) amplitude A correspondent to the mode and the respective contribution, in percentage, to the total acceleration response. Several parameters were required as inputs for the damping estimation, such as model order and details about mode clustering (minimum number of points needed to define a cluster/mode), but the damping ratios demonstrated low dependency to these factors. Thus, the default values depicted in Figure 10, based on the users' previous experience, were always used for the final estimations. Finally, it can also be seen that the algorithm may also detect spurious modes that can be easily disregarded given its low contribution (in the example presented here, the spurious Mode 2 contributes only 3.3% to the total acceleration amplitude).
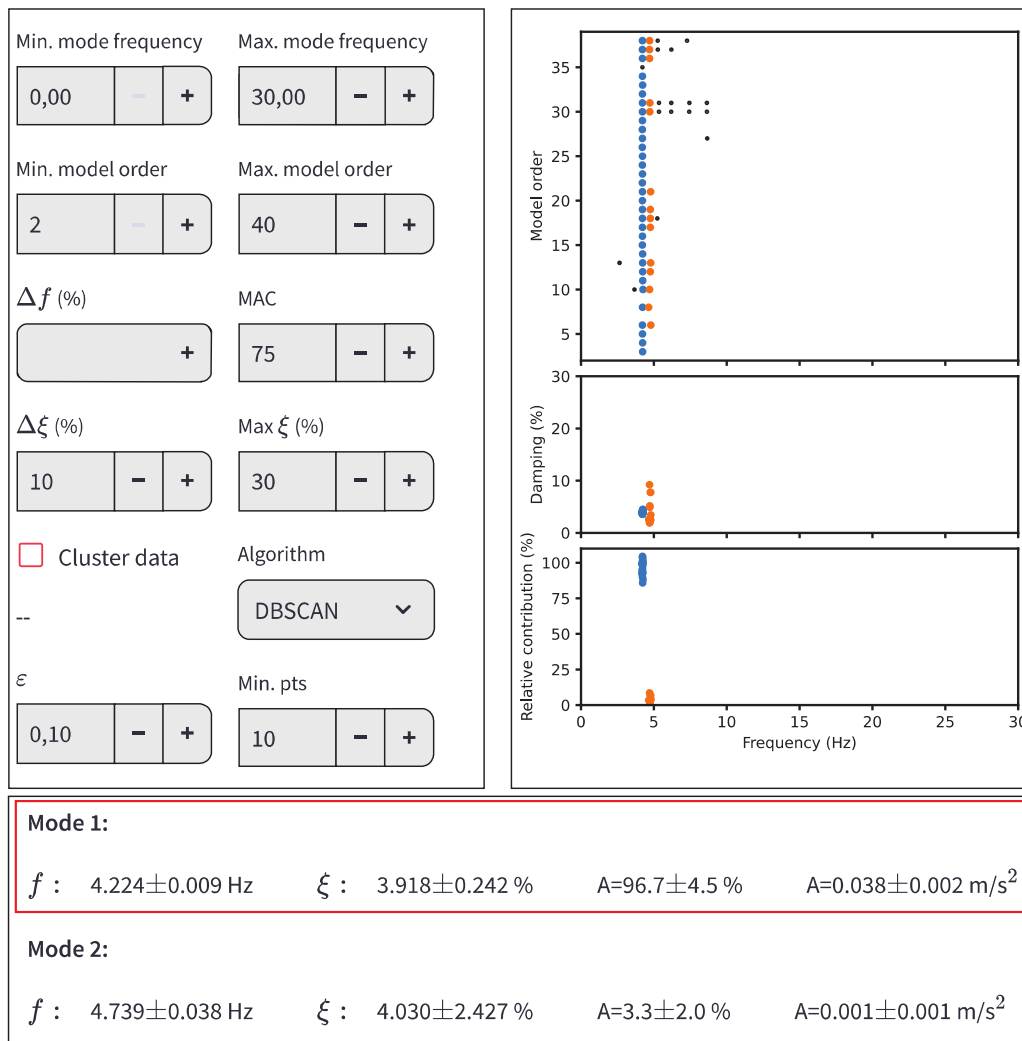
Figure 10: Step 3 – Identification of the fundamental mode through its frequency and calculation of damping ratio (example with the DB InfraGO EÜ über Stöckener Straße bridge – ID4500 in Germany – $f_1 = 4.224$ Hz, $\xi_1 = 3.918$ %, $A_1 = 0.038\,m/s^2$, which contributes 96.7 % to the total acceleration amplitude).

3.2.4 Least squares ratio function estimation incorporated in MATLAB's "modalfit" built-in function

The tests under forced excitation, described in Section 2.5.2, consisted of applying a sinusoidal force with constant amplitude to the deck, sweeping through various frequencies within a given range, in order to induce the bridge to resonance states when these matched the natural frequency of any of its modes. Since the records obtained from the tests performed in Sweden by KTH do not contain free decay periods, a different approach has been adopted to estimate damping based on the procedure described by Andersson et al. (2021) and Albright et al. (2025). This method estimates critical damping ratios for each mode using the least squares ratio function estimation formulated in detail by Ozdemir and Gumussoy (2017) and it was executed through the built-in MATLAB® (2023a) function *"modalfit"* contained in the System Identification Toolbox™.

For the present work, a MATLAB® routine has been developed by KTH and UPORTO to estimate damping through the aforementioned method for each sweep test. The main inputs of this routine consisted of the force (test input) and acceleration (test output) time series, which have been used to compute the correspondent FRF through Equation (1), as shown in the example plotted in Figure 11 related with the 5 kN, 10 kN and 20 kN input force tests performed in the Sidensjövägen bridge. Modal damping has been always estimated

considering the responses measured at the accelerometers located at midspan (A6 for the example presented in Figure 11). It can be observed that the FRF fitted using the *"modalfit"* built-in function shows good agreement with the experimental one for both detected modes. Depending on the test and the corresponding frequency sweep, one or more modes may be detected and analysed using this method.

a)

b)
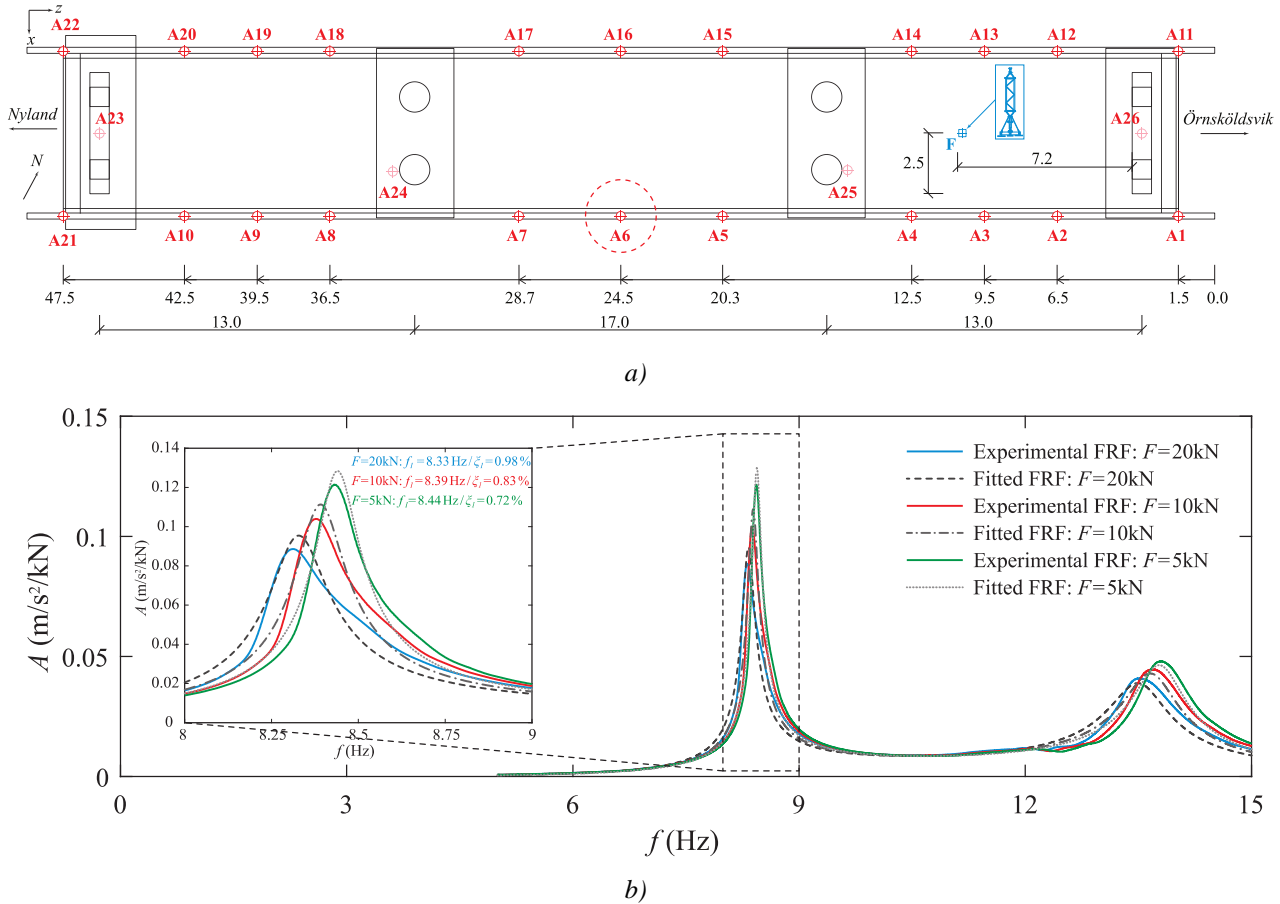
Figure 11: Application of the "modalfit" method to estimate damping using results from the tests under forced excitation performed in Sweden (example with the Trafikverket Sidensjövägen bridge in Sweden – results for accelerometer A6 located at midspan): a) instrumentation setup and b) FRF computed from the output response measured in A6 and corresponding fit through the MATLAB® (2023a) "modalfit" function to estimate frequency and damping on the detected modes.

3.3 Analysis of the free decay period

3.3.1 Foreword

A procedure to automatize the choice of the initial time t_0 of the free response for damping estimation has been developed and is presented in Section 3.3.2. This method could be validated with the help of the Portuguese measurement dataset, since it includes data obtained in optical sensors installed on both bridge's extremities to detect precisely the arrival and the departure of the train over the bridge. Additionally, rules to select the duration of signal, or ending time of the considered free response t_{end} have been defined and presented in Section 3.3.3.

3.3.2 Estimation of the initial free-decay instant

Two different methods were developed, both of which found a fairly accurate match with the optically detected departure time. The instrumentation setups, using accelerometers and optical sensors on Portuguese bridges, are described in Silva et al. (2023). Optical sensors were positioned as close as possible to the bearings

of six bridges (Braço do Cortiço (noted as no.1), Canelas (no.2), Cascalheira (no.3), Peixinhos (no.4), Sangalhos (no.5), and Vale da Negra (no.6)) and were directed towards the train axles. In this dataset, accelerometers were positioned only at mid-span, so initial time estimations were based on this assumption.

3.3.2.1   Statistical sigma method

The statistical sigma method involves calculating the standard deviation ("*sigma*") of acceleration during a train passage. The departure time is estimated by identifying the last time the acceleration exceeds the sigma threshold through the following procedure:

- Detection of the train passage: the duration of the train passage is calculated thanks to the 1s rolling-RMS (Root Mean Square) or moving-std $L_{eq,1s}$ value on the full signal. The train passage time boundaries are defined as the moments where $\max\{L_{eq,1s}\} - 40\text{dB}$ are reached.

- Calculation of sigma: the standard deviation of acceleration during train passage is computed on the 600 Hz low-pass filtered signal. This high cutoff frequency allows to keep a broader statistical distribution of the acceleration values.

- Train departure time: The departure time or initial time the free-response t_0 is the time of last exceedance of the sigma value.

Figure 12 depicts the procedure. The base signal st_{acc} is obtained after a 600 Hz low-pass filtering then only the signal between detected boundaries st_{train} is considered for the standard deviation calculation. The last exceedance represents the estimated t_0.
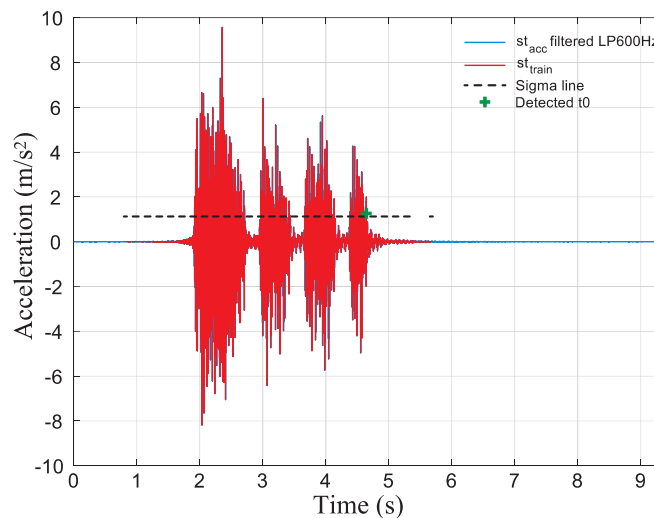
Figure 12: Detection of t₀ with the sigma method.

3.3.2.2   Displacement analysis method

In the displacement analysis method, train departure time is estimated thanks to the study of the displacement signal. It has been noticed on the dataset that the last significant displacement peak matches with the optical sensor detection. Displacement levels being sensitive to low frequencies, peaks presumably match passages of each bogie. The process involves the following steps:

- Double integration of acceleration to get displacement, applying a 1 Hz high-pass filter to avoid drifting.

- Detection of the last significant peak: this is a sensitive step because signals levels can vary significantly between passages and bridges; An automated procedure has been set up to detect the last peak. It

involves steps of normalization, peak detection and weighing and thresholding to remove spurious peaks.

Figure 13 presents the result of last peak detection on a signal after double integration to obtain a displacement signal.

Figure 13: Detection of t_0 with displacement peak method.

3.3.2.3   Validation with data from the optical sensors

Both methods were compared and validated through the measured references from optical sensors on the Portuguese dataset (6 bridges). Figure 14a shows the gap between t_0 estimates obtained with the 2 methods described above and the reference from optic sensors for each train passage. Additionally, median values for each method are represented. Figure 14b sh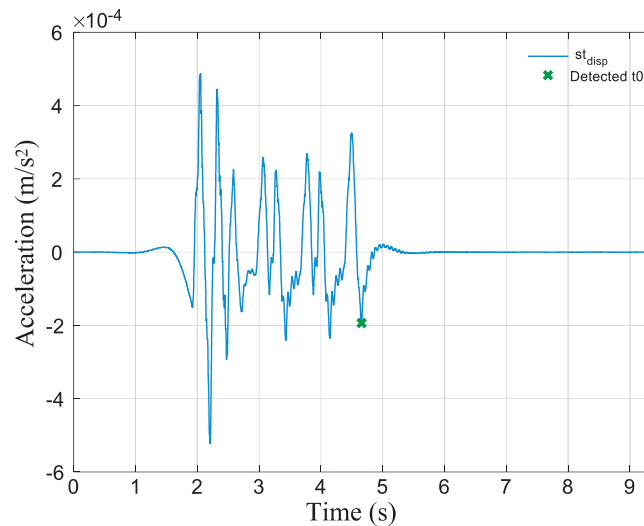ows the same values but with the train speed for each passage highlighted with different colours according to the presented scale. Speed was estimated by relating the time between the passage of the first and last axles detected by the optical sensors to the known distance between them. It may contain spurious values as optic sensors did not give relevant data on some passages, however, the speed tendencies per bridge are accurate. Observing Figure 14 allows the following inferences:

- The absolute error values are mostly inferior to 100 ms, For comparison, crossing 4 meters (half span of an 8 meters bridge corresponding to the distance between the accelerometer and support) at 100 km/h requires 144 ms.

- Bridges no.2, no.3 and especially no.4 show higher scattering for the t_0 detection.

- Standard deviation method (sigma method) shows better results on 5 out of 6 bridges with absolute median error values from 37.6ms to 0.488ms (bridge no.4 excluded).

- Results on bridge no.4 are notably worse than on other bridges and this is likely to be linked to the globally low speed of trains (often in the [20 ~ 60] km/h range),

- Bridge span is also likely to influence results as observed on bridge no.2 and no.3, which are about 11m-long. In these cases, median errors with sigma method reach about 30ms. For reference, an axle crossing half a 11m span at 70km/h requires 283ms and 220ms at 90km/h, so the method is precise enough to fall below this value.
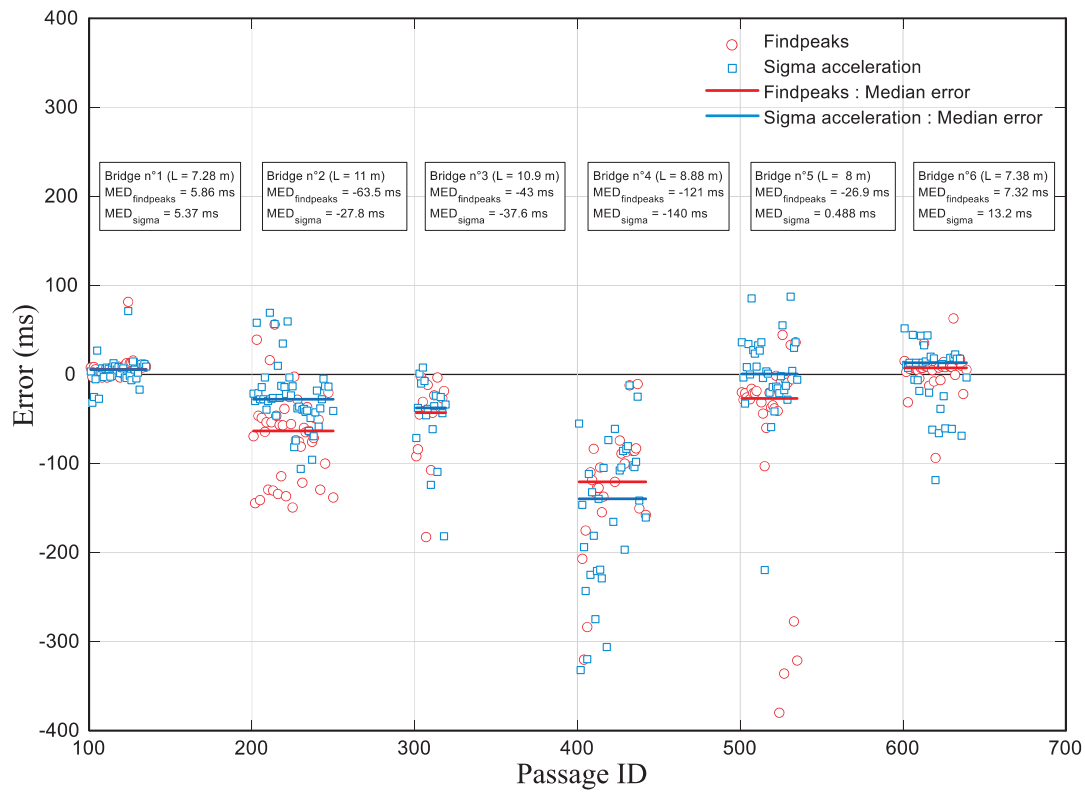
a)
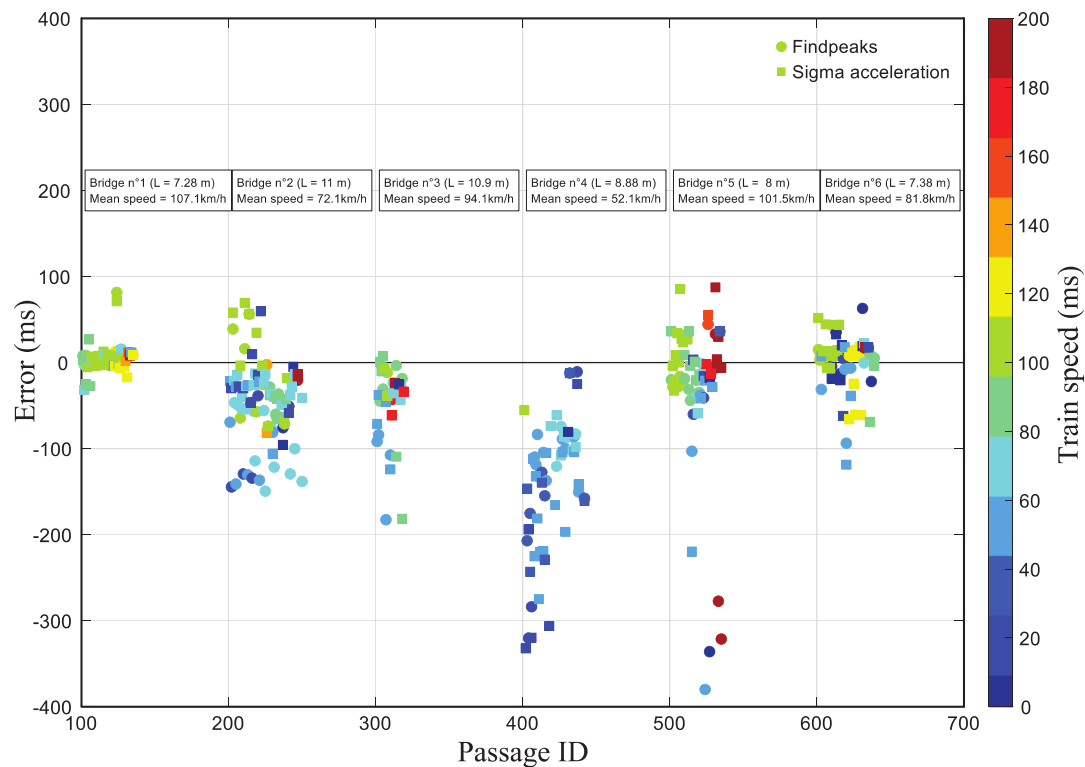
b)

Figure 14: Estimation error between the two t_0 detection methods against optical sensor reference: a) with median estimators, b) with train speed estimation.

3.3.3 Selection of the free-decay duration

The length of the considered signal, i.e. the duration of the free-decay, can also influence the damping estimation. The time of the end of considered free-decay response is called t_{end}. Two approaches have been applied to set rules for the selection of this parameter:

- UPORTO (SSI-COV method): Duration is set as a fixed number of periods of the lowest detected frequency, 10 periods were considered in this case. For example, a 5Hz mode who imply a duration of 2 seconds.

- AVLS (MCO method): t_{end} is calculated thanks the 1s moving-RMS value and corresponds to the point where RMS value dropped 40dB as compared to t_0. This corresponds to a ratio of 100 on amplitude between starting and ending times.

Depending on passages, the t_0 and t_{end} value could be adjusted manually in order to focus damping estimation on certain parts of the signal or avoid disruptive parts.

3.4 Methods comparisons and benchmarking

3.4.1 Foreword

This section aims to compare the performance of the two adopted methods to estimate damping with the free decay period obtained from the time series measured in the tests under railway traffic, namely the MCO, used by AVLS, and the SSI-COV, adopted by UPORTO. The comparison is divided in a series of tests that can be summarized as:

- Artificially generated time series with linear damping (see Section 3.4.2).

- Artificially generated time series with nonlinear damping (see Section 3.4.3)

- Artificially generated time series obtained from train-bridge-interaction (TBI) analysis carried out in a finite element method (FEM) model (see Section 3.4.4).

- Benchmarks performed with real signals obtained in the tests under railway traffic in bridges from different countries (see Section 3.4.5).

3.4.2 Linear damping test cases

The first validation tests involved estimating damping from artificially generated time series with known characteristics. These test cases provided a controlled environment where all input variables, including damping coefficients, were previously defined. By applying the MCO and SSI-COV methods to these synthetic signals, their performance was systematically evaluated by comparing the estimated outputs to the known inputs. This process assessed the tools' accuracy and reliability, confirming their ability to recover the correct damping coefficients under ideal conditions. Additionally, this benchmarking approach enabled a comparative analysis of the two algorithms' behaviour from different partners.

The time series $s(t)$ used in this first test consisted of an artificially generated signal depicting a free-decay vibration response composed of a portion of steady-state regime and a portion of damped decay given by

$$s(t) = \sum_{i=1}^{Ndof} A_i \cdot e^{-\omega_i \cdot \xi_i \cdot t} \cdot \sin\left(\omega_i \cdot \sqrt{1 - \xi_i^2} \cdot t + \phi_i\right) + G(\mu_i = 0, \sigma_i = A_i R_i) \tag{7}$$

where N_{dof} means "number of degrees of freedom", A_i, ω_i, ξ_i and ϕ_i are the relative amplitude, frequency, damping ratio and phase angle of the degree of freedom i, t is the time vector and G represents added gaussian noise, which is dependent on the mean μ_i, standard deviation σ_i and amplitude ratio R_i of the signal relative to degree of freedom i.

For the present validation, 10 test signals have been generated with the parameters described in Table 5 to cover a wide range of scenarios (since frequency is represented in Hz, nomenclature ω has been replaced by f). For all the scenarios, the start of the free decay is $t_0 = 8$s and the end $t_{end} = 20$s

Table 5: Parameters of the artificially generated signals with linear damping.

Case No.	Ndof	f_i (Hz)	A_i (m/s^2)	ξ_i (%)	ϕ_i (rad)	Noise R_i (%)
1	1	$f_1 = 5$	$A_1 = 1$	$\xi_1 = 1$	$\phi_1 = \pi/2$	$R_1 = 0$
2	2	$f_1 = 5$ $f_2 = 1.3f_1$	$A_1 = 1$ $A_2 = A_1$	$\xi_1 = 1$ $\xi_2 = \xi_1$	$\phi_1 = \pi/2$ $\phi_2 = \phi_1 + \pi/2$	$R_1 = 0$ $R_2 = R_1$
3	3	$f_1 = 5$ $f_2 = 1.3f_1$ $f_3 = 1.8f_1$	$A_1 = 1$ $A_2 = A_1$ $A_3 = A_1$	$\xi_1 = 1$ $\xi_2 = \xi_1$ $\xi_3 = \xi_1$	$\phi_1 = \pi/2$ $\phi_2 = \phi_1 + \pi/2$ $\phi_3 = \phi_1 + \pi$	$R_1 = 0$ $R_2 = R_1$ $R_3 = R_1$
4	2	$f_1 = 5$ $f_2 = 1.3f_1$	$A_1 = 1$ $A_2 = A_1/2$	$\xi_1 = 1$ $\xi_2 = \xi_1$	$\phi_1 = \pi/2$ $\phi_2 = \phi_1 + \pi/2$	$R_1 = 0$ $R_2 = R_1$
5	2	$f_1 = 5$ $f_2 = 1.3f_1$	$A_1 = 1$ $A_2 = A_1$	$\xi_1 = 1$ $\xi_2 = \xi_1/2$	$\phi_1 = \pi/2$ $\phi_2 = \phi_1 + \pi/2$	$R_1 = 0$ $R_2 = R_1$
6	2	$f_1 = 5$ $f_2 = 1.3f_1$	$A_1 = 1$ $A_2 = A_1$	$\xi_1 = 1$ $\xi_2 = \xi_1$	$\phi_1 = \pi/2$ $\phi_2 = \phi_1 + \pi/2$	$R_1 = 1$ $R_2 = R_1$
7	2	$f_1 = 10$ $f_2 = 1.3f_1$	$A_1 = 1$ $A_2 = A_1$	$\xi_1 = 1$ $\xi_2 = \xi_1$	$\phi_1 = \pi/2$ $\phi_2 = \phi_1 + \pi/2$	$R_1 = 0$ $R_2 = R_1$
8	2	$f_1 = 5$ $f_2 = 1.3f_1$	$A_1 = 1$ $A_2 = A_1$	$\xi_1 = 2$ $\xi_2 = \xi_1$	$\phi_1 = \pi/2$ $\phi_2 = \phi_1 + \pi/2$	$R_1 = 0$ $R_2 = R_1$
9	2	$f_1 = 5$ $f_2 = 1.3f_1$	$A_1 = 1$ $A_2 = A_1$	$\xi_1 = 4$ $\xi_2 = \xi_1$	$\phi_1 = \pi/2$ $\phi_2 = \phi_1 + \pi/2$	$R_1 = 0$ $R_2 = R_1$
10	2	$f_1 = 5$ $f_2 = 1.3f_1$	$A_1 = 1$ $A_2 = A_1$	$\xi_1 = 1$ $\xi_2 = \xi_1$	$\phi_1 = \pi/2$ $\phi_2 = \phi_1 + \pi/2$	$R_1 = 5$ $R_2 = R_1$

The tests were analysed using both MCO and SSI-COV by using the time series as inputs and checking if the frequency, amplitude and damping matched those used to generate the signals. The results obtained for all the tests are summarized in

Table 6, while comparisons carried out for tests 3, 5 and 10 are exemplified in Figures 15, 16 and 17, respectively. For the SSI-COV, the amplitudes are given in relative percentage between modes, since the imposed amplitude is related to the whole time series, and it may be different in the free decay period. Note that, even for the scenarios with noise (tests 6 and 10), the correspondence between the imposed damping and frequencies and those obtained by both methods is highly consistent, demonstrating their accuracy in this context.
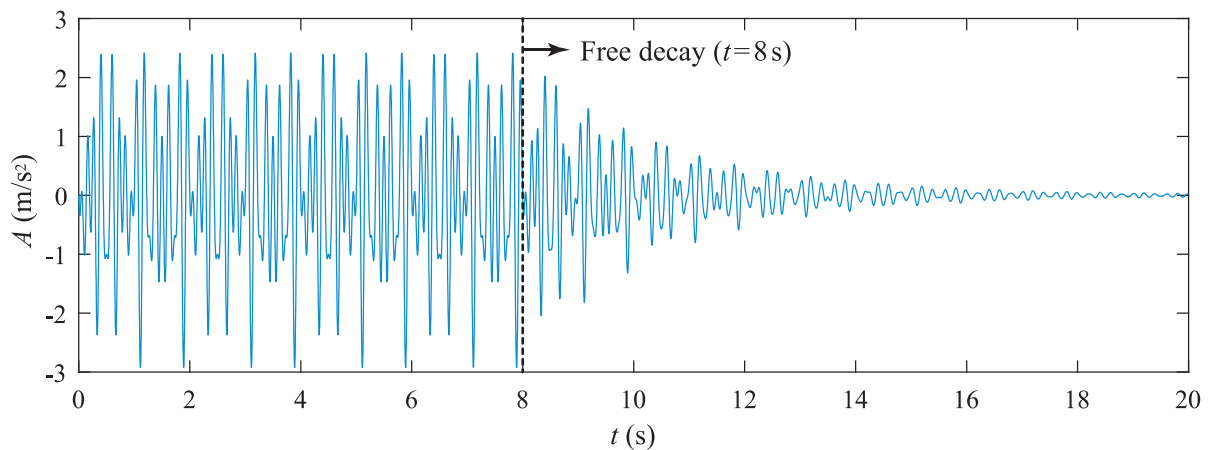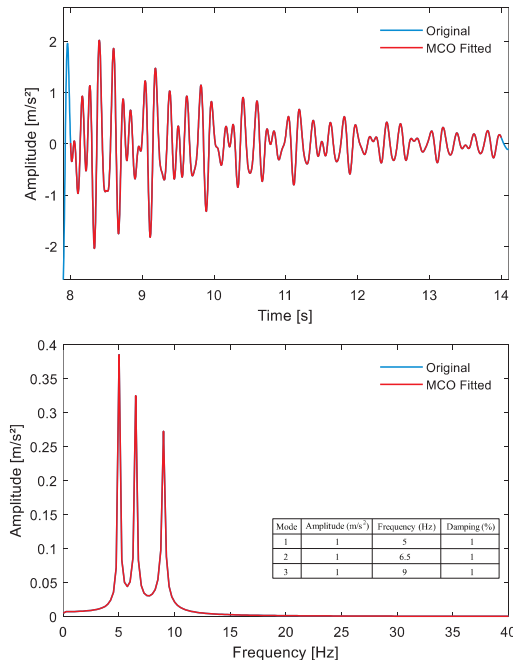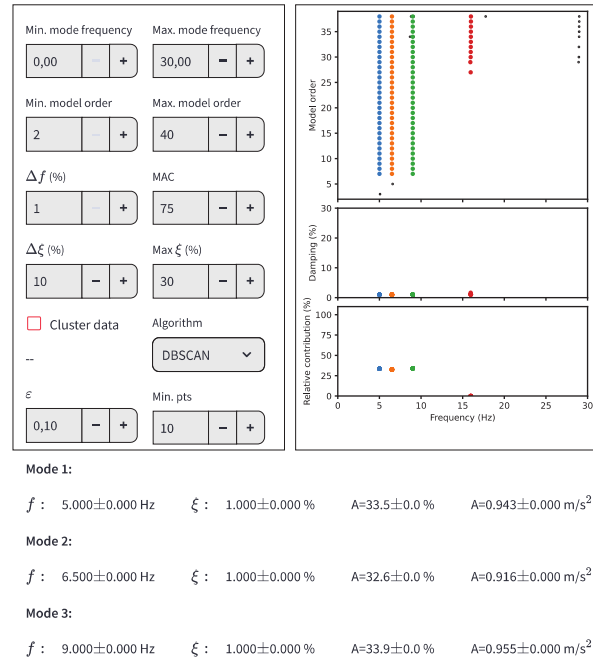
Figure 15: Validation test No. 3: a) artificially generated time series, b) identification with MCO and c) identification with SSI-COV.

a)

b)   *c)*

Figure 16: Validation test No. 5: a) artificially generated time series, b) identification with MCO and c) identification with SSI-COV.
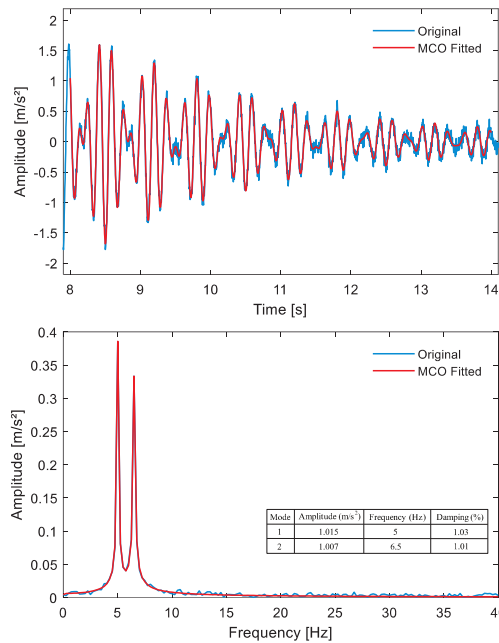
Figure 17: Validation test No. 10: a) artificially generated time series, b) identification with MCO and c) identification with SSI-COV.

Table 6: Results obtained with the two algorithms for the benchmark with linear test cases.

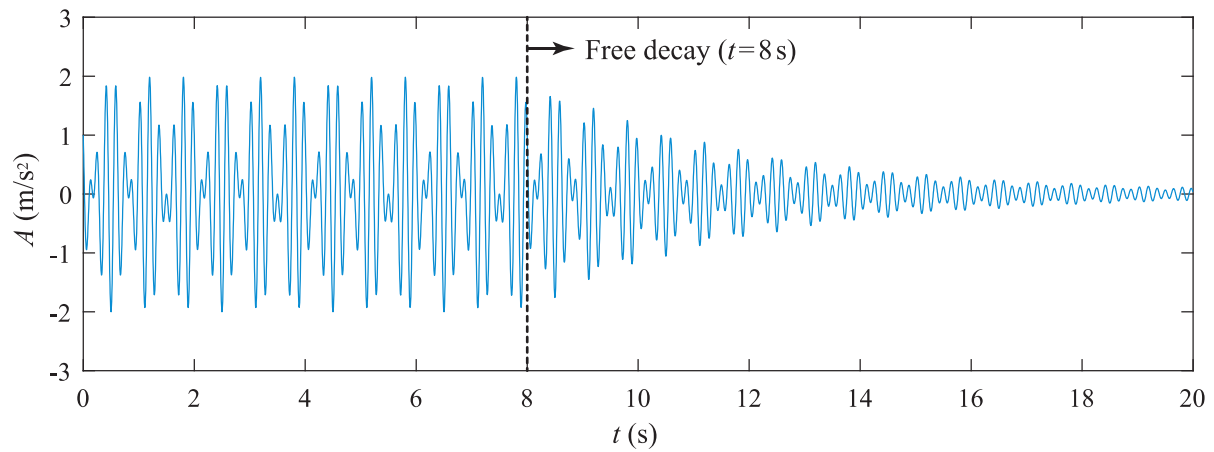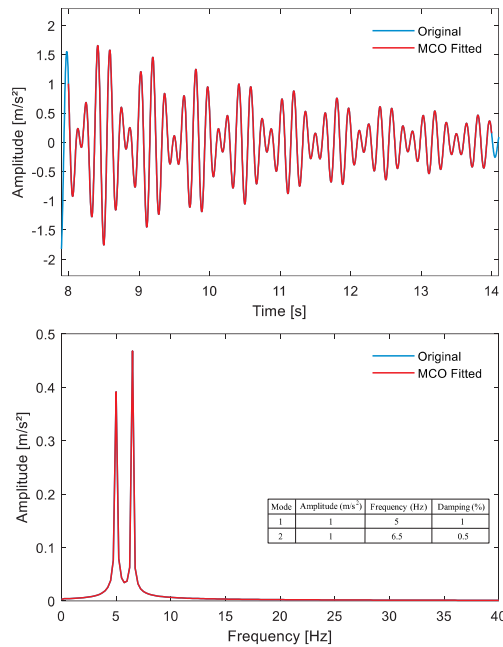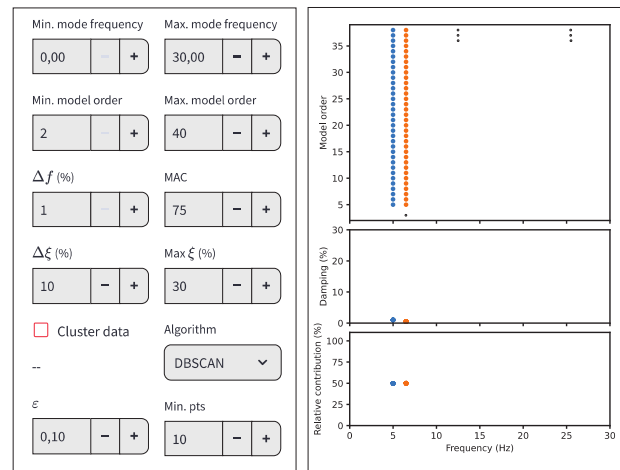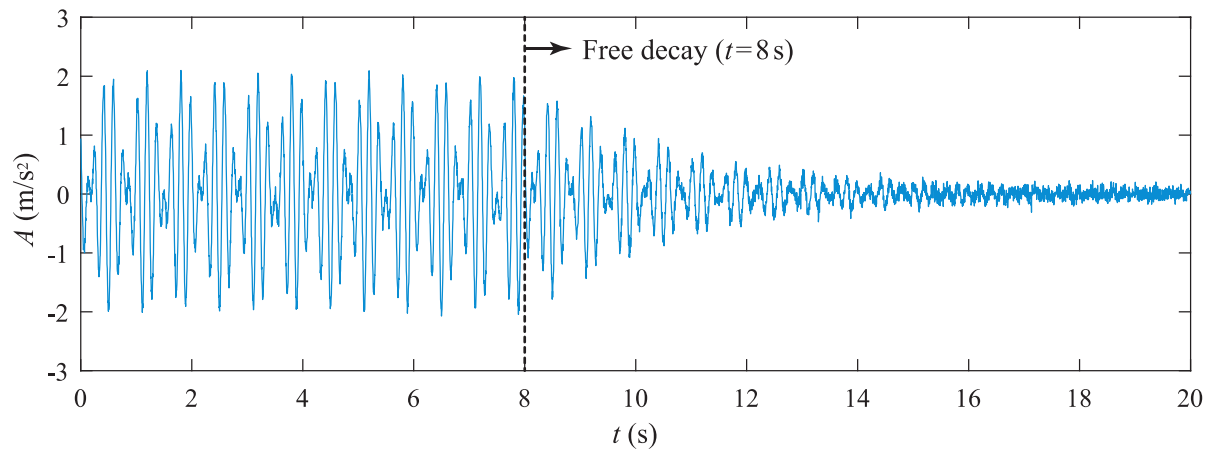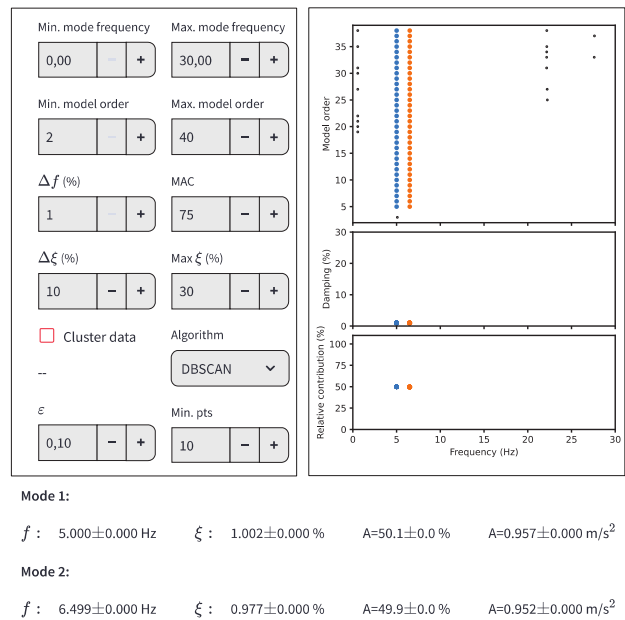| Case No.	Ndof	Noise	Signal properties (f_i (Hz), A_i (m/s² or %), ξ_i (%))		
			Imposed values	*Obtained with MCO*	*Obtained with SSI-COV*
1	1	No	$f_1 = 5$ $A_1 = 1$ $\xi_1 = 1$	$f_1 = 5.00$ $A_1 = 1$ $\xi_1 = 1.0$	$f_1 = 5$ $A_1 = 100\%$ $\xi_1 = 1.0$
2	2	No	$f_1 = 5 \; ; f_2 = 6.5$ $A_1 = A_2 = 1$ $\xi_1 = \xi_2 = 1$	$f_1 = 5.00 \; ; f_2 = 6.50$ $A_1 = A_2 = 1$ $\xi_1 = 1.0 \; ; \xi_2 = 1.0$	$f_1 = 5.00 \; ; f_2 = 6.50$ $A_1 = A_2 = 50\%$ $\xi_1 = 1.0 \; ; \xi_2 = 1.0$
3	3	No	$f_1 = 5 \; ; f_2 = 6.5 \; ;$ $f_3 = 9$ $A_1 = A_2 = A_3 = 1$ $\xi_1 = \xi_2 = \xi_3 = 1$	$f_1 = 5 \; ; f_2 = 6.5 \; ; f_3 = 9$ $A_1 = A_2 = A_3 = 1$ $\xi_1 = 1.0 \; ; \xi_2 = 1.0 ; \xi_3 = 1.0$	$f_1 = 5 \; ; f_2 = 6.5 \; ; f_3 = 9$ $A_1 = 33.5\% ; A_2 = 32.6\% \; ;$ $A_3 = 33.9\%$ $\xi_1 = 1.0 \; ; \xi_2 = 1.0 ; \xi_3 = 1.0$
4	2	No	$f_1 = 5 \; ; f_2 = 6.5$ $A_1 = 1 \; ; A_2 = 0.5$ $\xi_1 = \xi_2 = 1$	$f_1 = 5 \; ; f_2 = 6.5$ $A_1 = 1 \; ; A_2 = 0.5$ $\xi_1 = 1.0 \; ; \xi_2 = 1.0$	$f_1 = 5.00 \; ; f_2 = 6.50$ $A_1 = 67.4\% \; ; A_2 = 32.6\%$ $\xi_1 = 1.0 \; ; \xi_2 = 1.0$
5	2	No	$f_1 = 5 \; ; f_2 = 6.5$ $A_1 = A_2 = 1$ $\xi_1 = 1 \; ; \xi_2 = 0.5$	$f_1 = 5 \; ; f_2 = 6.5$ $A_1 = A_2 = 1$ $\xi_1 = 1 \; ; \xi_2 = 0.5$	$f_1 = 5 \; ; f_2 = 6$ $A_1 = A_2 = 50.0\%$ $\xi_1 = 1.0 \; ; \xi_2 = 0.5$
6	2	Yes (1%)	$f_1 = 5 \; ; f_2 = 6.5$ $A_1 = A_2 = 1$ $\xi_1 = \xi_2 = 1$	$f_1 = 5 \; ; f_2 = 6.5$ $A_1 = 0,999 \; ; A_2 = 1,002$ $\xi_1 = 1.0 \; ; \xi_2 = 1.0$	$f_1 = 5.00 \; ; f_2 = 6.50$ $A_1 = 49.9\% \; ; A_2 = 49.8\%$ $\xi_1 = 1.0 \; ; \xi_2 = 1.0$
7	2	No	$f_1 = 10 \; ; f_2 = 13$ $A_1 = A_2 = 1$ $\xi_1 = \xi_2 = 1$	$f_1 = 10 \; ; f_2 = 13$ $A_1 = A_2 = 1$ $\xi_1 = 1.0 \; ; \xi_2 = 1.0$	$f_1 = 10 \; ; f_2 = 13$ $A_1 = A_2 = 50.0\%$ $\xi_1 = 1.0 \; ; \xi_2 = 1.0$
8	2	No	$f_1 = 5 \; ; f_2 = 6.5$ $A_1 = A_2 = 1$ $\xi_1 = \xi_2 = 2$	$f_1 = 5 \; ; f_2 = 6.5$ $A_1 = A_2 = 1$ $\xi_1 = 2.0 \; ; \xi_2 = 2.0$	$f_1 = 5 \; ; f_2 = 6.5$ $A_1 = A_2 = 50.0\%$ $\xi_1 = 2.0 \; ; \xi_2 = 2.0$
9	2	No	$f_1 = 5 \; ; f_2 = 6.5$ $A_1 = A_2 = 1$ $\xi_1 = \xi_2 = 4$	$f_1 = 5 \; ; f_2 = 6.5$ $A_1 = A_2 = 1$ $\xi_1 = 4.0 \; ; \xi_2 = 4.0$	$f_1 = 5 \; ; f_2 = 6.5$ $A_1 = A_2 = 50.0\%$ $\xi_1 = 4.0 \; ; \xi_2 = 4.0$
10	2	Yes (5%)	$f_1 = 5 \; ; f_2 = 6.5$ $A_1 = A_2 = 1$ $\xi_1 = \xi_2 = 1$	$f_1 = 5 \; ; f_2 = 6.5$ $A_1 = 1,015 \; ; A_2 = 1,007$ $\xi_1 = 1.03 \; ; \xi_2 = 1.01$	$f_1 = 5 \; ; f_2 = 6.5$ $A_1 = 50.1\% \; ; A_2 = 49.9\%$ $\xi_1 = 1.00 \; ; \xi_2 = 0.98$

3.4.3 *Nonlinear viscous damping test cases*

It has been observed that real signals can present a nonlinear behaviour during a free-decay response with, for example, a non-exponential decrease of amplitude, which would imply a decreasing damping ratio over time and/or amplitude. There can also be an evolution of the natural frequencies of the bridge during the free-decay. This has been observed on light bridges, for instance, when the mass of the train is not negligible as compared to the bridge. Nonlinear test cases have then been created to evaluate the behaviour of damping estimation algorithms in such situation, since the methods adopted in this work are based on the linear

hypothesis. The goal is to identify whether the algorithms tend to obtain a lower boundary, a higher one or even an average estimate of damping.

In the present test case, the nonlinear free-decay time signal $s(t)$ is written in a similar way as in the previous test, but as a single degree of freedom response as

$$s(t) = A \cdot e^{-\omega \cdot \xi \cdot t} \cdot \sin\left(\omega . \sqrt{1 - \xi^2} \cdot t + \phi\right) + G(\mu = 0, \sigma = A \cdot R) \tag{8}$$

where the nonlinear damping ξ is studied with a model of viscous damping evolving as a first-order function of time given by

$$\xi = \alpha \cdot t + \beta \tag{9}$$

where t, A, ω, ϕ, G, R, μ and σ have been previously defined in Section 3.4.2 in relation to Equation (7), α and β are the slope and offset parameters, respectively, for defining the time-dependent nonlinear damping.

For the present validation, 4 test signals were generated with different damping decreasing rates (faster or slower decrease) and starting values as listed in Table 7 (since frequency is represented in Hz, nomenclature ω has been replaced by f). Figure 18 show the time signal and damping laws for the four test cases 1–2 and 3–4, respectively.

Table 7: Parameters of the artificially generated signals with nonlinear viscous damping.

Case No.	f (Hz)	A (m/s²)	ξ (%)	φ (rad)	R (%)	No. of cycles during decrease
1			$\xi = [6\% \dashrightarrow 3\%] \searrow$			20
2	5	1	$\xi = [6\% \dashrightarrow 3\%] \searrow$	0	0	75
3			$\xi = [3\% \dashrightarrow 1\%] \searrow$			30
4			$\xi = [3\% \dashrightarrow 1\%] \searrow$			75

a)   b)

Figure 18: Time series for the nonlinear test cases with damping decrease over time [6% to 3%]: a) test no. 1 with fast damping decrease rate and b) test no. 2 with slow damping decrease rate.
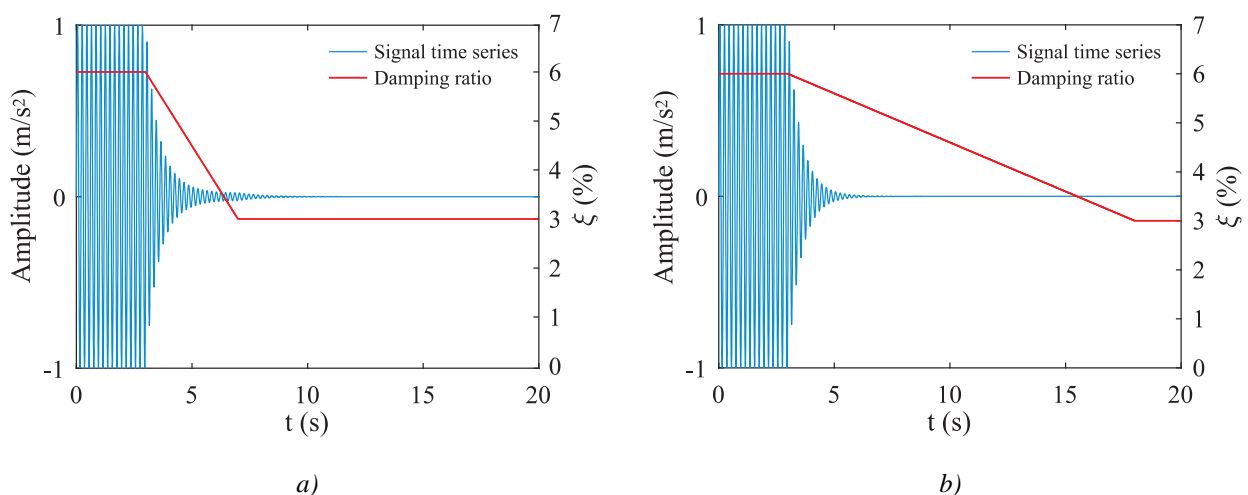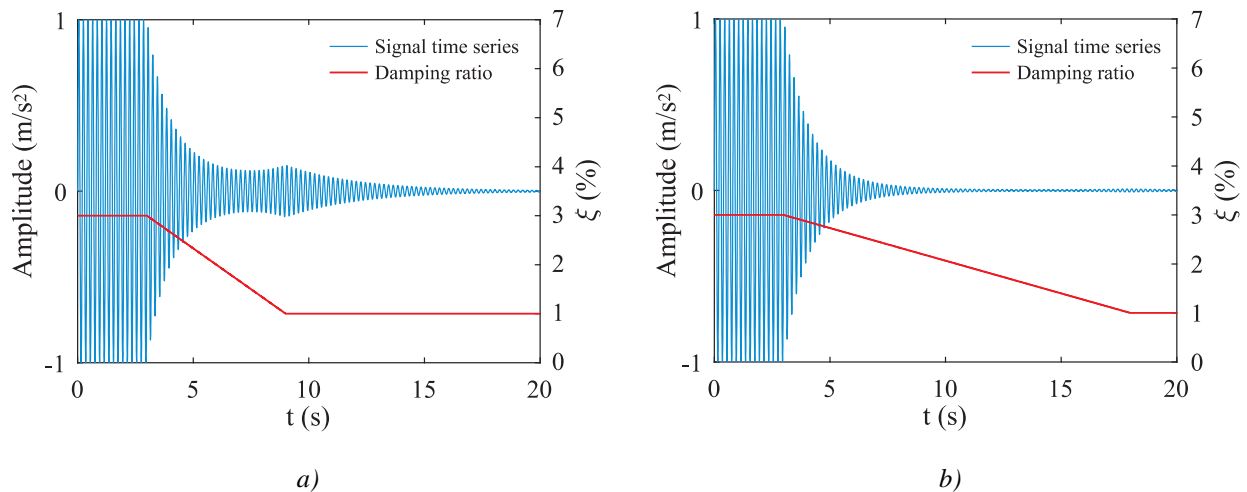
a)

b)

Figure 19: Time series for the nonlinear test cases with damping decrease over time [3% to 1%]: a) test no. 3 with fast damping decrease rate and b) test no. 4 with slow damping decrease rate.

Out of the four test signals, 5 subtests x.1 to x.2, where "*x*" is the test case, were defined depending on the portion of the signal studied. With different starting t_0 and ending t_{end} times, each subtest is cantered on a different damping ratio range. Table 8 lists all the subcases, their time parameters, the mean damping ratio on their range and the estimations by both methods.

Table 8: Results obtained with the two algorithms for the benchmark with nonlinear viscous test cases.

Test case ID	t_0 (s)	t_{end} (s)	Theoretical mean damping (%)	MCO damping (%)	SSI-COV damping (%)
1.1	3	4	5.63	5.32	3.80
1.2	3	5	5.25	5.07	5.08
1.3	3	6	4.88	4.95	4.97
1.4	3	7	4.50	4.77	4.98
1.5	5	7	3.75	1.68	3.37
2.1	3	6.75	5.63	5.71	5.70
2.2	3	10.5	5.25	5.70	6.01
2.3	3	14.25	4.88	5.70	5.76
2.4	3	18	4.50	5.70	6.08
2.5	4	11.5	5.05	5.27	5.55
3.1	3	4.5	2.75	2.58	2.31
3.2	3	6	2.50	2.26	2.91
3.3	3	7.5	2.25	2.02	3.08
3.4	3	9	2.00	1.91	3.24
3.5	4	7	2.17	1.50	2.22
4.1	3	6.75	2.75	2.68	3.30
4.2	3	10.5	2.50	2.66	2.89
4.3	3	14.25	2.25	2.65	2.97
4.4	3	18	2.00	2.65	2.81
4.5	4	11.5	2.37	2.36	2.74

Finally, estimations are compared to the theoretical mean damping ratio by calculating the gap $\xi_{estimated}$ - $\xi_{theoretical\_mean}$. Figure 20 summarizes these results for both methods. The closer the values are to zero, the closer the damping obtained by each method is to the average damping ratio. A clear trend of overestimating the theoretical mean damping is observed, as most of the results from both methods show positive gaps, particularly for the SSI-COV method. It is also noticeable that the longer the free-decay length considered (from subset x.1 to x.4), the greater the estimated damping value is compared to the theoretical mean. In this context of decreasing damping, both methods seem more sensitive to the initial cycles of oscillation, which exhibit higher damping values. Hence, the two methods are generally consistent with one another with less than 0.5 percentage-point of difference in their estimations. Some larger scatter up to 2%-point can be observed in cases 1.1, 1.5, 3.3 and 3.4 despite showing no specific feature linking them.
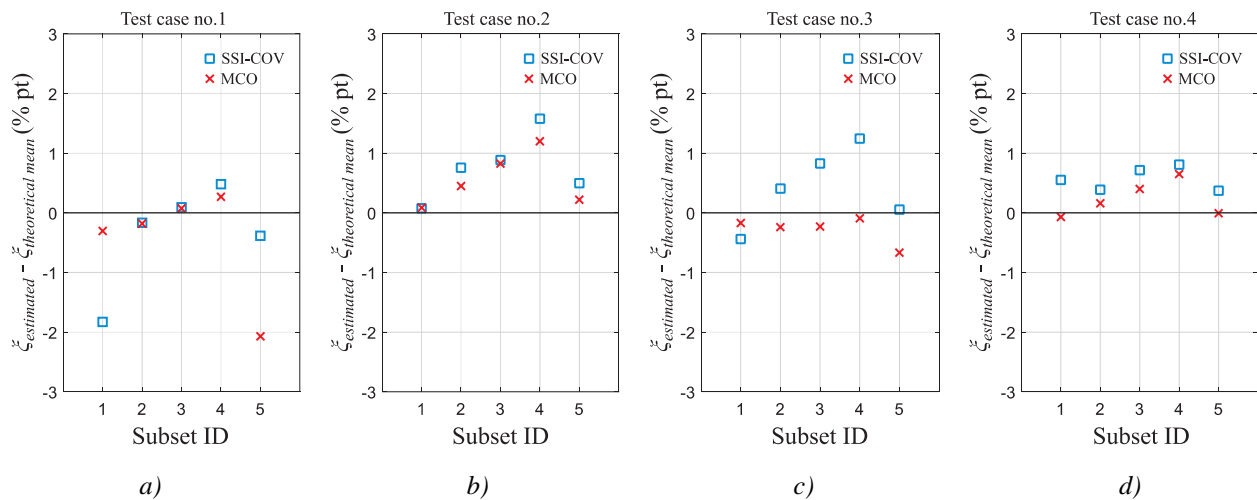

Figure 20: Comparisons of SSI-COV and MCO damping estimations referenced to the theoretical mean damping over the studied signal: test case a) no.1, b) no.2, c) no.3 and d) no.4.

3.4.4 FEM test case

Before advancing to the benchmarks in real signals from the database, a final comparison based on numerical results obtained in a dynamic analysis performed with the FEM has been carried. The test case consisted of simulating responses from one of the bridges from the database, the Cascalheira bridge in Portugal, through dynamic analysis using a train-bridge-interaction (TBI) dynamic analysis.

3.4.4.1 Bridge model

The Cascalheira bridge (see Figure 21a) is a 11 m length short-span filler beam bridge located at km 100.269 of the Northern Railway Line in Portugal that establishes the connection between Lisbon and Porto. A complex 3D model of the bridge (see Figure 21b), including the track, was developed in the FEM software ANSYS® (2019). To better simulate the transition zone in the abutments, an extension of the track was also modelled. Moreover, different materials were used to model the ballast on the longitudinal and transversal joints to allow the study of the degradation of the track in these regions. Regarding the type of elements adopted to develop the model, shell elements (SHELL63) were used to represent the concrete slabs, cantilevers and the retaining walls, while the embedded steel girders and the rails were modelled with three-dimensional beam elements capable of simulating eccentricities between the modelled position and the real position (BEAM44). Concerning the track, solid elements were used (SOLID45) for the ballast, as well as for the sleepers and rail pads. The non-structural elements, namely the restraining wall, were modelled with concentrated mass elements (MASS21), while the bearing supports were simulated through spring-dashpot elements

(COMBIN14) to take into consideration the vertical and longitudinal stiffness of the pot bearings. Finally, rigid beam (MPC184) elements were used to connect the deck to the ballast, and for the connection between the slabs of the deck to the cantilevers and retaining walls. The numerical model had a total of 13,266 finite elements, which contained 15,532 nodes and was numerically calibrated to match the experimental mode shapes and frequencies, as well as the deck's acceleration response under the passage of the Portuguese train Alfa Pendular. Details about the model, as well as its calibration can be found in Saramago et al. (2020).
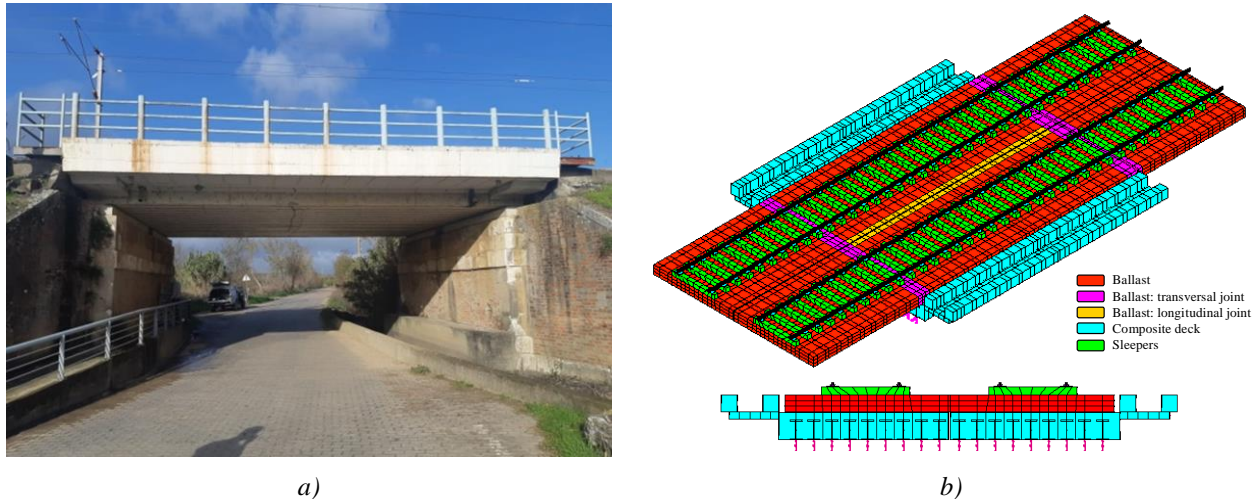

a)   *b)*

Figure 21: Cascalheira bridge: a) global view and b) numerical FEM model.

The numerical modal shapes of the first two modes of vibration (vertical bending and torsion) and its correspondent natural frequencies and damping coefficients imposed to the model according to the lower limit bound for this type of bridge stipulated in EN 1991-2 (2023), $\xi = 2.12\%$, are depicted in Figure 22.

$f_1 = 10.67$ Hz
$\xi_1 = 2.12\%$

$f_2 = 11.99$ Hz
$\xi_2 = 2.12\%$

a)   *b)*
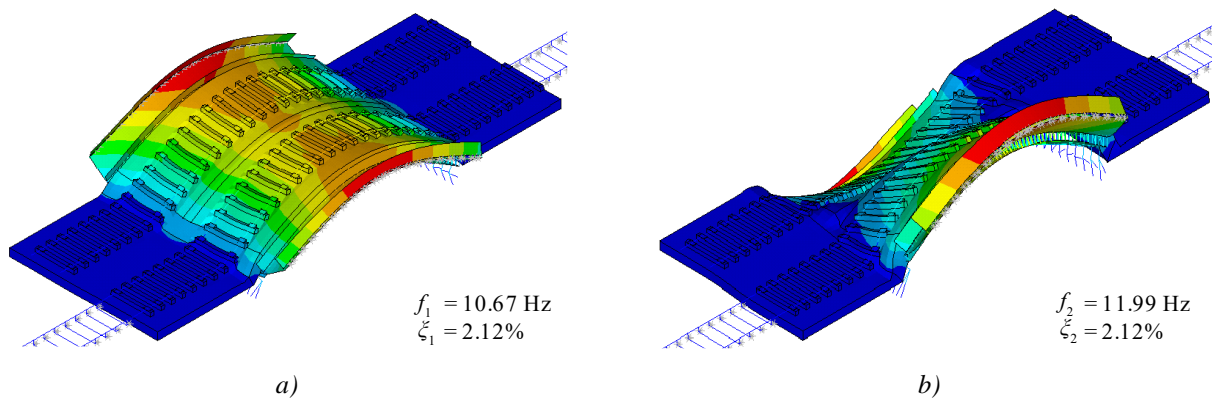
Figure 22: Numerical mode shapes of the Cascalheira bridge: a) bending and b) torsion.

3.4.4.2   Train model

As mentioned before, to take into consideration not only the dynamic effects imposed to the bridge by the moving loads corresponding to the train axle load, a TBI dynamic analysis has been carried out to also consider the effects of track irregularities, thus leading to more realistic and broader range of scenarios. Nevertheless, this type of analysis requires not only the bridge structural model, but also the train model as an independent structure that interacts with the former.

In this work, the Alfa Pendular train was modelled using ANSYS® (2019) through a multibody formulation. Figure 23 illustrates the dynamic model of one of its cars, including the location of the suspensions and centres

of gravity of the different components. In this figure, *k*, *c*, *m* and *I* represent stiffness, damping, mass and rotational inertia, respectively; *a*, *b* and *h* refer to the longitudinal, transversal and vertical distances, respectively; *s* represents the gauge and R_0 represents the nominal rolling radius. The subscripts *cb*, *b* and *w* refer to the carbody, bogie and wheelset, respectively. Concerning the suspensions, the subscripts 1 and 2 denote the primary and secondary ones, respectively, while the subscripts *x*, *y* and *z* designate the longitudinal, transversal and vertical directions, respectively. All the aforementioned geometrical and mechanical properties of the vehicle can be found in Saramago et al. (2020).
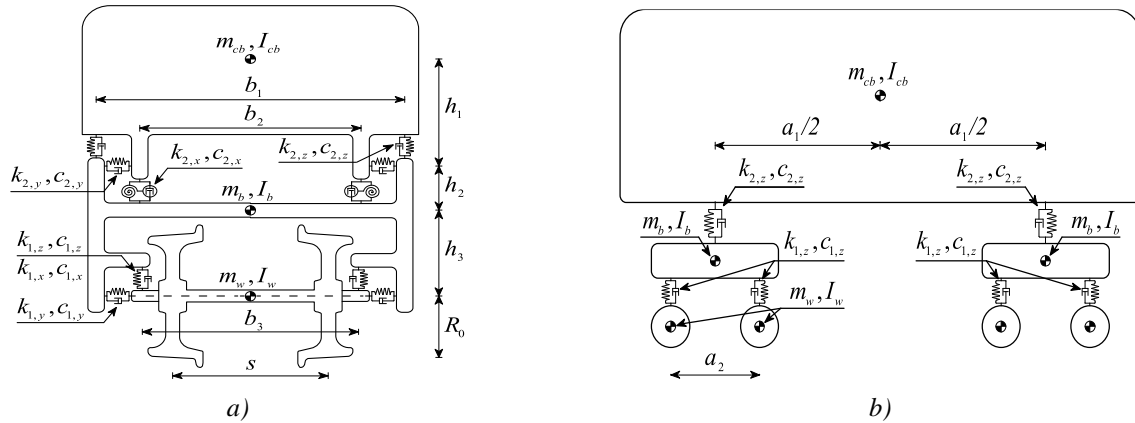

Figure 23: Dynamic model scheme of an Alfa Pendular's car: a) transversal and b) lateral views.

3.4.4.3   Dynamic analyses with TBI methodology

The dynamic analyses performed in the present study have been carried out with a TBI tool named "*VSI— Vehicle Structure Interaction Analysis*", developed and validated by Montenegro et al. (2015) and Montenegro and Calçada (2023) and used in several distinct applications (Ferreira et al., 2024; Montenegro et al., 2016; Montenegro et al., 2022), in which the train is coupled to the bridge through a wheel-rail contact model that accounts for the geometrical properties of both surfaces in contact, as well as the normal and tangential contact forces that arise in their interface.

For the present study, the Alfa Pendular train crossed the Cascalheira bridge under different speed and track condition scenarios. The scenarios consisted of two speeds, 135 km/h and 165 km/h, and four different types of vertical irregularities measured by the inspection vehicle EM120 from the Portuguese Infrastructure Manager, Infraestruturas de Portugal, corresponding to measurements carried out between 2018 and 2020, as depicted in Figure 8 (location of the bridge highlighted by the grey area), totalizing 8 tests.
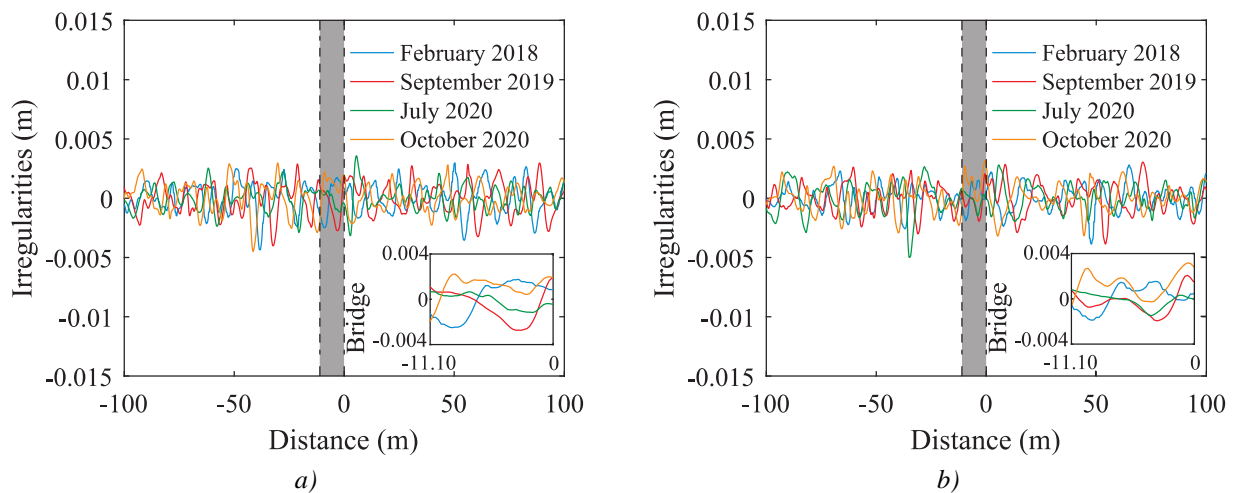

Figure 24: Vertical irregularities used in the dynamic analyses: a) left rail and b) right rail.

Given the nonlinear nature of the TBI tool due to the wheel-rail contact problem, VSI solves the system of dynamic equations through direct integration, thus invalidating the option of allocate individual damping ratio for each structural mode/frequency. Hence, for these TBI analysis, damping has been considered through the Rayleigh proportional matrix, as shown in Figure 25. A known target damping ratio of 2.12 % stipulated in EN 1991-2 (2023) has been set for the two global modes depicted in Figure 22 with the objective of benchmarking the two damping estimation methods used in this work. The benchmark aimed to evaluate whether these methods could distinguish the two modes, identify their frequencies, and accurately estimate the predetermined damping.
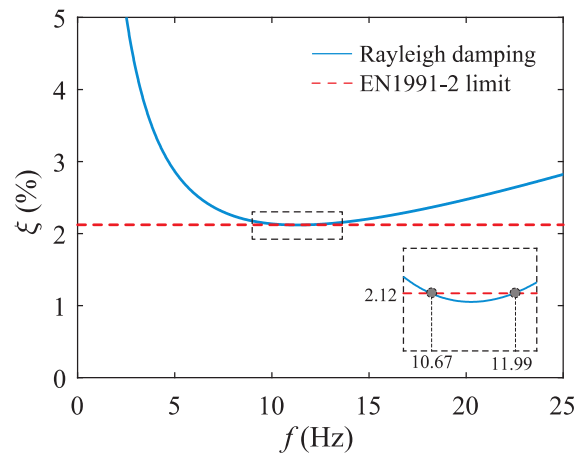
Figure 25: Rayleigh damping curve applied in the model for the benchmark fixing the target damping in the first global bending and torsional modes.

3.4.4.4 Benchmark results

The results obtained in this benchmark are presented in Table 9, where it is possible to compare the frequencies from the FEM model and the respective damping values imposed through Rayleigh damping with the estimations obtained by both methods (modes 1 and 2 correspond to the bending and torsional modes, respectively). To better visualize this comparison, the results are also presented in Figure 26. It can be observed that, with exception of the test case no.4, in which MCO significantly overestimated the damping of the bending mode (ξ_{MCO} = 5.17 % much higher than the target damping value of ξ_{FEM} = 2.12 %), the other estimations using both methods have a good agreement with the target damping imposed to the FEM model.

Figure 26: FEM benchmark damping results: a) mode 1 – bending, b) mode 2 - torsion.

Table 9: Results obtained with the two algorithms for the benchmark with FEM test cases.

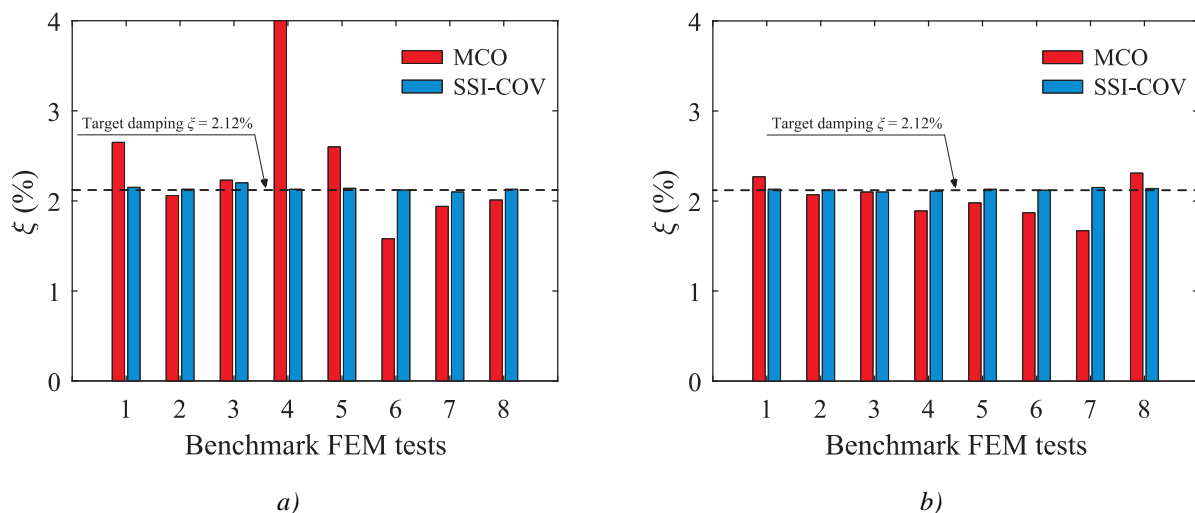| Test case ID	Irregularity	Train speed (km/h)	Mode	FEM		MCO		SSI-COV	
				f (Hz)	ξ (%)	f (Hz)	ξ (%)	f (Hz)	ξ (%)
1	Feb-18	135	1	10.67	2.12	10.66	2.15	10.66	2.65
			2	11.99		11.98	2.13	11.96	2.27
2	Sep-19		1	10.67	2.12	10.67	2.13	10.66	2.06
			2	11.99		11.98	2.12	11.98	2.07
3	Jul-20		1	10.67	2.12	10.66	2.20	10.66	2.23
			2	11.99		11.98	2.10	11.98	2.10
4	Oct-20		1	10.67	2.12	10.67	2.13	10.49	5.17
			2	11.99		11.98	2.11	11.96	1.89
5	Feb-18	165	1	10.67	2.12	10.67	2.14	10.59	2.60
			2	11.99		11.99	2.13	11.99	1.98
6	Sep-19		1	10.67	2.12	10.67	2.12	10.55	1.58
			2	11.99		11.98	2.12	12.04	1.87
7	Jul-20		1	10.67	2.12	10.67	2.10	10.62	1.94
			2	11.99		11.99	2.15	12.04	1.67
8	Oct-20		1	10.67	2.12	10.67	2.13	10.67	2.01
			2	11.99		11.98	2.14	11.96	2.31

3.4.5 Real signals test cases

While the test cases included artificially added noise to simulate real-world conditions, actual field signals present additional complexities. Real-world signals are not only affected by noise but also exhibit distorted decay patterns due to nonlinearities, transient phenomena, and other unpredictable factors. These challenges can significantly impact the accuracy of damping coefficient estimations, highlighting the necessity of controlled test cases. However, such cases alone are not entirely sufficient for validating the tools' performance in practical applications.

To further assess reliability, several passages from the database were selected to compare the SSI-COV and MCO methods using the same input data. A passage over the following bridges was chosen for benchmarking:

- Signals involving multiple low-damped modes: Guadiana bridge in Spain (Section 3.4.5.1).

- Signals involving high damping ratios: Braço do Cortiço bridge in Portugal and Ebr ü.Wenderterstraße and EÜ Str.Vinzelb.-Käth bridges in Germany (Section 3.4.5.2)

- Signal showing non-linear behaviour: Sermaize-les-Bains bridge in France (Section 3.4.5.3).

- Study of the mode amplitude estimation: Algodor bridge in Spain, Malay-le-Petit and Vinzelles bridges in France and Kerpen bridge in Germany (Section 3.4.5.4).

- Blind benchmark with non-fixed time parameters: Savigny-le-Temple (830000_036+790) bridge in France (Section 3.4.5.5

Finally, a synthesis of the results obtained in the present benchmark with real signal test cases is presented in Section 3.4.5.6.

3.4.5.1 Benchmark involving multiple low-damped modes

The Guadiana bridge in Spain (see Annex B) is a double-track bridge with two independent decks that share a ballast layer. The bridge is composed of two 11.93 m spans, where the concrete slabs rest on pre-stressed concrete girders. Galvín et al. (2021) identified five mode shapes below 30 Hz including bending and torsion modes.

The dynamic response after train passage exhibits high contribution from several of these modes. Hence, one train passage has been selected as a benchmark for damping estimation methods in this configuration. Five test cases were tested on this signal (Guadiana 01, channel 1) with different couples of starting and ending times (t_0 and t_{end}) as pictured in Figure 27. An example of results obtained by both methods on the test case 2 is presented in Figure 28. It can be noticed for instance that despite an accurate fit on the time signal, the MCO method does not show a good agreement on the first mode in the frequency domain which can lead to an underestimation of the damping ratio. In this example, the mode 1 damping ratio from MCO is indeed 0.5 %pt lower than the one estimated by SSI-COV, nevertheless a similar gap can be observed in reverse order on mode 2.

All damping ratio and frequency estimations are summed up in Table 10, where it is possible to observe that the frequency estimates generally show good agreement between the two methods. Regarding test case 3, MCO method could not get satisfactory results, hence the lack of data on this entry. The MCO method can lead to unrealistic negative damping values on modes with a low contribution despite an accurate fit on main modes. On main modes, in this case modes no.2 and no.3, both methods agree with a gap near 0.5 %pt on test cases 1 and 2. Test cases 3, 4 and 5 start later on the decay response and present a weak mitigation over time leading to low damping values.

A graphical overview of all results and their discussions can be found in Section 3.4.5.6.
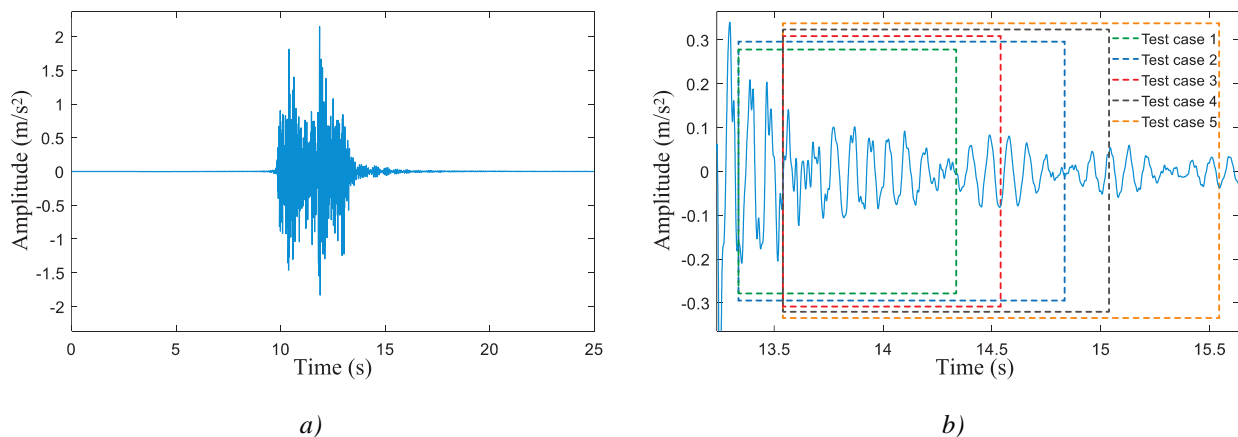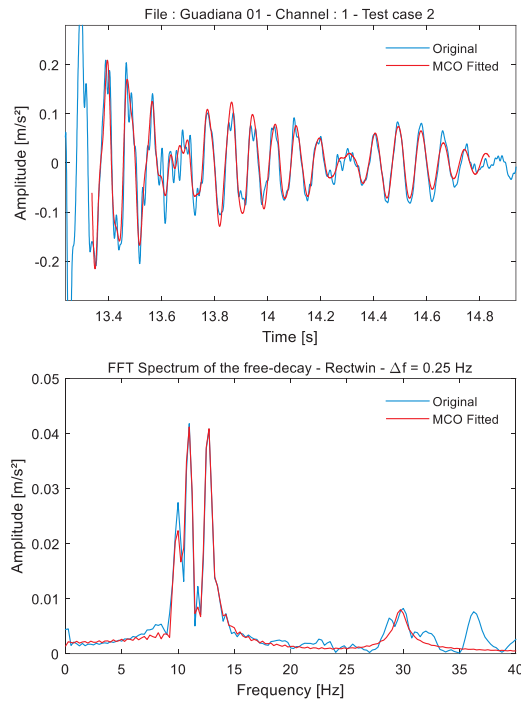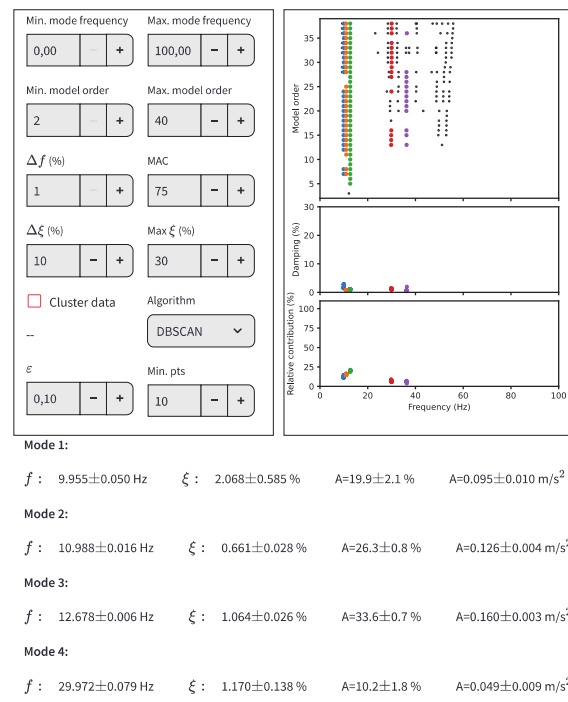

a)   *b)*

Figure 27: Response of the Guadiana bridge test case: a) whole time signal and b) zoom on free decay.

a)   *b)*

Figure 28: Guadiana test case no.2: identification with a) MCO and with b) SSI-COV.

Table 10: List of Guadiana test cases and SSI-COV and MCO estimates of damping and frequency.

Test case ID	t_0 (s)	t_{end} (s)	Mode	SSI-COV ξ_i (%)	MCO ξ_i (%)	SSI-COV f_i (Hz)	MCO f_i (Hz)
Guadiana 1	13.34	14.34	1	0.47	-0.14	9.72	9.57
			2	2.02	2.50	11.01	11.00
			3	1.20	1.44	12.65	12.63
			4	0.99	0.91	29.85	29.90
Guadiana 2	13.34	14.84	1	2.07	1.29	9.96	9.69
			2	0.66	1.18	10.99	11.04
			3	1.06	1.36	12.68	12.66
			4	1.17	1.67	29.97	29.74
Guadiana 3	13.54	14.54	1	2.47	-	9.73	-
			2	0.25	-	11.03	-
			3	0.96	-	12.66	-
			4	2.38	-	28.07	-
Guadiana 4	13.54	15.04	1	2.45	3.60	9.89	9.67
			2	0.45	-3.10^{-7}	10.94	10.83
			3	1.10	0.88	12.66	12.58
			4	1.90	3.81	27.92	29.91
Guadiana 5	13.54	15.54	1	3.17	3.64	9.89	9.69
			2	0.61	0.13	10.86	10.84
			3	0.97	0.86	12.67	12.63
			4	1.08	4.95	29.90	33.14

3.4.5.2 Benchmark involving high damping ratios

Estimating high damping ratios is more complex due to fast amplitude changes over a short period of time, especially if several modes are contributing. Signals from three bridges displaying such dynamic behaviour have been studied as benchmarks. A graphical overview of all results and their discussions can be found in Section 3.4.5.6.

a) *Braço do Cortiço bridge (Portugal)*

Braço do Cortiço in Portugal is a short filler beam bridge with a span of 7m (see Annex B). Each of the two railways is supported by an independent deck. The bridge is weakly resonant, meaning that after the train passes, the vibration response is rapidly damped, indicating a high damping ratio.

One train passage has been selected as a benchmark for damping estimation methods. Three test cases were selected on this signal (Braço do Cortiço 25, channel 1) with different couples of starting and ending times (t_0 and t_{end}) as pictured in Figure 29.

An example of results obtained by both methods on the test case no.1 is presented in Figure 30. The responses present three modes at 15.7 Hz, 21 Hz and 59 Hz. In this case, the considered response is 0.3 seconds short, causing ripples on the FFT.

All damping ratio and frequency estimations are summed up in Table 11. The two methods display consistent results on modes 1 and 3 (on test cases 1 and 2) and more scattering on mode 2, which weakly contributes to the response. Test case 3 has a longer duration than the others and in this case SSI-COV estimates a lower damping ratio than previously and has compared to MCO.
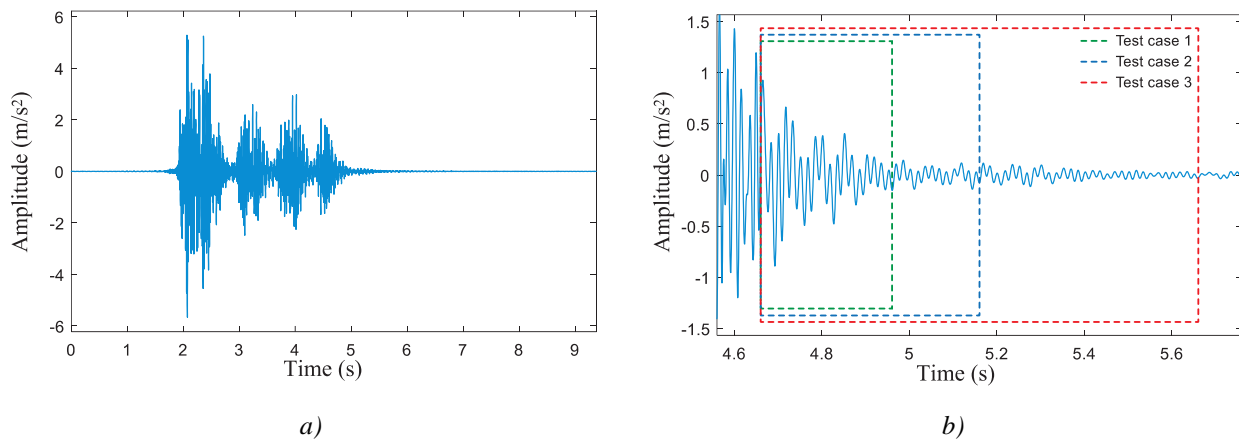

a)   *b)*

Figure 29: Response of the Braço do Cortiço bridge test case: a) whole time signal and b) zoom on free decay.
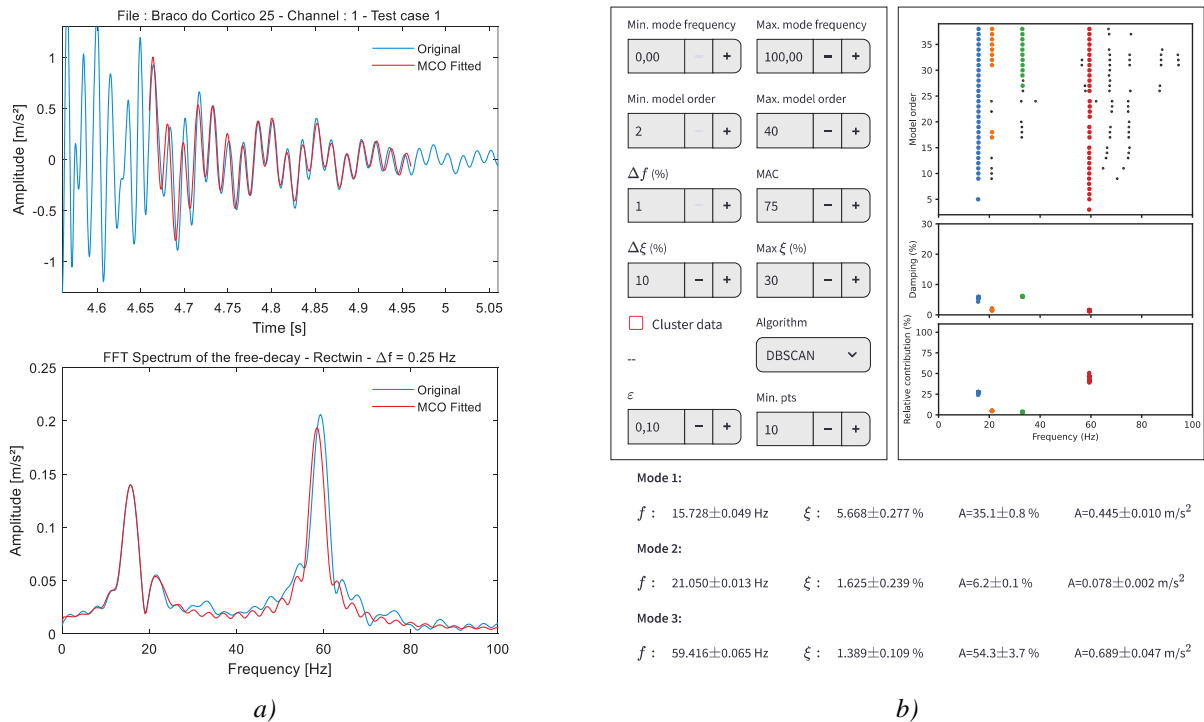
a) *b)*

Figure 30: Braço do Cortiço test case no.1: identification with a) MCO and with b) SSI-COV.

Table 11: List of Braço do Cortiço test cases and SSI-COV and MCO estimates of damping and frequency.

Test case ID	t_0 (s)	t_{end} (s)	Mode	SSI-COV ξ_i (%)	MCO ξ_i (%)	SSI-COV f_i (Hz)	MCO f_i (Hz)
Braco do Cortiço 1	4.66	4.96	1	5.67	6.20	15.73	15.76
			2	1.63	3.52	21.05	20.86
			3	1.39	1.47	59.42	58.50
Braco do Cortiço 2	4.66	5.16	1	5.89	5.79	15.78	15.73
			2	2.97	4.45	20.99	21.26
			3	1.39	1.81	59.55	58.57
Braco do Cortiço 3	4.66	5.66	1	3.96	5.41	15.75	15.74
			2	2.40	4.77	22.22	21.28
			1	5.65	6.20	15.73	15.76

b)   Ebr ü.Wenderterstraße and EÜ Str.Vinzelb.-Käth bridges in Germany

Ebr ü.Wenderterstraße bridge in Germany (see Annex B) is a concrete slab beam bridge with a span of 22.6m. Each of the two railways is supported by an independent deck. One train passage has been selected (Sarsted 01, channel 2) and 4 test cases with different couples of starting and ending times (t_0 and t_{end}) as pictured in Figure 31. EÜ Str.Vinzelb.-Käth bridge in Germany (see Annex B) is a filler beam bridge with a span of 12.86m. Each of the two railways is supported by an independent deck. One train passage has been selected (Vinzelberg 03, channel 2) and 3 test cases as pictured in Figure 34.

An example of results obtained by both methods on the Ebr ü.Wenderterstraße bridge (test case 2) is presented in Figure 33, while an example from EÜ Str.Vinzelb.-Käth bridge (test case 2) is presented in Figure 34. All damping ratio and frequency estimations are summarized in Table 12. By observing the results, it is possible to conclude that damping estimations of both models are in match with a typical margin of 0.5

%pt except for Ebr ü.Wenderterstraße test case no.3 and EÜ Str.Vinzelb.-Käth test no.1. In this latter cases, MCO result are inconsistent with the other test cases, revealing a possibly spurious result.
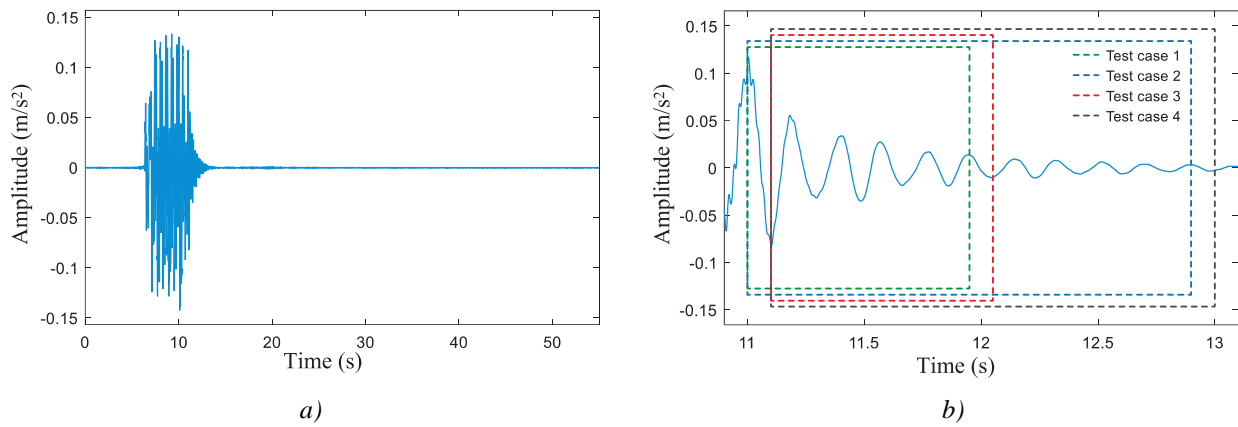

Figure 31: Response of the Ebr ü.Wenderterstraße bridge test case: a) whole time signal and b) zoom on free decay.
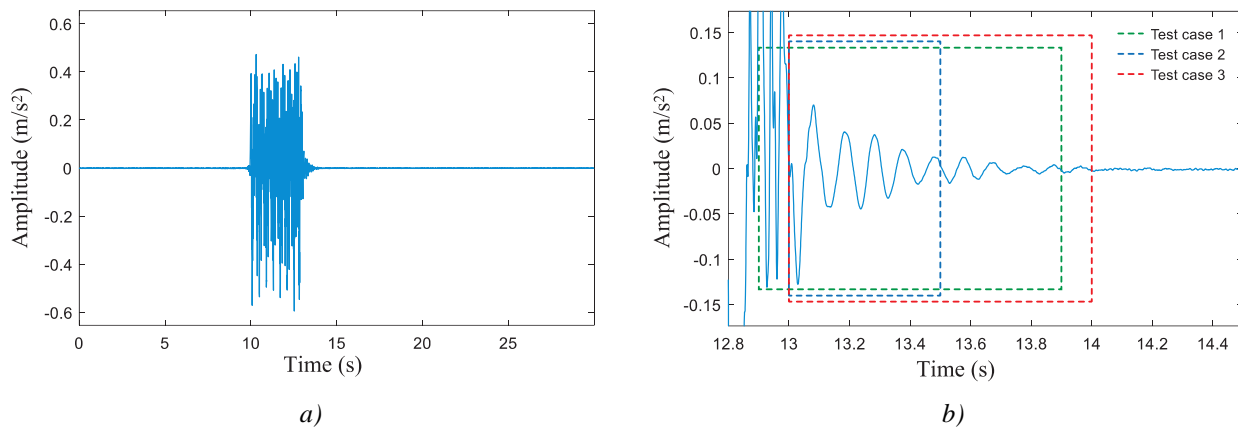

Figure 32: Response of the EÜ Str.Vinzelb.-Käth bridge test case: a) whole time signal and b) zoom on free decay.
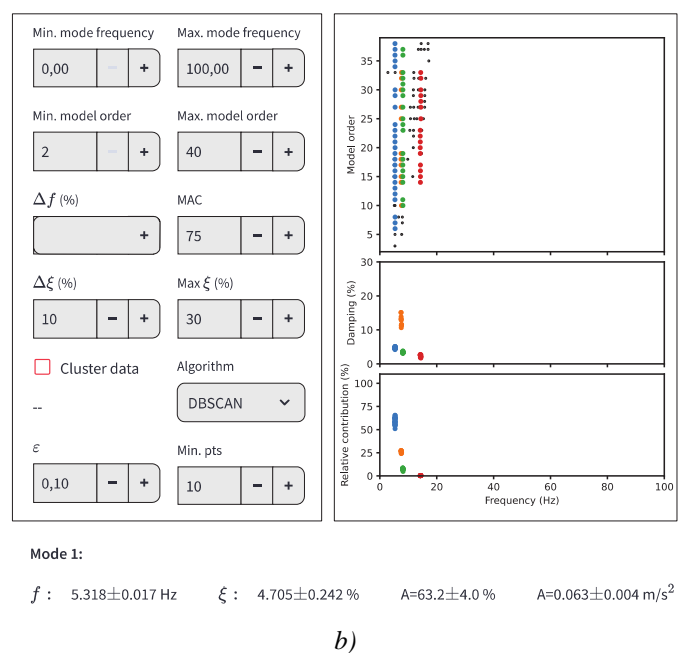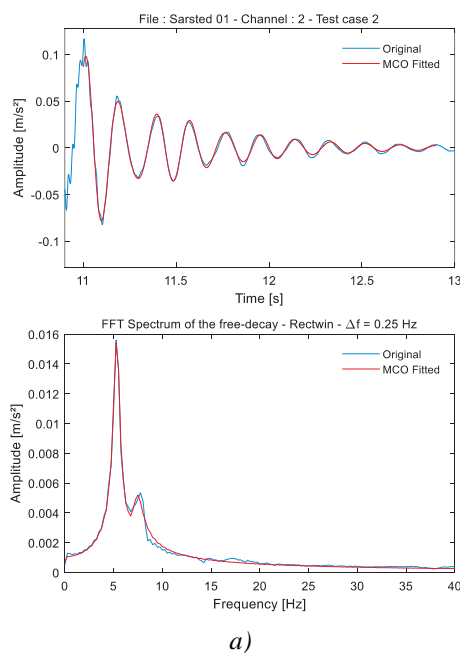

Figure 33: Ebr ü.Wenderterstraße test case no. 2: identification with a) MCO and with b) SSI-COV.
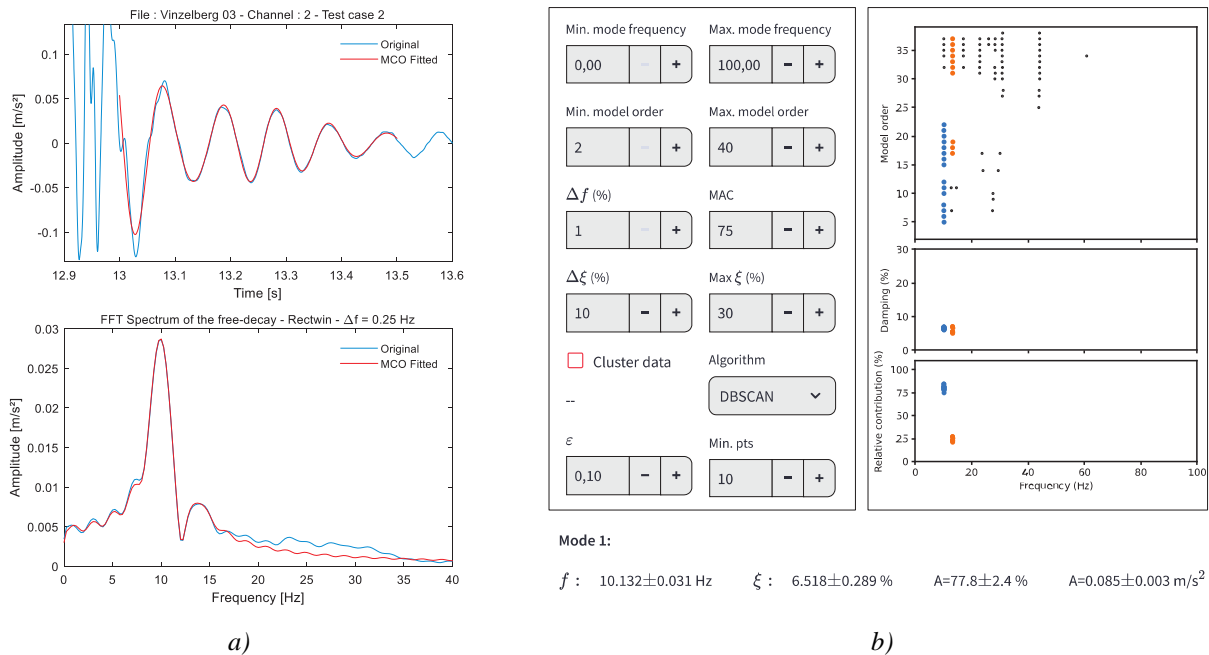
a)   *b)*

Figure 34: EÜ Str.Vinzelb.-Käth test case no.2: identification with a) MCO and with b) SSI-COV.

Table 12: List of Ebr ü.Wenderterstraße (Sarsted) and EÜ Str.Vinzelb.-Käth (Vinzelberg) test cases and SSI-COV and MCO estimates of damping and frequency.

Test case ID	t_0 (s)	t_{end} (s)	Mode	SSI-COV ξ_i (%)	MCO ξ_i (%)	SSI-COV f_i (Hz)	MCO f_i (Hz)
Sarsted 1	11	11.95	1	5.48	5.98	5.31	5.30
Sarsted 2	11	12.9	1	4.71	5.49	5.32	5.32
Sarsted 3	11.1	12.05	1	5.15	2.82	5.32	5.35
Sarsted 4	11.1	13	1	4.67	4.82	5.32	5.31
Vinzelberg 1	12.9	13.9	1	6.01	4.42	10.03	10.13
Vinzelberg 2	13	13.5	1	6.52	6.56	10.13	10.09
Vinzelberg 3	13	14	1	6.07	6.29	10.16	10.12

3.4.5.3   Benchmark involving non-linear behaviour

Sermaize-les-bains bridge in France (also noted 070000_230+956, see Annex B) is a short *"U"*-shaped steel bridge with a span of 6m, in which each platform carries one railway. This light bridge displays a non-linear dynamic behaviour in terms of frequency and amplitude of decay as the frequency of oscillations evolves along the decay from about 16 Hz to 2 0Hz. This is possibly linked to rapid quasi-static loading of the bridge when the train's axle load is not negligible as compared to modal mass.

One train passage has been selected (Sermaize 52, channel 1) as depicted in Figure 35 and obtained results by both methods are presented in Figure 36. Damping ratio and frequency estimations are given in Table 13.

In that context, estimation methods present gaps in damping values of 1 %pt and in frequency values of about 1 Hz. A classical logarithmic decrement estimation of damping on that signal, considering a mean frequency of 17 Hz leads to 6% damping estimate.
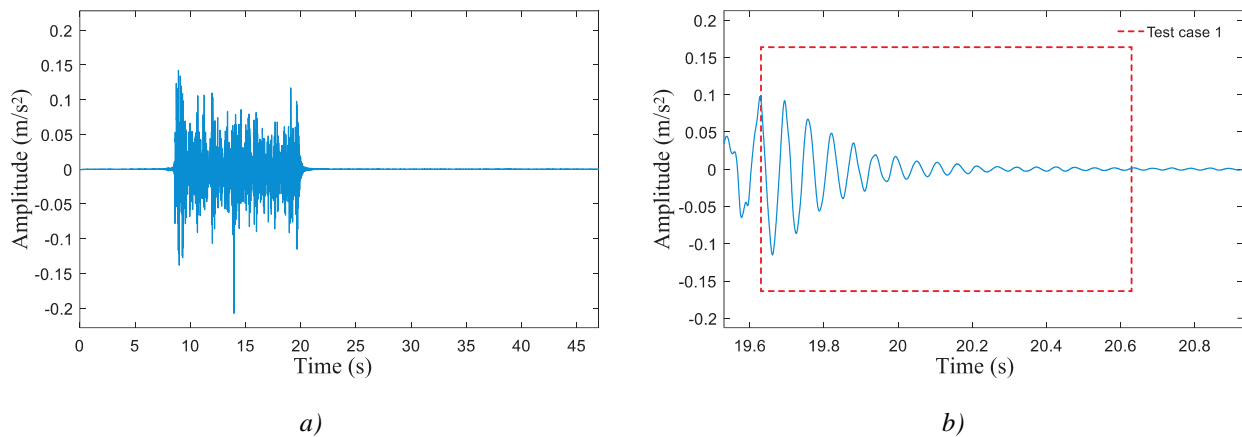
a)

b)

Figure 35: Response of the Sermaize-les-bains bridge test case: a) whole time signal and b) zoom on free decay.
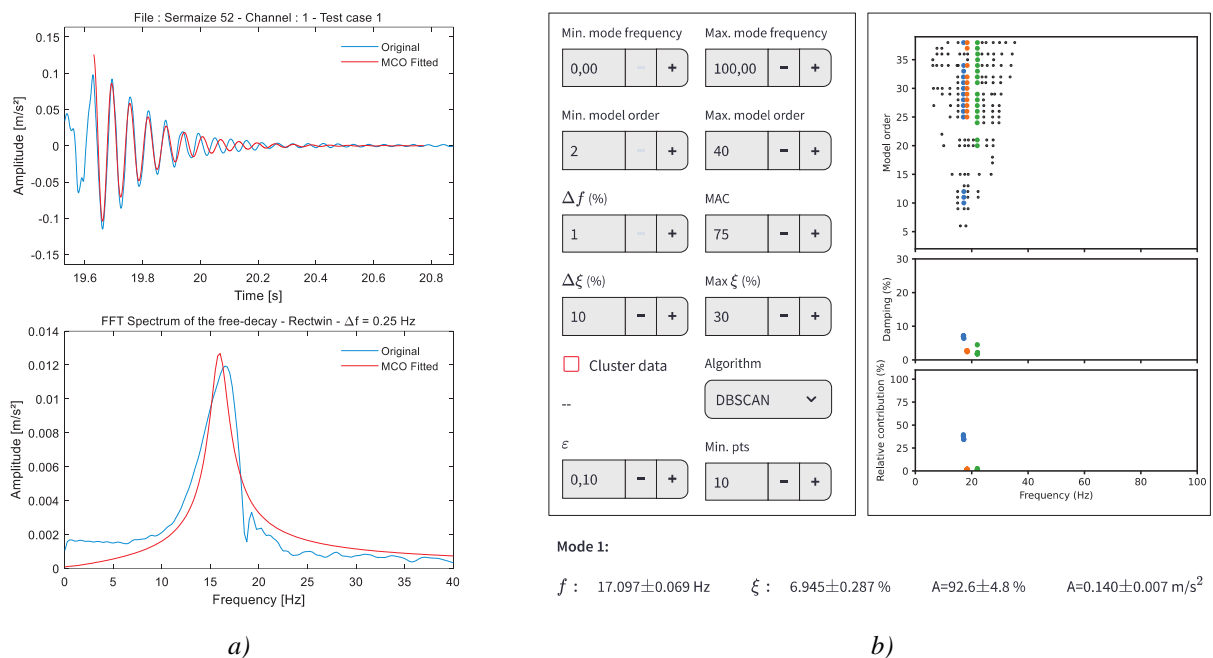

a)

b)

Figure 36: Sermaize-les-bains test case no.1: identification with a) MCO and with b) SSI-COV.

Table 13: Sermaize-les-Bains test case and SSI-COV and MCO estimates of damping and frequency.

Test case ID	t_0 (s)	t_{end} (s)	Mode	SSI-COV ξ_i (%)	MCO ξ_i (%)	SSI-COV f_i (Hz)	MCO f_i (Hz)
Sermaize 52	19.63	20.78	1	6.94	6.12	17.10	15.92

3.4.5.4 Benchmarks on mode amplitude estimation

In addition to the estimation of damping ratios, another important aspect to study is the amplitude of oscillations to analyse the importance of each mode for the global bridge response. The amplitude value that is calculated in this part corresponds to the initial acceleration value of each mode on the time signal and is called A_i in Equation (7).

Eight train passages on several bridges were then selected to benchmark the amplitude estimations by SSI-COV and MCO methods. The testes bridges were (see Annex B for details):

- EÜ über477 bei Kerpen (Germany): filler beam bridge with a span of 15.92m.

- Algodor (Spain): filler beam bridge with 3 spans (selected span of 10.25m).

- Malay - 752000_083+112 (France): filler beam bridge with 2 spans, selected span of 34.4m.

- Vinzelles - 752000_335+986 (France): filler beam bridge with 3 spans, selected span of 11.42m.

Figures 37 to 40 present examples of vibration signals measured on these bridges after train passage and the considered signal portions for damping estimations within the free decay period.
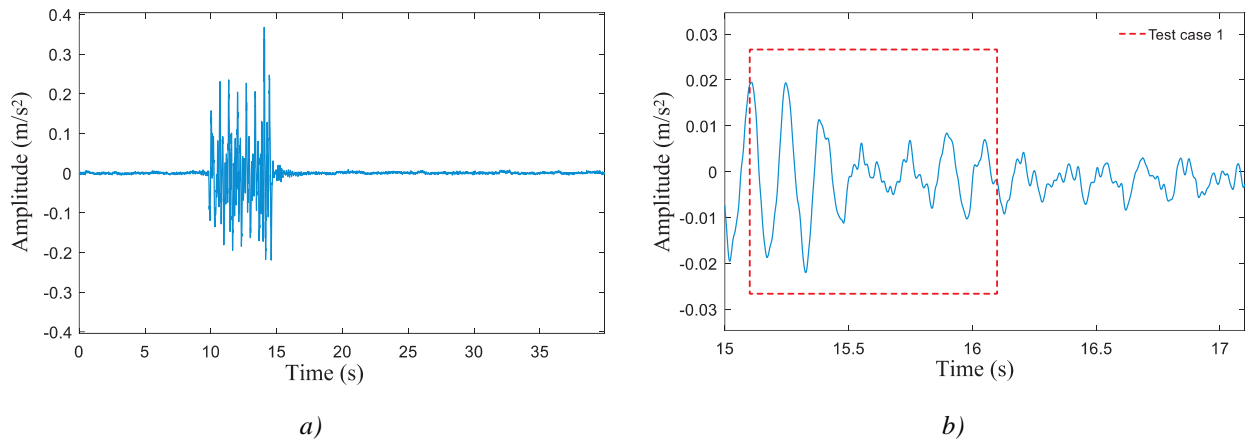

a) *b)*

Figure 37: Response of the EÜ über477 bei Kerpen bridge test case: a) whole time signal and b) zoom on free decay.
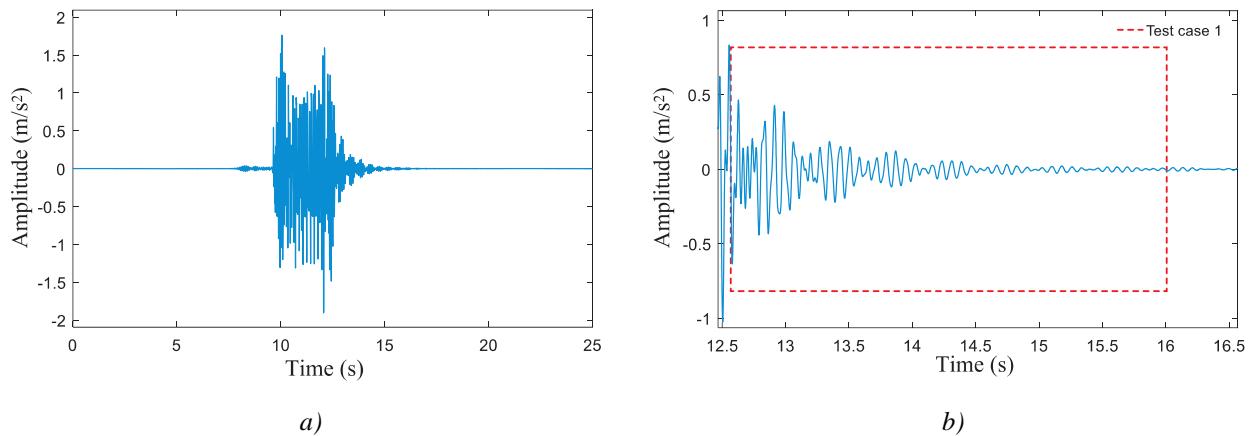

a) *b)*

Figure 38: Response of the Algodor bridge test case: a) whole time signal and b) zoom on free decay.
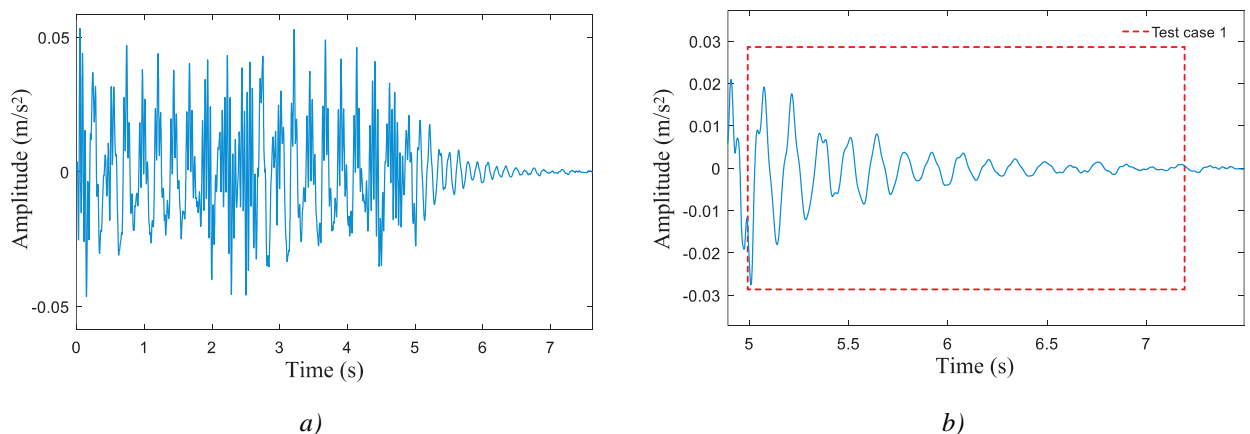

a) *b)*

Figure 39: Response of the Malay (752000_083+112) bridge test case: a) whole time signal and b) zoom on free decay.
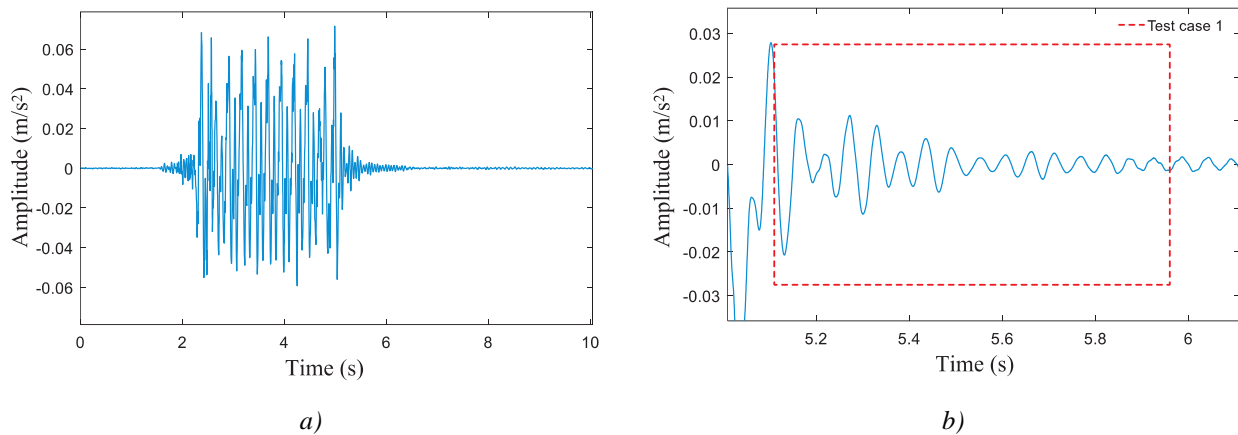
Figure 40: Response of the Vinzelles (752000_335+986) bridge test case: a) whole time signal and b) zoom on free decay.

a) EÜ über477 bei Kerpen

EÜ über477 bei Kerpen bridge in Germany is a filler beam bridge with a span of 15.92m, in which each of the two railways is supported by an independent deck. Four train passages have been selected (Kerpen 04-channel 15, Kerpen 07-channel 15, Kerpen 16-channel 3 and Kerpen 17-channel 15). An example of results obtained by both methods on Kerpen 07 is presented in Figure 41, while the whole set of results is presented in Table 14.
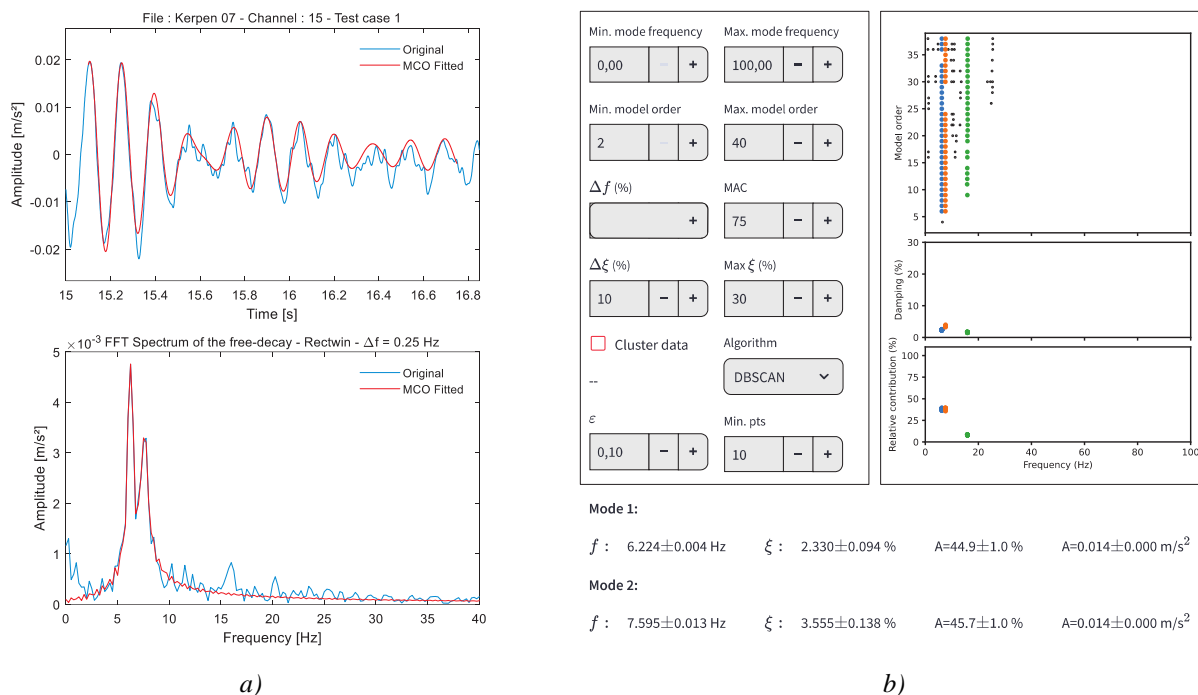
Figure 41: Kerpen 07 test case: a) identification with MCO, b) identification with SSI-COV.

b) Algodor

Algodor in Spain is a filler beam bridge with 3 spans, the selected span being 10.25m. The passages Algodor 04 – channel 1 and Algodor 12 – channel 1 have been selected. According to Galvín et al. (2021) modal analysis, this bridge exhibits very close modes due to coupling between adjacent span with close dimensions. Estimation results are presented in Table 14.

c) *Malay*

Malay (752000_083+112, France) is a filler beam bridge with 2 spans, the selected span being 34.4m. The passage 752000_083+112 31, channel 1 has been selected. Estimation results are presented in Table 14.

d) <u>Vinzelles</u>

Vinzelles (752000_335+986, France) is a filler beam bridge with 3 spans, the selected span being 11.42m. The passage 752000_335+986 21, channel 1 has been selected. Estimation results are presented in Table 14.

e) *Results summary*

In terms of frequencies, both methods show a good agreement in all the test cases. Regarding damping, most test cases show satisfactory agreement, except for Kerpen 17 and Malay 31. The amplitude estimations are also close for the two methods expect for the Kerpen 17 and the two Algodor cases. However, as mentioned previously, the Algodor bridge is likely to have very close modes and indeed SSI-COV detected supplementary ones, 13.4 Hz and 13.7 Hz for instance (results are not displayed here) while MCO could not differentiate so close contributions. Hence with more detected modes, contributions are shared and can explain the differences in amplitude estimations.

Table 14 – List of amplitude test cases and SSI-COV and MCO estimates of damping and frequency.

Test case ID	t_0 (s)	t_{end} (s)	Mode	SSI-COV ξ_i (%)	MCO ξ_i (%)	SSI-COV f_i (Hz)	MCO f_i (Hz)	SSI-COV A_i (m/s²)	MCO A_i (m/s²)
Kerpen 04-channel 15	14.40	16.05	1	2.80	3.44	6.23	6.31	1.40x10⁻²	1.54x10⁻²
			2	3.46	3.11	7.48	7.39		1.31x10⁻²
Kerpen 07-channel 15	15.10	16.75	1	2.33	2.37	6.22	6.24	1.20x10⁻²	1.16x10⁻²
			2	3.56	3.67	7.60	7.57		1.20x10⁻²
Kerpen 16-channel 3	14.50	16.15	1	3.10	3.11	6.16	6.17	1.35x10⁻¹	1.18x10⁻¹
Kerpen 17-channel 15	14.20	15.85	1	3.22	6.81	6.16	6.28	1.12x10⁻¹	2.14x10⁻¹
Algodor 4	10.34	14.59	1	1.95	1.48	11.38	11.40	1.71x10⁻¹	1.63x10⁻¹
			2	1.68	1.37	13.57	13.55	1.84x10⁻¹	3.40x10⁻¹
Algodor 12	12.57	15.99	1	2.06	2.36	11.48	11.42	1.46x10⁻¹	3.26x10⁻¹
			2	1.92	1.48	13.41	13.56	1.83x10⁻¹	3.16x10⁻¹
Malay 31	4.99	7.12	1	4.55	6.29	4.54	5.06	3.00x10⁻³	2.00x10⁻³
			2	4.18	4.22	7.20	7.08	1.60x10⁻²	2.10x10⁻²
Vinzelles 21	5.11	5.96	1	7.99	7.47	12.38	12.30	1.00x10⁻²	1.00x10⁻²
			2	3.12	3.12	18.15	18.15	1.40x10⁻²	1.50x10⁻²

In terms of damping estimations, the test cases show good agreement except for the Kerpen 17 and Malay 31 results. The amplitude estimations are also close for the two methods expect for the Kerpen 17 and the two Algodor cases. However, as mentioned previously, the Algodor bridge is likely to have very close modes and indeed SSI-COV detected supplementary ones, 13.4 Hz and 13.7 Hz for instance (results are not displayed here) while MCO could not differentiate so close contributions. Hence with more detected modes, contributions are shared and can explain the differences in amplitude estimations.

In addition to the previous test cases, four of them on Spanish and French bridges were repeated with the SSI-COV method with different t_{end} values set to include 10 cycles of the mainly oscillating mode in order to

focus the estimations on the very beginning of the free-decay response. Results are listed below in Table 15 with the "bis" suffix. These additional tests display better correlations on Algodor amplitude estimates, as compared to initial MCO values.

Table 15 – List of repeated tests on Algodor, Malay and Vinzelles cases (bis) and SSI-COV estimates.

Test case ID	t_0 (s)	t_{end} (s)	Mode	SSI-COV ξ_i (%)	SSI-COV f_i (Hz)	SSI-COV A_i (m/s²)
Algodor 4bis	10.34	11.21	1	2.24	11.41	2.09×10^{-1}
			2	0.93	13.53	3.05×10^{-1}
Algodor 12bis	12.57	13.44	1	2.58	11.42	2.94×10^{-1}
			2	1.15	13.52	2.54×10^{-1}
Malay 31bis	4.99	7.19	1	4.75	4.56	5.00×10^{-3}
			2	4.24	7.20	2.30×10^{-2}
Vinzelles 21bis	5.11	5.92	1	7.67	12.32	1.10×10^{-2}
			2	2.99	18.16	1.40×10^{-2}

3.4.5.5   Blind benchmark with non-fixed time parameters

The last benchmark, referred to as "blind" because the starting and ending values were not communicated between the UPORTO and AVLS teams using SSI-COV and MCO methods, respectively. These cases help to evaluate the overall estimations when the teams do not always have the same parameters such as starting and ending times or signal filtering.

This benchmark has been conducted with the Savigny (830000_036+790) bridge in France, a *"U"*-shaped composite bridge with a span of 14m (see Annex C for details). Five train passages have been selected (830000_036+790 33, 830000_036+790 60, 830000_036+790 62, 830000_036+790 71 and 830000_036+790 81, channel 1) to compare frequency, damping and modal amplitude estimations between both methods.

Figure 42 displays an example of signal for the Savigny 62 train passage and obtained results by both methods on this case are presented in Figure 43. All estimations are given in Table 16.

As seen in the previous example, since the studied part of the signal can differ significantly, the amplitudes also vary in a similar way. Consequently, results of amplitude values can differ by a ratio up to 3 on the 830000_036+790 71 example. However, damping ratio estimations with the two methods stay within a margin of 0.5 %pt.
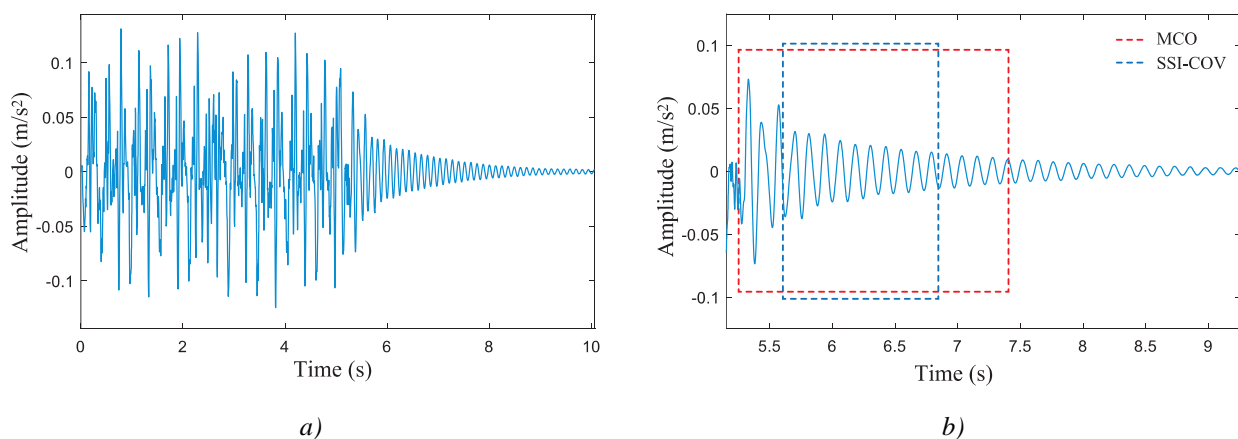

Figure 42: Response of the Savigny bridge 62 test case: a) whole time signal and b) zoom on free decay.
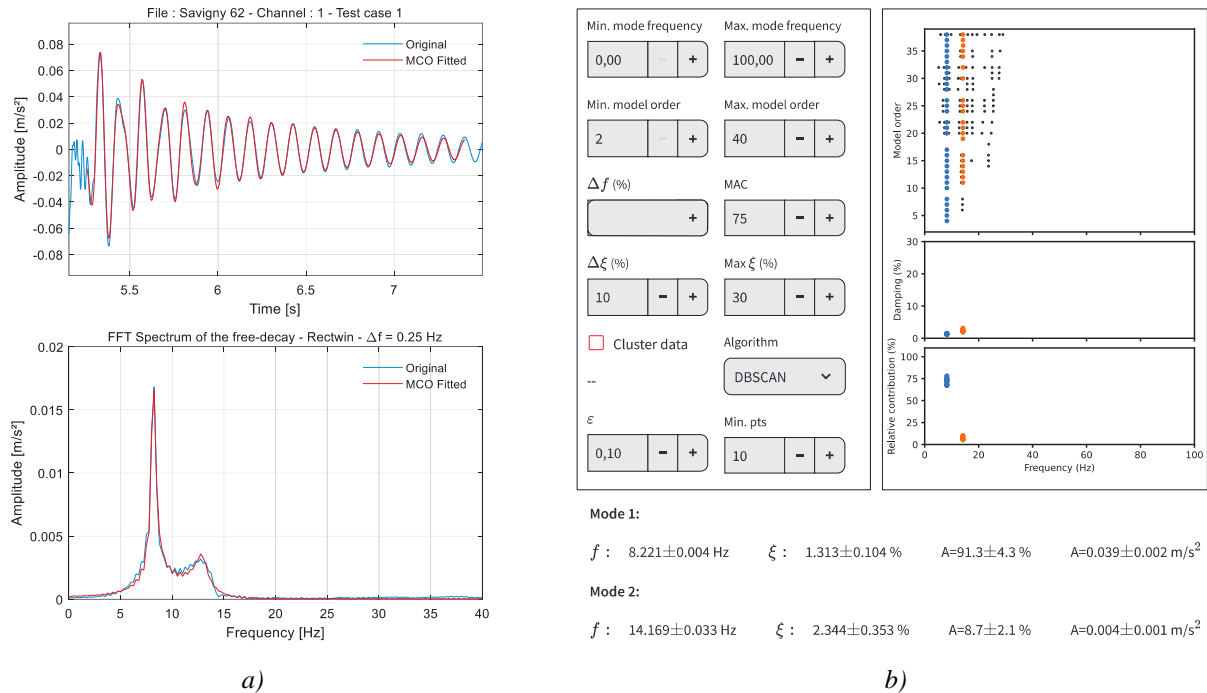
a)   *b)*

Figure 43: Savigny 62 test case: a) identification with MCO, b) identification with SSI-COV.

Table 16 – List of Savigny test cases and SSI-COV and MCO estimates of damping and frequency.

Test case id	t_0 (s)	t_{end} (s)	Mode	SSI-COV ξ_i (%)	MCO ξ_i (%)	SSI-COV f_i (Hz)	MCO f_i (Hz)	SSI-COV A_i (m/s²)	MCO A_i (m/s²)
830000_036+790 33	-	-	1	1.40	1.84	8.21	8.16	0.076	0.070
830000_036+790 60	-	-	1	1.17	1.36	8.25	8.21	0.025	0.023
830000_036+790 62	-	-	1	1.31	1.80	8.22	8.18	0.039	0.055
830000_036+790 71	-	-	1	1.18	1.03	8.33	8.22	0.016	0.013
830000_036+790 81	-	-	1	1.19	1.86	8.27	8.23	0.032	0.044

3.4.5.6 Benchmarks synthesis and analysis

As a synthesis, the present section summarizes the different benchmarks presented previously and discuss their results.

a) *Frequency estimations*

Firstly, Figure 44 compares the first mode frequency estimations of both methods. Results are consistent with a usual margin of 0.2 Hz except for a couple cases, especially for Sermaize non-linear benchmark which notably involves a non-stationary modal frequency. Frequency estimations on modes of higher order fall also into this margin.
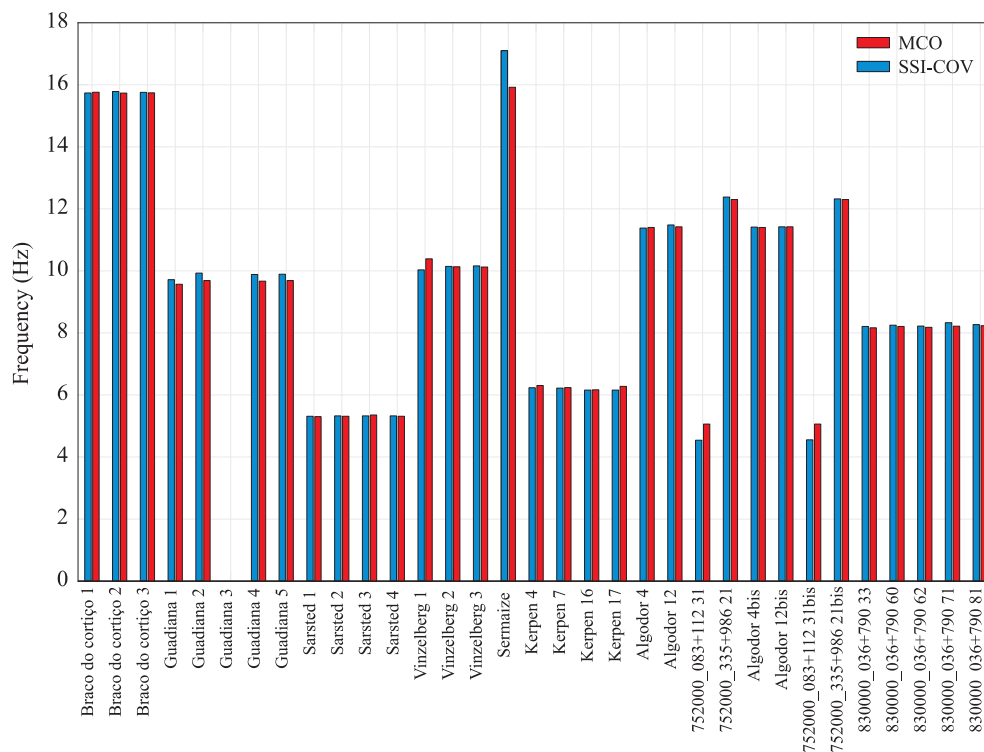
Figure 44: First mode frequency estimations of SSI-COV and MCO methods on benchmarks.

b)   *Damping estimations*

Damping estimations results on the first detected natural frequency are summed up in Figure 45. Additionally, the gap in values $\Delta\xi$ between SSI-COV and MCO are plotted in Figure 46a and the histogram of the $\Delta\xi$ values in Figure 46b. The comparison of damping ratio estimations shows a general agreement between both methods despite several large discrepancies or even a negative value (Guadiana 1). The gaps between estimations and their histogram show that the majority of test cases present a margin of 0.5 %pt in absolute values. Moreover, with a most occurring gap falling in [-0.5 %pt, 0], it can be noticed that MCO tends to overestimate damping values as compared to SSI-COV.

Large discrepancies have appeared in the following situations:

- Non-linear behaviour as in the Sermaize example.

- Complex signal: Some test cases are notably complex with very short or very long duration, large frequency content or noise level such as in the Braço do Cortiço 3, Sarstedt 3, Vinzelberg1 or Kerpen 17 examples.

- Mode 1 is not predominant: The first mode is not always the main contribution in the response and consequently is more difficult to identify like in the Guadiana 4 or Malay 31 (752000_083+112) cases.
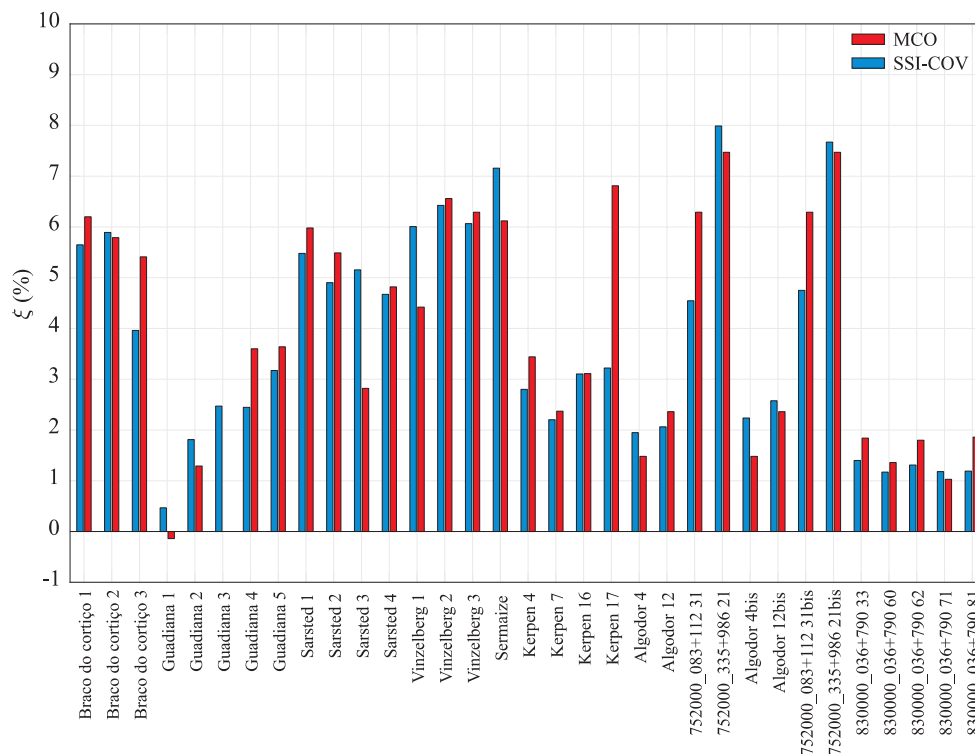
Figure 45: First mode damping ratio estimations of SSI-COV and MCO methods on benchmarks

a)	*b)*

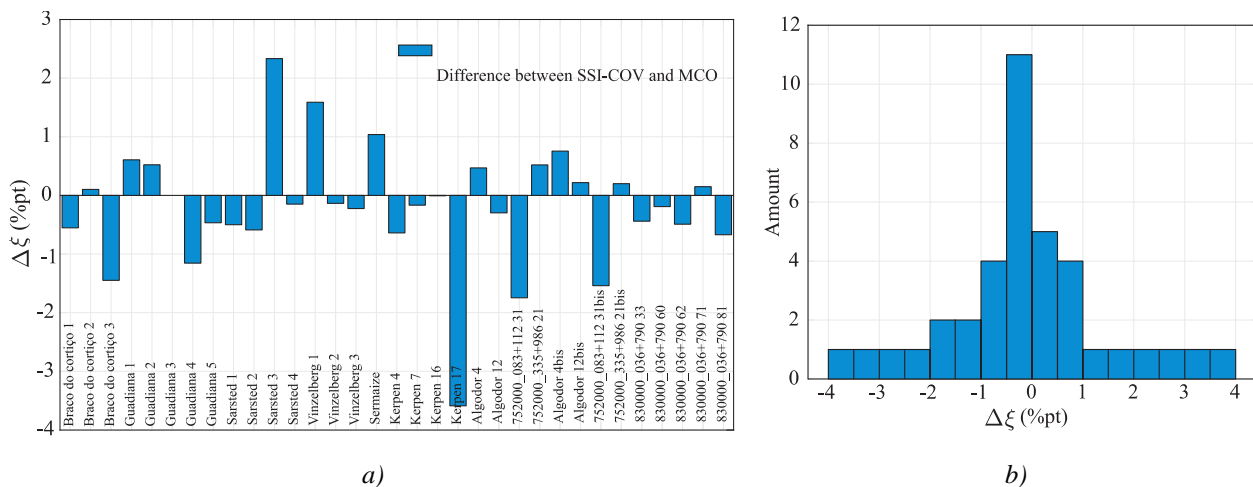*Figure 46: SSI-COV and MCO gap values on first mode damping ratio. a) Δξ values per test case b) Histogram of Δξ values*

Estimations on the second mode, when applicable, are compared in Figure 47. It can be observed a similar margin of 0.5 %pt on the estimations. Unrealistically low values were obtained for the Guadiana 4 and 5 test cases due to the consideration of an almost non-decaying signal.
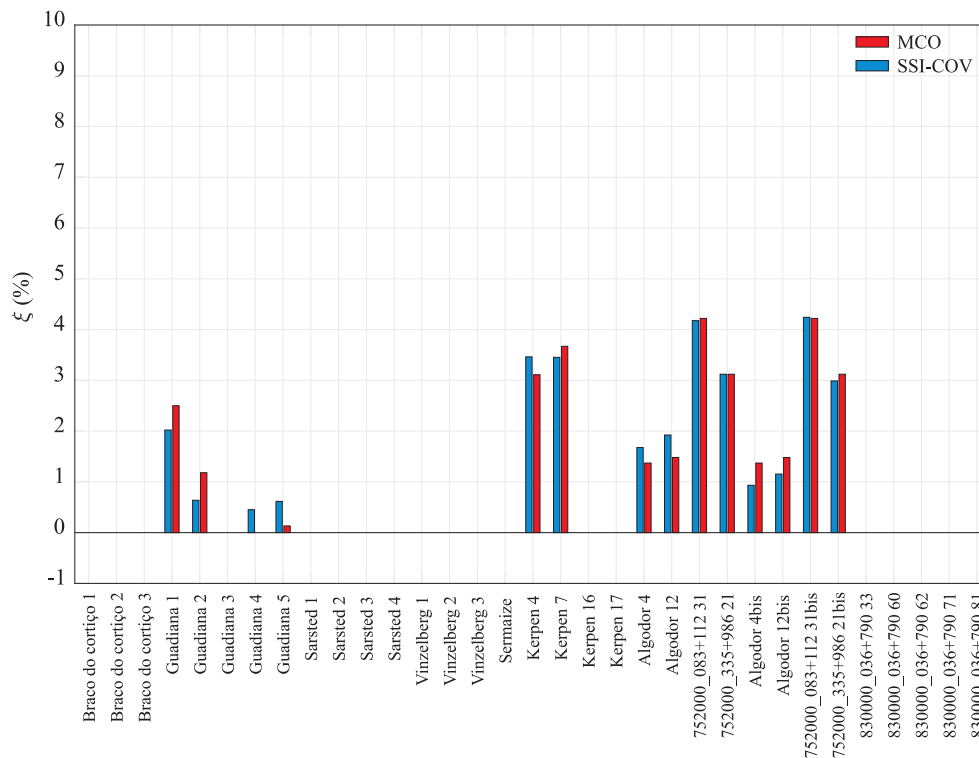
Figure 47: Second mode damping ratio estimations of SSI-COV and MCO methods on benchmarks

c) *Modal amplitude estimations*

Modal amplitude estimations on the first and second modes are presented below on Figure 48. As discussed previously in Section 3.4.5.4, larger discrepancies observed on test cases Algodor 4 and Algodor 12 are presumably linked to a complex dynamic behaviour with very close modes that cannot be captured equally by both methods. Cases on the 830000 036+790 (Savigny) bridge were the "blind" benchmarks presented in Section 3.4.5.5. Since initial time and studied durations differ between the two teams, amplitude values are not expected to be equal. It is nevertheless stated that amplitude orders of magnitude are consistent between test cases and despite occurring large ratios between SSI-COV and MCO, the obtained damping estimations in these conditions also fall in a consistent range of values.
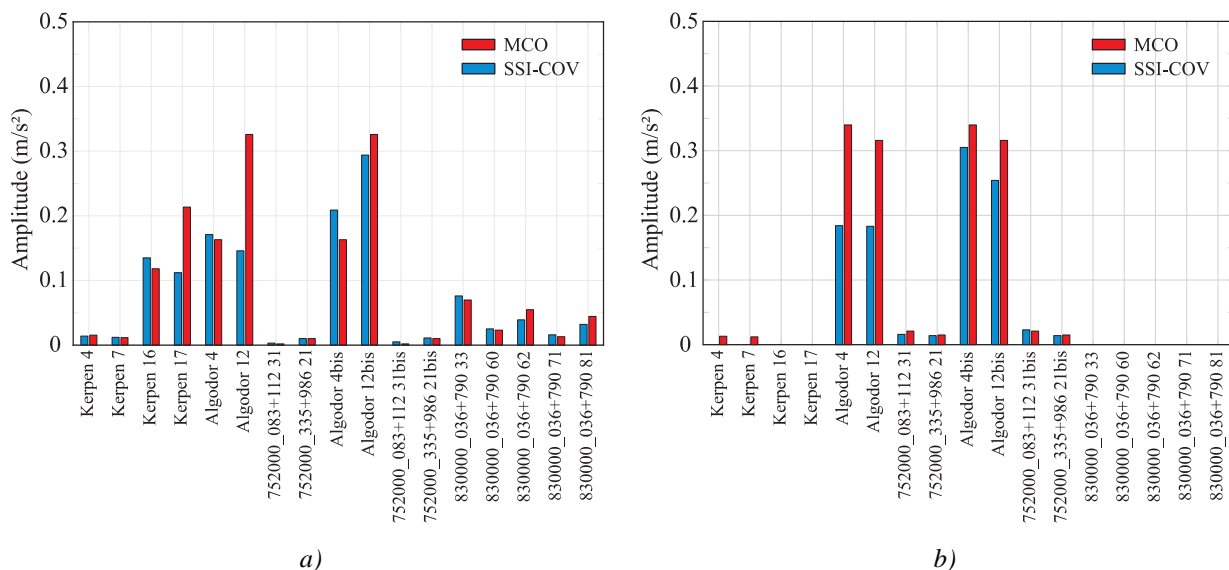

Figure 48: Initial amplitude estimations by SSI-COV and MCO methods on benchmarks: a) first and b) second modes.

4 DAMPING ESTIMATION RESULTS

4.1 Initial considerations

This section aims to present the outcomes of Task 4.2 from the InBridge4EU project which consist of the damping ratios estimated for all the studied bridges through the algorithms presented before in Chapter 3. In total, approximately 1150 train passages over about 90 railway bridges from Portugal, Sweden, Spain, Germany and France have been analysed. AVLS performed the damping estimations using the MCO method on French (filler beam, concrete, steel and part of the composite) and Spanish bridges, while UPORTO used SSI-COV to estimate damping on Portuguese, German, Swedish and French (composite only) bridges. First, Section 4.2 introduces the procedure for preparing the data used in damping estimation, focusing on the selection of train passages and sensors. Then, to provide a comprehensive overview of the results, Section 4.3 presents the estimated damping coefficients for the fundamental vertical bending mode of all analysed bridges and measurements as a function of span L and bridge type. The results are summarised in table format in Annex A and in the bridge datasheets in Annex B. These annexes, in addition to including the main bridge properties and damping values, also present the range of estimated frequencies and response amplitudes.

4.2 Preparation of data for damping estimation

Before presenting the results overview, it is important to understand how the available data has been selected to be used as inputs to the methods described before in Chapter 3.

For methods that estimate damping based on the bridge response to railway traffic (MCO and SSI-COV), the train passage selection has been focused on those presenting a clearer resonance during free response as these provide the most meaningful data for analysis. A preliminary assessment of the resonance was conducted visually by analysing the time signal and the Fast Fourier Transforms (FFTs) of train passages, ensuring that the selected passages were the most suitable for accurate damping estimation. However, later in Chapter 5, Section 5.4, a more robust procedure is introduced to clearly identify scenarios closer to the resonant area, allowing for a more accurate definition of damping.

As for the channel selection (sensor position), ideally the sensor positioned at the centre of the structure would typically provide the most accurate measurements for analysis of the fundamental vertical bending mode. In double-track bridges, priority was given to the sensors located on the side where the train crossed. However, in practice, it was sometimes necessary to select alternative sensors due to the presence of excessive noise in the central sensor's data. This noise would compromise the quality of the measurements and, consequently, the accuracy of the estimations. For example, on the Tirteafuera bridge in Spain, as shown in Figure 49, sensors A2, A14 and A23, set midspan, were used for damping estimations, depending on the travelled track and quality of response.
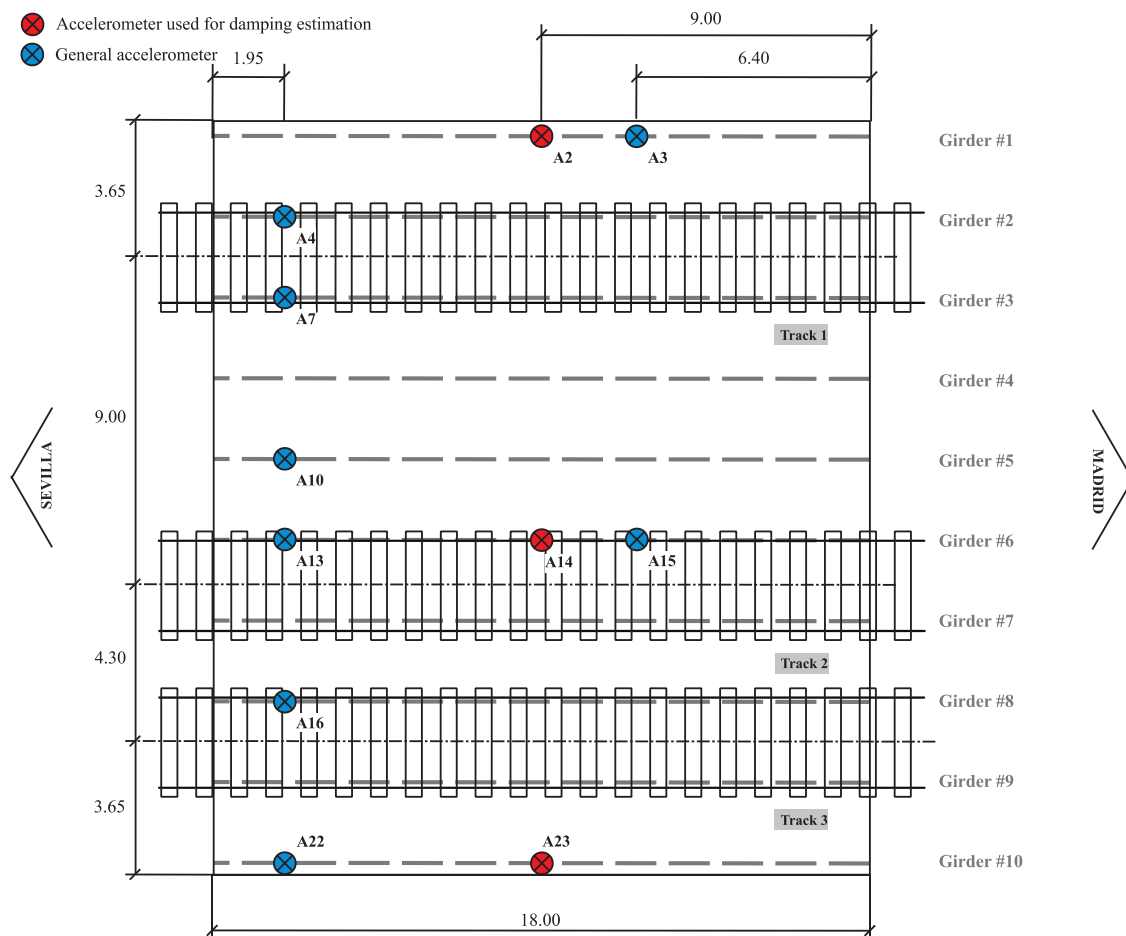
Figure 49: Sensor locations on Tirteafuera bridge (Spain) – Sensors A2, A14 and A23 were used for damping estimation.

Regarding the methods used to estimate damping based on the free decay part of the bridge response, both compute damping ratios from several modes if they contribute to the free response. The validation of an estimation is based on the expertise of the user through the following simple procedures:

- MCO method (adopted by AVLS): fit quality on the time signal and on the FFT spectrum.
- SSI-COV method (adopted by UPORTO): critical analysis of a stabilisation diagram.

After validation, two modes are selected among all detected modes: the fundamental vertical bending mode of the bridges (usually that with lowest frequency and previously assessed through dynamic reports provided by the Infrastructure Managers, as referred later in Section 3.2) and the one with maximum amplitude (corresponding to maximal value on the free-decay time signal attributed to this mode), but only if do not correspond to the fundamental bending mode. Indeed, on a same bridge different passages can excite different modes so picking several modes shows the variety of excited modes and allows to evaluate the influence of higher-order mode damping in the bridge dynamics.

4.3 Estimated damping values

The damping coefficients estimated by AVLS and UPORTO for all analysed bridges and measurements as function of span *L* categorized by the bridge type specified in EN 1991-2 (2023) are plotted in Figure 50. As there is no specific type for portal frame bridges in this code, they have been included here with filler beam and reinforced concrete bridges due to their closer structural similarity to the latter. All the damping

coefficients ξ_1 presented in this figure correspond only to the first fundamental vertical bending mode of vibration, which is the mode more prone to resonance given its lower frequency. As expected, a large scatter is observed, but most of the values are significantly above the current normative limit specified in EN 1991-2 (2023). Nevertheless, values below the normative curves can also be found and will be further discussed in Chapter 5 dedicated to Task 4.3.
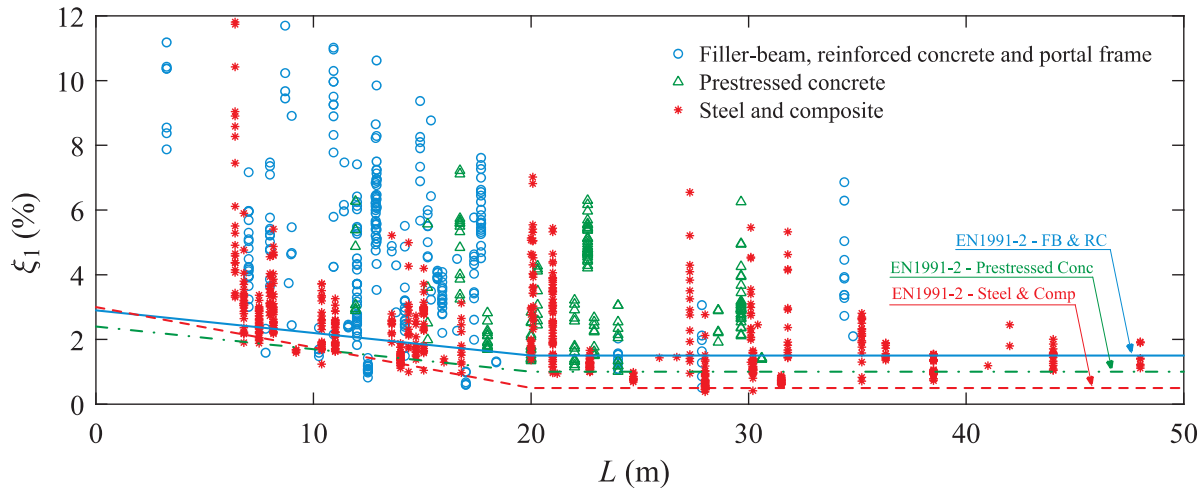

Figure 50: Damping coefficients related to the first fundamental bending mode as function of span and Eurocode bridge type.

For a better visualization of the results, Figure 51 depicts the damping as function of span L obtained in all the three bridge types separately and according to the country to which the bridge belongs. Note that the tests under forced excitation carried out in Sweden are represented through a different marker, where it can be observed that, in general, the higher vibration amplitudes imposed by the actuator to the bridges lead to higher damping ratios. A detailed analysis of this results will be addressed later in Chapter 5. The range of estimated damping, frequencies and response amplitudes are summarized in table format in Annex A, while a more detailed presentation of the bridges and respective dynamic properties are presented in the bridge datasheets in Annex B.

Following the damping estimations performed in Task 4.2, the next step involved a thorough analysis of the results to discuss insights into damping dispersion, justifications for lower values, the potential definition of new bridge types, and trends that may lead to improved normative damping values. This analysis, which falls within the objectives of Task 4.3 of the InBridge4EU project, is presented next in Chapter 5, while the normative recommendations for EN 1991-2 (2023) that arise from it are presented later in Chapter 5.1.
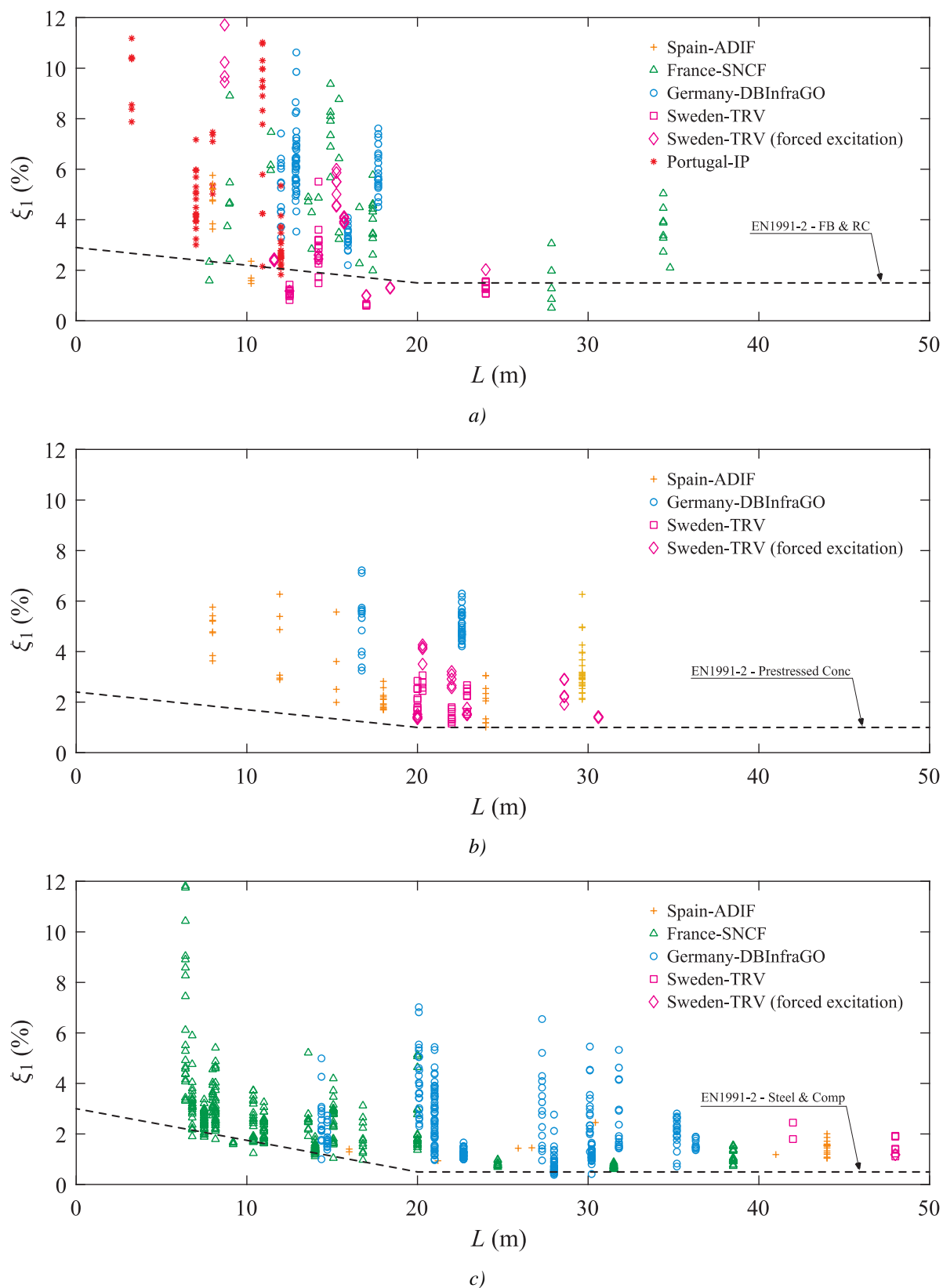
Figure 51: Damping coefficients related to the first fundamental bending mode as function of span for each Eurocode bridge type and country: a) Filler beam and reinforced concrete (including portal frames), b) Prestressed concrete and c) Steel and composite.

5 DAMPING DATA PROCESSING AND ANALYSIS

5.1 Initial considerations

The damping database developed within Task 4.2 has been extensively analysed in Task 4.3 by UPORTO to study the potential correlations between various factors that may influence damping. The following actions have been taken within this regard, which will be detailed in the next sections:

- Evaluation of the influence of amplitude of the bridge response in the estimated damping values (see Section 5.2).

- Evaluation of the possibility of establishing new damping bridge types distinct from those currently defined in EN 1991-2 (2023) (see Section 5.3).

- Evaluation of the contribution of the fundamental vertical bending mode for the bridge response in damping assessment (see Section 5.4).

- Analysis of value deviations that may condition the lower bounds of damping ratios (see Section 5.6).

Taking into consideration the analysis carried out within the present section based on the actions referred above, recommendations for possible changes in the normative definition currently specified in EN 1991-2 (2023) will be proposed in Chapter 6

5.2 Influence of the response amplitude in the damping values

As a first approach, the correlation between amplitude and damping was analysed, considering all damping estimations conducted in Task 4. The study by the ERRI D214 committee (ERRI D214/RP3, 1999) suggested a slight correlation between the amplitude of the free decay response of bridges and the estimated damping. However, this correlation was not linear, and in some cases, it was absent altogether, as illustrated by the examples from ERRI D214/RP3 (1999) in Figure 52. For instance, while the Vieux Briollay and Valenton bridges exhibit an increase in damping with response amplitude, this correlation is either unclear or non-existent for OA 49/25 and Bip (Paris-Lille).

a)

b)

c)

d)
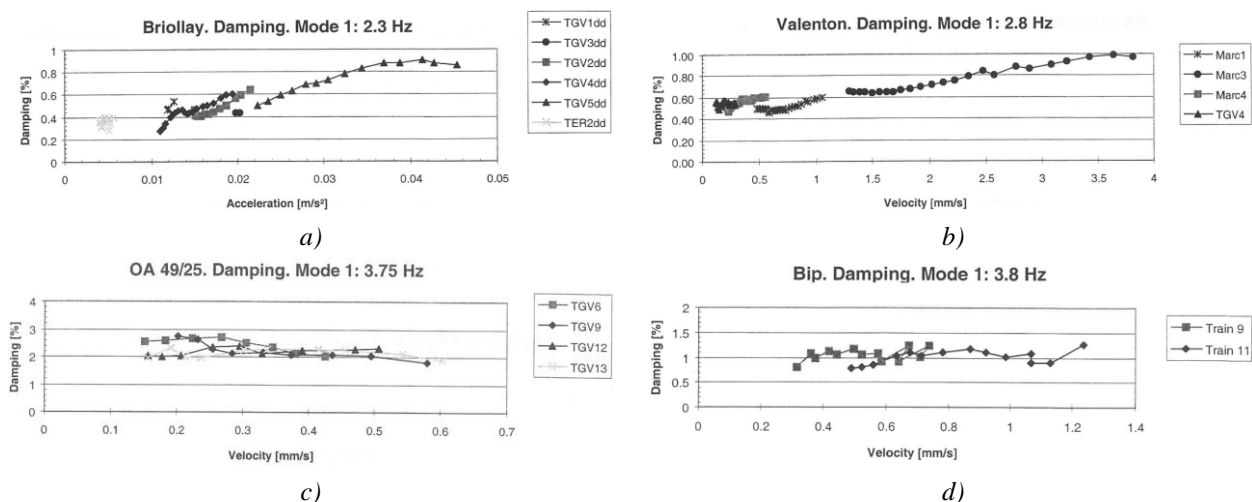
Figure 52: Relation between response amplitude and estimated damping from bridges studied in ERRI D214/RP3 (1999): a) Vieux Briollay, b) Valenton, c) OA 49/25 and d) Bip (Paris-Lille).

Figure 53 presents the same damping values previously shown in Figure 51, but as a function of the maximum acceleration amplitude during the free vibration period, considering the first fundamental mode's contribution. No clear correlation between amplitude and damping can be observed, making it difficult to draw definitive conclusions regarding the influence of acceleration amplitude on damping. Nevertheless, most tests conducted under forced excitation by KTH in Sweden generated significantly higher acceleration amplitudes

than those performed under railway traffic, generally resulting in higher damping values. Additionally, it is important to note that acceleration amplitude naturally depends on both the sensor's position on the bridge and the bridge's dynamic behaviour. Regarding the sensor placement, most damping estimations were based on sensors positioned as close as possible to midspan and on the train's passage side. However, due to placement constraints in different setups, this was not always feasible. As for the bridge's dynamic behaviour, the results in Figure 53 provide only a general overview of the relationship between damping and vibration amplitude for each bridge individually. They are not intended for direct comparisons between different bridges, as each structure exhibits unique dynamic characteristics.
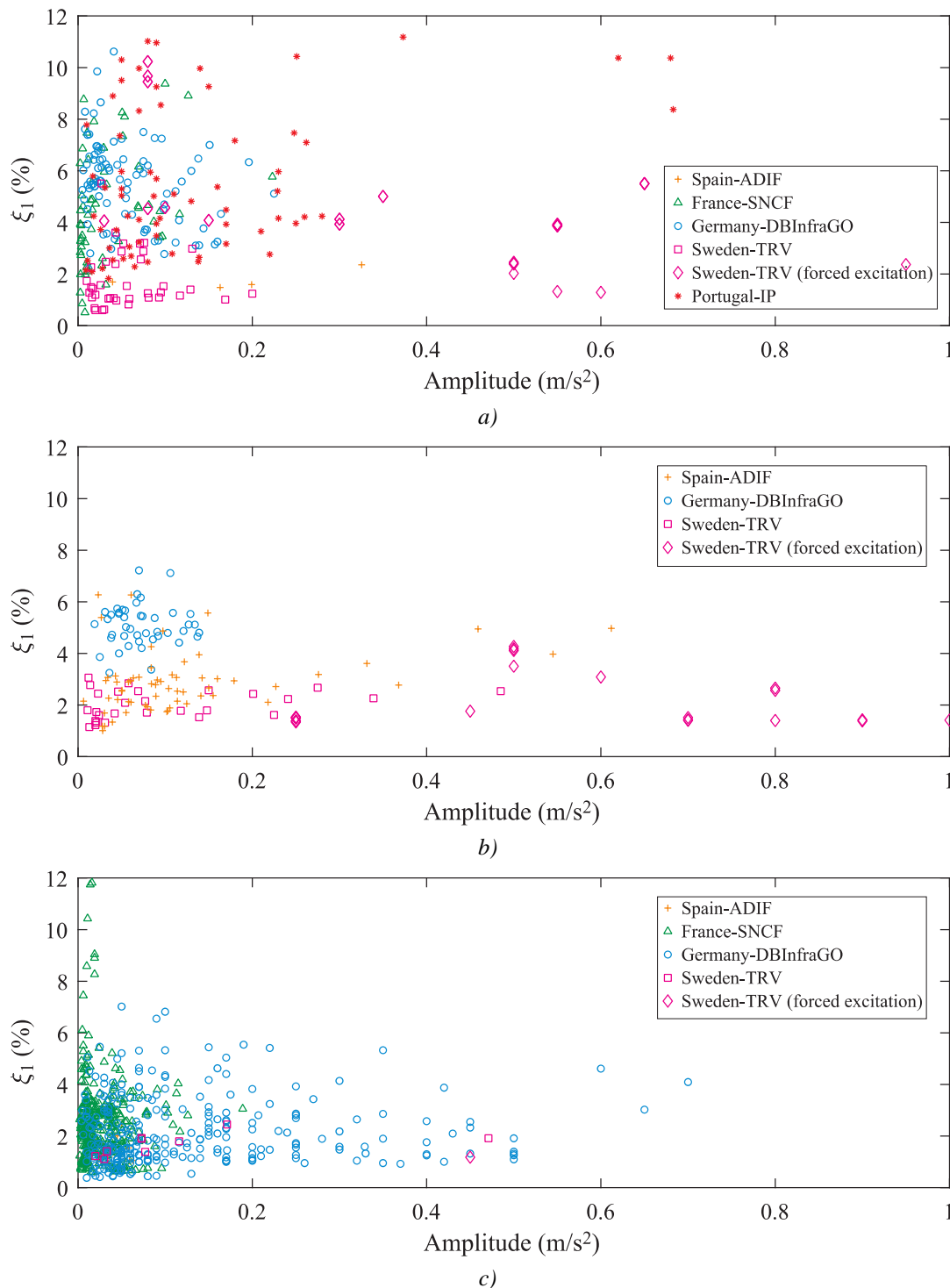

Figure 53: Damping coefficients related to the first fundamental bending mode as function of the acceleration amplitude of the free vibration period for each Eurocode bridge type and country: a) Filler beam and reinforced concrete, b) Prestressed concrete and c) Steel and composite.

By observing the global picture depicted in Figure 53 it is difficult to find clear correlations between response amplitude and damping. Moreover, as mentioned before, this figure aims only to give a general overview of the results, rather than making direct relative comparisons between bridges. Therefore, for exemplification purposes, the damping coefficients related to the first fundamental bending mode as function of the acceleration amplitude of seven isolated bridges examples are plotted in Figure 54 (given the different scale of amplitudes of the free decay period in the different bridges and measurements, the results are separated into two subfigures). As observed, some bridges, such as Taxinge and 00100-186+312, exhibit generally higher damping ratios with increasing amplitude, while others do not follow the same trend. Therefore, the analysis indicates that drawing significant conclusions about damping based on the amplitude factor is challenging due to the lack of a consistent correlation.
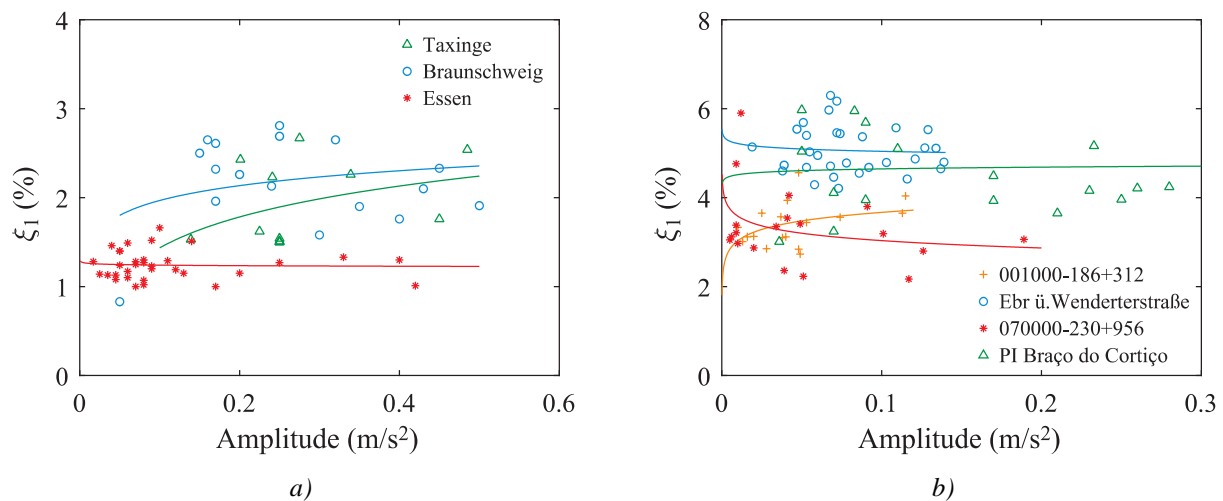

Figure 54: Damping coefficients related to the first fundamental bending mode as function of the acceleration amplitude of isolated bridges: bridges with maximum amplitude of a) 0.3 m/s² and b) 0.6 m/s².

5.3 Evaluation of the possibility to establish new normative bridge types for damping

Given the greater representativeness of the bridges and measurements used to estimate damping compared to those available for the work carried out by the ERRI D214/RP3 (1999) committee (see Table 1), it would be worthwhile to assess whether the current bridge types established by EN 1991-2 (2023) for damping should be maintained or revised. The main reason for conducting this assessment is that having a limited number of bridge families may constrain the normative damping ratios to overly low values associated to the lower bounds of a specific subtype, potentially leaving other subtypes in an excessively conservative situation.

To understand the advantage of establishing possible new bridge types, first it is important to understand which current types may be split. According to EN 1991-2 (2023), the bridge types for the purpose of damping definition consists of *i)* filler beam and reinforced concrete, *ii)* prestressed concrete and *iii)* steel and composite. Therefore, as a first step, the damping ratios depicted before in Figure 51 obtained for types *i)* and *iii)* have been split in order to understand if there is any trend in the different subtypes, namely filler beam *vs* reinforced concrete (and also portal frames, which were not analysed by the ERRI D214 committee, but in Figure 51 were included in this type) and steel *vs* composite bridges, as presented in Figure 55.

By observing Figure 55a, it is possible to observe that there is no trend that may justify a separation between filler beams and reinforced concrete, but it is clear that the portal frame bridges are characterized by a significant higher damping. Such behaviour, attributed to the radiation damping provided by the backfill soil, has also been observed in several recent studies (Heiland et al., 2024; Zangeneh, 2021; Zangeneh et al., 2018), where the damping consistently exceeded 7% in most of the analysed cases. Regarding the other two subtypes,

it is important to highlight that most of the reinforced concrete bridges in the database come from the Swedish dataset. These bridges are characterized by 1.5 m to 2.0 m over-sails (deck sections extending beyond the support) and continuous decks with integrated wingwalls and backwalls that interact with the adjacent embankment (integral abutments), making them not particularly typical structural solutions within the European bridge landscape.

In summary, the analysis suggests that it may be worthwhile to explore the possibility of defining a new bridge type for normative purposes, portal frame bridges, while keeping filler beam and reinforced concrete bridges grouped together.

With respect to Figure 55b, the lower bounds of both steel and composite bridges do not significantly differ, but in general, steel bridges present slightly lower values, which can give some hints regarding this new possible bridge type split. Moreover, as discussed in Section 5.4, some of the lower bounds correspond to scenarios where the first fundamental vertical bending mode, the mode most susceptible to resonance, is not the dominant factor in the response. Consequently, these scenarios are far from resonance conditions, where damping plays a significant role, thus not so important for the normative damping definition. Details about this topic will be explained in the next section. Hence, the present analysis indicates that is worthwhile to explore the possibility of splitting the current steel and composite bridge type into two.
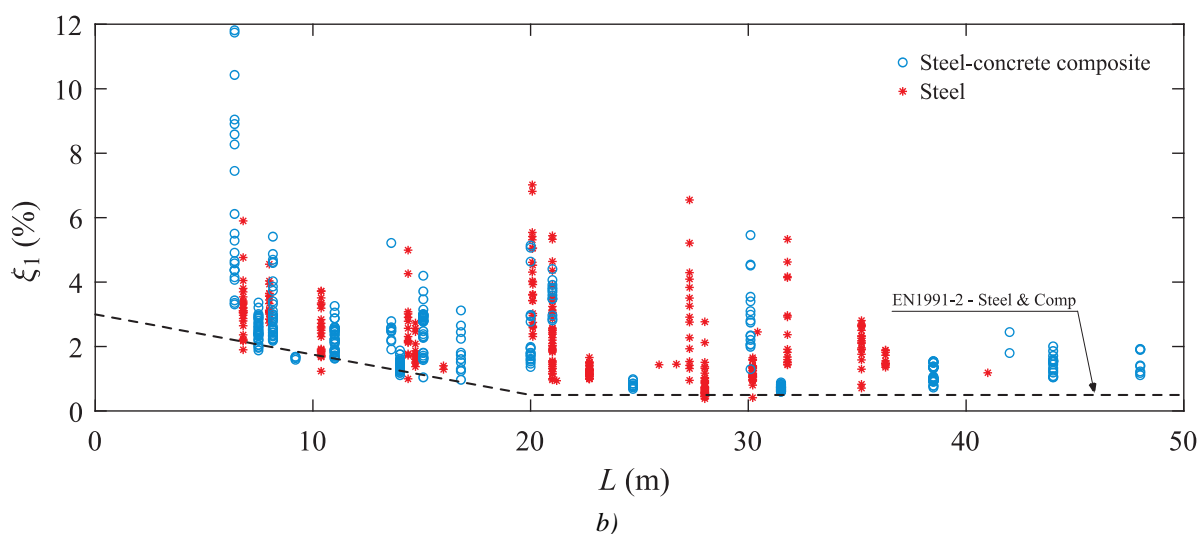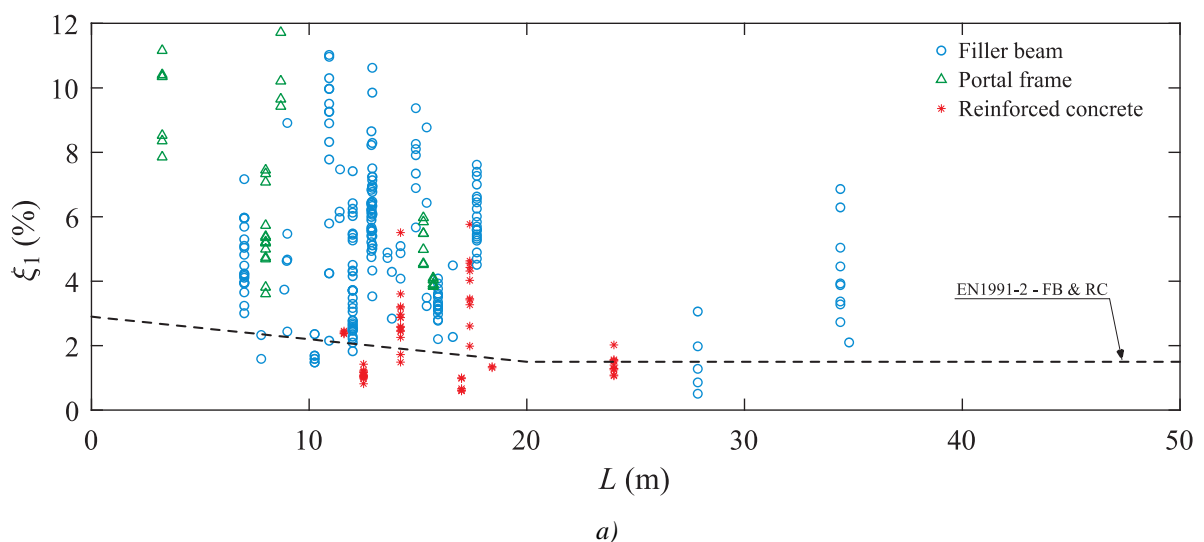

a)

b)

Figure 55: Damping coefficients related to the first fundamental bending mode as function of span identified by subtypes: a) filler beam, reinforced concrete, portal frames and b) steel and composite.
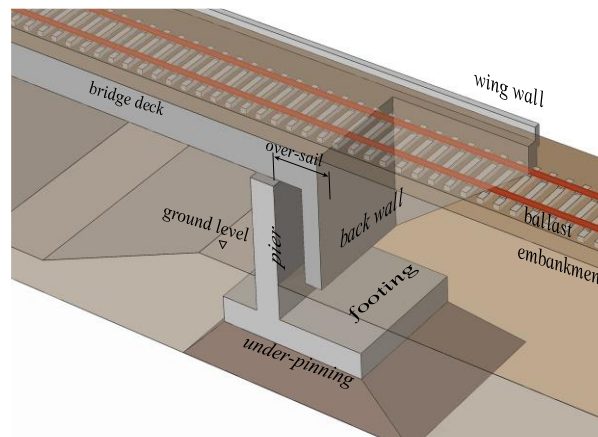
Figure 56: Illustration of a typical integral abutment in the Swedish bridges (Andersson et al., 2021).

Finally, regarding the prestressed concrete bridge type stipulated in EN 1991-2 (2023), it is worth noting that ERRI D214/RP3 (1999) does not differentiate between reinforced and prestressed concrete bridges until the final part of the report, which covers the final normative recommendations proposed by the committee. By examining the final results of this report, which can be consulted in Figure 57, it can be observed that the only concrete bridge falling between the *"Filler beam and reinforced concrete"* and *"Prestressed concrete"* types is the Hengelo bridge in the Netherlands (NS database), with a 7.4m span. In addition to the lack of explicit information in the report regarding whether this bridge is prestressed, a single bridge alone would not justify the difference in the curves. The only plausible explanation is that prestressed concrete bridges are much less prone to cracking, which could potentially result in lower damping. However, this explanation is not stated in the report and lacks supporting data. Therefore, since the rationale behind the ERRI D214 committee's proposal for a lower normative damping ratio for this bridge type is not totally clear, damping in this particular type of bridges will be examined in detail in the following sections, separately from the other concrete bridges.
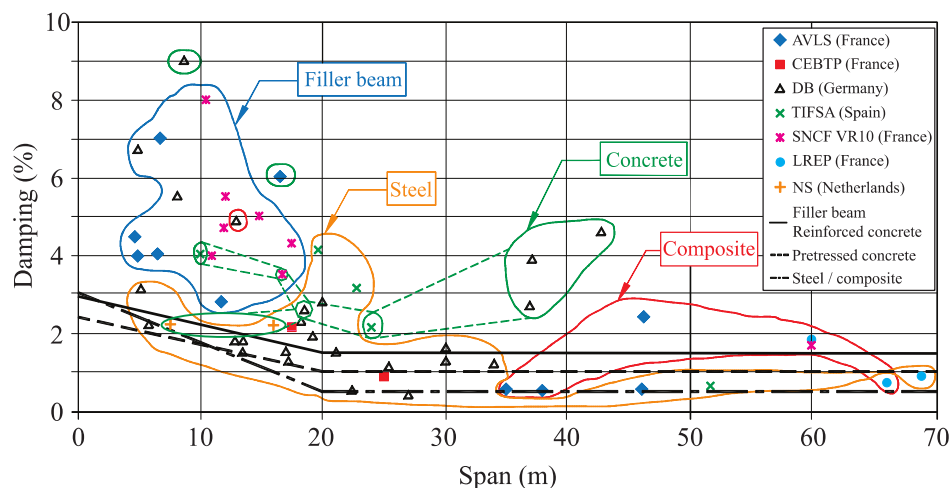

Figure 57: ERRI D214 database and recommendations for damping on railway bridges according to their type (adapted from ERRI D214/RP3 (1999))

5.4 Evaluation of the contribution of the fundamental vertical bending mode for the bridge response in damping assessment

5.4.1 Description of the procedure

With the analysis of amplitude influence conducted in Section 5.2 and the pre-definition of possible new bridge types for normative recommendations proposed in Section 5.3, the next step involved selecting cases that closely approximate resonant scenarios, as damping plays a particularly significant role in bridge design under these conditions (ERRI D214/RP3, 1999). Figure 58 extracted from ERRI D214/RP3 (1999) clearly shows this, where it possible to observe that the maximum acceleration at the midspan of a given simply supported bridge is only significantly affected by damping at the resonance speed, in this particular case around 270 km/h. Naturally, not all the measured scenarios fit within these characteristics, and some may lead to the estimation of damping levels that are not compatible with the resonance conditions that actually influence the structural design of the bridge. In fact, damping estimated from scenarios far from resonant area may lead to misleading results and should be avoided. Hence, it is important to establish a clear and consistent procedure for identifying scenarios that can be classified as near-resonant.

In bridges more prone to resonance, such as simply supported ones, vertical resonance caused by the repetitive passage of train axle loads typically occurs due to the global bending or torsional modes of the deck. In terms of bending, the fundamental mode carries the most energy and is therefore the most susceptible to resonance. For higher-order modes (second, third, etc.), if the axle spacing matches the frequency of the bridge, some axles apply force on upward-moving sections while others act on downward-moving sections, which may result in partial cancellation of resonance, reducing the significance of these modes in the overall bridge response. With respect to global torsional modes, they can also be susceptible to resonance, especially in double-track bridges prone to torsion when a train crosses it in one of the ways. Sometimes, the first global torsional mode can even be coupled or closely spaced with the bending mode (e.g. Silva et al. (2023)), leading to difficulties on decoupling them for damping estimation. Therefore, the near-resonant scenarios should be those mostly dominated by these first global modes. Naturally, other local modes may also influence the bridge response, but global modes should be prioritized for damping estimation, as they are the most relevant from a bridge design perspective.

Thus, recognizing that the first fundamental global modes are generally the most susceptible to resonance induced by a passing train, damping values should be estimated primarily from scenarios where these modes dominate the response. The first bending mode is relatively easy to capture in a simple experimental setup (e.g., a single accelerometer at midspan may be sufficient), whereas the torsional mode requires larger setups with multiple accelerometers, which are not always available. Moreover, in this study, the dynamic reports provided by Infrastructure Managers included only the frequency of the first bending mode, limiting access to other global modes. While both SSI-COV and MCO methods can identify additional modes, the absence of mode shape information introduces uncertainty about their true nature. As a result, taking into consideration the uncertainties that may arise in relation to other modes, near-resonant scenarios are defined here as those where the bridge response is predominantly influenced by the first global vertical bending mode and only damping values under these circumstances should be considered for normative recommendations, as non-resonant cases may lead to misleading results. Such an analysis, in itself, constitutes an alternative to what was previously developed by the D214 committee and documented in ERRI D214/RP3 (1999), which did not include a quantitative assessment of the contribution of the first mode. However, studies involving damping estimations for higher global modes may be carried out in the future to check their significance in the bridge design point of view, as recommended ahead in this document in Section 6.5.
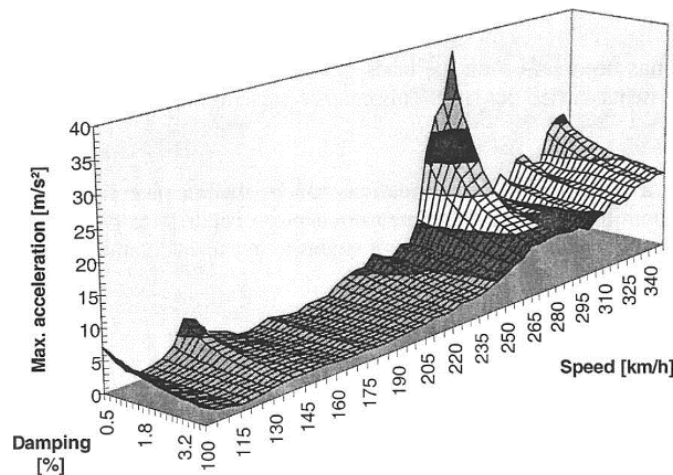
Figure 58: Maximum acceleration at a given bridge as function of damping and train speed (adapted from ERRI D214/RP3 (1999)).

In summary, the approach to evaluate the damping in scenarios that most closely resemble those used in the design of bridges, i.e., scenarios within the resonance area, may be carried out through the following procedure:

1) Estimate the frequency of the bridge's fundamental vertical bending mode f_1 using dynamic reports from the Infrastructure Managers (e.g., reports from DB InfraGO for German bridges and SNCF for French bridges) or through ambient vibration tests conducted during measurements (e.g., conducted by UPORTO, KTH, and UJI/UdS in the Portuguese, Swedish and Spanish bridges, respectively). This step will help determine the fundamental mode frequency in advance, making it easier to identify it in the subsequent analysis.

2) Apply a low-pass filter to the time series with a cutoff frequency f_{cut} given by the following equation proposed by DB InfraGO in its dynamic measurement reports:

$$f_{cut} = \max\{30 \text{ Hz}, 9f_1\} \tag{10}$$

where the 30 Hz threshold is based on the procedure outlined in EN 1990-Annex A2 (2023) for evaluating deck acceleration, while the $9f_1$ value corresponds to an internal procedure from DB InfraGO used to assess the contribution of higher-frequency modes.

3) Isolate the free decay segment of the time series using the procedure described in Section 0, with manual verification by the operator (see previous example in Figure 9). For the SSI-COV approach (adopted by UPORTO), the free decay duration was set to 10 vibration cycles (depending on the first mode frequency) to minimize interference from cycles with very low amplitude in the damping ratio evaluation. For the MCO (adopted by AVLS), the free decay duration was computed based on the method presented in Section 3.3.3. Although based on different approaches, the benchmarks presented in Section 3.4 shown a general good agreement between both methods.

4) Estimate the damping of the fundamental vertical bending mode using one of the available methods (MCO or SSI-COV) based on the free decay segment identified in the previous step (note that step 1 helped to identify the fundamental mode, since its frequency was known a priori). Both methods provide not only the damping ratio ξ_1, but also the mode's frequency f_1. Additionally, it is also possible to extract the vibration (acceleration) amplitude A corresponding to the mode, along with its percentage contribution to the total acceleration response

5) Consider damping estimations only from measurements where the contribution of the fundamental bending mode of vibration is dominant, meaning its contribution to the overall response is the highest compared to other modes captured in the analysis. This evaluation ensures that only damping ratios derived from measurements resembling resonant scenarios, typically characterized by responses governed by the fundamental mode, are considered for drafting the normative recommendation.

As an example, Figure 59a illustrates the free decay response of one of the measurements (measurement 26) carried out in the German bridge Ebr ü.Wenderterstraße, where the fundamental first vertical bending mode is dominant. In this case, the percentage contribution to the total acceleration amplitude, after filtering the time-series with a cutoff frequency f_{cut} according to Equation (8), i.e., considering a vast range of frequencies and modes, is 82 %. In contrast, Figure 59b depicts a scenario (measurement 43 from the French bridge 001000_459+633) that is not clearly dominated by the fundamental mode, as its contribution to the global response is only 17 %. In the present work, only the damping ratios derived from scenarios equivalent to those shown in Figure 59a were considered for normative recommendations.
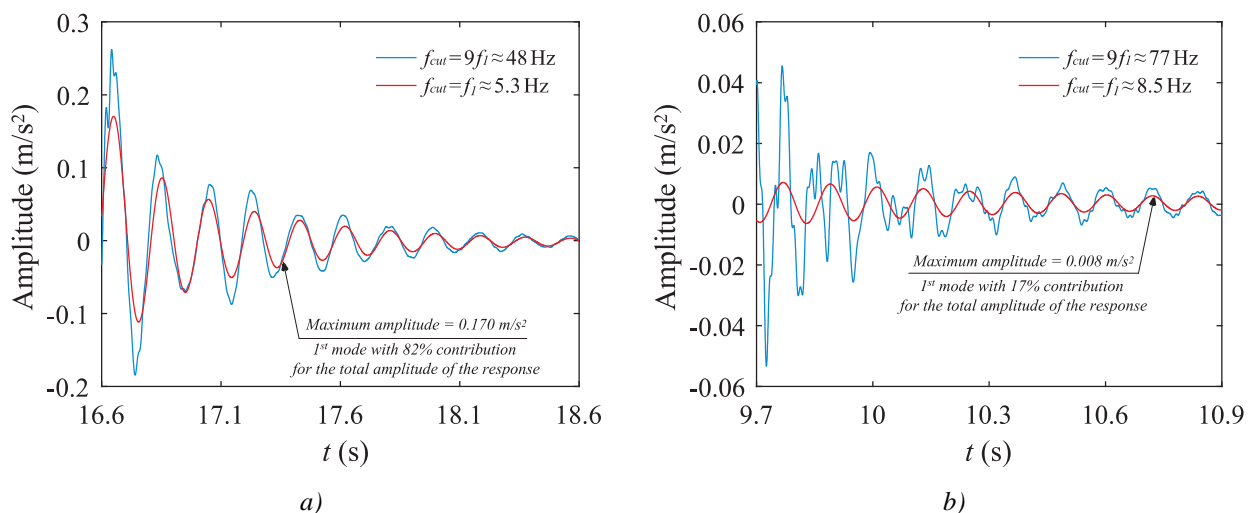

Figure 59: Example of a free decay response where: a) the fundamental first vertical bending mode is dominant, i.e., it has the highest contribution to the global response (bridge Ebr ü. Wenderterstraße in Germany); and b) the fundamental mode is not dominant, as higher modes, less prone to resonance, contribute more significantly to the overall response (bridge 001000_459+633 in France).

Considering the procedure described in this section, the following sections present the results and a critical analysis focusing only on the damping ratios obtained from near-resonant scenarios for each bridge type specified in Section 5.3.

5.4.2 Study of the "filler beam and reinforced concrete" bridge type

Figure 60 presents the estimated damping ratios for the *"filler beam and reinforced concrete"* bridge type as function of span and country. The damping ratios derived from near-resonant scenarios, following the procedure described in Section 5.4.1, are plotted with colour, while those obtained from scenarios where the fundamental bending mode was not dominant are shown in grey and should be disregarded for normative recommendations. For this particular bridge family, while some damping ratios that should be disregarded are notably close to the lower bound, certain valid estimated values still fall below the current normative proposal specified in EN 1991-2 (2023). It is noteworthy that most of these lowest damping values belong to the Swedish bridges, which in some cases, even considering the estimations obtained from forced vibration tests, are below the normative limit. Such behaviour may be related with the fact that these bridges have a particular

structural configuration when compared to the remaining ones, in which part of the abutment is integrated in the bridge deck through an over-sail (see Figure 56), resulting in an increased soil-structure interaction due to the back walls and wing walls that may influence both the frequency and damping of the resulting structure. To evaluate the possibility of proposing normative recommendations for this bridge type, these Swedish outliers and other relevant cases will be discussed further in Section 5.6.
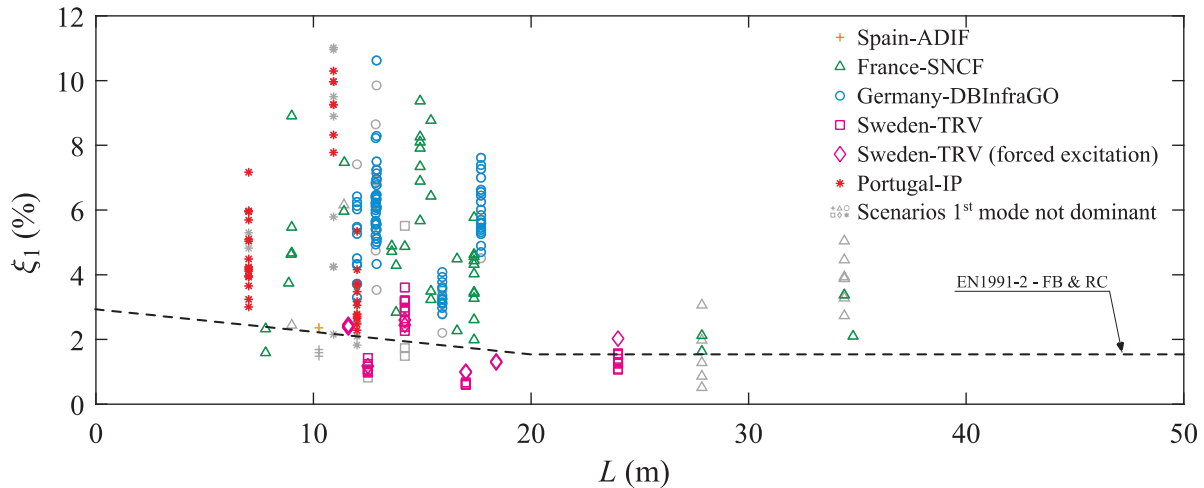

Figure 60: Identification of the damping ratios in the bridge type "filler beam and reinforced concrete" that are not majorly controlled by the fundamental vertical bending mode.

5.4.3 Study of the "portal frame" bridge type

Figure 61 presents the damping ratios estimated for the *"portal frame "* bridge type as function of span and country, in which the values derived from near-resonant scenarios, following the procedure described in Section 5.4.1, are plotted with colour, while those obtained from scenarios where the fundamental bending mode was not dominant are shown in grey. Since portal frames are not currently addressed in EN 1991-2 (2023), the normative curve depicted in Figure 61 corresponds to the *"filler beam and reinforced concrete"* bridge family, as it is the closest in structural terms to the former. By observing the figure, it is clear that the damping ratios are well above the aforementioned normative curve, since, as stated in Section 5.3, portal frame bridges exhibit significant structural damping primarily due to the radiation damping provided by the backfill soil.

An exception to the aforementioned trend can be observed in the two longer-span bridges (Gesällgatan North and South), which exhibit lower damping values closer to those of the current normative family, *"filler beam and reinforced concrete"*. Such behaviour may be justified by the fact that, for larger spans, the influence of soil-structure interaction that occurs through the abutments tends to diminish in the overall structural response. As a result, these bridges may also be typically classified under more common bridge types, such as reinforced or prestressed concrete bridges. For the particular cases of these bridges, since they are prestressed, they are also included in *"prestressed concrete"* bridge family, as will be seen next in Section 5.4.4. The same consideration for the Laguna Blanca bridge in Spain with 8 m span, since it is also prestressed. For this reason, these three bridges are highlighted in Figure 61
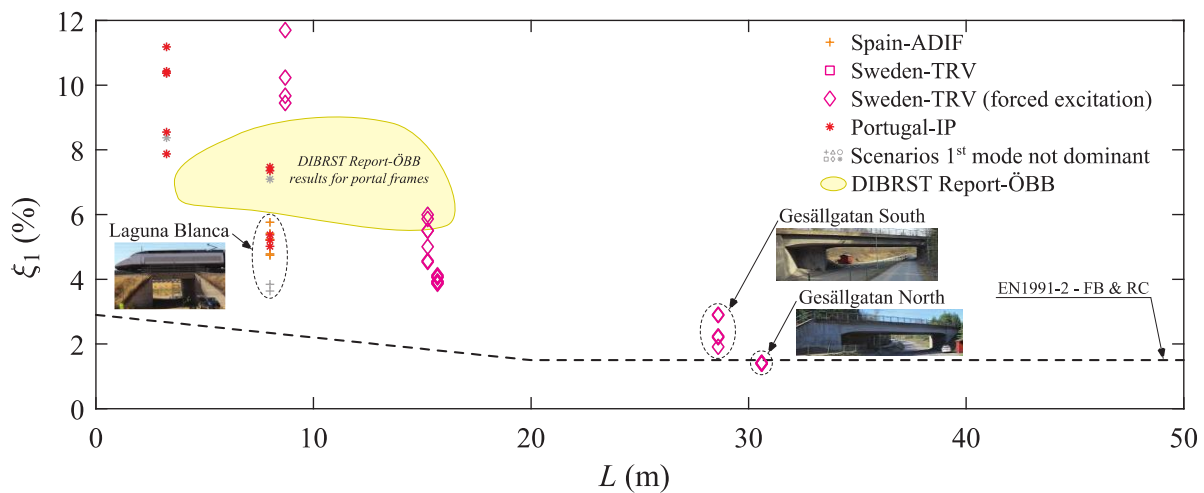
Figure 61: Identification of the damping ratios in the bridge type "portal frame" that are not majorly controlled by the fundamental vertical bending mode.

Finally, the CEN/TC250/SC1 drafted a report on the dynamic interface between railway bridges and rolling stock (DIBRST, 2023), which includes a catalogue of dynamic measurements conducted on existing portal frame bridges with spans up to 20 m by several Infrastructure Managers (DB InfraGO, ÖBB-Infra, Trafikverket, and Infraestruturas de Portugal), including damping estimations. While the damping values from Trafikverket and Infraestruturas de Portugal are those presented in this study, conducted during In2Track2 (2018) by KTH and UPORTO, respectively, the specific estimations carried out by ÖBB-Infra in each bridge are not publicly available, but the main envelope can be also observed in Figure 61. Although obtained with different algorithms, the damping values estimated by ÖBB-Infra range from 8.8% to 5.5% for spans between of 4 m to 16 m, aligning closely with the estimations made within InBridge4EU. Such results further justify a recommendation for possible inclusion of this bridge type in the definition of normative damping in railway bridges, as will be discussed in Chapter 6. Lower damping values were obtained by DB InfraGO at the time of these measurements, but these deviant/abnormal values will be discussed in Section 5.6.3.

5.4.4   Study of the "prestressed concrete" bridge type

The estimated damping ratios for the *"prestressed concrete"* bridge type are plotted in Figure 62 as function of span and country. As in the previous sections, the values obtained from scenarios where the fundamental bending mode was not dominant are shown in grey to distinguish the valid values from those that should be disregarded for normative recommendations, in accordance with the procedure described in Section 5.4.1. Once more, most of the damping ratios obtained from scenarios far from the resonant area present low values, some of them very close to the current normative curve for the prestressed concrete bridge type. By disregarding these values, it is possible to observe that the lower bound of the damping ratio obtained from the measurements is generally higher than the current value defined by the normative curve, thereby opening the possibility of increasing the normative damping for this type of bridge. Furthermore, the proposal from ERRI D214/RP3 (1999) is not entirely clear regarding the differentiation between prestressed and reinforced concrete bridges, which further supports the aforementioned suggestion. Therefore, recommendations for improvement the current normative curve will be addressed further in Chapter 6.

It is also important to note that, as observed previously for the reinforced concrete bridge type, the Swedish bridges show once more general lower damping values. Although these bridges are prestressed, the general structural configuration is similar to that presented before in Figure 56, which may justify the general lower damping from these bridges. Moreover, the two Swedish bridges, Gesällgatan North and South, with spans of

approximately 30 m, as well as the Spanish bridge, Laguna Blanca, with an 8 m span, may also be considered portal frames (see Section 5.4.3), since they have a fully closed continuous integral abutment. For this reason, they appear on both Figures 61 and 62.
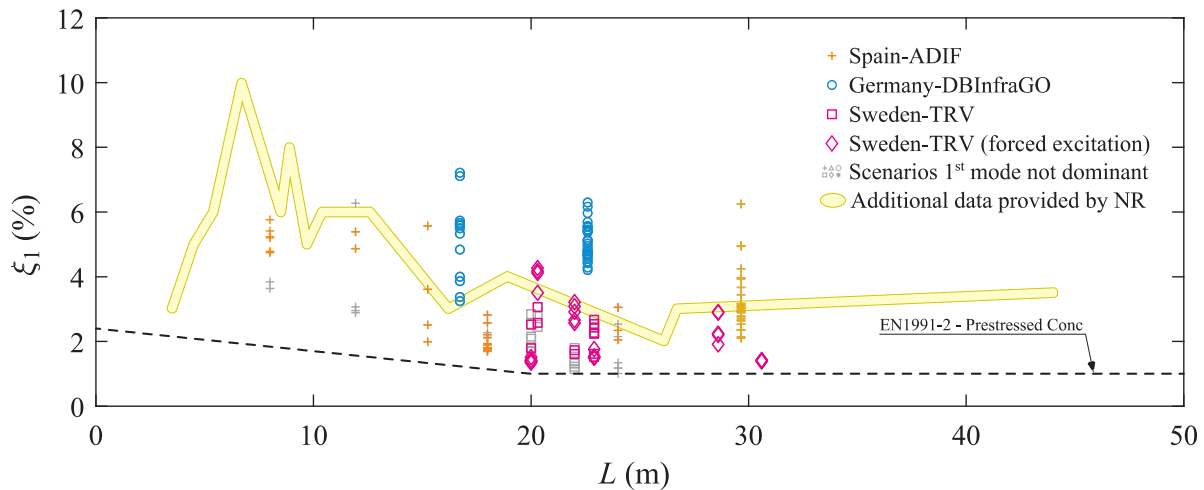

Figure 62: Identification of the damping ratios in the bridge type "prestressed concrete" that are not majorly controlled by the fundamental vertical bending mode.

Finally, damping estimations provided by Network Rail (NR) from 10 bridges with spans $3.5\,m < L < 15.0$ m, 3 bridges with spans $15.0\,m < L < 20.0\,m$ and 3 bridges with spans $25.0\,m < L < 45.0\,m$ are also included in Figure 62 for informational purposes only, indicating estimated critical damping values related to the first bending mode of $3\% < \xi_1 < 10\%$, $3\% < \xi_1 < 4\%$ and $2\% < \xi_1 < 3\%$, respectively. However, according to NR, these structures are reconstructed bridges, built to replace older ones using prestressed concrete elements installed during a single weekend closure of the railway line. As a result, unlike typical new bridges where prestressed elements are overlain by concrete slabs, these elements are allowed to move independently between them. This relative movements may generate friction at the joints, which can increase damping values beyond those typically expected for prestressed concrete. Moreover, these values were not estimated using the same procedures as in InBridge4EU and they should not be directly combined with those obtained in the project. Nevertheless, despite these conditions, this data may still provide support for the damping estimations conducted in InBridge4EU and is therefore also included in Figure 69 for informational purposes only.

5.4.5 *Study of the "steel-concrete composite" bridge type*

As mentioned in Section 5.3, the present work will study the possibility of splitting the current normative family steel and composite into two different bridge types. Hence, Figure 63 presents the damping ratios estimated for the newly proposed *"steel-concrete composite"* bridge type as function of span and country. Values from near-resonant scenarios, as described in Section 5.4.1, are in colour, while those from non-dominant bending modes appear in grey. Once again, the trend of low damping ratios in non-resonant scenarios persists for some of the bridges belonging from this bridge family, but, especially for bridges with spans smaller than 15 m, the lower bound continues to be defined by the current normative curve. However, except for one French bridge with span $L = 31.5\,m$ (bridge 242000_138+166), the lower bound of damping for longer-span bridges is slightly higher than the current normative curve, which also includes purely steel bridges. This suggests potential adjustments to the current curve, to be discussed in Chapter 6.
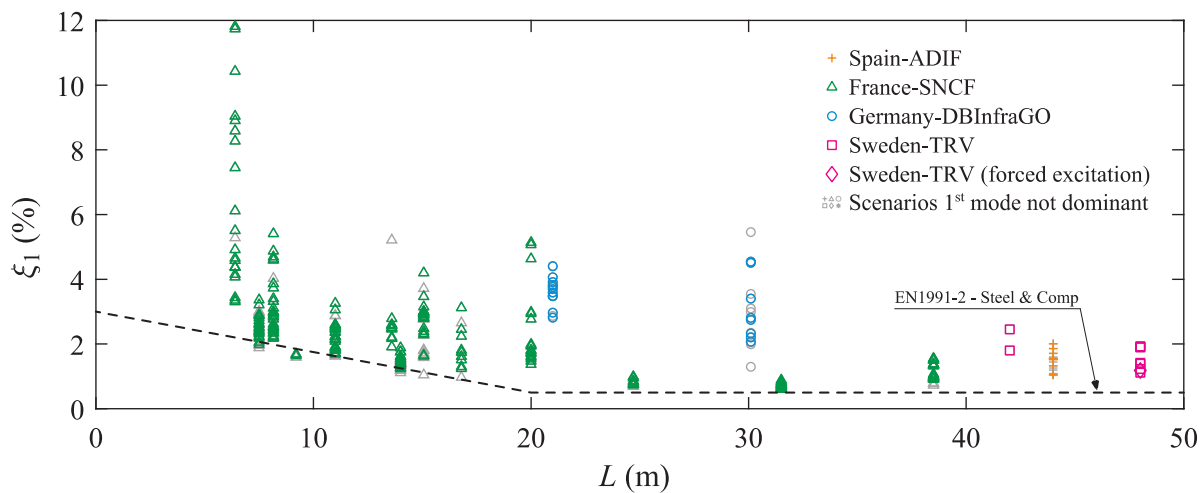
Figure 63: Identification of the damping ratios in the bridge type "steel-concrete composite" that are not majorly controlled by the fundamental vertical bending mode.

5.4.6   Study of the "steel" bridge type

Figure 64 presents the damping ratios estimated for the *"steel "* bridge type as function of span and country. Values from near-resonant scenarios, as described in Section 5.4.1, are in colour, while those from non-dominant bending modes appear in grey. For this bridge family, even excluding damping ratios from non-resonant scenarios, the overall lower bound closely aligns with the current normative curve. A large scatter is observed in all bridges, but unlike composite bridges, it is particularly pronounced in those with longer spans. No noticeably deviations or abnormal cases that significantly differ from the overall lower bound are observed in this bridge family, as will be discussed later in Section 5.6.6. Discussion about possible recommendations for changing the current normative curve will be presented in Chapter 6.

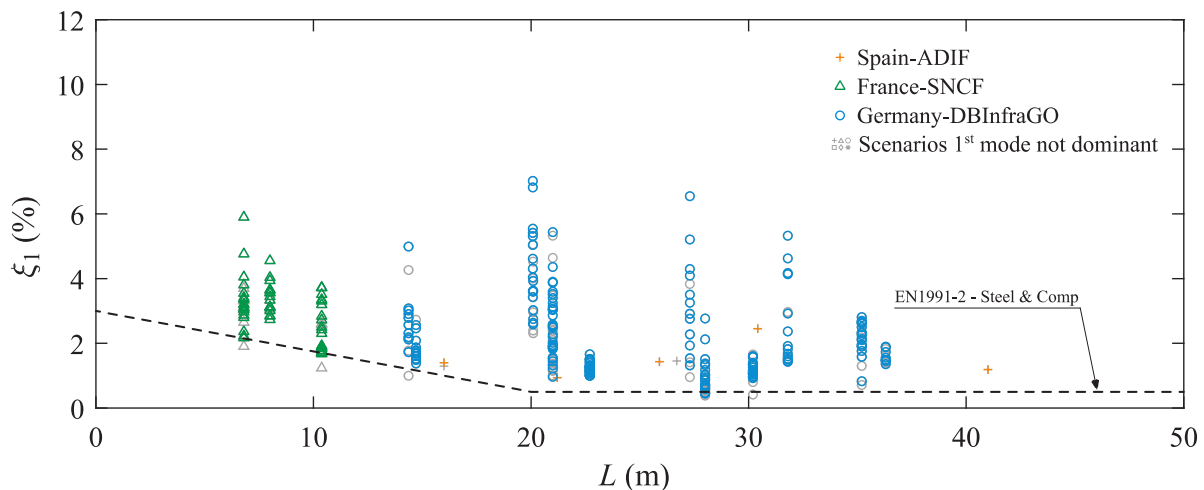*Figure 64: Identification of the damping ratios in the bridge type "steel" that are not majorly controlled by the fundamental vertical bending mode.*

5.5   Statistical analysis of the results

5.5.1   Foreword

Although the results presented in Section 5.4 are based on estimates from a wide range of bridge measurements (approximately 1,150 measurements conducted on about 90 bridges across five European

countries), the challenges of carrying out a large number of tests make it difficult to obtain a statistically representative dataset. Nevertheless, a statistical analysis of the results based on the procedure proposed by the Austrian norm ÖBB-Regelwerk 08.01.05 (2023), whose basis rely on the specifications defined in EN 1990-Annex D (2023), has been carried out for some bridges to check its validity on defining statistically reliable lower bounds of damping.

5.5.2 Analysis procedure

According to the procedure proposed by EN 1990-Annex D (2023) for the statistical determination of a single property, and adopted by ÖBB-Regelwerk 08.01.05 (2023) for the specific assessment of bridge damping based on dynamic tests, the determination of the 5% fractile of the variable (characteristic value) should follow the following assumptions:

- All variables follow either a Normal or a Log-Normal distribution.

- There is no prior knowledge about the mean value.

- The coefficient of variation V_x may or may not be known a priori.

Based on these assumptions, the damping value ξ_d is determined as the 5% fractile value of the tests for a 75% confidence level as

$$\xi_d = \eta_d \cdot \left(\bar{\bar{\xi}} - k_n \sigma\right) \tag{11}$$

where $\bar{\bar{\xi}}$ is the empirical mean obtained with the available test results, which, according to ÖBB-Regelwerk 08.01.05 (2023), should be at least 5, σ is the empirical standard deviation, η_d is a conversation factor dependent on the data quality, that should be taken as 1.0 or 0.9 if the data quality is good or average, respectively, and k_n is a factor given in Table 17 retrieved from EN 1990-Annex D (2023) or ÖBB-Regelwerk 08.01.05 (2023) that depends on the prior knowledge of the standard deviation. For damping assessment, since there is no prior knowledge of this quantity, only the k_n values for unknown standard deviations are considered. By looking to the values presented in Table 17, it is clear that k_n decreases significantly with a larger number of tests *n* and asymptotically approaches the value of 1.64, which corresponds to the 95% value of a standard normal distribution. Therefore, a high number of individual tests should be aimed to achieve the highest possible statistically secured fractile values.

Table 17: Values k_n for calculating the 5% fractiles with unknown standard deviations.

n	3	4	5	6	8	10	20	30	∞
k_n	3.37	2.63	2.33	2.18	2.00	1.92	1.76	1.73	1.64

To evaluate whether the assumption regarding the Normal or Log-Normal distribution of the damping is valid, the results obtained by KTH from the long-term monitoring of the Bryngeån bridge in Sweden have been analysed. This monitoring system, installed during the Shift2Rail In2Track2 (2018) project and still ongoing within InBridge4EU, consists of a series of sensors, including accelerometers, that continuously capture the bridge's response at various locations due to railway traffic. The bridge, which is part of the InBridge4EU database and has been used in WP4 for damping estimation (see Annex B), is a 48 m simply supported, single-track, steel-concrete composite bridge. To date, approximately 35,000 train passages have been recorded, with around 50% of them consisting of the X62 train type, also known as the Alstom Coradia Nordic.

The natural frequency and damping of the first bending mode have been estimated based on the free vibration response following train passages between June 2021 and February 2023. During positive temperatures, the average natural frequency was approximately 2.48 Hz, while the damping ratio was around 1.9%. These variations are illustrated in Figure 65, which includes only results obtained under positive temperatures and for the same train type, the X62. The frequency distribution aligns relatively well with a generalized extreme value (GEV) distribution, whereas the damping distribution does not conform to any conventional distribution functions. Its kurtosis β_2 exceeds 40, in contrast to the typical $\beta_2 = 3$ for a normal distribution, resulting in significantly thinner tails. This effect is evident in Figure 65b, where a narrower "bell" shape can be observed. Such an analysis, based on a much broader range of samples, indicates that the assumption of damping following a Normal or Log-Normal distribution is not entirely valid. Nevertheless, the statistical analysis mentioned above was still conducted to provide a clearer interpretation of the results.
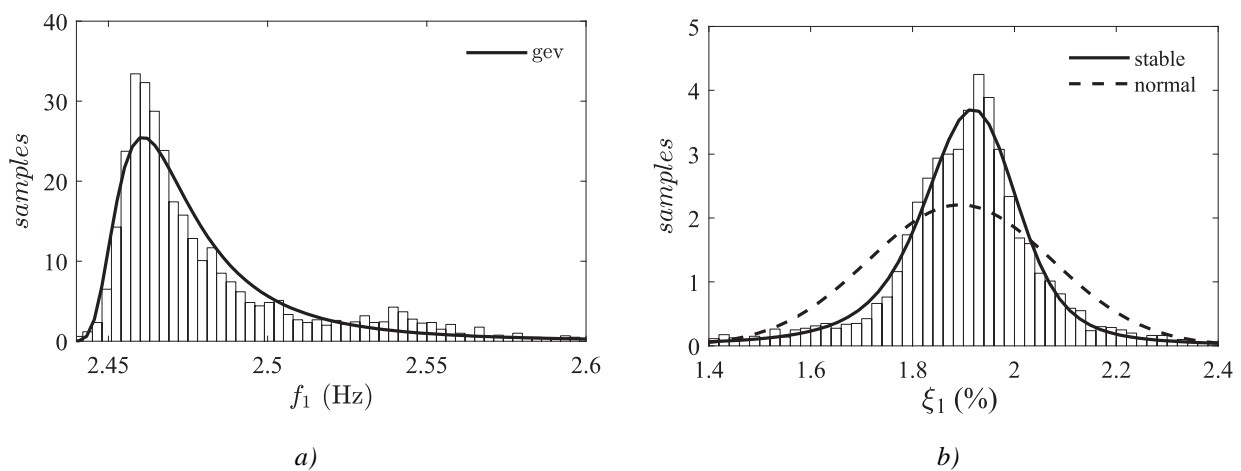

Figure 65: Distributions for the modal properties obtained with the passage of the X62 train: a) fundamental bending frequency and b) respective damping ratio.

By applying the aforementioned procedure, it is possible to perform a statistical analysis even with a limited number of measurements. In this project, an average of approximately 10 measurements is available per bridge. However, in cases of high damping scatter and, consequently, a large standard deviation, this statistical approach may result in extremely low values for the 5% fractile. This analysis is presented in the following sections.

5.5.3 Statistical analysis

The statistical analysis described in Section 5.5.2 has been conducted on a limited number of bridges to assess its suitability for studying damping. The selected bridges, whose span and estimated damping ranges, are presented in Table 18, were chosen to encompass all bridge types, varying spans and number of valid measurements and different levels of scatter in damping ratios. Thus, by applying Equation (11) to the damping estimation results obtained in each bridge, and taking into consideration the respective number of valid measurements n and factor k_n according to Table 17, it was possible to determine the 5% fractile value of damping ξ_d, as it can also be seen in Table 18 (ξ_d computed with η_d=1.0 considering good quality data).

By examining the results in Table 18, it becomes evident that, due to the significant scatter in damping across most bridges and the limited amount of data, the statistical 5% fractile value of damping is, in most cases, even lower than the estimated lower bound. Naturally, in cases with a larger number of valid measurements (e.g., Ebr ü.Wenderterstraße - ID5046 or Essen - ID17028 | 17553), this gap tends to decrease, as the empirical dataset approximates a normal distribution, leading to a scenario where the 5% fractile aligns

more closely with the empirical measurements. Moreover, in scenarios where the standard deviation is low when compared to the mean value (e.g., 282.943 - Ponte de Canelas or Aspan), even with a lower number of valid measurements, the gap between the lower bound of damping and 5% fractile tends to be less, as well.

On the other hand, in cases such as the 590000_235+895 and Bracea bridges, where there is either excessively high scatter (ξ =3.31% to 11.81%) or a very limited empirical dataset (only four valid measurements), respectively, the 5% fractile becomes extremely conservative and significantly lower than the lowest estimated damping value. In the latter case, the 5% fractile even results in a non-physical negative damping value, which should obviously be disregarded.

To clearly see the gap between the lower bound of estimated damping and the respective 5% fractile, Figure 66 plots the empirical estimated damping dataset of each of the aforementioned statistically studied bridges (the estimated damping values presented before in Section 5.4), as well as the 5% fractile.

Table 18: Selected bridges for statistical analysis and respective parameters and 5% fractile value ξ_d.

| Bridge name	Country	Type	Span (m)	n	k_n	Range ξ (%)	$\bar{\bar{\xi}}$ (%)	σ (%)	ξ_d (%)
Nuthe Drewitz - ID23194	Germany	Filler beam and reinforced concrete	17.70	20	1.76	4.70 – 7.61	6.02	0.84	4.55
Aspan	Sweden		24.00	10	1.92	1.07 – 2.03	1.41	0.28	0.86
282.943 - Ponte de Canelas	Portugal		12.00	13	1.87	1.61 – 5.34	3.25	0.83	1.69
Sodra Kungsvägen	Sweden	Portal frame	15.25	7	2.09	4.54 – 6.00	5.28	0.59	4.05
Bracea	Spain	Prestressed concrete	15.25	4	2.63	1.99 – 5.57	3.42	1.58	-0.75
Ebr ü.Wenderterstraße - ID5046	Germany		22.60	31	1.73	4.21 – 6.30	5.06	0.54	4.13
590000_235+895	France	Steel-concrete composite.	6.40	22	1.75	3.31 – 11.81	6.30	2.74	1.50
242000_138+166	France		31.50	21	1.76	0.60 – 0.89	0.71	0.08	0.57
Augsburg - ID31962	Germany	Steel	20.08	11	1.90	3.43 – 7.02	5.01	1.18	2.77
Essen - ID17028 | 17553	Germany		22.70	35	1.72	1.00 – 1.66	1.24	0.16	0.96
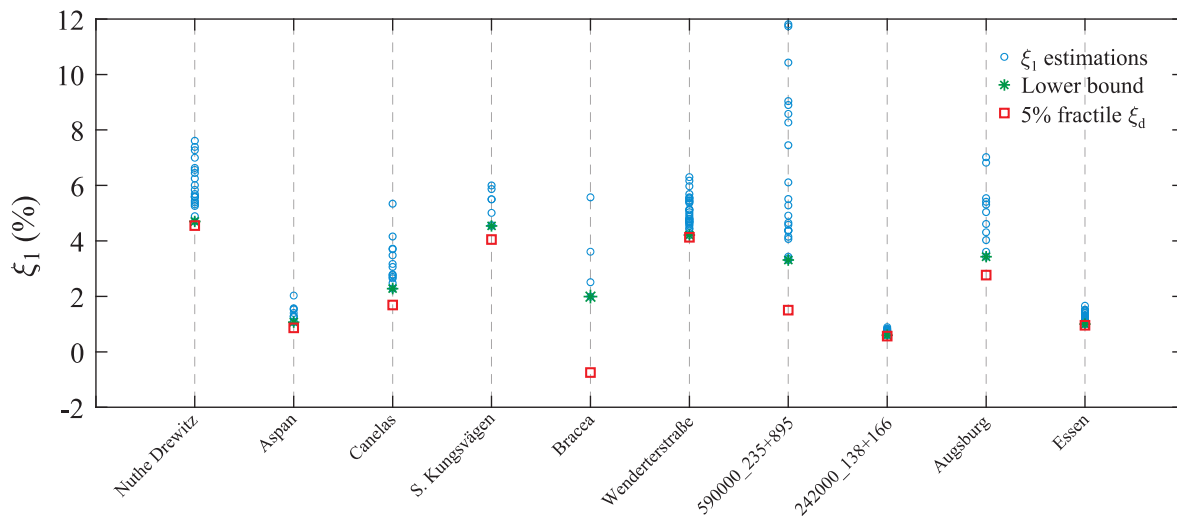
Figure 66: Empirical estimated damping dataset of measurements in the statistically studied bridges, together with the obtained 5% fractile.

Large damping scatter generally observed in most of the studied bridges in this project (see Figures 60 to 64) is a common outcome when measurements are conducted under railway traffic that can jeopardize an accurate statistical analysis of the results. In such cases, numerous uncontrolled variables influence damping, including energy dissipation within materials and supports, friction within assemblies, bridge condition (e.g., cracking or damage), and radiation damping through soil-structure interaction. Additionally, the limited amount of data, due to the time-consuming and economically costly nature of conducting measurements, along with the lack of evidence that damping may follow a normal distribution, as observed in the example of the Bryngeån bridge in Section 5.5.2, further challenges the statistical approach prescribed in EN 1990-Annex D (2023) and, for the particular case of damping estimation in railway bridges, specified in ÖBB-Regelwerk 08.01.05 (2023). As a result, a statistical approach based on fractiles tends to be overly conservative and should not be relied upon for proposing modifications to the current normative damping curves. For this reason, lower bounds of the estimated damping values for each bridge will be the main determinants and drivers of potential normative recommendations for railway bridge damping. However, particular damping value deviations that may overconservatively influence the normative proposals will be addressed next in Section 5.6, before concluding with final recommendations in Chapter 6.

5.6   Analysis of deviations that may condition the lower bounds of damping ratios

5.6.1   Foreword

By analysing and isolating the damping ratios estimated from measurements that closely resembled resonant scenarios in the previous section, a general increase in the overall lower bound for each bridge family was observed. This analysis offers an alternative to the approach previously developed by the D214 committee and documented in ERRI D214/RP3 (1999), which did not include a quantitative assessment of the contribution of the first mode more prone to resonance. As a result, all valid measurements were considered for the normative recommendation proposed by this committee, leading to excessively conservative lower bounds. Hence, the analysis presented in Section 5.4 aligns with the procedure recommended in the ERA Technical Note (2022) that led to the present project's call, which states that while conservative lower-bound damping values should be specified, low damping values from tests may be excluded if a valid justification for their exclusion is provided. However, even considering this upgrade, it is important to further examine the results obtained so far, particularly by assessing the significance of certain exceptionally low values of damping ratios, which may negatively influence the overall lower bound. This section aims to

conduct such an analysis for each bridge family, providing a critical interpretation of the obtained values to prevent excessively conservative recommendations. Ultimately, the identification of the final valid damping ratios will serve as the basis for the normative recommendation proposals discussed in Chapter 6.

5.6.2   Damping deviations in the "filler beam and reinforced concrete" bridge type

By observing Figure 60 in Section 5.4.2, it is possible to conclude that most of the damping values below the current normative limit belong to Swedish bridges, including those obtained from force vibration tests. Given that these bridges are particularly common in Sweden, special recommendations could be proposed in the form of a national annex to prevent a specific bridge type from influencing the overall normative damping ratios. However, even if the Swedish bridges were excluded from the general recommendation, there are still values below or very close to the current damping curve, particularly from France and Portugal. Naturally, given the successful experience in bridge design over the past 30 years using the current normative damping ratios, lowering the existing curve is clearly not recommended. Thus, based on the overall results presented in Figure 60, the authors do not find engineering rationale that may support its modification.

5.6.3   Damping deviations in the "portal frame" bridge type

The results presented in Figure 61 from Section 5.4.3 demonstrate a clear overall trend, consistently well above the current normative damping curve for the closest structurally comparable bridge family, the reinforced concrete bridge category. The only exception is the Gesällgatan North bridge, with a 30.6 m span, whose damping ratio is very close to the value currently specified in the code of 1.5 %. Nevertheless, portal frame bridges are particularly common in Europe for shorter spans, typically below 20 m, so this deviation does not compromise the normative recommendation for this new bridge category. Moreover, given their large spans and prestressed concrete construction, the Gesällgatan North and South bridges may also fit within the prestressed concrete bridge family, as will be addressed later.

Finally, it is worth noting that the CEN/TC250/SC1 draft report on the dynamic interface between railway bridges and rolling stock (DIBRST, 2023) also presented damping estimations for portal frames with spans shorter than 20 m from various Infrastructure Managers (DB InfraGO, ÖBB-Infra, Trafikverket, and Infraestruturas de Portugal), as briefly mentioned in Section 5.4.3. While most results align well with those estimated in this work within InBridge4EU, some exceptions were found in the estimations from DB InfraGO, where generally low damping values were obtained. However, DB InfraGO clarified that these estimations were derived using basic LD methods with automatically processed sensor data, without human intervention in data analysis. Given these factors, along with the use of different algorithms and assumptions from those applied in this study (as described in Chapter 3), these anomalous results will not be considered in the normative recommendations proposed in Chapter 6.

5.6.4   Damping deviations in the "prestressed concrete" bridge type

Prestressed concrete bridges do not show any particular low damping ratio that may not fit in the overall trend of results, as it can be seen in Figure 62 from Section 5.6.4. As mentioned before, the overall lower bound, after disregarding scenarios far from the resonant area, is above the current normative curve defined in EN 1991-2 (2023) for this type of bridge. The lowest damping values of ξ_1 of 1.34 % and 1.38 % are attributed to the Swedish bridges Enköpingsvägen ($L = 20.0$ m) and Gesällgatan North ($L = 30.6$ m), respectively.

Regarding Enköpingsvägen, it is interesting to note that, unlike most other Swedish bridges, which exhibit higher damping values when estimated from tests under forced excitation, this bridge shows the opposite trend, since its damping ratios obtained from tests under railway traffic are higher ($\xi_1 = 1.79{\sim}2.52$ % under railway traffic and $\xi_1 = 1.34{\sim}1.51$ % under forced excitation, see Appendix B). Another example exhibiting this behaviour is the Taxinge bridge ($L = 22.9$ m), also in Sweden, with damping ratios of $\xi_1 = 1.53{\sim}2.67$ % under

railway traffic and $\xi_1 = 1.50 \sim 1.76$ % under forced excitation (see Appendix B). However, in this case, the maximum amplitude levels recorded in both tests are similar ($A_1 = 0.139 \sim 0.485$ m/s^2 under railway traffic and $A_1 = 0.250 \sim 0.450$ m/s^2 under forced excitation, see Appendix B). In contrast, for Enköpingsvägen, the amplitude recorded in the forced excitation test is significantly higher than that observed under railway traffic ($A_1 = 0.046 \sim 0.148$ m/s^2 under railway traffic against $A_1 = 0.250 \sim 0.700$ m/s^2 under forced excitation, see Appendix B). Although no clear correlation between amplitude and damping was identified (see Section 5.2), this similarity in amplitude levels makes the results from the Taxinge bridge more directly comparable, whereas Enköpingsvägen clearly stands out as an anomalous case.

With respect to Gesällgatan North, no valid damping estimations could be obtained through measurements under railway traffic, but given this bridge's similarity to a portal frame, it is not entirely comparable to the other more typical prestressed bridges, such as girder bridges or box girders. Nevertheless, the lowest damping value is very close to the current normative value of 1.5 % for the filler beam and reinforced concrete bridges, pointing to a lack of justification to separate the prestressed bridges from the former in terms of normative damping. Moreover, as mentioned before, the proposal from ERRI D214/RP3 (1999) to differentiate these two bridge categories is not clear according to the results obtained at the time, which also supports a possible change in the normative curve, as will be addressed in Chapter 6.

5.6.5 *Damping deviations in the "steel-concrete composite" bridge type*

For the larger span lengths, above 20 m, composite bridges show an overall lower bound of damping slightly above the current value defined for the steel bridges of 0.5 %. Two French bridges, however, namely 810000_097+770 (L = 24.7 m) and 242000_138+166 (L = 31.5 m) show damping estimations with small scatter, but with particular low value, namely $\xi_1 = 0.73 \sim 0.99$ % and $\xi_1 = 0.60 \sim 0.89$ %, respectively. This bridge's structural solution differs slightly from the full "U"-shaped bridges for spans up to 20 m with a steel sheet at the bottom (see example in Figure 67a), which, according to SNCF Réseau, are almost exclusively used in France (all French composite bridges studied in this work with L < 20 m are of this type, see Annex B). Instead, the two bridges mentioned above have the lower flanges of the upper lateral inclined girders connected by transversal spaced steel girders encased in concrete, as shown in Figure 67b, and are typically used in France for single-track bridges with spans ranging from 20 m to 30 m. According to SNCF Réseau, this bridge solution is commonly adopted when replacing ballastless bridges within this span range or to accommodate specific gauge constraints and are characterized by low mass (for these cases around 11 t/m), which likely explains the low damping observed. Therefore, although the damping values observed in these composite sub-bridge type are still above the current normative value for steel-composite bridges of 0.5%, they will be treated as exceptions in the proposal for the new steel-concrete composite bridge type presented later in Chapter 6.
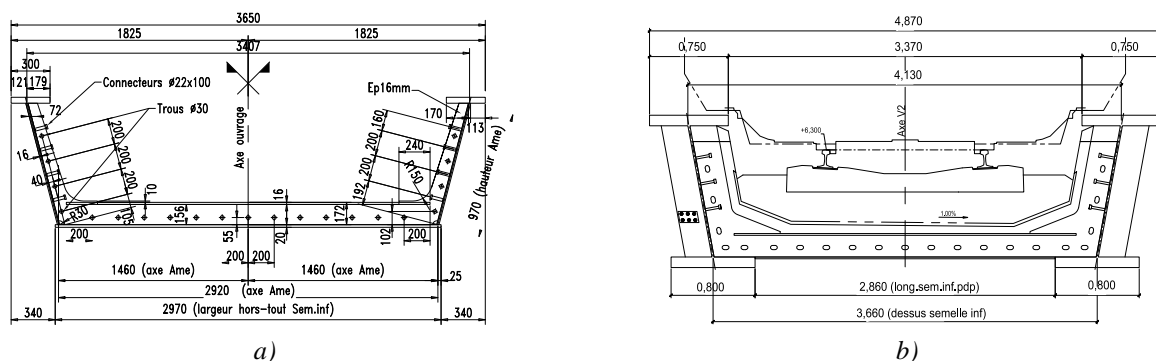

a)   *b)*

Figure 67: Cross-section of the French composite bridges: a) "U"-shape composite with steel sheet in the bottom 070000_219+422 (L = 9.2 m) and b) Upper lateral inclined girders composite connected by spaced steel transversal beam at the bottom 810000_097+770 (L = 24.7 m).

For a broader analysis, the results obtained by the ERRI D214 committee in the 1990s for composite bridges (ERRI D214/RP3, 1999) have also been revisited in this work. Although the damping ratios were estimated using different algorithms, which may make a direct comparison less reliable due to the lack of benchmarking between the methods used in this study and those applied by the ERRI D214 committee, it is still valuable to conduct a general analysis of the results for comparison purposes. Table 19 presents the results obtained in ERRI D214/RP3 (1999) for the steel-concrete bridges, together with some information provided in the report.

By examining Table 19, it is important to highlight two points:

- All damping ratios from these bridges were estimated using the simplest available method, the Logarithmic Decrement (LD). This method has significant limitations, particularly when the first mode is not clearly isolated, as the presence of other modes with similar natural frequencies may adversely affect the estimation, leading to less accurate results.

- There is some lack of coherence in the number of cycles used to estimate damping, ranging from 5 in the Massy-Lyon line, Pompadour sector OA49/25 bridge to 88 in the estimation carried out by LREP in the Paris-Lille line, Saint Denis PK6.382. Such a situation may reduce the reliability of comparisons.

Next, assuming that the previously mentioned limitations are acknowledged, the following conclusions can be drawn from the data presented ERRI D214/RP3 (1999) summarized in Table 19:

- Massy-Lyon line – Pompadour sector OA49/25: this bridge presents a considerable high damping, therefore, it would not affect the lower bound.

- Le Mans-Angers line – Vieux Briollay PK 293.020: This bridge exhibits notably low damping ($\xi_1 = 0.57\%$), and all the results presented in ERRI D214/RP3 (1999) appear to be reliable. The amplitude of the free decay recorded for the passage of one of the six analysed trains (TGV5dd) is significantly higher than that observed for the other five trains (approximately 0.04 m/s² for the TGV5dd, compared to values below 0.02 m/s² for the others), resulting in a higher estimated damping (around $\xi_1 = 0.90\%$). Nevertheless, despite the use of the less accurate LD method for damping estimation, the lower bound remains $\xi_1 = 0.57\%$, which stands as an exception compared to the other bridges.

- Paris-Lille line – bridge on the Bip: the report establishes a damping lower bound of $\xi_1 = 0.54\%$ in the final recommendation graphic (previously shown in Figure 57) as well as in its Annexes C and D. However, in Annex B – Figure 3.12 of ERRI D214/RP3 (1999), the minimum estimated damping appears to fall between 0.75% and 1.00%, with most of the estimations clearly above the latter. Since AVLS is also part of the InBridge4EU consortium, it was possible to verify this discrepancy in the original AVLS report, confirming that the correct lower value is $\xi_1 = 0.87\%$.

- Paris-Lille line – Saint Denis PK6.382: this bridge has been studied by two entities with considerably different lower bound damping values ($\xi_1 = 0.85\%$ by LREP vs $\xi_1 = 1.60\%$ by SNCF-VR10). However, by observing the information given in the D214/RP3 report and summarized in Table 19, the authors state that they used an excessive number of cycles and a not so accurate method, namely a graphically calculated decrement with log paper. In addition to this point, the amplitude of the free decay used by SNCF-VR10 is 10 times larger than that of LREP, which further supports the suggestion that the results obtained by the former ($\xi_1 = 1.60\%$) is more credible.

- Paris-Saint Lazare region – Maison Lafitte: the results obtained for these bridges raised the following concerns to the ERRI/D214 committee: i) the excessive number of cycles considered for the free decay, and ii) the measured eigenfrequency for a 66 m span bridge was too high (14.3 Hz) for this kind of

spans, leading them to consider one-tenth of its value (1.43 Hz). Based on these concerns from the ERRI/D214 committee, the authors of the present deliverable believe that the estimated damping of $\xi_1 = 0.70\%$ may present some doubts and lack of reliability and should not be considered for a normative recommendation.

- Bebra-Göttingen line – PK 238.220: this bridge presents a considerable high damping, therefore, it would not affect the lower bound.

In summary, from the six steel-concrete composite bridges analysed by the ERRI/D214 committee, three of them showed considerable high damping above 1% (Massy-Lyon line – Pompadour sector OA49/25, Paris-Lille line – Saint Denis PK6.382 and Bebra-Göttingen line – PK 238.220), one presented a damping ratio close to 1% (Paris-Lille line – bridge on the Bip), one presented low damping but with unreliable results due to the method used and the misleading frequency (Paris-Saint Lazare region – Maison Lafitte) and one presented credible low damping values between 0.57 % and 0.90 % (Le Mans-Angers line – Vieux Briollay PK 293.020). Therefore, and although direct comparisons with the results obtained in InBridge4EU should not be carried out due to the differences in the methods used to estimate damping, all of them, except the latter, present results that fit in the steel-concrete composite overall lower bound presented in Figure 63. This topic will be revisited later in Chapter 6 when drawing the final conclusions and normative recommendations.

Table 19: Damping estimations for steel-concrete composite bridges in ERRI D214/RP3 (1999).

Bridge name	Responsible entity	Structural solution	Span (m)	ξ_1 (%)	Information provided in ERRI D214/RP3 (1999)
Massy-Lyon line, Pompadour sector OA49/25	AVLS (France)	Steel girders with concrete slab on the top	46.00	1.90	Signal filtered around first eigenfrequency, followed by LD over 5 cycles
Le Mans-Angers line, Vieux Briollay PK 293.020	AVLS (France)	Steel girders with concrete slab on the top	38.00	0.57	Signal filtered around first eigenfrequency, followed by LD at the beginning and end of the free decay
Paris-Lille line, bridge on the Bip	AVLS (France)	Steel girders with concrete slab on the top	34.90	0.54 0.87	Signal filtered around first eigenfrequency, followed by LD over 20 cycles (discrepancy in the damping ratio)
Paris-Lille line, Saint Denis PK6.382	LREP (France)	Steel girders with concrete slab on the top	59.80	0.85	LD calculated graphically in log paper over 88 cycles with oscillations of the order of 0.2 mm at midspan (excessive number of cycles)
	SNCF – VR10 (France)			1.60	No information, except that the oscillations at the midspan were of the order of 3 mm
Paris-Saint Lazare region, Maison Lafitte	LREP (France)	Steel girders with concrete slab on the top	66.00	0.70	LD calculated graphically in log paper over 88 cycles with oscillations of the order of 0.2 mm at midspan (excessive number of cycles). Warning: 1st eigenfrequency measured of 14.3 Hz very high for a 66 m span bridge, therefore, the frequency was replaced by 1.43 Hz.
Bebra-Göttingen line, PK 238.220	DB (Germany)	Steel girders with concrete slab on the top	13.00	4.90	Computed through the LD (no more information provided)

5.6.6   Damping deviations in the "steel" bridge type

As mentioned in Section 5.4.6, a particularly large scatter of results can be observed for large-span bridges (see Figure 64). However, the overall lower bound, even after disregarding non-resonant scenarios, closely aligns with the current normative curve for steel bridges as stipulated in EN 1991-2 (2023). Similarly, for the *"filler beam and reinforced concrete"* bridge category, no noticeably deviations or abnormal cases significantly differing from the overall lower bound are observed. While a few cases fall slightly below the curve, they should not be considered, given the successful track record of bridge design over the past 30 years using the current normative damping ratios. It is also worth mentioning that a significant number of steel bridges were analysed by the ERRI/D214 committee (see Figure 57). For some of these bridges with spans greater than 20 m, the estimated damping values are very close to, or in some cases even lower than, the currently specified normative damping of 0.5%. Therefore, based on the available data, there is a lack of engineering rationale for proposing changes to the normative curve for the *"steel"* bridge family currently specified in the code.

6   NORMATIVE RECOMMENDATIONS AND CONCLUSIONS

6.1   Initial considerations

While Chapter 4 presented the damping ratios estimated for all 88 bridges studied in this work, based on more than 1,000 measurements, Chapter 5 focused on processing these results and critically analysing them to identify scenarios that should not be considered for normative recommendations due to their non-resonant nature. Furthermore, scientific and engineering reasoning was applied to understand the causes of values that deviate from the overall trend. This analysis aimed to support the development of normative proposals that could be incorporated into current codes, promoting more economically efficient bridge design without compromising structural integrity or the train running safety. Therefore, the normative recommendations will be presented in the following sections related to each bridge type (Sections 6.2.1 to 6.2.5), culminating with a summary of those proposals in Section 6.3 and conclusions and future recommendations in Section 6.4.

6.2   Normative recommendations for each bridge type

6.2.1   Normative recommendations for the "filler beam and reinforced concrete" bridge type

As mentioned before in Section 5.4.2, even after disregarding scenarios that not aligned with near-resonant situations, certain valid estimated values continue to be aligned with the current normative curve for *"filler beam and reinforced concrete"* bridges and some of them even fall below it, in particular those from the Swedish bridges, but also some from Portugal and France. Hence, taking into consideration the available data, which exhibits, in general, an overall lower bound even lower than that obtained by the ERRI/D214 committee presented in ERRI D214/RP3 (1999) and transposed to Figure 57, the authors do not find engineering rationale that may support an enhancement of the current normative curve for this bridge type. Nevertheless, the observation of the results presented in Figure 60 suggests, in general, that the damping values estimated from tests under forced excitation show slightly higher values than those obtained from tests under railway traffic (see also Andersson et al. (2021)). The authors recommend that, in the future, additional tests under forced excitation should be conducted on other more typical bridge types (such as simply supported bridges) to assess their suitability for achieving larger damping ratios. This type of testing allows for exciting the bridge at controlled frequencies that resemble the structure's natural frequency, thereby inducing controlled resonance scenarios from which more accurate damping estimations may be obtained. Results obtained by Reiterer et al.

(2017) also indicate a more accurate estimation of damping using controlled tests under forced excitation, both in terms of higher damping values and reduced scatter between measurements.

6.2.2 Normative recommendations for the "portal frame" bridge type

Portal frame bridges are not currently addressed in EN 1991-2 (2023) in terms of bridge damping. However, the results presented in Section 5.4.3 indicate that, for spans shorter than 20 m, there is a clear trend of significantly higher damping compared to the closest bridge type in structural terms, the *"reinforced concrete"* bridge type. Thus, a new normative damping curve is proposed from the results that arise from this project that covers the current observed lower bounds plotted in Figure 61 and simultaneously respects the lower values observed in the two only large span portal frames / prestressed concrete bridges studied in this work, the Swedish Gesällgatan North and South. Moreover, and although computed with different algorithms, it also covers the values estimated by ÖBB-Infra and presented in the report on the dynamic interface between railway bridges and rolling stock (DIBRST, 2023), which point to damping ratios ranging from 8.8% to 5.5% for spans between of 4 m to 16 m (see Section 5.4.3 and the cloud plotted in Figure 61, since the specific values cannot be published due to confidentiality reasons).

Figure 68 presents the original damping curve stipulated in EN 1991-2 (2023) for the *"filler beam and reinforced concrete"* bridges together with the lower bound damping estimations and the newly proposed curve based on the results obtained in this project. It can be observed that the recommended curve for the *"portal frame"* bridge type successfully covers the lower bound of estimated damping (including those studied by ÖBB, see cloud plotted in Figure 68) while still significantly increasing the values currently prescribed by the standard. Regarding larger span bridges ($L > 20$ m), the lack of data and the results obtained in Gesällgatan North and South point to a damping value in the same order of magnitude of the current curve. Finally, to avoid a sudden discontinuity in damping values at $L = 20$m, an intermediate segment has been added for a smoother transition in the range 15 m $\leq L \leq 20$ m (the data in this area is scarce). Thus, the piecewise function curve that defines the damping for the portal frame bridges as function of their span L and plotted in Figure 68 is given by:

$$\begin{cases} \xi = 3.00 + 0.15 \cdot (20 - L) & ; \quad L < 15 \text{ m} \\ \xi = 1.50 + 0.45 \cdot (20 - L) & ; \quad 15 \text{ m} \leq L < 20 \text{ m} \\ \xi = 1.50 & ; \quad L \geq 20 \text{ m} \end{cases} \tag{12}$$
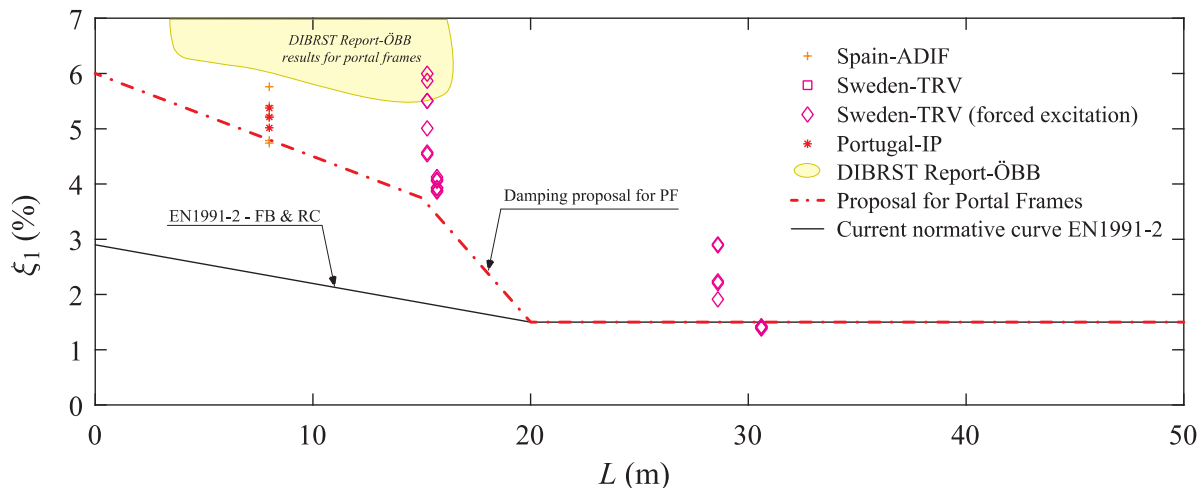

Figure 68: Comparison between the current stipulated curve in EN 1991-2 (2023) for the "filler beam and reinforced concrete" bridge type and the newly proposed curve for the "portal frame" bridge category.

6.2.3   Normative recommendations for the "prestressed concrete" bridge type

As observed in Section 5.4.4, when disregarding non-near-resonant scenarios, the overall lower bound of the damping ratio is generally higher than the value currently defined by the normative curve for "prestressed concrete" bridges. Additionally, the ERRI D214/RP3 (1999) does not clearly differentiate between prestressed and reinforced concrete bridges, as no damping values related to the former bridge type appear between their damping normative curves, as seen in Figure 57 and discussed in Section 5.3. In fact, ERRI D214/RP3 (1999) does not explicitly distinguish between these two bridge types in its core report or annexes. Given these considerations, a revision of the current curve is justified, which consists of merging the *"prestressed concrete"* type in the current *"filler beam and reinforced concrete"* bridge category. Such merge allows a 0.5% increase in damping for the prestressed concrete bridges without violating the lower bounds observed in the measurements. The only exception stands for the Swedish Enköpingsvägen bridge ($L = 20.0$ m) and Gesällgatan North ($L = 30.6$ m), but as mentioned in Section 5.6.4, the former is a clear outlier, while the latter presents a minimum damping ratio of $\xi_1 = 1.38$ %, which is very close to 1.5 %. Moreover, all the Swedish bridges, including those studied in the reinforced concrete family, presented general lower damping values, which can be justified by the particular structural type of these bridges with continuous decks with integrated wingwalls and backwalls that interact with the adjacent embankment (integral abutments). For this reason, the authors propose a damping normative curve that is not conditioned by these deviant/abnormal situations (see Figure 69), and that can be expressed by the piecewise function that it is currently associated only to the reinforced concrete bridges given by:

$$\begin{cases} \xi = 1.50 + 0.07 \cdot (20 - L) & ; \quad L < 20 \text{ m} \\ \xi = 1.50 & ; \quad L \geq 20 \text{ m} \end{cases} \tag{13}$$
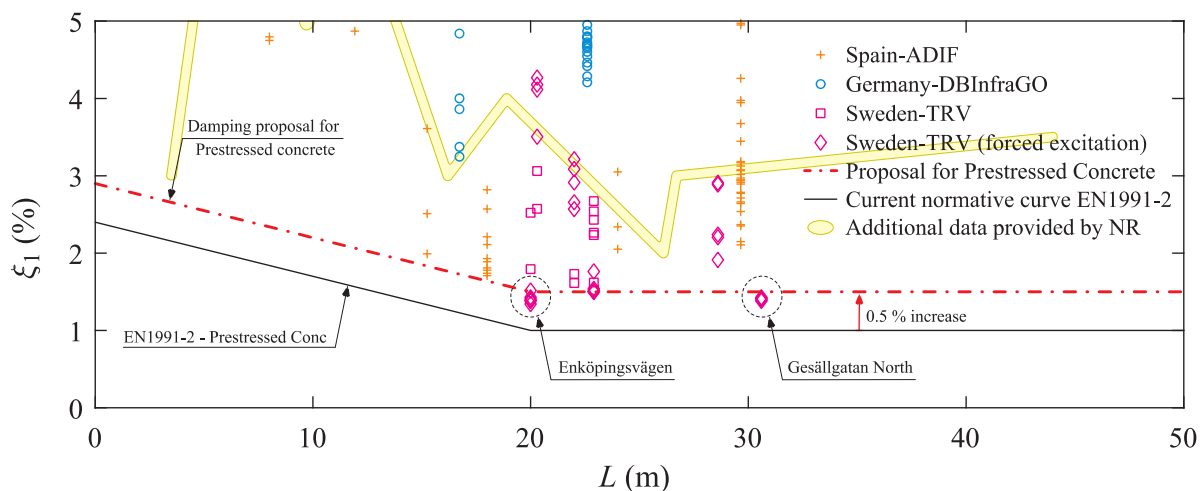

Figure 69: Comparison between the current stipulated curve in EN 1991-2 (2023) for the "prestressed concrete" bridge type and the newly proposed curve for this category.

The data available to support this modification, however, pertains to bridges with spans ranging from approximately 8 m to 31 m. Nevertheless, data provided by Network Rail from 10 bridges with spans 3.5 m < L < 15.0 m, 3 bridges with spans 15.0 m < L < 20.0 m and 3 bridges with spans 25.0 m < L < 45.0 m indicate estimated critical damping values related to the first bending mode of 3% < ξ_1 < 10%, 3% < ξ_1 < 4% and 2% < ξ_1 < 3%, respectively. Since these values were not estimated using the same procedures as in InBridge4EU, they are presented here and plotted in Figure 69 for informational purposes only. However, caution should be exercised when interpreting these values from NR, as explained in Section 5.4.4. Therefore, while these values

may help support the proposed recommendations for prestressed concrete bridges, the evaluation of damping in the ranges below 8 m and above 31 m should be considered an open issue at this stage.

6.2.4   Normative recommendations for the "steel-concrete composite" bridge type

Steel-concrete composite bridges are currently classified within the same normative damping family as steel bridges, with a lower damping bound of 0.5% for spans greater than 20 m. However, composite bridges are generally heavier than steel bridges due to the presence of concrete, typically in the form of a top (or bottom) slab, which often results in higher structural damping. As an example, the composite bridges BadOldesloe ($L = 30.10$ m) and Banafjällsån ($L = 42.00$ m) weigh 13.14 t/m and 16.93 t/m, respectively, while the steel bridges Boppard ($L = 31.80$ m), Braunschweig ($L = 35.20$ m) and Duisburg ($L = 30.20$ m) weigh only 8.93 t/m, 4.09 t/m and 5.90 t/m, respectively (see Annex B). Thus, considering the results presented in Figure 63, along with the extensive evaluation and justification for the low damping deviations observed in both the current database and the ERRI D214/RP3 (1999) dataset, this work will propose a normative revision for composite bridge damping, separating them from steel bridges.

The present proposal consists of keeping the current normative curve specified in EN 1991-2 (2023) for spans shorter than 20 m and increasing the damping from 0.5 % to 1.0 % in the larger spans, where the bridges tend to behave somewhere between steel bridges and reinforced/prestressed concrete bridges. However, similar to the portal frame bridge proposal, to avoid discontinuities in the damping curve at $L = 20$m, an additional segment been added to it for a smoother transition in the range $15\,\text{m} \leq L \leq 20\,\text{m}$. Hence, the piecewise function curve that defines the damping for the steel-concrete composite bridges as function of their span L is presented in and given by the following equation:

$$\begin{cases} \xi = 0.50 + 0.125 \cdot (20 - L) & ; \quad L < 15\,\text{m} \\ \xi = 1.00 + 0.025 \cdot (20 - L) & ; \quad 15\,\text{m} \leq L < 20\,\text{m} \\ \xi = 1.00 & ; \quad L \geq 20\,\text{m} \end{cases} \tag{14}$$

The newly proposed curve for the *"steel-concrete composite"* bridges, as defined by Equation (14), is shown in Figure 70, alongside the current normative curve specified in the code and the lowest damping values obtained from the estimations within the InBridge4EU project. It can be observed that, for spans shorter than 20 m, there are still a few French bridges whose lower bounds of damping fall below the current curve. However, as seen in other cases (such as the *"filler beam and reinforced concrete"* family), lowering the current curve is not recommended, given the successful experience in bridge design to date. As for longer spans, and as discussed in Section 5.6.5, the two French bridges 810000_097+770 ($L = 24.7$ m) and 242000_138+166 ($L = 31.5$ m), highlighted in the figure, are clearly below the proposed recommendation of $\xi = 1.00$ %. This may be associated with the explanation provided earlier in Section 5.6.5, where it was indicated that the mass of this subtype of composite bridge (upper lateral inclined girders composite connected by spaced steel transversal beams,, see Figure 67b) is lower compared to other composite bridges, such as those with steel girders and a heavy concrete slab on top (or sometimes on the bottom), which may consequently reduce their structural damping. Thus, unless further information proves otherwise, it is proposed that these upper lateral inclined girders composite connected by spaced steel transversal beams with spans longer than 20 m be excluded from this normative proposal for general composite bridges and be included in the *"steel"* bridge family, as described in Section 6.2.5. However, a more generic criterion that includes the ratios between concrete and steel, as well as their contribution to the global bending mode of the bridge, would

be worth studying if more data were available. Such criterion should be recognized as an open point for future revisions.

Finally, it is important to note that the damping values obtained for the composite bridges studied ERRI D214/RP3 (1999) have also been included in Figure 70 for a clearer comparison with the results from InBridge4EU (a detailed discussion about the ERRI D214 committee damping estimations is presented in Section 5.6.5). Note that, since the graphs are limited to $L = 50$ m, the damping from the Saint Denis PK6.382 ($L = 59.80$ m) and Maison Lafitte ($L = 66.00$ m) bridges (see Table 19) are plot in $L = 50$ m for fitting purposes. Although three bridges show damping below the proposed recommendations, only Vieux Briollay PK 293.020 ($L = 38.00$ m) is a clear outlier. With respect to the other two, the bridge on the Bip has its lowest damping value of $\xi_1 = 0.87\%$, which is very close to 1 % (but with most of the estimations shown in ERRI D214/RP3 (1999) well above this value), and may be considered to fit in the proposed recommendation. As for the Maison Lafitte bridge, the authors of ERRI D214/RP3 (1999) clearly warn the readers about the uncertainty in the estimated damping ratio's reliability ($\xi_1 = 0.70\%$), given the lack of confidence in the bridge's frequency assessment (the authors refer that the obtained frequency of 14.3 Hz is completely inconsistent with the expected frequency range for bridges of this span) and the use of an excessive number of cycles in the damping evaluation. In addition to these limitations, as described in Section 5.6.5, it is worth noting that all these bridges have been analysed using the most simplified damping method, the LD, which is known for not producing very accurate results in certain situations where the free decay is not clearly defined. Considering the aforementioned rationale, it is suggested that the Vieux Briollay PK 293.020 outlier should not condition the overall damping lower bound and, consequently, the proposed increase in damping for composite bridges with longer spans.
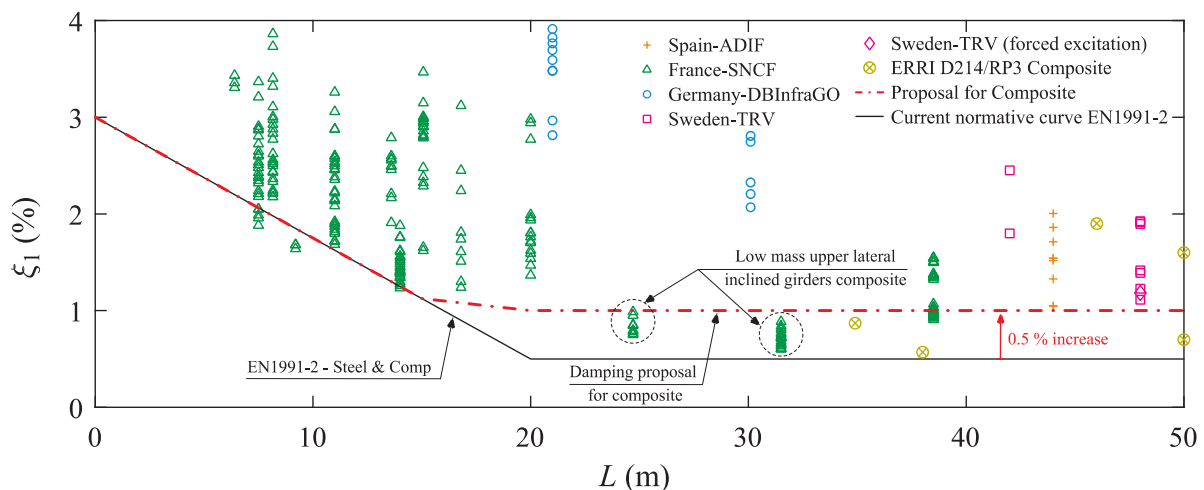

Figure 70: Comparison between the current stipulated curve in EN 1991-2 (2023) for the "steel and composite" bridge type and the newly proposed curve for the "steel-concrete composite" bridge category.

6.2.5 Normative recommendations for the "steel" bridge type

With respect to the *"steel"* bridge type, and as referred in Section 5.4.6 and depicted in Figure 64, the overall lower bound, even after disregarding non-resonant scenarios, closely aligns with the current normative curve for steel bridges as stipulated in EN 1991-2 (2023). No important deviations or abnormal cases that could condition the overall lower bound of damping have been observed and the majority of the results obtained in this work match well with those presented by the ERRI/D214 committee. In fact, some of the lowest damping values obtained in both studies are slightly below the current normative curve, but they cannot be attributed to a specific structural configuration. In conclusion, the results from this work do not provide any engineering

rationale to disregard certain results or propose higher damping values for steel bridges, which justifies proposing that the current normative curve for this type of bridge remains unchanged in future revisions of the code. Nonethless, as mentioned in Section 6.2.1 for the *"filler beam and reinforced concrete"* bridges, the authors recommend that additional tests under controlled forced excitation be conducted on these or other bridges to create scenarios closer to resonance and determine whether this could positively affect the damping estimation, i.e., lead to higher values.

6.3 Summary of the proposed normative recommendations

The results presented at the end of this report led to normative recommendations on bridge damping, with the aim of enhancing the damping curves currently stipulated in EN 1991-2 (2023). While increasing damping as much as possible would ideally be beneficial for bridge cost-efficiency, such an increase can only be proposed with a well-supported scientific and engineering rationale. This is often challenging to achieve, especially for a topic like bridge damping, as it is a highly nonlinear quantity that cannot be directly measured by any specific sensor. Furthermore, the uncertainty surrounding damping is considerable, due to both the limitations of the methods used to estimate it (all methods have inherent limitations) and the difficulty in identifying the main sources that most contribute to the overall damping of the bridge.

Even considering the aforementioned challenges, this work, which is the culmination of all the research made within WP4 from the InBridge4EU project, led to new recommendations on railway bridge damping, which include definition of new bridge types, new normative lower limits and proposals for even further enhancements. Thus, as proposed by ERRI D214/RP3 (1999), bridge damping should continue to be defined as a function of the span, as its determination is always straightforward and indisputable (unlike frequency-related damping, which relies on measurements that may be prone to errors). Table 20 summarizes the proposed normative recommendations for bridge damping as function of its span and compares with the values currently specified in the code EN 1991-2 (2023). This comparison is graphically presented in Figure 71.

Table 20: Summary of damping recommendations and comparison with the current normative values specified in EN 1991-2 (2023).

|	Lower limit of percentage of critical damping ξ (%)					
	$L < 15\ m$		$15\ m \leq L < 20\ m$		$L \geq 20\ m$	
	EN 1991-2	*Proposal*	*EN 1991-2*	*Proposal*	*EN1991-2*	*Proposal*
Filler beam and reinforced concrete	1.50+0.07(20-L)	1.50+0.07(20-L)	1.50+0.07(20-L)	1.50+0.07·(20-L)	1.50	1.50
Prestressed concrete	1.00+0.07(20-L)		1.00+0.07(20-L)		1.00	
Portal frame	-	3.00+0.15(20-L)	-	1.50+0.45·(20-L)	-	1.50
Steel-concrete composite	0.50+0.125(20-L)	0.50+0.125(20-L)	0.50+0.125(20-L)	1.00+0.025·(20-L)	0.50	1.00
Steel	$0.50 + 0.125(20 - L)$		$0.50 + 0.125(20 - L)$		0.50	
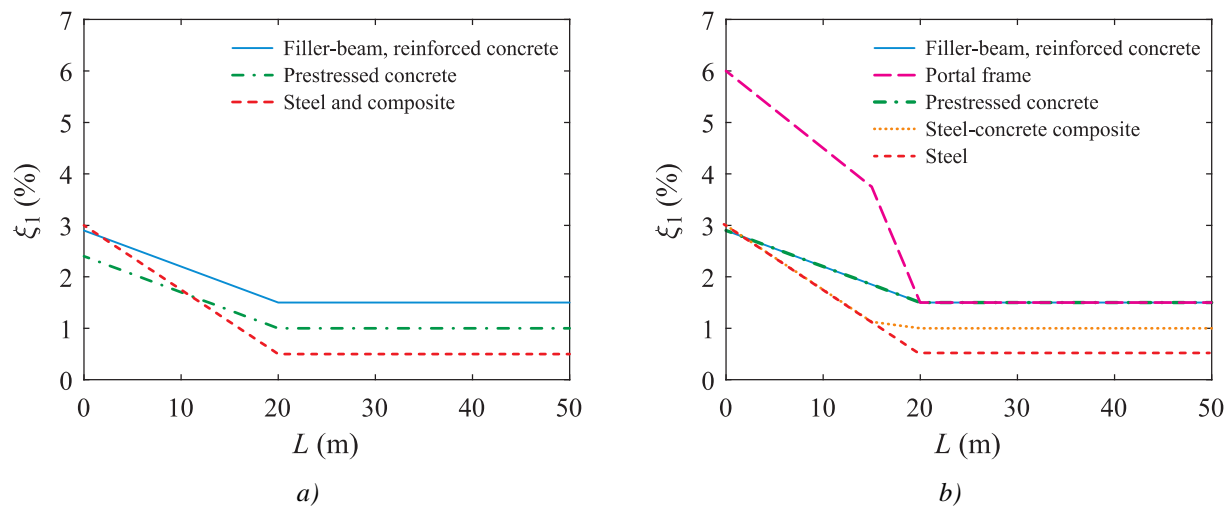
Figure 71: Graphical comparison of the current normative damping curves with the proposed recommendations: a) current curves stipulated in EN 1991-2 (2023) and b) proposed recommendations.

6.4 Conclusions

Based on the above, in summary, the following can be concluded:

- Over 1,000 damping estimations from nearly 90 bridges across five countries (France, Germany, Portugal, Spain, and Sweden) were performed using two algorithms: MCOMCO and SSI-COV. This database represents a substantial increase compared to the work previously conducted by the ERRI D214 committee (Chapter 2).

- Both algorithms were benchmarked using artificially generated linear and nonlinear known free decays, numerically simulated bridge responses through TBI analysis, and real cases from the measurement database gathered by the InBridge4EU consortium. Overall, both algorithms demonstrated a satisfactory agreement (Chapter 3).

- All damping estimates obtained from measurements obtained in tests under railway traffic (with an average of more than 10 train passages per analysed bridge) and forced excitation tests carried out by KTH in Sweden have been presented graphically in the main report and summarized in Annexes A and B. The latter include bridge datasheets containing detailed information on all bridges in the dataset, including mass, stiffness, number of valid measurements, estimated frequency and damping, among other parameters (Chapter 4).

- A comprehensive critical analysis of all the results has been conducted to assess the validity of the estimations (Chapter 5). Key conclusions from this analysis are summarized in the following points.

- Initially, the influence of amplitude of the bridge response on damping values was examined, but no significant correlations were observed.

- In the second stage, a methodology was developed to identify the measurements that most closely resemble near-resonant scenarios, as damping has the greatest impact on bridge response under these circumstances and estimations obtained from situations far from resonance can be misleading. This methodology evaluates the contribution of the first fundamental vertical bending mode to the overall response, as this mode, due to its low natural frequency, is generally the most susceptible to resonance from passing trains. By isolating scenarios closer to resonance, it is the authors' opinion that this

approach enhances the previous work carried out by the ERRI D214 committee, which did not include a quantitative assessment of the first mode's contribution. As a result, many damping values that previously influenced the lower bound were found to be associated with misleading scenarios and could be disregarded for normative considerations.

- In the third stage, a statistical analysis was conducted following the procedures outlined in EN 1990-Annex D (2023) and adopted by the Austrian railways in their bridge dynamics assessment recommendations (ÖBB-Regelwerk 08.01.05, 2023). However, the results raised several concerns, namely: *i)* by observing the results from a long-term monitoring system installed in one of the Swedish bridges, it was possible to conclude that damping did not clearly follow a Normal or Log-Normal distribution, which is a key assumption in EN 1990-Annex D (2023); *ii)* due to the large scatter and limited dataset, applying the statistical methodology prescribed in these codes resulted in overly conservative outcomes, as the 5% fractile value was, in most cases, even lower than the lowest damping value obtained in the tests for each bridge. Consequently, the statistical analysis based on fractiles was not adopted in this study. Instead, the lower bounds of the estimated damping values for each bridge were the primary determinants to shape the normative recommendations for railway bridge damping proposed in this work.

- Finally, the fourth stage of analysis involved a detailed examination of whether the lowest damping estimations could be considered outliers or abnormal values that might skew the overall lower bound of damping, potentially leading to overly conservative results. This step was crucial, as the ERA Technical Note (2022), which prompted this project, explicitly stated that low damping values from tests may be excluded, but only if their exclusion is justified by a sound engineering rationale. The refinement introduced earlier, which involved disregarding non-resonant scenarios, already led to less conservative results. However, it remained essential to further scrutinize the findings after applying that methodology, particularly by evaluating the significance of exceptionally low damping ratio values and providing a critical interpretation of their impact.

- The analysis of the abnormal values led to the following conclusions for each bridge type:

    i) The damping lower bound for the *"filler beam and reinforced concrete"* bridge type closely follows the current curve stipulated in the norm, with several cases presenting even lower damping values.

    ii) When non-near-resonant scenarios are disregarded, *"prestressed concrete"* bridges generally exhibit a higher lower bound of damping compared to the current curve, which could justify an enhancement.

    iii) The *"portal frame"* bridges clearly stood out, leading to the conclusion of a possible introduction of a new bridge family with considerable higher damping.

    iv) The *"steel-concrete composite"* bridge family could be separated from the steel bridges, given their usual higher mass, due to the presence of concrete and, consequently, higher damping. A thorough analysis of two outliers from the French network with considerably lower damping led to the conclusion that the upper lateral inclined girders composite connected by spaced steel transversal beams , given their low mass when compared with other composite structural solutions, should be excluded from the newly proposed composite bridge family. Other results obtained by the ERRI D214 committee were also analysed, where sound scientific rationale was found to justify some of the lower damping values estimated at the time.

v) The steel bridges, now split from the composite, shown a damping lower bound that aligns very well with the current curve, thus justifications for enhancing the damping in this bridge family could not be drawn.

- The work performed gave origin to the following recommendations (this proposals do not address any additional damping related to vehicle-bridge interaction, which has already been removed from the current version of EN 1991-2 (2023)):

i) The *"filler beam and reinforced concrete"* curve should remain unchanged.

ii) The *"prestressed concrete"* bridges should be merged with the *"filler beam and reinforced concrete"*, forming a single bridge family.

iii) Portal frames should be classified under a newly proposed *"portal frame"* bridge family.

iv) The current steel and composite bridge family should be split into two: a newly defined *"steel-concrete composite"* bridge type with higher damping for longer span bridges ($L > 20$ m) and a *"steel"* bridge type, which retains the existing curve.

6.5 Possible future recommendations

- The present proposals suggest a general increase of damping in some of the bridge families. Although a thorough analysis of the near-resonant scenarios was carried out to decrease the probability of estimating misleading damping ratios, all the proposals are based on damping from the fundamental vertical bending mode. Future studies involving damping estimation for higher global modes may be carried out to check their significance in the bridge design point of view.

- It is suggested that additional tests under forced excitation be conducted to better understand their effectiveness in reducing damping scatter and to create more realistic, controlled scenarios closer to resonance. Special attention should be given to more traditional bridge types that better represent the European bridge landscape, such as simply supported bridges. The only available data for this work from tests under controlled forced excitation were related to Swedish bridges with over-sails and integral abutments, which are not as common in the European context.

- In the particular case of prestressed concrete bridges, although the estimated damping values from Network Rail provide an optimistic perspective on the newly proposed curve, the evaluation of damping for spans below 8 m and above 31 m, using the same algorithms applied in this study for a fairer comparison, should be recognized as an open point at this stage.

- For the newly proposed steel-concrete composite category, a more generic criterion that includes the ratios between concrete and steel, as well as their contribution to the global bending mode of the bridge, would be worth studying if more data were available. Such criterion should be recognized as an open point for future revisions.

7 REFERENCES

Albright, A., Battini, J. M., & Andersson, A. (2025). Dynamic soil-structure interaction of a single-span railway bridge, forced vibration testing and simulation. *Structure and Infrastructure Engineering, 21*(1), 39-48. doi:10.1080/15732479.2023.2184395

Andersson, A., Allahvirdizadeh, R., Zangeneh, A., Silva, A., Ribeiro, D., Ferreira, G., Montenegro, P. A., Museros, P., Karoumi, R., & Calçada, R. (2021). *In2Track2 - Research into enhanced track and switch and crossing system 2* (Report No. D5.2.5 – High-speed low-cost bridges final report).

ANSYS®. (2019). Canonsburg, PA, USA: Academic Research, Release 19.2, ANSYS Inc.

DIBRST (2023). *Dynamic interface between Railway Bridges and Rolling Stock - State of the art report,* Draft Report, CEN Technical Committee 250 "Structural Eurocodes", Subcommittee SC1 - EN1991-2 (CEN/TC250/SC1). Brussels.

EN 1990-Annex A2 (2023). *Eurocode - Basis of structural and geotechnical design - Annex A.2: Application for bridges,* European Committee for Standardization (CEN). Brussels.

EN 1990-Annex D (2023). *Eurocode - Basis of structural and geotechnical design - Annex D: Design assisted by testing,* European Committee for Standardization (CEN). Brussels.

EN 1991-2 (2023). *Eurocode 1 - Actions on structures - Part 2: Traffic loads on bridges and other civil engineering works,* European Committee for Standardization (CEN). Brussels.

ERA Technical Note (2022). *ERA1193-TD-01-2022 - ERA technical note on work needed for closing TSI open points on bridge dynamics,* European Union Agency for Railways (ERA). Valenciennes.

ERRI D214/RP3 (1999). *Rail bridges for speeds > 200 km/h: Recommendations for calculating damping in rail bridge decks,* European Rail Research Institute. Utrecht.

Ferreira, G., Montenegro, P., Andersson, A., Henriques, A. A., Karoumi, R., & Calçada, R. (2024). Critical analysis of the current Eurocode deck acceleration limit for evaluating running safety in ballastless railway bridges. *Engineering Structures, 312*. doi:10.1016/j.engstruct.2024.118127

Galvín, P., Romero, A., Moliner, E., De Roeck, G., & Martínez-Rodrigo, M. D. (2021). On the dynamic characterisation of railway bridges through experimental testing. *Engineering Structures, 226*, 111261. doi:10.1016/j.engstruct.2020.111261

Heiland, T., Stempniewski, L., & Stark, A. (2024). The dynamic characteristics of railway portal frame bridges: a comparison between measurements and calculations. *Applied Sciences, 14*(4), 1493. doi:10.3390/app14041493

In2Track2 (2018). Research into enhanced track and switch and crossing system 2. Retrieved from https://projects.shift2rail.org/s2r_ip3_n.aspx?p=IN2TRACK2

In2Track3 (2023). Research into optimised and future railway infrastructure. Retrieved from https://projects.shift2rail.org/s2r_ip3_n.aspx?p=IN2TRACK3

InBridge4EU-Database (2024). InBridge4EU - Database of bridges. Retrieved from https://computeruse.us.es/inbridge4eu/index/

Magalhães, F. (2010). *Operational modal analysis for testing and monitoring of bridges and special structures.* (PhD), Faculty of Engineering of the University of Porto, Porto, Portugal.

Magalhães, F., & Cunha, A. (2011). Explaining operational modal analysis with data from an arch bridge. *Mechanical Systems and Signal Processing, 25*(5), 1431-1450. doi:10.1016/j.ymssp.2010.08.001

MATLAB®. (2023a). Natick, MA, USA: Release R2023a, The MathWorks Inc.

Montenegro, P. A., & Calçada, R. (2023). Wheel–rail contact model for railway vehicle–structure interaction applications: development and validation. *Railway Engineering Science, 31*(3), 181–206. doi:10.1007/s40534-023-00306-4

Montenegro, P. A., Calçada, R., Vila-Pouca, N., & Tanabe, M. (2016). Running safety assessment of trains moving over bridges subjected to moderate earthquakes. *Earthquake Engineering & Structural Dynamics, 45*, 483–504. doi:10.1002/eqe.2673

Montenegro, P. A., Carvalho, H., Ortega, M., Millanes, F., Goicolea, J. M., Zhai, W. M., & Calçada, R. (2022). Impact of the train-track-bridge-wind system characteristics in the runnability of high-speed trains against crosswinds - Part I: running safety. *Journal of Wind Engineering and Industrial Aerodynamics, 224*, 104974. doi:10.1016/j.jweia.2022.104974

Montenegro, P. A., Neves, S. G. M., Calçada, R., Tanabe, M., & Sogabe, M. (2015). Wheel-rail contact formulation for analyzing the lateral train-structure dynamic interaction. *Computers & Structures, 152*, 200-214. doi:10.1016/j.compstruc.2015.01.004

ÖBB-Regelwerk 08.01.05 (2023). *Dynamische Messung von Eisenbahnbrücken,* ÖBB-Infrastruktur AG. Wien.

Ozdemir, A. A., & Gumussoy, S. (2017). Transfer Function Estimation in System Identification Toolbox via Vector Fitting. *IFAC-PapersOnLine, 50*(1), 6232-6237. doi:10.1016/j.ifacol.2017.08.1026

Peeters, B., & De Roeck, G. (1999). Reference-Based Stochastic Subspace Identification for output-only modal analysis. *Mechanical Systems and Signal Processing, 13*(6), 855-878. doi:10.1006/mssp.1999.1249

Pimenta, F., Pedrelli, V. L., Vanelli, T., & Magalhães, F. (2024a). On the effect of nonlinear damping sources in output-only identification methods applied to floating wind turbines. *Energies, 17*, 1671. doi:10.3390/en17071671

Pimenta, F., Ribeiro, D., Román, A., & Magalhães, F. (2024b). Modal properties of floating wind turbines: Analytical study and operational modal analysis of an utility-scale wind turbine. *Engineering Structures, 301*, 117367. doi:10.1016/j.engstruct.2023.117367

Reiterer, M., Lachinger, S., Fink, J., & Bruschetini-Ambro, S. Z. (2017). Ermittlung der dynamischen Kennwerte von Eisenbahnbrücken unter Anwendung von unterschiedlichen Schwingungsanregungsmethoden. *Bauingenieur, 92*(10), 2-13. doi:10.37544/0005-6650-2017-10-24

Sánchez-Quesada, J. C., Moliner, E., Romero, A., Galvín, P., & Martínez-Rodrigo, M. D. (2021). Ballasted track interaction effects in railway bridges with simply-supported spans composed by adjacent twin single-track decks. *Engineering Structures, 247*, 113062. doi:10.1016/j.engstruct.2021.113062

Sánchez-Quesada, J. C., Romero, A., Galvín, P., Moliner, E., & Martínez-Rodrigo, M. D. (2023). 3D analysis of railway induced vibrations on skew girder bridges including ballast track–bridge interaction effects. *Engineering Structures, 279*, 115546. doi:10.1016/j.engstruct.2022.115546

Saramago, G., Montenero, P. A., Ribeiro, D., Silva, A., Santos, S., & Calçada, R. (2020). Experimental Validation of a Double-Deck Track-Bridge System under Railway Traffic. *Sustainability, 14*, 5794. doi:10.3390/su14105794

Silva, A., Ribeiro, D., Montenegro, P. A., Ferreira, G., Andersson, A., Zangeneh, A., Karoumi, R., & Calçada, R. (2023). New Contributions for Damping Assessment on Filler-Beam Railway Bridges Framed on In2Track EU Projects. *Applied Sciences, 13*, 2636. doi:10.3390/app13042636

Van Rossum, G., & Drake, F. L. (2009). *Python 3 Reference Manual*. Scotts Valley, CA, USA: CreateSpace Independent Publishing Platform.

Vandekerckhove, J., & Oldenhuis, R. (2009). GODLIKE (Global Optimum Determination by Linking and Interchanging Kindred Evaluators) - A robust single-& multi-objective optimizer. Retrieved from https://www.mathworks.com/matlabcentral/fileexchange/24838-godlike-a-robust-single-multi-objective-optimizer

Zangeneh, A. (2021). *Dynamic soil-structure interaction analysis of high-speed railway bridges: efficient modeling techniques and experimental testing.* (PhD Thesis), Royal Institute of Technology (KTH), Stockholm, Sweden. Retrieved from https://kth.diva-portal.org/smash/record.jsf?pid=diva2%3A1552654&dswid=-24

Zangeneh, A., Svedholm, C., Andersson, A., Pacoste, C., & Karoumi, R. (2018). Identification of soil-structure interaction effect in a portal frame railway bridge through full-scale dynamic testing. *Applied Sciences, 159*, 299-309. doi:10.1016/j.engstruct.2018.01.014

ANNEX A – SUMMARY OF DAMPING ESTIMATION RESULTS

Legend of the summary table:

- FB/RC: Filler beam and reinforced concrete.

- PSC: Prestressed concrete.

- COMP: Steel-concrete composite.

- STL: Steel.

- PF: Portal-frame.

- f_1: frequency of the first vertical bending mode (fundamental mode).

- ξ_1: damping of the first vertical bending mode (fundamental mode).

- A_1: amplitude of vibration the first vertical bending mode (fundamental mode).

- MCO: Multi-criteria optimization method (used for damping estimation in tests under railway traffic).

- SSI-COV: Covariance driven stochastic subspace identification method (used for damping estimation in tests under railway traffic).

- 'modalfit': Least squares ratio function estimation incorporated in MATLAB's "modalfit" built-in function (used for damping estimation in tests under forced excitation).

List of bridges:

- A.1. Bridges from France (SNCF Réseau)

- A.2. Bridges from Germany (DBInfraGo)

- A.3. Bridges from Portugal (Infraestruturas de Portugal)

- A.4. Bridges from Spain (ADIF)

- A.5. Bridges from Sweden (Trafikverket)

A.1. Bridges from France (SNCF Réseau)

Bridge designation	Country	Structural type (normative type)	Span (m)	f1 (Hz)	ξ1 (%)	A1 (m/s2)	Method
070000_205+406	France	U-shaped composite, simply supported (COMP)	16.80	6.96 – 7.25	0.97 – 3.12	0.007 – 0.051	MCO
070000_219+422	France	U-shaped composite, simply supported (COMP)	9.20	16.41 – 16.51	1.59 – 1.68	0.012 – 0.052	MCO
070000_230+956	France	U-shaped steel, simply supported (STL)	6.80	17.22 – 18.82	2.17 – 5.90	0.005 – 0.189	MCO
070000_231+572	France	U-shaped composite, simply supported (COMP)	20.00	5.81 – 6.01	1.37 – 5.14	0.005 – 0.025	SSI-COV
070000_383+560	France	Filler beam, simply supported (FB/RC)	16.60	6.24 – 6.98	2.27 – 4.49	0.010 – 0.017	MCO
070000_384+378	France	Filler beam, simply supported (FB/RC)	15.40	7.24 – 7.41	3.23 – 8.77	0.005 – 0.012	MCO
070000_470+164	France	Filler beam, simply supported (FB/RC)	9.00	10.57 – 10.70	4.67 – 8.91	0.033 – 0.126	MCO
070000_484+884	France	Filler beam, simply supported (FB/RC)	8.97	13.66	4.63	0.006	MCO
070000_492+208	France	Filler beam, simply supported (FB/RC)	11.40	9.02	5.96	0.030	MCO
070000_496+533	France	High upper side beams, simply supported (COMP)	38.50	3.10 – 3.15	0.91 – 1.55	0.004 – 0.379	SSI-COV
830000_034+307	France	Filler beam, simply supported (FB/RC)	14.90	7.51 – 9.02	5.67 – 9.37	0.018 – 0.100	MCO
830000_036+790	France	U-shaped composite, simply supported (COMP)	14.00	8.22 – 8.35	1.11 – 1.88	0.011 – 0.088	SSI-COV
830000_351+364	France	U-shaped composite, simply supported (COMP)	7.50	16.15 – 18.18	1.88 – 3.37	0.003 – 0.031	SSI-COV

Bridge designation	Country	Structural type (normative type)	Span (m)	f1 (Hz)	ξ1 (%)	A1 (m/s2)	Method
830000_380+357	France	U-shaped composite, simply supported (COMP)	11.00	12.33 – 12.89	1.62 – 3.26	0.004 – 0.075	SSI-COV
830000_697+966	France	Filler beam, simply supported (FB/RC)	8.86	10.05	3.74	0.015	MCO
830000_699+425	France	Filler beam, simply supported (FB/RC)	14.20	8.27	4.87	0.015	MCO
830000_739+502	France	Filler beam, simply supported (FB/RC)	13.80	8.86 – 9.08	2.84 – 4.29	0.003 – 0.011	MCO
752000_083+112	France	Filler beam, simply supported (FB/RC)	34.40	2.50 – 2.52	1.64 – 2.12	0.010- 0.011	MCO
752000_185+353	France	Filler beam, simply supported (FB/RC)	27.85	4.61	3.38	0.011	MCO
752000_241+136	France	Slab, simply supported (FB/RC)	17.38	6.48 – 6.81	1.99 – 5.77	0.003 – 0.223	MCO
752000_249+715	France	Filler beam, continuous (FB/RC)	13.60	8.32 – 8.36	4.72 – 4.89	0.016 – 0.020	MCO
752000_287+961	France	Filler beam, continuous (FB/RC)	7.80	17.91 – 17.95	1.59 – 2.33	0.027 – 0.032	MCO
752000_318+837	France	Filler beam, continuous (FB/RC)	34.80	2.11	2.10	0.012	MCO
752000_335+986	France	Filler beam, continuous (FB/RC)	11.42	12.30	7.47	0.010	MCO
590000_261+703	France	U-shaped steel, simply supported (STL)	10.38	11.38 – 12.18	1.68 – 3.73	0.003 – 0.063	MCO
590000_235+895	France	U-shaped composite, simply supported (COMP)	6.40	22.22 – 25.66	3.31 – 11.81	0.004 – 0.019	SSI-COV
810000_097+770	France	Upper lateral inclined girders composite, simply supported (COMP)	24.70	4.38 – 4.52	0.73 – 0.99	0.009 – 0.080	SSI-COV
001000_186+312	France	U-shaped steel,	8.00	19.21 –	2.73 – 4.56	0.010 –	MCO

Bridge designation	Country	Structural type (normative type)	Span (m)	f1 (Hz)	ξ1 (%)	A1 (m/s2)	Method
		simply supported (STL)		19.71		0.115	
001000_459+633	France	U-shaped composite, simply supported (COMP)	15.07	4.46 – 8.49	1.62 – 4.20	0.005 – 0.103	SSI-COV
242000_138+166	France	Upper lateral inclined girders composite, simply supported (COMP)	31.50	2.82 – 2.88	0.60 – 0.89	0.015 – 0.096	SSI-COV
272000_048+164	France	U-shaped composite, simply supported (COMP)	13.60	9.41 – 9.59	1.91 – 2.79	0.027 – 0.058	SSI-COV
570000_041+757	France	U-shaped composite, simply supported (COMP)	8.16	14.73 – 15.93	1.79 – 5.41	0.004 – 0.109	SSI-COV

A.2. Bridges from Germany (DBInfraGo)

Bridge designation	Country	Structural type (normative type)	Span (m)	f1 (Hz)	ξ1 (%)	A1 (m/s2)	Method
EÜ Milde bei Beese - ID24193	Germany	Filler beam, simply supported (FB/RC)	12.90	8.39 – 8.77	4.33 – 10.62	0.008 – 0.225	SSI-COV
EÜ Str.Vinzelb.-Käth - ID26496	Germany	Filler beam, simply supported (FB/RC)	12.86	10.05 – 10.28	4.94 – 8.93	0.018 – 0.130	SSI-COV
EÜ über477 bei Kerpen - ID20726	Germany	Filler beam, simply supported (FB/RC)	15.92	6.10 – 6.22	2.78 – 4.08	0.011 – 0.160	SSI-COV
Nuthe Drewitz - ID23194	Germany	Filler beam, simply supported (FB/RC)	17.70	5.30 – 5.66	4.70 – 7.61	0.005 – 0.151	SSI-COV
Straßenunterführung - ID12391	Germany	Filler beam, simply supported (FB/RC)	12.00	7.98 – 8.12	3.30 – 6.42	0.006 – 0.098	SSI-COV
Ebr ü.Wenderterstraße - ID5046	Germany	Slab beam, simply supported (PSC)	22.60	5.20 – 5.37	4.21 – 6.30	0.019 – 0.139	SSI-COV
Hamminkelner Landstr - ID34492	Germany	Slab beam, simply supported (PSC)	16.73	8.62 – 8.82	3.25 – 7.22	0.025 – 0.106	SSI-COV
Friedrich Allee - ID7341	Germany	Steel trough cross-section, simply supported (STL)	14.71	8.03 – 8.17	1.38 – 2.56	0.015 – 0.116	SSI-COV
Augsburg - ID31962	Germany	Steel trough cross-section, simply supported (STL)	20.08	4.36 – 4.85	3.43 – 7.02	0.020 – 0.600	SSI-COV
BadOldesloe - ID24517	Germany	Steel hollow box with concrete slab, simply supported (COMP)	30.10	2.78 – 3.97	2.07 – 4.54	0.009 – 0.207	SSI-COV
Bonn - ID7342 | 7343	Germany	Steel trough cross-section, simply supported (STL)	14.37	8.58 – 9.01	1.73 – 4.99	0.035 – 0.170	SSI-COV
Boppard - ID7640	Germany	Steel trough cross-section, simply supported (STL)	27.30	4.59 – 5.06	1.32 – 6.55	0.035 – 0.700	SSI-COV
Boppard - ID7641	Germany	Steel trough cross-section, simply supported (STL)	31.80	3.55 – 3.73	1.43 – 5.33	0.019 – 0.350	SSI-COV
Braunschweig - ID3648	Germany	Steel trough cross-section, simply supported (STL)	35.20	3.35 – 3.45	0.83 – 2.81	0.050 – 0.500	SSI-COV
Duisburg - ID15906 | 16955	Germany	Steel trough cross-section, simply supported (STL)	30.20	3.72 – 3.85	0.93 – 1.60	0.025 – 1.100	SSI-COV

Bridge designation	Country	Structural type (normative type)	Span (m)	f1 (Hz)	ξ1 (%)	A1 (m/s2)	Method
Essen - ID17028 | 17553	Germany	Steel trough cross-section, simply supported (STL)	22.70	4.68 – 5.24	1.00 – 1.66	0.017 – 0.420	SSI-COV
Halle - ID11874 | 11875	Germany	Steel trough cross-section, simply supported (STL)	28.00	4.11 – 4.30	0.44 – 2.77	0.010 – 0.100	SSI-COV
HannoverLeinhausen - ID4500	Germany	Girder grid with concrete slab, simply supported (COMP)	21.00	4.16 – 4.26	2.81 – 4.40	0.030 – 0.200	SSI-COV
Karlsruhe - ID6007 | 6008	Germany	Steel trough cross-section, simply supported (STL)	21.00	7.00 – 7.46	0.97 – 5.44	0.035 – 0.450	SSI-COV
Langenhorn - ID23875	Germany	Steel trough cross-section, simply supported (STL)	36.30	4.04 – 4.13	1.36 – 1.89	0.140 – 0.300	SSI-COV
Sehnde - ID15894 | 18019	Germany	Steel trough cross-section, simply supported (STL)	20.10	5.15 – 5.69	2.59 – 3.93	0.004 – 0.650	SSI-COV

A.3. Bridges from Portugal (Infraestruturas de Portugal)

Bridge designation	Country	Structural type (normative type)	Span (m)	f1 (Hz)	ξ1 (%)	A1 (m/s2)	Method
95.965 - PI Braço do Cortiço	Portugal	Filler beam, simply supported (FB/RC)	7.02	15.35 – 16.09	3.01 – 7.17	0.036 – 0.280	SSI-COV
100.629 - PI da Cascalheira	Portugal	Filler beam, simply supported (FB/RC)	10.92	9.06 – 10.14	7.78 – 10.30	0.010 – 0.150	SSI-COV
282.943 - Ponte de Canelas	Portugal	Filler beam, simply supported (FB/RC)	12.00	7.77 – 8.36	1.64 – 5.34	0.026 – 0.220	SSI-COV
Sangalhos	Portugal	Portal Frame, closed (PF)	8.00	17.46 – 20.16	5.02 – 7.47	0.048 – 0.262	SSI-COV
Pausinho	Portugal	Portal Frame, closed (PF)	3.25	46.56 – 56.41	7.88 – 11.18	0.095 – 0.683	SSI-COV

A.4. Bridges from Spain (ADIF)

Bridge designation	Country	Structural type (normative type)	Span (m)	f1 (Hz)	ξ1 (%)	A1 (m/s2)	Method
Algodor	Spain	Filler beam, simply supported (FB/RC)	10.25	11.40	2.36	0.326	MCO
Bracea	Spain	Girder deck, simply supported (PSC)	15.25	9.20 – 9.43	1.99 – 5.57	0.077 – 0.331	MCO
Guadiana	Spain	Girder deck, simply supported (PSC)	11.93	9.70 – 9.90	4.87 – 5.39	0.027 – 0.097	MCO
Jabalon	Spain	Girder deck, simply supported (PSC)	24.00	6.17 – 6.19	2.05 – 3.05	0.089 – 0.142	MCO
Laguna Blanca	Spain	Portal Frame, closed (PF) / Prestressed concrete (PSC)	8.00	21.78 – 23.42	4.74 – 5.78	0.069 – 0.284	SSI-COV
Tirteafuera	Spain	Girder deck, simply supported (PSC)	18.00	8.06 – 8.20	1.71 – 2.82	0.046 – 0.105	MCO
Arroyo Corbones: PC029_100017615	Spain	Truss, simply supported (STL)	30.42	7.62	2.45	0.050	MCO
Barranco Bancal Redo: PC030_100017609	Spain	Truss, simply supported (STL)	16.00	10.02	1.40	0.015	MCO
Barranco De Los Corrimientos: PC040_100016018	Spain	Truss, simply supported (STL)	21.20	8.01	0.94	0.035	MCO
Tejería: PC041_100015418_ Lateral	Spain	Truss, simply supported (STL)	25.90	8.14	1.44	0.036	MCO
Tejería: PC041_100015418_ Central	Spain	Truss, simply supported (STL)	41.00	5.08	1.19	0.036	MCO
Arroyo de las Piedras	Spain	Steel box with concrete slab, continuous (COMP)	44.00	3.99 – 4.05	1.05 – 2.01	0.022 – 0.063	SSI-COV
Casamisarro	Spain	Girder deck, simply supported (PSC)	29.65	5.05 – 5.45	2.11 – 6.27	0.043 – 0.612	SSI-COV

A.5. Bridges from Sweden (Trafikverket)

Note: in the Swedish bridges, "i)" refers to results relative to tests under railway traffic, while "ii)" refers to tests under forced excitation.

Bridge designation	Country	Structural type (normative type)	Span (m)	f1 (Hz)	ξ1 (%)	A1 (m/s2)	Method
Banafjällsån	Sweden	Steel beam with concrete slab, simply supported (COMP)	42.00	i) 3.25 – 3.26	i) 1.80 – 2.45	i) 0.116 – 0.171	i) SSI-COV
Hästhovsgatan	Sweden	Slab full, simply supported (FB/RC)	14.20	i) 11.87 – 12.45 ii) 11.53 – 11.54	i) 2.26 – 3.61 ii) 2.45 – 2.60	i) 0.015 – 0.131 ii) 2.900	i) SSI-COV ii) 'modalfit'
Bryngeån	Sweden	Steel beam with concrete slab, simply supported (COMP)	48.00	i) 2.49 – 2.60 ii) 2.45	i) 1.11 – 1.92 ii) 1.18	i) 0.020 – 0.471 ii) 0.450	i) SSI-COV ii) 'modalfit'
Bodavägen	Sweden	Beam, simply supported (PSC)	22.00	i) 8.16 – 8.38 ii) 7.38 – 7.62	i) 1.61 – 1.73 ii) 2.57 – 3.21	i) 0.021 – 0.024 ii) 0.600 – 1.400	i) SSI-COV ii) 'modalfit'
Aspan	Sweden	Slab full, simply supported (FB/RC)	24.00	i) 6.58 – 6.69 ii) 6.39	i) 1.07 – 1.57 ii) 2.03	i) 0.013 – 0.024 ii) 0.500	i) SSI-COV ii) 'modalfit'
Enköpingsvägen	Sweden	Beam, continuous (PSC)	20.00	i) 7.96 – 8.04 ii) 7.74 – 7.83	i) 1.79 – 2.52 ii) 1.34 – 1.51	i) 0.046 – 0.148 ii) 0.25 – 0.70	i) SSI-COV ii) 'modalfit'
Fanna	Sweden	Beam, continuous (PSC)	20.30	i) 8.10 – 8.19 ii) 8.02 – 8.06	i) 2.57 – 3.06 ii) 3.50 – 4.27	i) 0.012 – 0.150 ii) 0.500	i) SSI-COV ii) 'modalfit'
Sidensjövägen	Sweden	Slab full, continuous (FB/RC)	17.00	i) 8.50 – 8.52 ii) 8.33	i) 0.60 – 0.67 ii) 0.98 – 1.01	i) 0.019 – 0.030 ii) 1.800 – 2.000	i) SSI-COV ii) 'modalfit'
Taxinge	Sweden	Slab full, continuous (PSC)	22.90	i) 5.43 – 5.59 ii) 5.39 – 5.50	i) 1.53 – 2.67 ii) 1.50 – 1.76	i) 0.139 – 0.485 ii) 0.250 – 0.450	i) SSI-COV ii) 'modalfit'
Sveavägen	Sweden	Slab full, continuous (FB/RC)	11.60	ii) 13.72 – 13.82	ii) 2.37 – 2.46	ii) 0.500 – 0.950	ii) 'modalfit'

Bridge designation	Country	Structural type (normative type)	Span (m)	f1 (Hz)	ξ1 (%)	A1 (m/s2)	Method
Vasavägen	Sweden	Slab full, continuous (FB/RC)	12.50	i) 12.28 – 12.64 ii) 12.19	i) 0.98 – 1.43 ii) 1.18	i) 0.017 – 0.200 ii) 1.700	i) SSI-COV ii) *'modalfit'*
Pershagen	Sweden	Slab full, continuous (FB/RC)	18.40	ii) 7.82	ii) 1.29 – 1.32	ii) 0.550 – 0.600	ii) *'modalfit'*
Degermyran	Sweden	Portal Frame, open (PF)	8.70	ii) 30.42 – 31.58	ii) 9.45 – 12.85	ii) 0.080	ii) *'modalfit'*
Faresmyren	Sweden	Portal Frame, open (PF)	8.70	ii) 29.10 – 29.17	ii) 14.45 – 20.03	ii) 0.150 – 0.600	ii) *'modalfit'*
Gesällgatan North	Sweden	Portal Frame (PF) / Beam, continuous abutment (PSC)	30.60	ii) 6.54 – 6.55	ii) 1.38 – 1.43	ii) 0.800 – 1.000	ii) *'modalfit'*
Gesällgatan South	Sweden	Portal Frame (PF) / Beam, continuous abutment (PSC)	28.60	ii) 5.65 – 5.67	ii) 1.91 – 2.91	ii) 2.200	ii) *'modalfit'*
Norra Kungsvägen	Sweden	Portal Frame, open (PF)	15.70	ii) 16.36 – 16.43	ii) 3.86 – 4.13	ii) 0.030 – 0.550	ii) *'modalfit'*
Sodra Kungsvägen	Sweden	Portal Frame, open (PF)	15.25	ii) 15.33 – 15.90	ii) 4.54 – 6.00	ii) 0.080 – 1.200	ii) *'modalfit'*

ANNEX B – BRIDGE DATASHEETS

Legend of the table datasheets:

- FB/RC: Filler beam and reinforced concrete.

- PSC: Prestressed concrete.

- COMP: Steel-concrete composite.

- STL: Steel.

- PF: Portal-frame.

- f_1: frequency of the first vertical bending mode (fundamental mode).

- ξ_1: damping of the first vertical bending mode (fundamental mode).

- A_1: amplitude of vibration the first vertical bending mode (fundamental mode).

- MCO: Multi-criteria optimization method (used for damping estimation in tests under railway traffic).

- SSI-COV: Covariance driven stochastic subspace identification method (used for damping estimation in tests under railway traffic).

- 'modalfit': Least squares ratio function estimation incorporated in MATLAB's "modalfit" built-in function (used for damping estimation in tests under forced excitation).

List of bridges:

- B.1. Bridges from France (SNCF Réseau)

- B.2. Bridges from Germany (DBInfraGo)

- B.3. Bridges from Portugal (Infraestruturas de Portugal)

- B.4. Bridges from Spain (ADIF)

- B.5. Bridges from Sweden (Trafikverket)
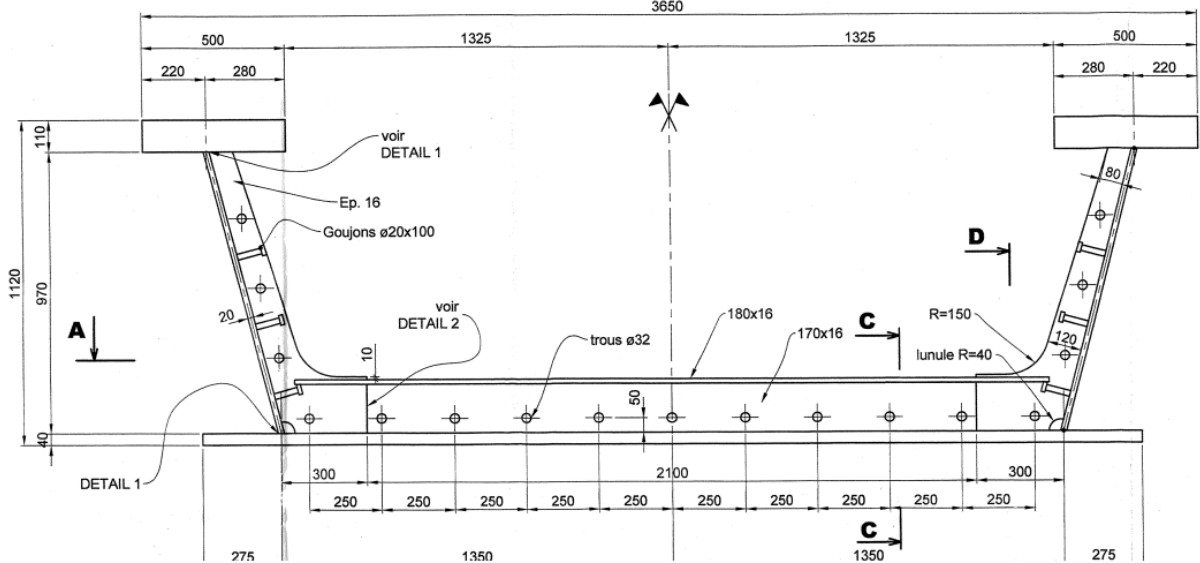
B.1. Bridges from France (SNCF Réseau)
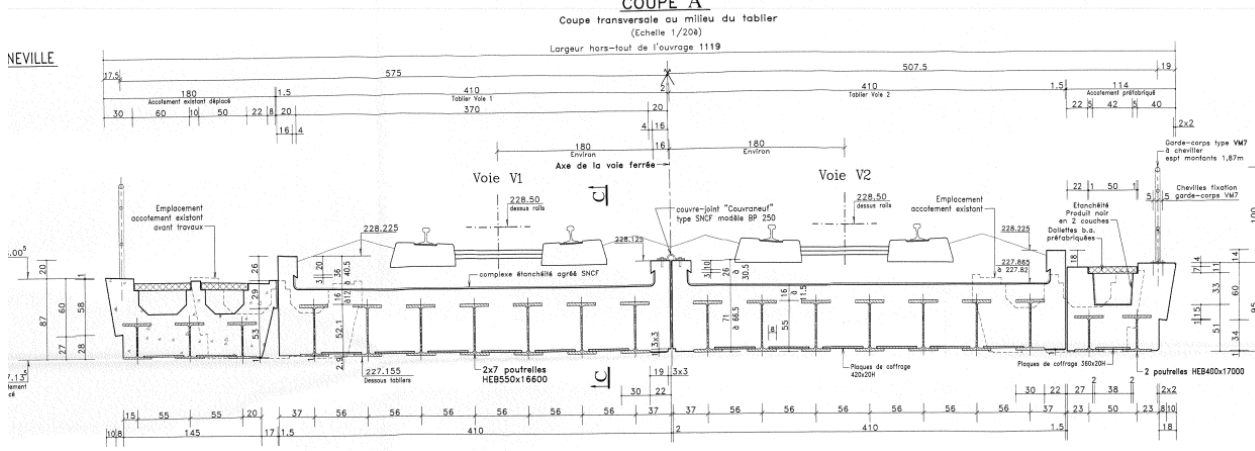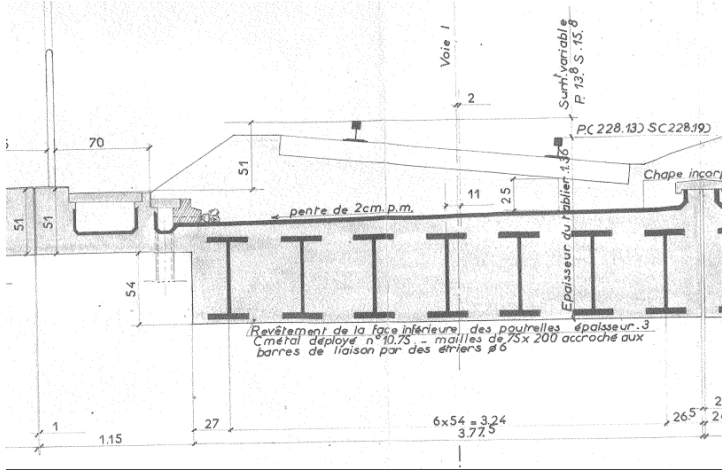
070000_205+406			
Country	**Line designation**	**Maximum speed**	**Infrastructure Manager**
France	070000: Paris Est - Strasbourg Ville	160 km/h	SNCF RÉSEAU

Structural properties			
Span (m)	16.80	**Type**	U-shaped composite
Mass (t/m)	7.23	**Configuration**	Simply supported
EI **(N.m^2)**	1.20×10^{10}	**Normative type**	COMP
Dynamic properties			
Test type	Under railway traffic	**Method**	MCO
Range f_1 (Hz)	6.96 – 7.25	**Range ξ_1 (%)**	0.97 – 3.12
Range A_1 (m/s^2)	0.007 – 0.051	**No. valid measurements**	10
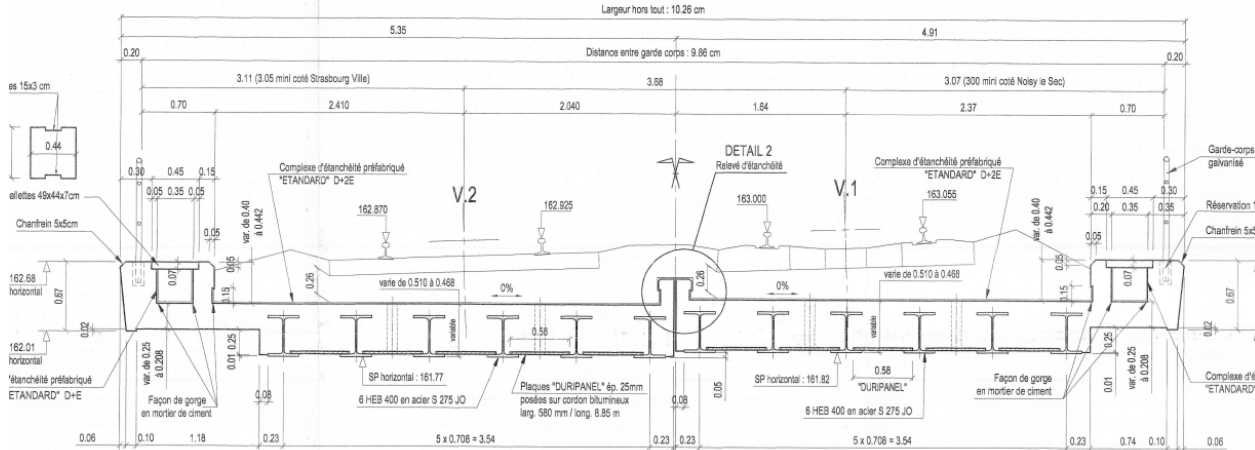
070000_219+422			
Country	**Line designation**	**Maximum speed**	**Infrastructure Manager**
France	070000: Paris Est - Strasbourg Ville	160 km/h	SNCF RÉSEAU

Coupe transversale st H-H Ech : 1/50

Structural properties			
Span (m)	9.20	**Type**	U-shaped composite
Mass (t/m)	6.13	**Configuration**	Simply supported
EI (N.m^2)	4.89×10^9	**Normative type**	COMP
Dynamic properties			
Test type	Under railway traffic	**Method**	MCO
Range f_1 (Hz)	16.41 – 16.51	**Range ξ_1 (%)**	1.59 – 1.68
Range A_1 (m/s^2)	0.012 – 0.052	**No. valid measurements**	4
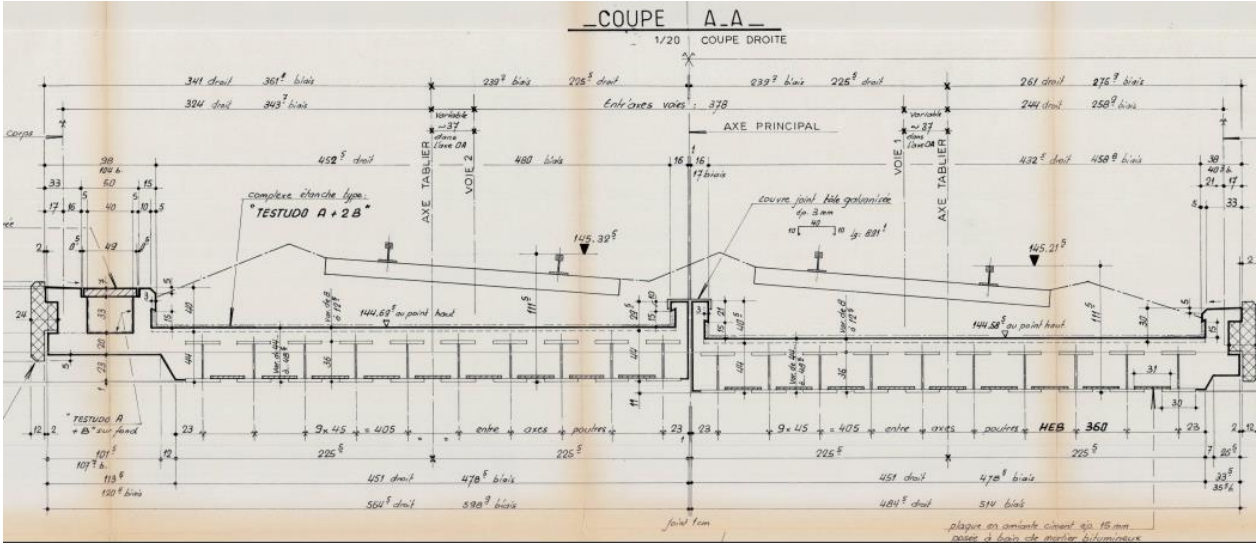
070000_230+956			
Country	**Line designation**	**Maximum speed**	**Infrastructure Manager**
France	070000: Paris Est - Strasbourg Ville	160 km/h	SNCF RÉSEAU

Structural properties			
Span (m)	6.80	**Type**	U-shaped steel
Mass (t/m)	5.00	**Configuration**	Simply supported
EI (N.m^2)	4.54×10^9	**Normative type**	STL
Dynamic properties			
Test type	Under railway traffic	**Method**	MCO
Range f_1 (Hz)	17.22 – 18.82	**Range ξ_1 (%)**	2.17 – 5.90
Range A_1 (m/s^2)	0.005 – 0.189	**No. valid measurements**	19
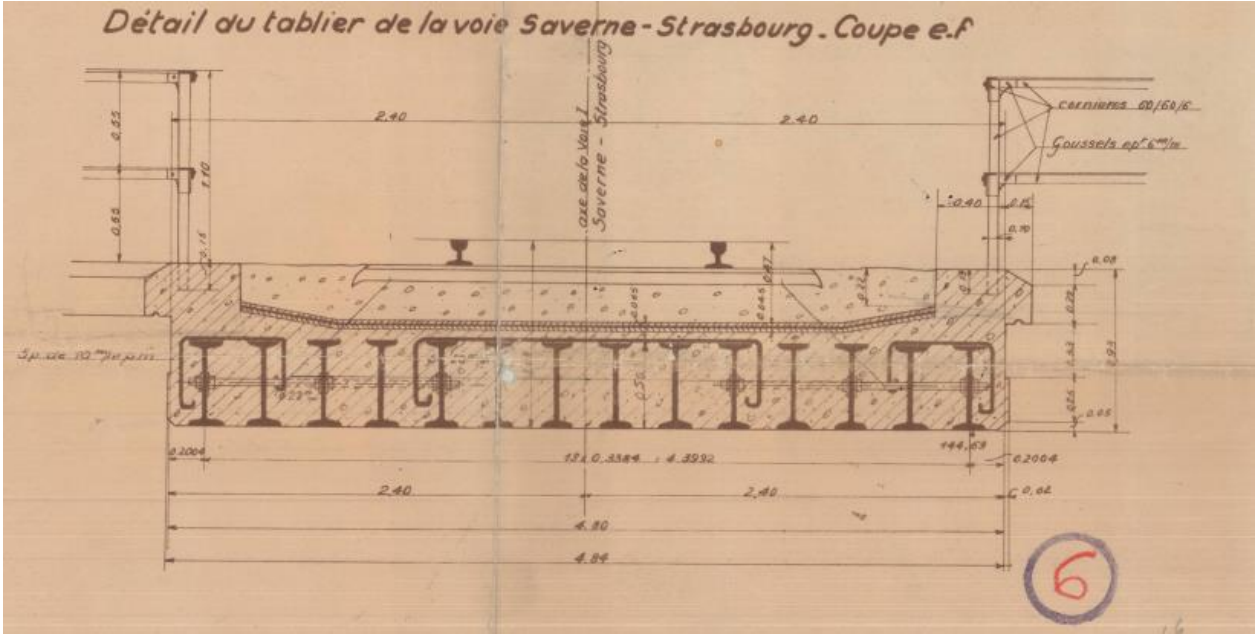
070000_231+572			
Country	**Line designation**	**Maximum speed**	**Infrastructure Manager**
France	070000: Paris Est - Strasbourg Ville	160 km/h	SNCF RÉSEAU

ELEVATION CADRES N°2 A 20
ECH. 1/10

Structural properties			
Span (m)	20.00	**Type**	U-shaped composite
Mass (t/m)	7.03	**Configuration**	Simply supported
EI (N.m^2)	1.48×10^{10}	**Normative type**	COMP
Dynamic properties			
Test type	Under railway traffic	**Method**	SSI-COV
Range f_1 (Hz)	5.81 – 6.01	**Range ξ_1 (%)**	1.37 – 5.14
Range A_1 (m/s^2)	0.005 – 0.025	**No. valid measurements**	19
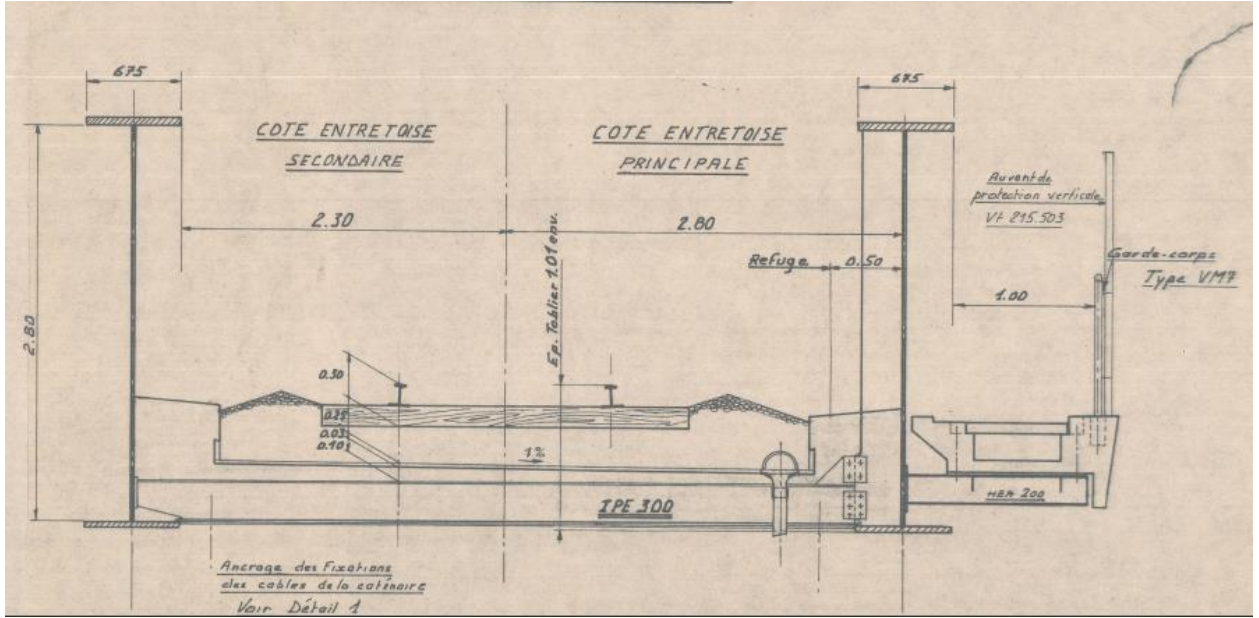
070000_383+560			
Country	**Line designation**	**Maximum speed**	**Infrastructure Manager**
France	070000: Paris Est - Strasbourg Ville	150 km/h	SNCF RÉSEAU

Structural properties			
Span (m)	16.60	**Type**	Filler beam
Mass (t/m)	11.60	**Configuration**	Simply supported
EI **(N.m^2)**	5.40×10^9	**Normative type**	FB/RC
Dynamic properties			
Test type	Under railway traffic	**Method**	MCO
Range f_1 (Hz)	6.24 – 6.98	**Range ξ_1 (%)**	2.27 – 4.49
Range A_1 (m/s^2)	0.010 – 0.017	**No. valid measurements**	2
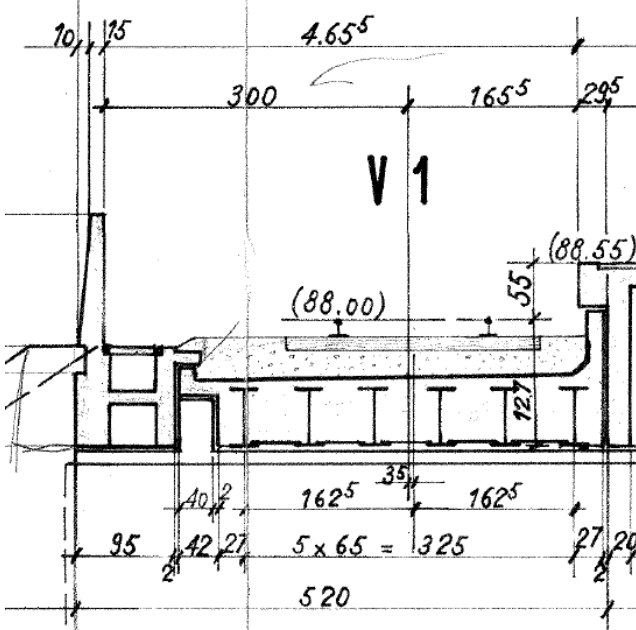
070000_384+378			
Country	**Line designation**	**Maximum speed**	**Infrastructure Manager**
France	070000: Paris Est - Strasbourg Ville	150 km/h	SNCF RÉSEAU

Structural properties			
Span (m)	15.40	**Type**	Filler beam
Mass (t/m)	13.10	**Configuration**	Simply supported
EI (N.m²)	5.91×10^9	**Normative type**	FB/RC
Dynamic properties			
Test type	Under railway traffic	**Method**	MCO
Range f_1 (Hz)	7.24 – 7.41	**Range ξ_1 (%)**	3.23 – 8.77
Range A_1 (m/s²)	0.005 – 0.012	**No. valid measurements**	4
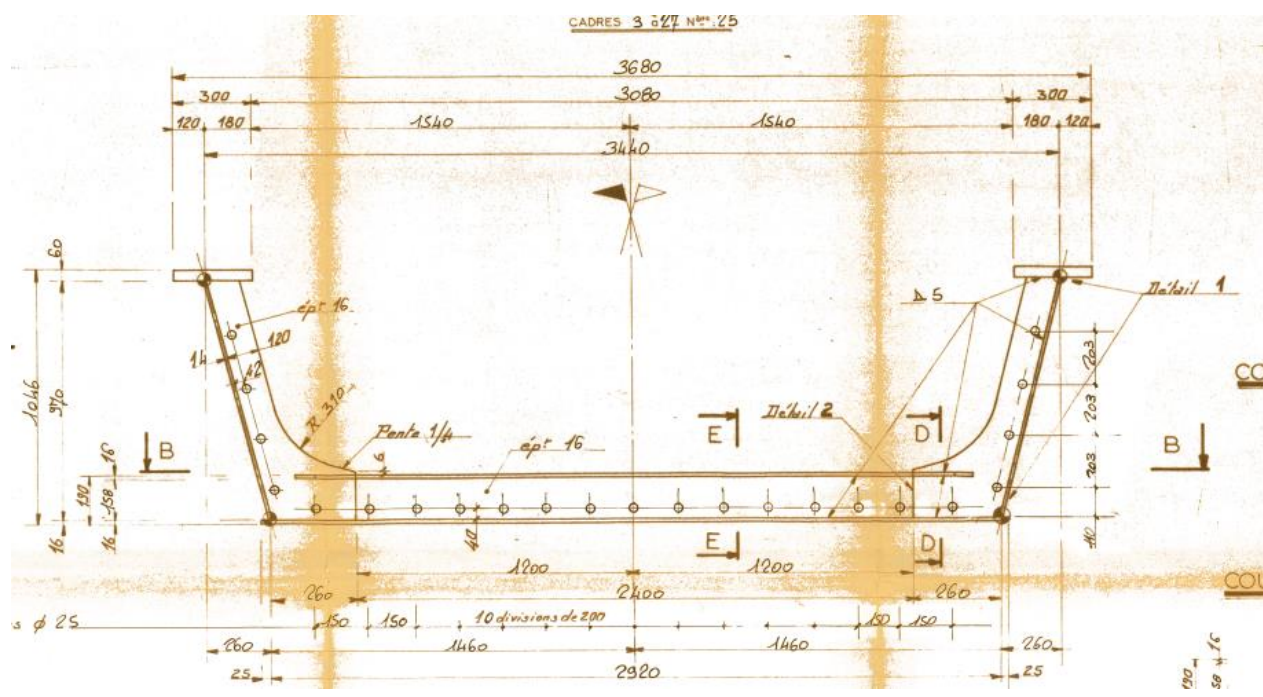
070000_470+164			
Country	**Line designation**	**Maximum speed**	**Infrastructure Manager**
France	070000: Paris Est - Strasbourg Ville	160 km/h	SNCF RÉSEAU

Structural properties			
Span (m)	9.00	**Type**	Filler beam
Mass (t/m)	11.00	**Configuration**	Simply supported
EI (N.m²)	1.84×10^9	**Normative type**	FB/RC
Dynamic properties			
Test type	Under railway traffic	**Method**	MCO
Range f_1 (Hz)	10.57 – 10.70	**Range ξ_1 (%)**	4.67 – 8.91
Range A_1 (m/s²)	0.033 – 0.126	**No. valid measurements**	3
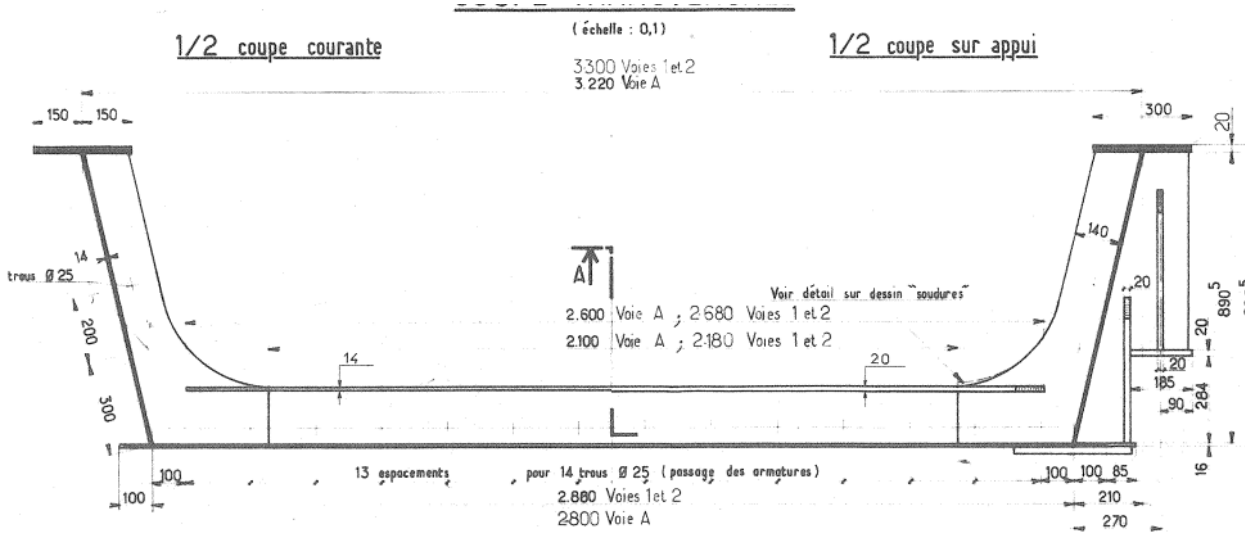
070000_484+884			
Country	**Line designation**	**Maximum speed**	**Infrastructure Manager**
France	070000: Paris Est - Strasbourg Ville	160 km/h	SNCF RÉSEAU

Structural properties			
Span (m)	8.97	**Type**	Filler beam
Mass (t/m)	11.85	**Configuration**	Simply supported
EI (N.m²)	2.08×10^9	**Normative type**	FB/RC
Dynamic properties			
Test type	Under railway traffic	**Method**	MCO
Range f_1 (Hz)	13.66	**Range ξ_1 (%)**	4.63
Range A_1 (m/s²)	0.006	**No. valid measurements**	1
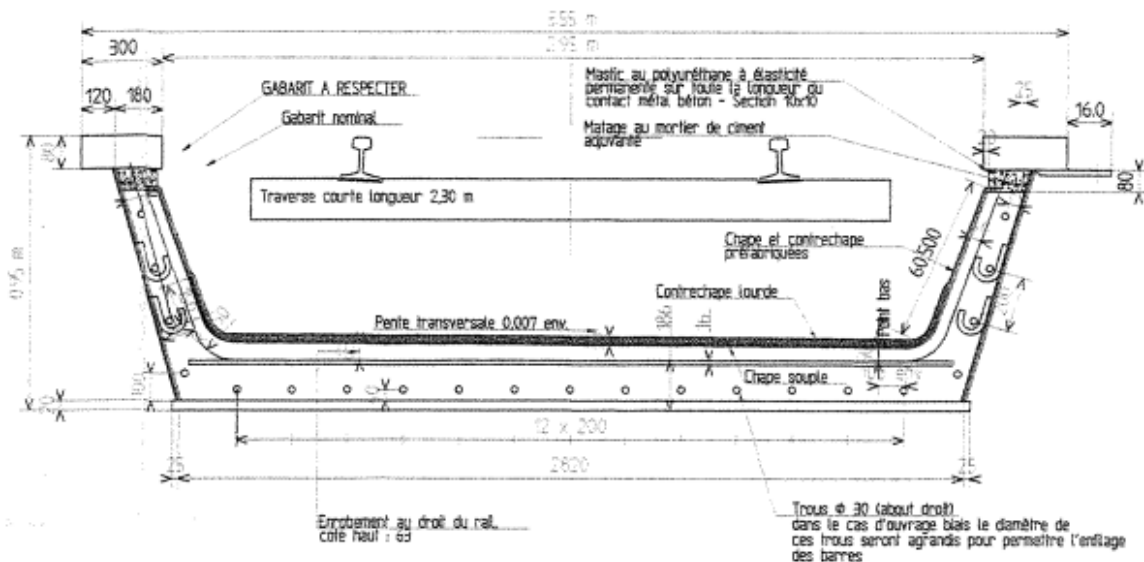
070000_492+208			
Country	**Line designation**	**Maximum speed**	**Infrastructure Manager**
France	070000: Paris Est - Strasbourg Ville	160 km/h	SNCF RÉSEAU

Structural properties			
Span (m)	11.40	**Type**	Filler beam
Mass (t/m)	13.10	**Configuration**	Simply supported
EI (N.m^2)	4.00×10^9	**Normative type**	FB/RC
Dynamic properties			
Test type	Under railway traffic	**Method**	MCO
Range f_1 (Hz)	9.02	**Range ξ_1 (%)**	5.96
Range A_1 (m/s^2)	0.030	**No. valid measurements**	1
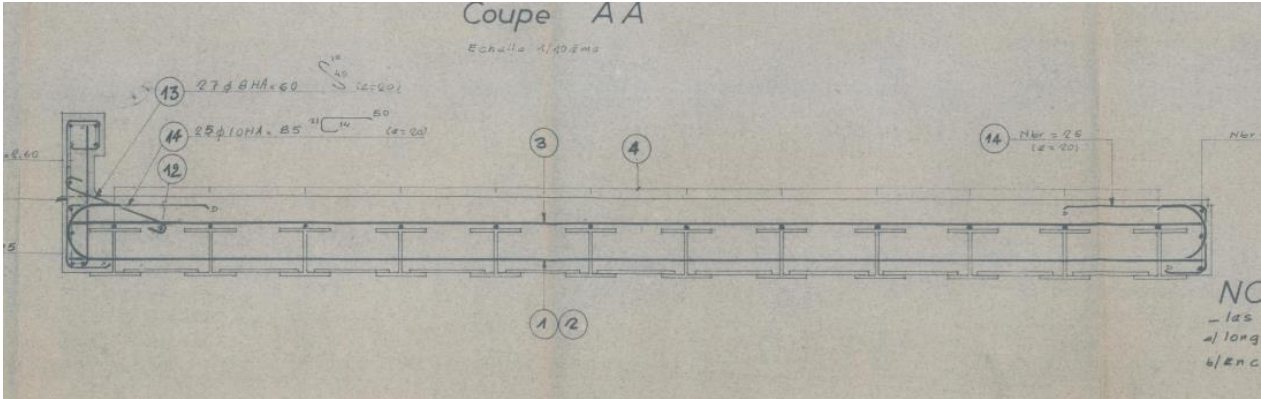
070000_496+533			
Country	**Line designation**	**Maximum speed**	**Infrastructure Manager**
France	070000: Paris Est - Strasbourg Ville	160 km/h	SNCF RÉSEAU

Structural properties			
Span (m)	38.50	**Type**	High upper side beams composite
Mass (t/m)	14.42	**Configuration**	Simply supported
EI (N.m^2)	1.17×10^{11}	**Normative type**	COMP
Dynamic properties			
Test type	Under railway traffic	**Method**	SSI-COV
Range f_1 (Hz)	3.10 – 3.15	**Range ξ_1 (%)**	0.91 – 1.55
Range A_1 (m/s^2)	0.004 – 0.379	**No. valid measurements**	37
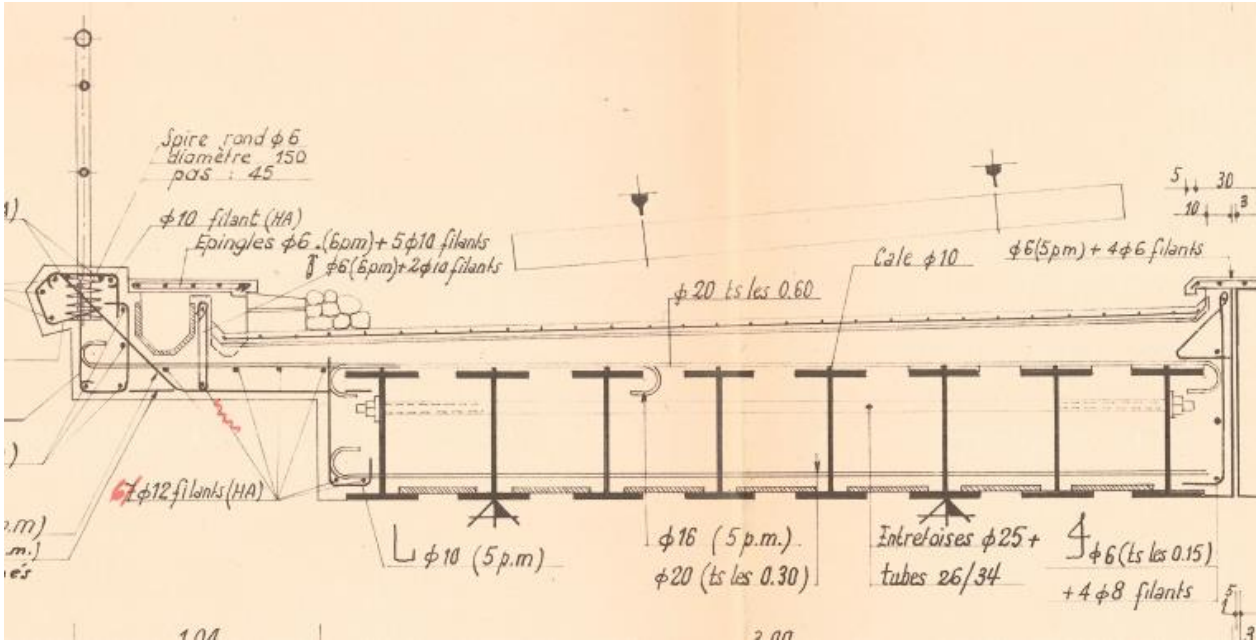
830000_034+307			
Country	**Line designation**	**Maximum speed**	**Infrastructure Manager**
France	830000: Paris Lyon - Marseille Saint Charles	160 km/h	SNCF RÉSEAU

Structural properties			
Span (m)	14.90	**Type**	Filler beam
Mass (t/m)	11.30	**Configuration**	Simply supported
EI (N.m²)	5.17×10^9	**Normative type**	FB/RC
Dynamic properties			
Test type	Under railway traffic	**Method**	MCO
Range f_1 (Hz)	7.51 – 9.02	**Range ξ_1 (%)**	5.67 – 9.37
Range A_1 (m/s²)	0.018 – 0.100	**No. valid measurements**	7

830000_036+790			
Country	**Line designation**	**Maximum speed**	**Infrastructure Manager**
France	830000: Paris Lyon - Marseille Saint Charles	160 km/h	SNCF RÉSEAU

Structural properties			
Span (m)	14.00	**Type**	U-shaped composite
Mass (t/m)	6.11	**Configuration**	Simply supported
EI (N.m²)	5.32×10^9	**Normative type**	COMP
Dynamic properties			
Test type	Under railway traffic	**Method**	SSI-COV
Range f_1 (Hz)	8.22 – 8.35	**Range ξ_1 (%)**	1.11 – 1.88
Range A_1 (m/s²)	0.011 – 0.088	**No. valid measurements**	28

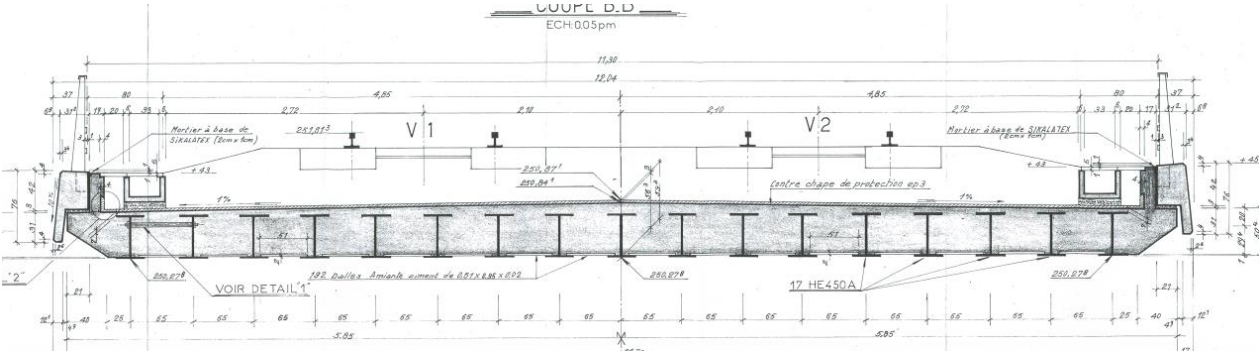| 830000_351+364			
Country	**Line designation**	**Maximum speed**	**Infrastructure Manager**
France	830000: Paris Lyon - Marseille Saint Charles	160 km/h	SNCF RÉSEAU

Structural properties			
Span (m)	7.50	**Type**	U-shaped composite
Mass (t/m)	5.42	**Configuration**	Simply supported
EI (N.m^2)	3.06×10^9	**Normative type**	COMP

Dynamic properties			
Test type	Under railway traffic	**Method**	SSI-COV
Range f_1 (Hz)	16.15 – 18.18	**Range ξ_1 (%)**	1.88 – 3.37
Range A_1 (m/s^2)	0.003 – 0.031	**No. valid measurements**	26

830000_380+357			
Country	**Line designation**	**Maximum speed**	**Infrastructure Manager**
France	830000: Paris Lyon - Marseille Saint Charles	160 km/h	SNCF RÉSEAU

Structural properties			
Span (m)	11.00	**Type**	U-shaped composite
Mass (t/m)	5.80	**Configuration**	Simply supported
EI (N.m²)	5.06×10^9	**Normative type**	COMP
Dynamic properties			
Test type	Under railway traffic	**Method**	SSI-COV
Range f_1 (Hz)	12.33 – 12.89	**Range ξ_1 (%)**	1.62 – 3.26
Range A_1 (m/s²)	0.004 – 0.075	**No. valid measurements**	33
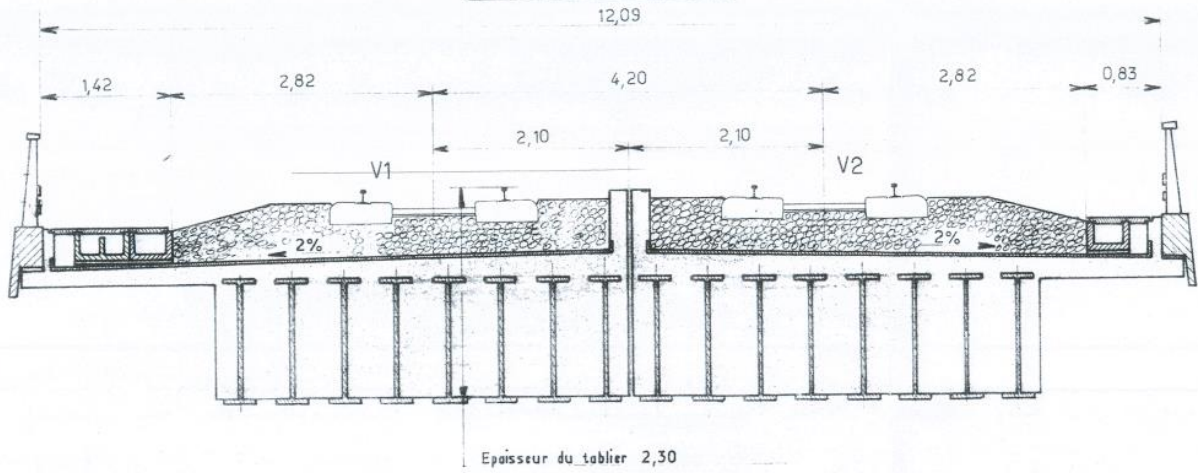
830000_697+966			
Country	**Line designation**	**Maximum speed**	**Infrastructure Manager**
France	830000: Paris Lyon - Marseille Saint Charles	160 km/h	SNCF RÉSEAU

Structural properties			
Span (m)	8.86	**Type**	Filler beam
Mass (t/m)	10.57	**Configuration**	Simply supported
EI (N.m²)	$2.36{\times}10^9$	**Normative type**	FB/RC
Dynamic properties			
Test type	Under railway traffic	**Method**	MCO
Range f_1 (Hz)	10.05	**Range ξ_1 (%)**	3.74
Range A_1 (m/s²)	0.015	**No. valid measurements**	1
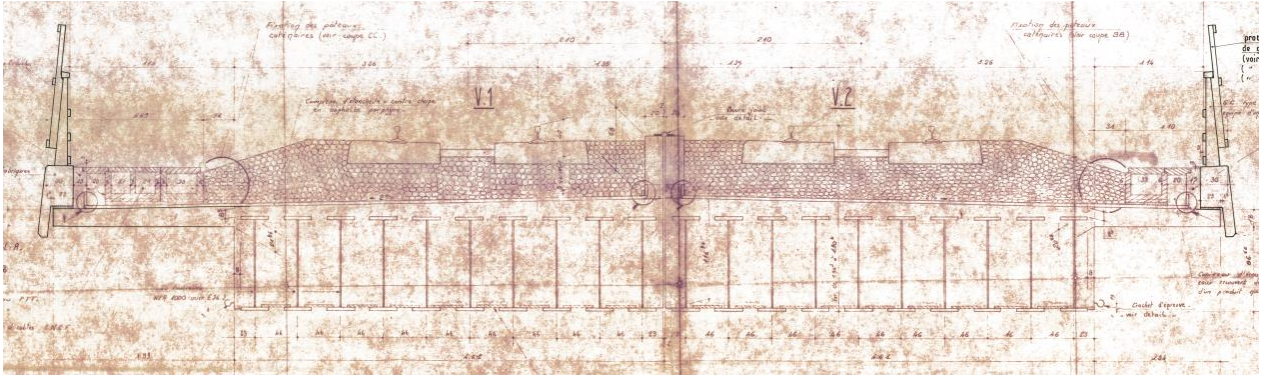
830000_699+425			
Country	**Line designation**	**Maximum speed**	**Infrastructure Manager**
France	830000: Paris Lyon - Marseille Saint Charles	160 km/h	

Structural properties			
Span (m)	14.20	**Type**	Filler beam
Mass (t/m)	12.23	**Configuration**	Simply supported
EI (N.m^2)	5.55×10^9	**Normative type**	FB/RC
Dynamic properties			
Test type	Under railway traffic	**Method**	MCO
Range f_1 (Hz)	8.27	**Range ξ_1 (%)**	4.87
Range A_1 (m/s^2)	0.015	**No. valid measurements**	1
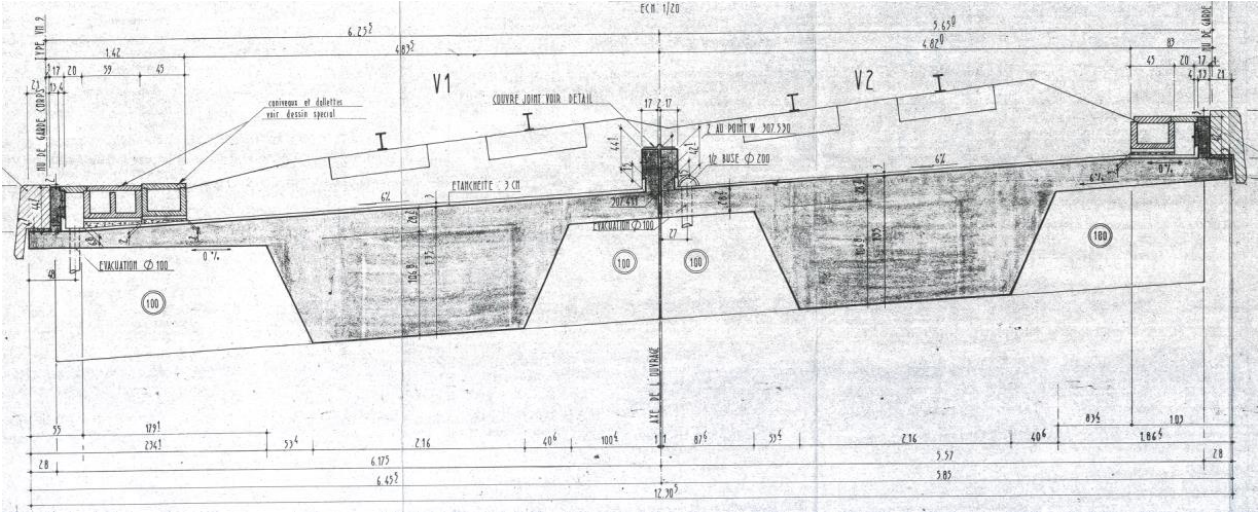
830000_739+502			
Country	**Line designation**	**Maximum speed**	**Infrastructure Manager**
France	830000: Paris Lyon - Marseille Saint Charles	160 km/h	SNCF RÉSEAU
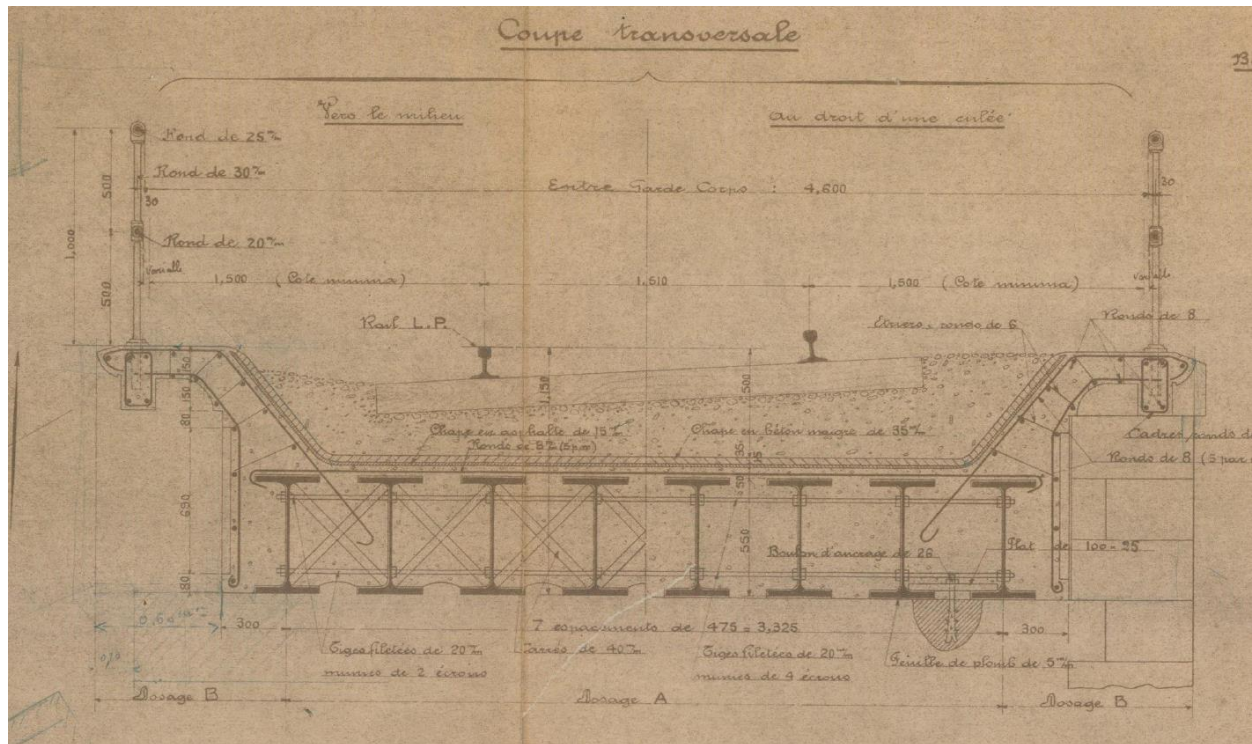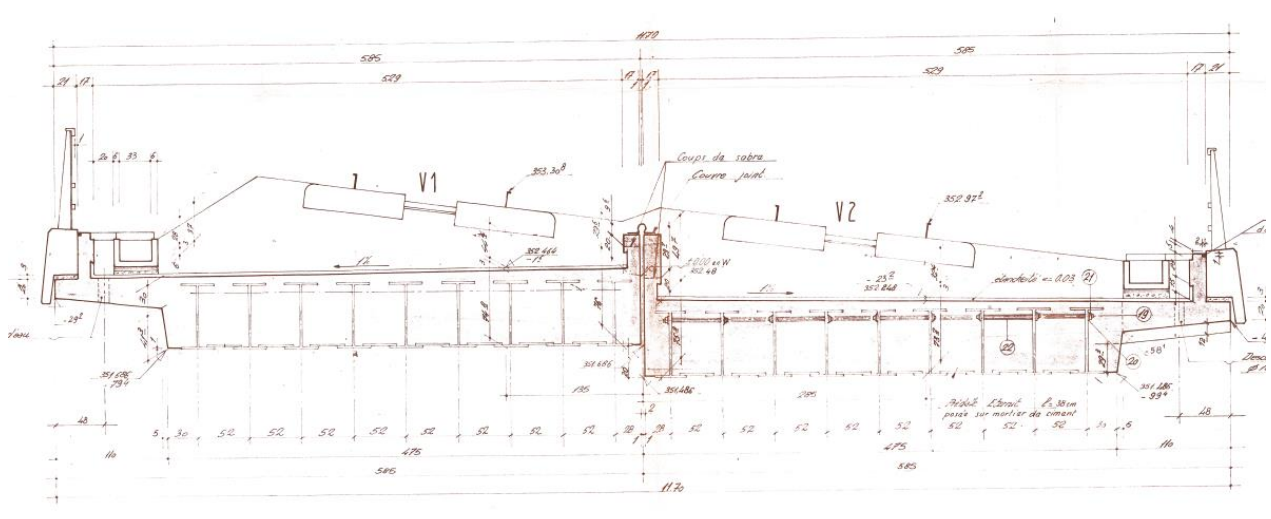
Structural properties			
Span (m)	13.80	**Type**	Filler beam
Mass (t/m)	12.32	**Configuration**	Simply supported
EI (N.m²)	4.49×10^9	**Normative type**	FB/RC
Dynamic properties			
Test type	Under railway traffic	**Method**	MCO
Range f_1 (Hz)	8.86 – 9.08	**Range ξ_1 (%)**	2.84 – 4.29
Range A_1 (m/s²)	0.003 – 0.011	**No. valid measurements**	2
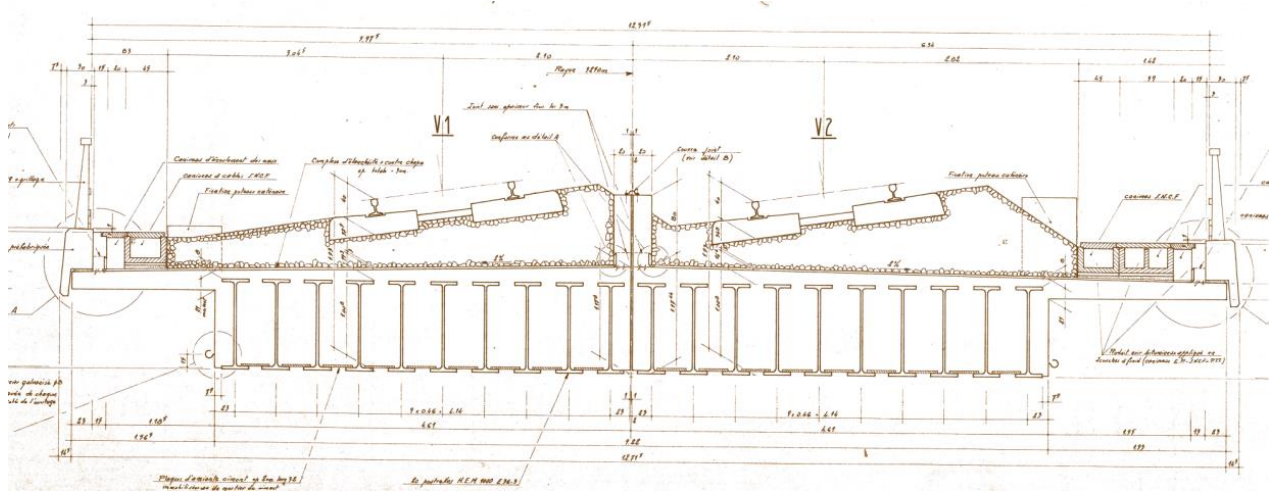
752000_083+112			
Country	**Line designation**	**Maximum speed**	**Infrastructure Manager**
France	752000: Paris - Lyon	300 km/h	SNCF RÉSEAU

Structural properties			
Span (m)	34.40	**Type**	Filler beam
Mass (t/m)	24.20	**Configuration**	Simply supported
EI (N.m²)	5.274×10^{10}	**Normative type**	FB/RC
Dynamic properties			
Test type	Under railway traffic	**Method**	MCO
Range f_1 (Hz)	2.50 – 2.52	**Range ξ_1 (%)**	1.64 – 2.12
Range A_1 (m/s²)	0.010-0.011	**No. valid measurements**	2
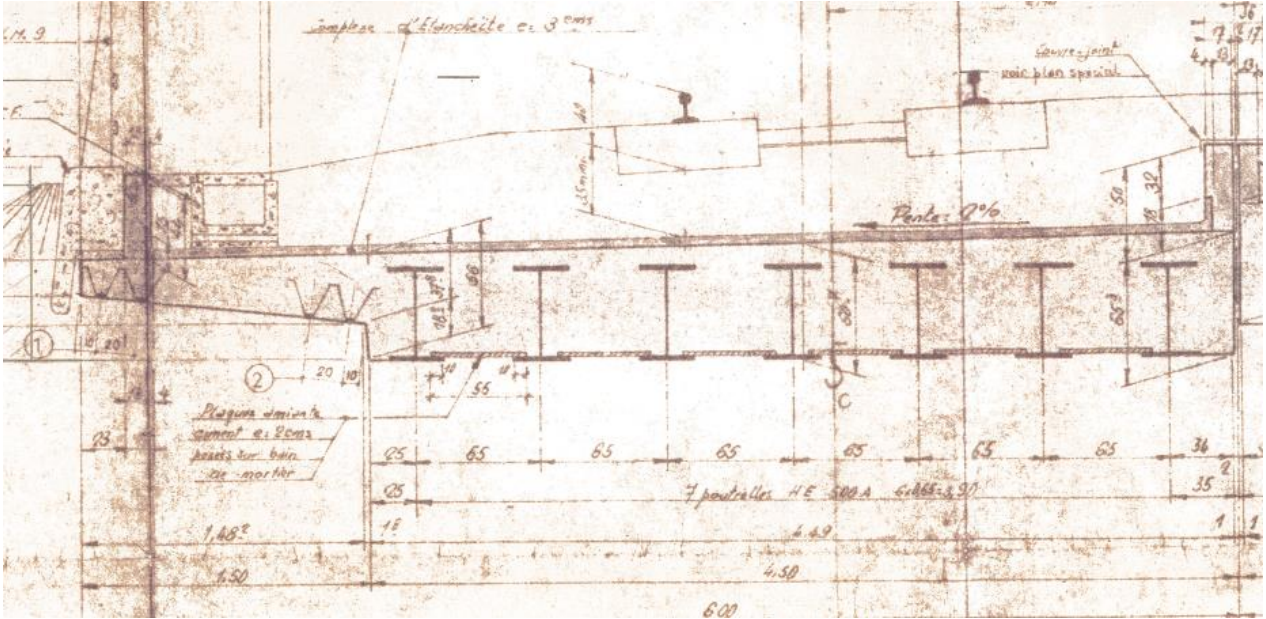
752000_185+353			
Country	**Line designation**	**Maximum speed**	**Infrastructure Manager**
France	752000: Paris - Lyon	300 km/h	SNCF RÉSEAU

Structural properties			
Span (m)	27.85	**Type**	Filler beam
Mass (t/m)	21.60	**Configuration**	Simply supported
EI (N.m^2)	2.87×10^{10}	**Normative type**	FB/RC
Dynamic properties			
Test type	Under railway traffic	**Method**	MCO
Range f_1 (Hz)	4.61	**Range ξ_1 (%)**	3.38
Range A_1 (m/s^2)	0.011	**No. valid measurements**	1
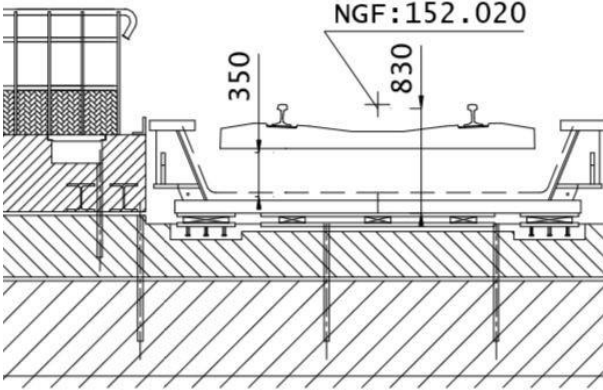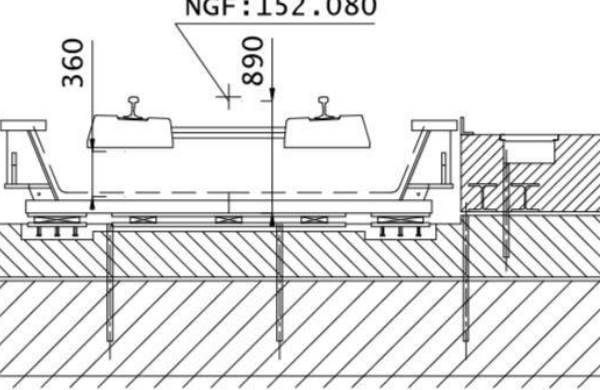
752000_241+136

Country	Line designation	Maximum speed	Infrastructure Manager
France	752000: Paris - Lyon	300 km/h	SNCF RÉSEAU

Structural properties

Span (m)	17.38	Type	Slab
Mass (t/m)	13.70	Configuration	Simply supported
EI (N.m^2)	2.31×10^{10}	Normative type	FB/RC

Dynamic properties

Test type	Under railway traffic	Method	MCO
Range f_1 (Hz)	6.48 – 6.81	Range ξ_1 (%)	1.99 – 5.77
Range A_1 (m/s^2)	0.003 – 0.223	No. valid measurements	11
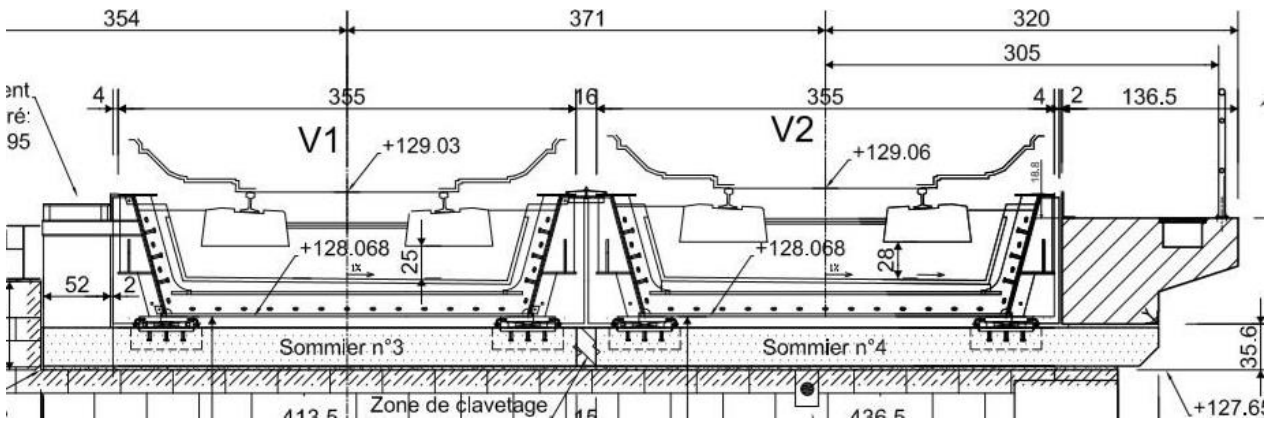
752000_249+715			
Country	**Line designation**	**Maximum speed**	**Infrastructure Manager**
France	752000: Paris - Lyon	300 km/h	SNCF RÉSEAU

Structural properties			
Span (m)	13.60	**Type**	Filler beam
Mass (t/m)	17.30	**Configuration**	Continuous
EI (N.m^2)	8.81×10^9	**Normative type**	FB/RC
Dynamic properties			
Test type	Under railway traffic	**Method**	MCO
Range f_1 (Hz)	8.32 – 8.36	**Range ξ_1 (%)**	4.72 – 4.89
Range A_1 (m/s^2)	0.016 – 0.020	**No. valid measurements**	2
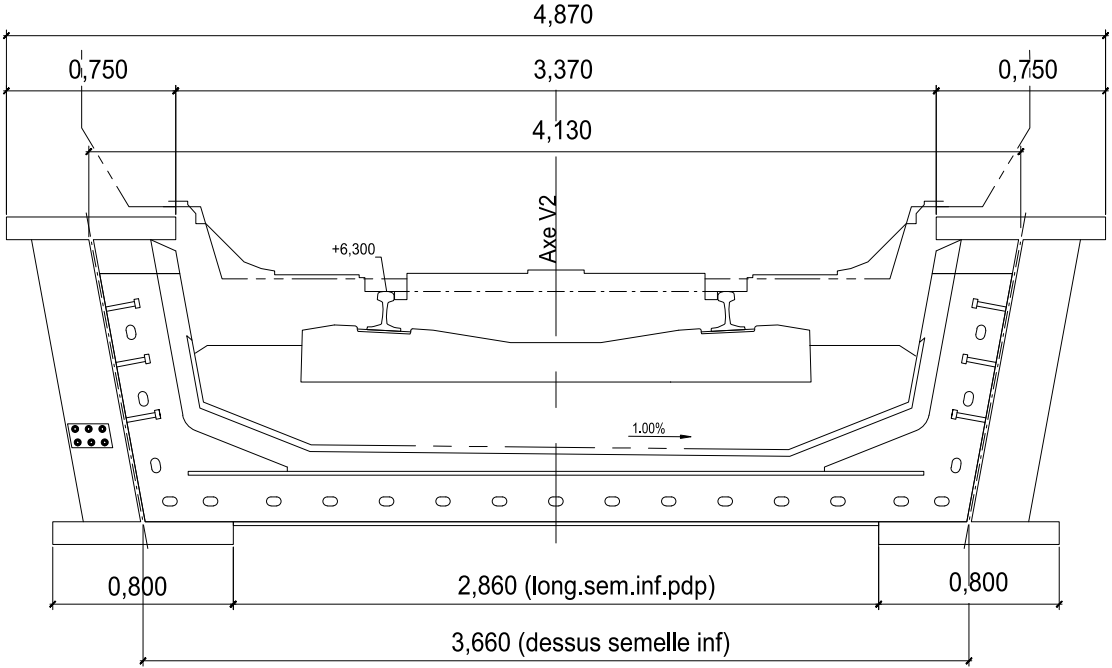
752000_287+961			
Country	**Line designation**	**Maximum speed**	**Infrastructure Manager**
France	752000: Paris - Lyon	270 km/h	SNCF RÉSEAU

Structural properties			
Span (m)	7.80	**Type**	Filler beam
Mass (t/m)	28.00	**Configuration**	Continuous
EI (N.m^2)	6.35×10^9	**Normative type**	FB/RC
Dynamic properties			
Test type	Under railway traffic	**Method**	MCO
Range f_1 (Hz)	17.91 – 17.95	**Range ξ_1 (%)**	1.59 – 2.33
Range A_1 (m/s^2)	0.027 – 0.032	**No. valid measurements**	2
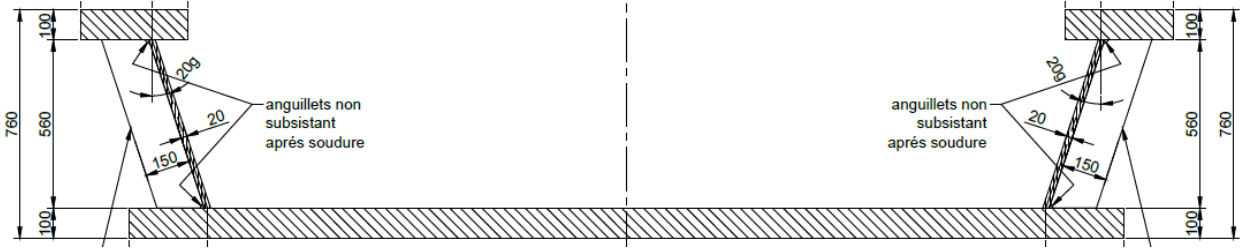
752000_318+837			
Country	**Line designation**	**Maximum speed**	**Infrastructure Manager**
France	752000: Paris - Lyon	270 km/h	SNCF RÉSEAU

Structural properties			
Span (m)	34.80	**Type**	Filler beam
Mass (t/m)	22.60	**Configuration**	Continuous
EI (N.m^2)	2.87×10^{10}	**Normative type**	FB/RC
Dynamic properties			
Test type	Under railway traffic	**Method**	MCO
Range f_1 (Hz)	2.11	**Range ξ_1 (%)**	2.10
Range A_1 (m/s^2)	0.012	**No. valid measurements**	1
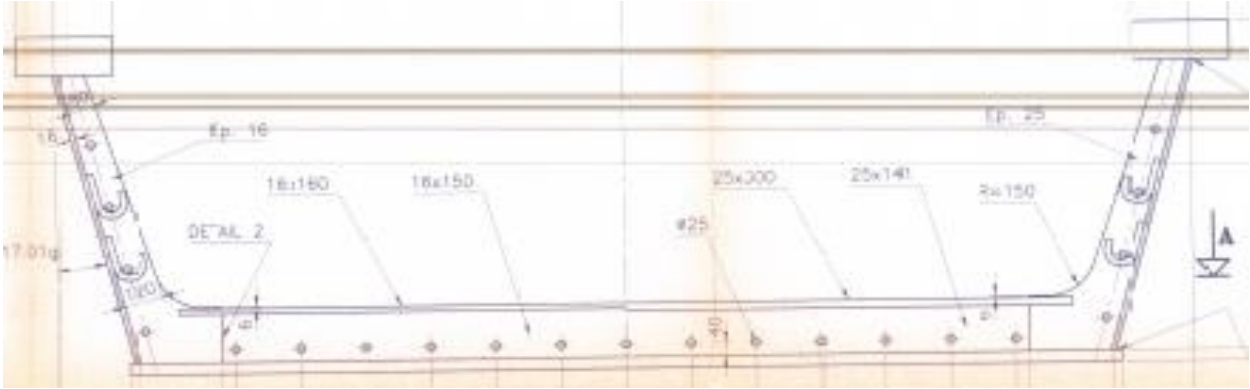
752000_335+986			
Country	**Line designation**	**Maximum speed**	**Infrastructure Manager**
France	752000: Paris - Lyon	270 km/h	SNCF RÉSEAU

Structural properties			
Span (m)	11.42	**Type**	Filler beam
Mass (t/m)	14.60	**Configuration**	Continuous
EI (N.m²)	3.84×10^9	**Normative type**	FB/RC
Dynamic properties			
Test type	Under railway traffic	**Method**	MCO
Range f_1 (Hz)	12.30	**Range ξ_1 (%)**	7.47
Range A_1 (m/s²)	0.010	**No. valid measurements**	1
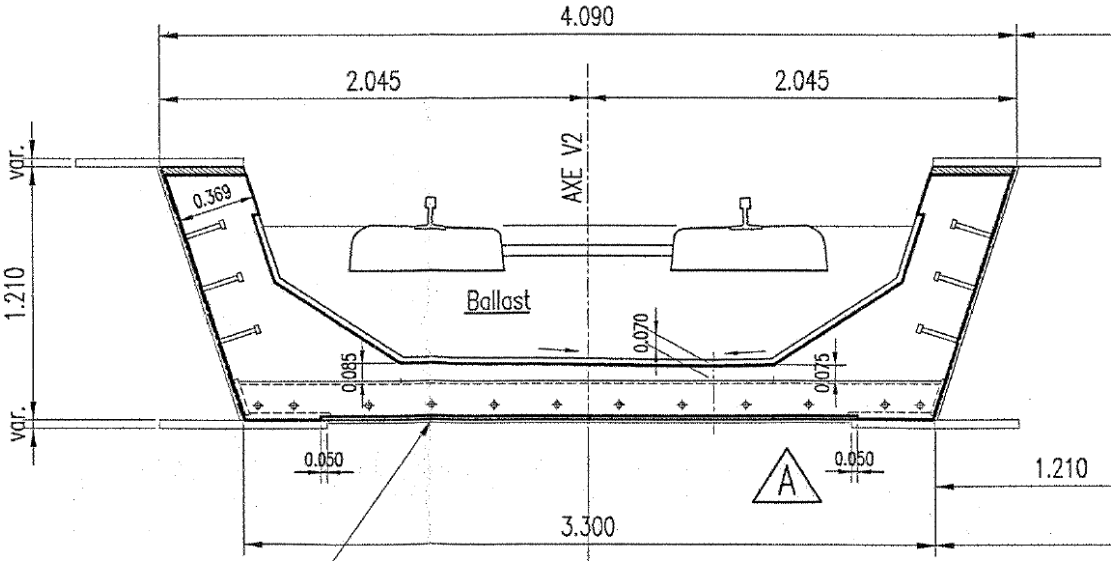
590000_261+703			
Country	**Line designation**	**Maximum speed**	**Infrastructure Manager**
France	590000: Aubrais Orléans - Montauban Ville Bourbon	160 km/h	SNCF RÉSEAU

Structural properties			
Span (m)	10.38	**Type**	U-shaped steel
Mass (t/m)	5.63	**Configuration**	Simply supported
EI (N.m^2)	4.65×10^9	**Normative type**	STL
Dynamic properties			
Test type	Under railway traffic	**Method**	MCO
Range f_1 (Hz)	11.38 – 12.18	**Range ξ_1 (%)**	1.68 – 3.73
Range A_1 (m/s^2)	0.003 – 0.063	**No. valid measurements**	21
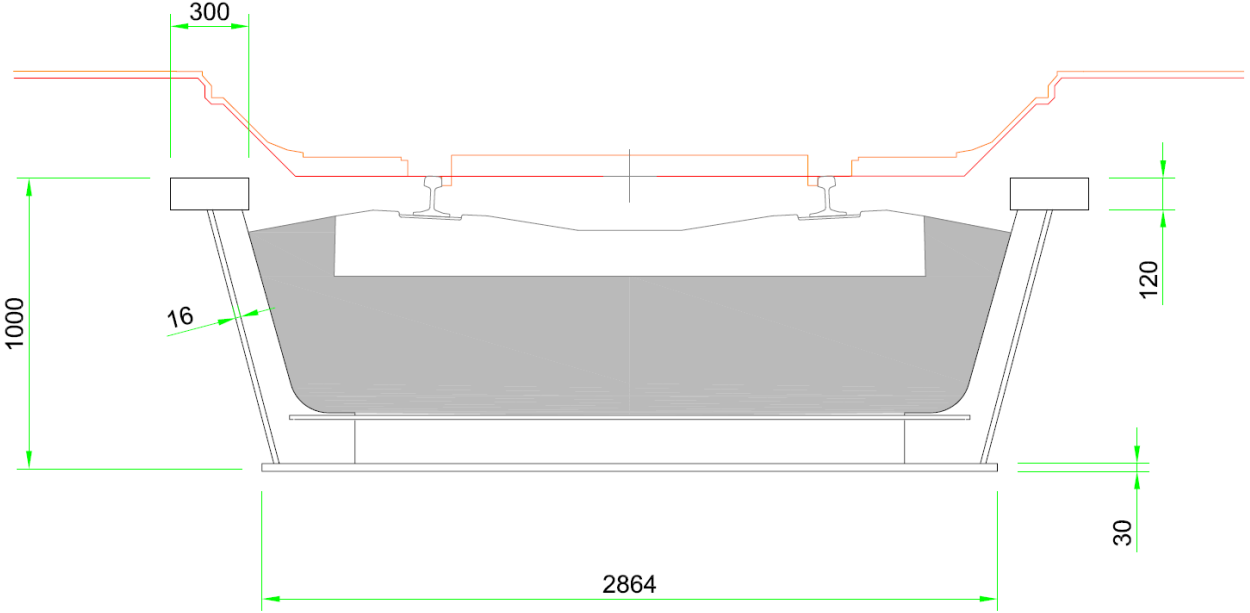
590000_235+895			
Country	**Line designation**	**Maximum speed**	**Infrastructure Manager**
France	590000: Aubrais Orléans - Montauban Ville Bourbon	160 km/h	SNCF RÉSEAU

Structural properties			
Span (m)	6.40	**Type**	U-shaped composite
Mass (t/m)	5.85	**Configuration**	Simply supported
EI (N.m^2)	3.62×10^9	**Normative type**	COMP

Dynamic properties			
Test type	Under railway traffic	**Method**	SSI-COV
Range f_1 (Hz)	22.22 – 25.66	**Range ξ_1 (%)**	3.31 – 11.81
Range A_1 (m/s^2)	0.004 – 0.019	**No. valid measurements**	22
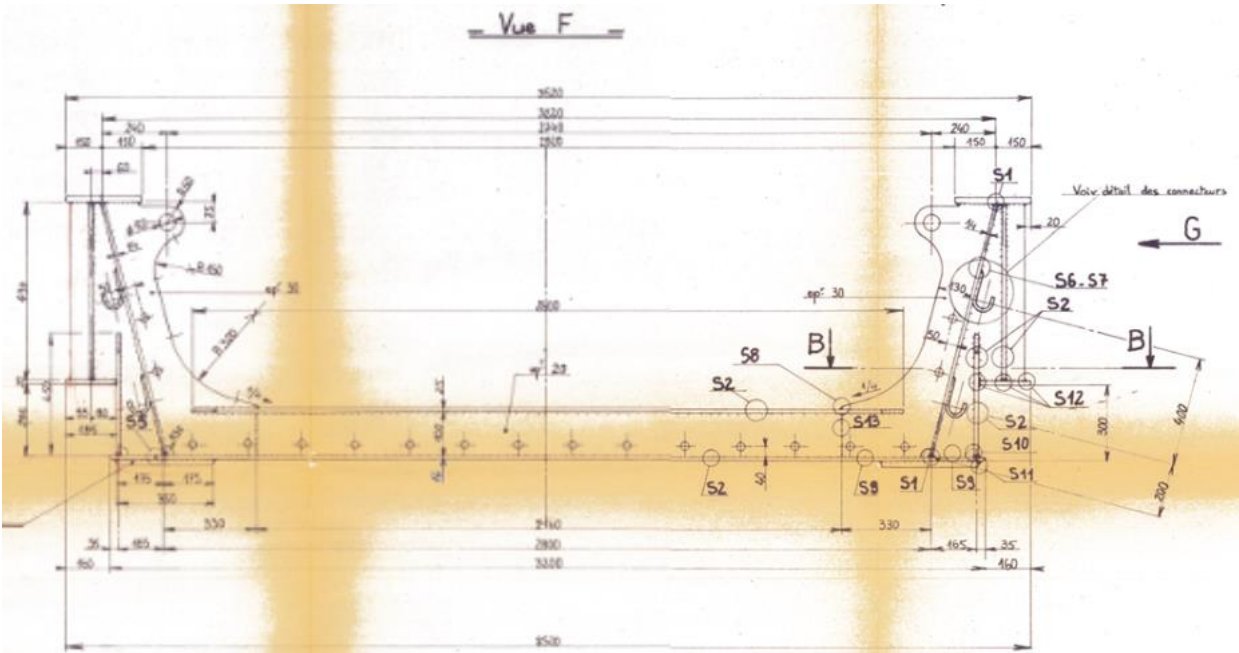
810000_097+770			
Country	**Line designation**	**Maximum speed**	**Infrastructure Manager**
France	810000: Tarascon - Sète Ville	160 km/h	SNCF RÉSEAU

Structural properties			
Span (m)	24.70	**Type**	Upper lateral inclined girders composite
Mass (t/m)	11.34	**Configuration**	Simply supported
EI (N.m^2)	2.98×10^{10}	**Normative type**	COMP
Dynamic properties			
Test type	Under railway traffic	**Method**	SSI-COV
Range f_1 (Hz)	4.38 – 4.52	**Range ξ_1 (%)**	0.73 – 0.99
Range A_1 (m/s^2)	0.009 – 0.080	**No. valid measurements**	9

001000_186+312			
Country	**Line designation**	**Maximum speed**	**Infrastructure Manager**
France	001000: Paris Est - Mulhouse Ville	160 km/h	SNCF RÉSEAU

Structural properties			
Span (m)	8.00	**Type**	U-shaped steel
Mass (t/m)	6.01	**Configuration**	Simply supported
EI (N.m²)	5.82×10^9	**Normative type**	STL
Dynamic properties			
Test type	Under railway traffic	**Method**	MCO
Range f_1 (Hz)	19.21 – 19.71	**Range ξ_1 (%)**	2.73 – 4.56
Range A_1 (m/s²)	0.010 – 0.115	**No. valid measurements**	17

001000_459+633			
Country	**Line designation**	**Maximum speed**	**Infrastructure Manager**
France	001000: Paris Est - Mulhouse Ville	160 km/h	SNCF RÉSEAU

Structural properties			
Span (m)	15.07	**Type**	U-shaped composite
Mass (t/m)	7.35	**Configuration**	Simply supported
EI (N.m²)	9.40×10^9	**Normative type**	COMP
Dynamic properties			
Test type	Under railway traffic	**Method**	SSI-COV
Range f_1 (Hz)	4.46 – 8.49	**Range ξ_1 (%)**	1.62 – 4.20
Range A_1 (m/s²)	0.005 – 0.103	**No. valid measurements**	24
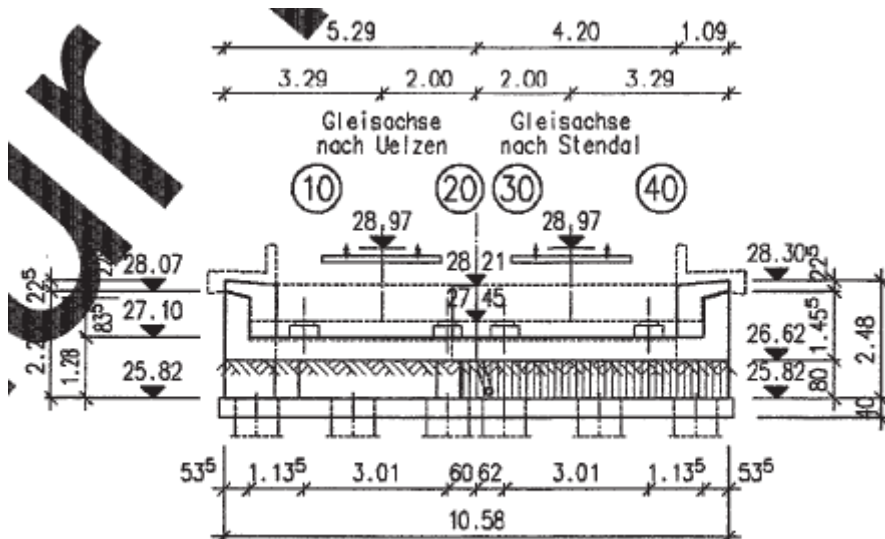
242000_138+166			
Country	**Line designation**	**Maximum speed**	**Infrastructure Manager**
France	242000: Creil - Jeumont	160 km/h	SNCF RÉSEAU

Structural properties			
Span (m)	31.50	**Type**	Upper lateral inclined girders composite
Mass (t/m)	11.42	**Configuration**	Simply supported
EI (N.m²)	2.68×10^{10}	**Normative type**	COMP
Dynamic properties			
Test type	Under railway traffic	**Method**	SSI-COV
Range f_1 (Hz)	2.82 – 2.88	**Range ξ_1 (%)**	0.60 – 0.89
Range A_1 (m/s²)	0.015 – 0.096	**No. valid measurements**	21
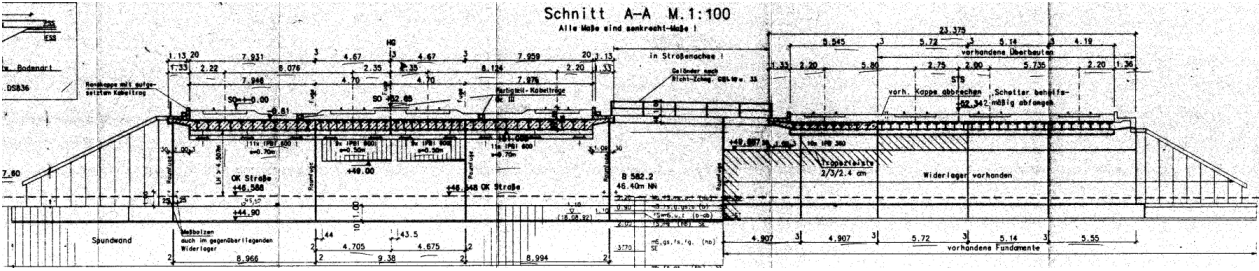
272000_048+164			
Country	**Line designation**	**Maximum speed**	**Infrastructure Manager**
France	272000: Paris Nord - Lille	160 km/h	SNCF RÉSEAU

Structural properties			
Span (m)	13.60	**Type**	U-shaped composite
Mass (t/m)	6.59	**Configuration**	Simply supported
EI (N.m²)	7.60×10^9	**Normative type**	COMP
Dynamic properties			
Test type	Under railway traffic	**Method**	SSI-COV
Range f_1 (Hz)	9.41 – 9.59	**Range ξ_1 (%)**	1.91 – 2.79
Range A_1 (m/s²)	0.027 – 0.058	**No. valid measurements**	10
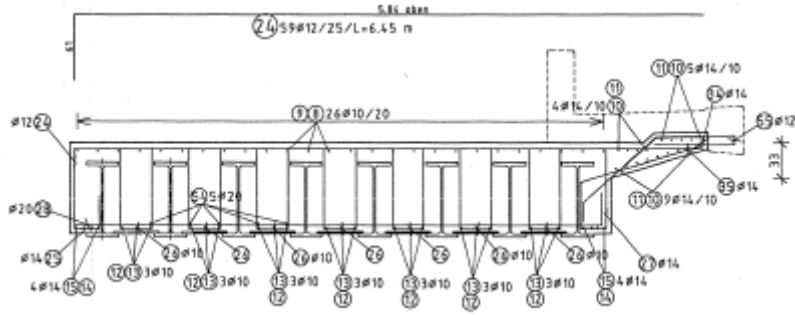
570000_041+757			
Country	**Line designation**	**Maximum speed**	**Infrastructure Manager**
France	570000: Paris Austerlitz - Bordeaux Saint Jean	150 km/h	SNCF RÉSEAU

Structural properties			
Span (m)	8.16	**Type**	U-shaped composite
Mass (t/m)	5.73	**Configuration**	Simply supported
EI **(N.m^2)**	2.19×10^9	**Normative type**	COMP
Dynamic properties			
Test type	Under railway traffic	**Method**	SSI-COV
Range f_1 (Hz)	14.73 – 15.93	**Range ξ_1 (%)**	1.79 – 5.41
Range A_1 (m/s^2)	0.004 – 0.109	**No. valid measurements**	31
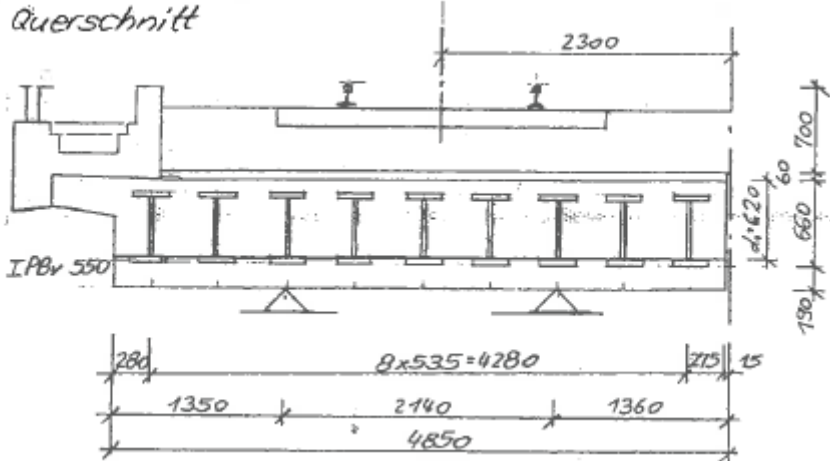
B.2. Bridges from Germany (DBInfraGO)
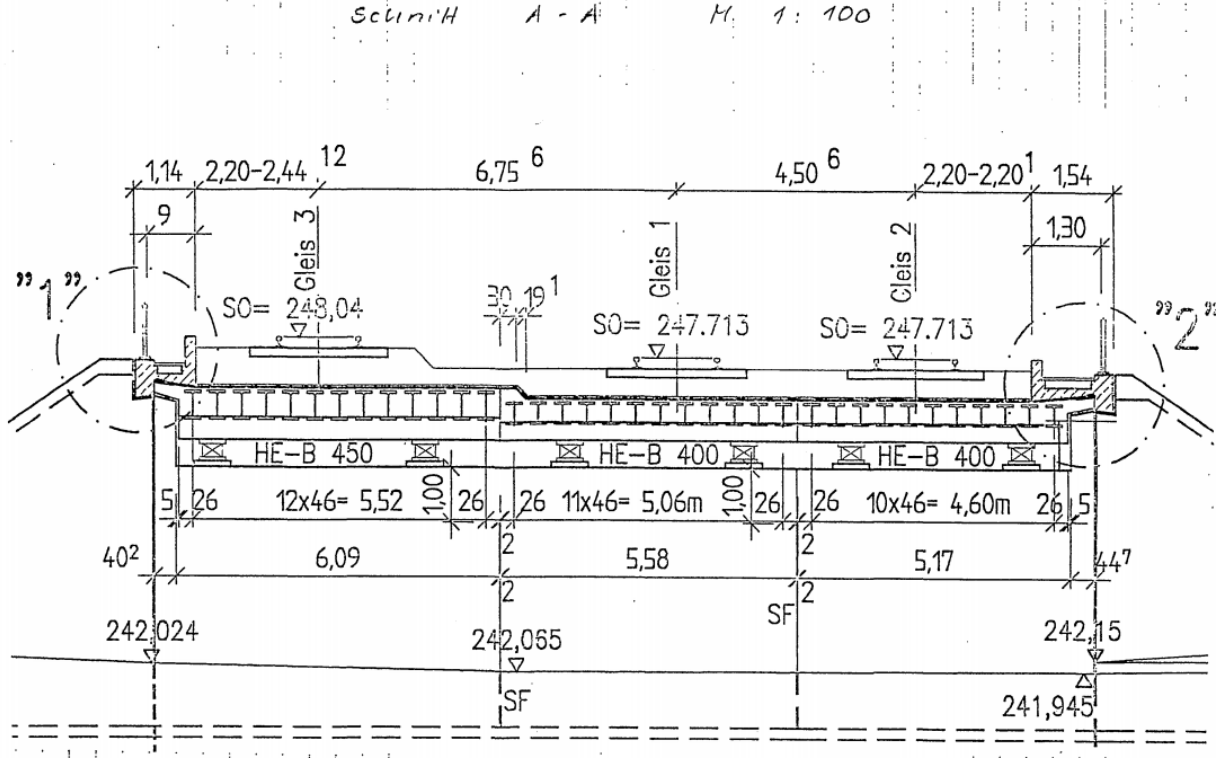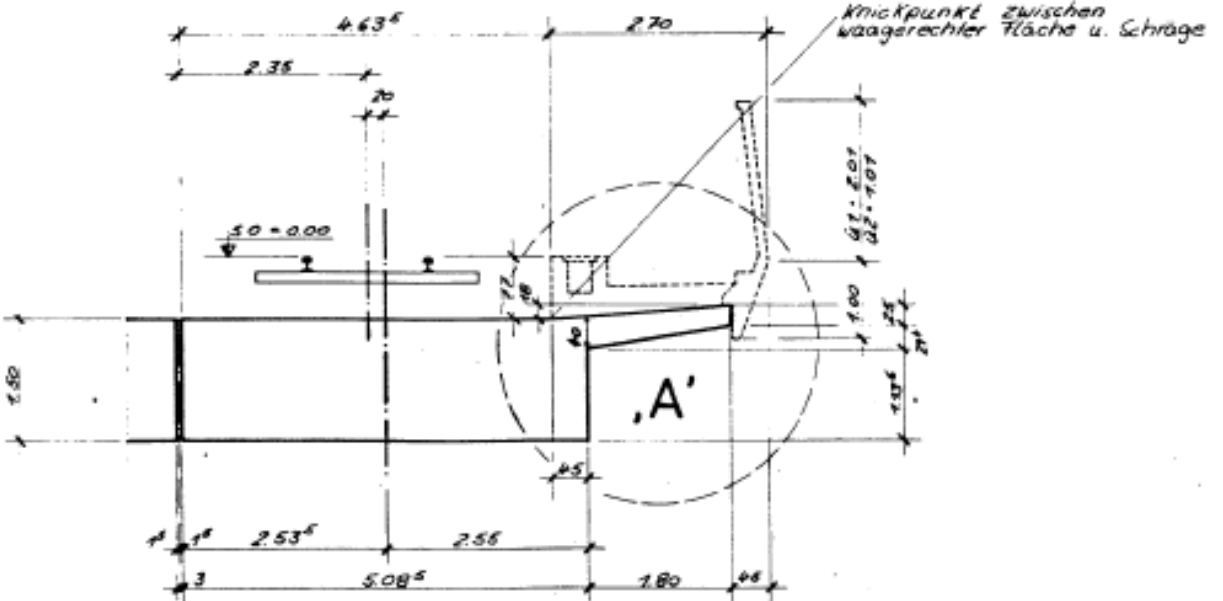
EÜ Milde bei Beese - ID24193			
Country	**Line designation**	**Maximum speed**	**Infrastructure Manager**
Germany	6899: Stendal Uelzen RiGI	160 km/h	DB InfraGO

Structural properties			
Span (m)	12.90	**Type**	Filler beam
Mass (t/m)	15.80	**Configuration**	Simply supported
EI (N.m^2)	3.73×10^9	**Normative type**	FB/RC
Dynamic properties			
Test type	Under railway traffic	**Method**	SSI-COV
Range f_1 (Hz)	8.39 – 8.77	**Range ξ_1 (%)**	4.33 – 10.62
Range A_1 (m/s^2)	0.008 – 0.225	**No. valid measurements**	19
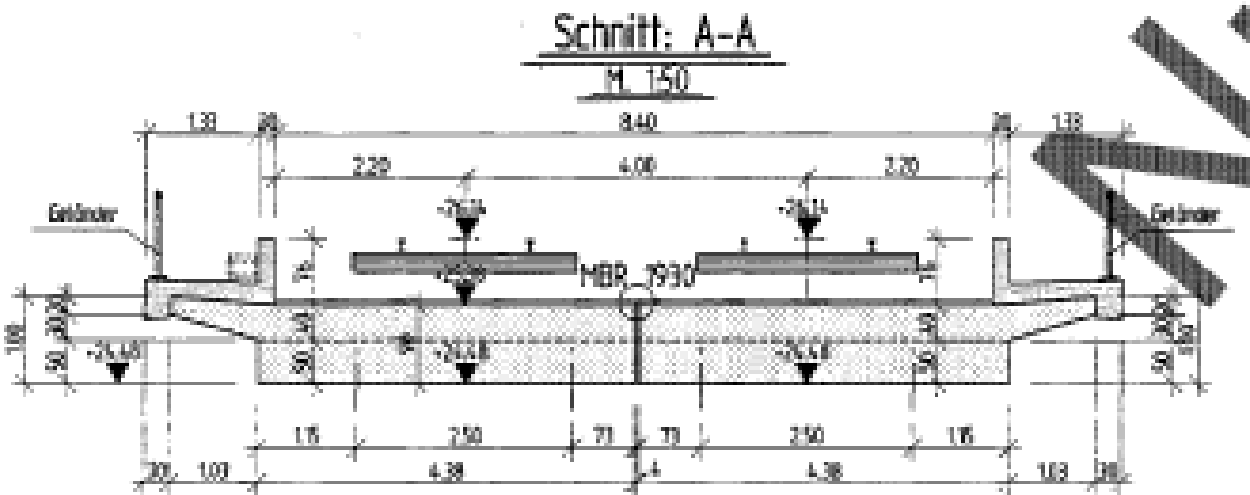
EÜ Str.Vinzelb.-Käth - ID26496			
Country	**Line designation**	**Maximum speed**	**Infrastructure Manager**
Germany	6185: Berlin Spandau – Oebisfelde GeRiGI	250 km/h	**DB InfraGO**

Structural properties			
Span (m)	12.86	**Type**	Filler beam
Mass (t/m)	16.56	**Configuration**	Simply supported
EI **(N.m²)**	$3.91{\times}10^9$	**Normative type**	FB/RC

Dynamic properties			
Test type	Under railway traffic	**Method**	SSI-COV
Range f_1 (Hz)	10.05 – 10.28	**Range ξ_1 (%)**	4.94 – 8.93
Range A_1 (m/s²)	0.018 – 0.130	**No. valid measurements**	16
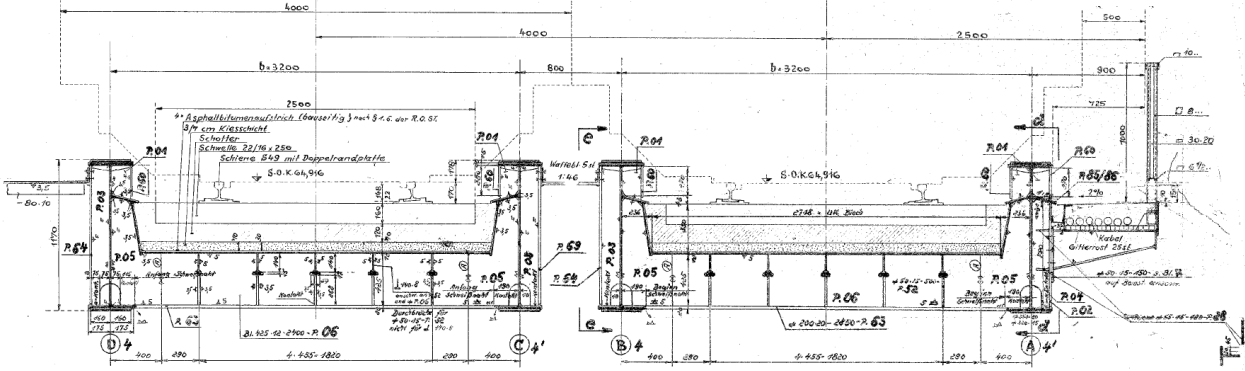
EÜ über477 bei Kerpen - ID20726			
Country	**Line designation**	**Maximum speed**	**Infrastructure Manager**
Germany	2600: Köln - Aachen	250 km/h	**DB** InfraGO

Structural properties			
Span (m)	15.92	**Type**	Filler beam
Mass (t/m)	20.87	**Configuration**	Simply supported
EI (N.m^2)	1.26×10^{10}	**Normative type**	FB/RC
Dynamic properties			
Test type	Under railway traffic	**Method**	SSI-COV
Range f_1 (Hz)	6.10 – 6.22	**Range ξ_1 (%)**	2.78 – 4.08
Range A_1 (m/s^2)	0.011 – 0.160	**No. valid measurements**	14
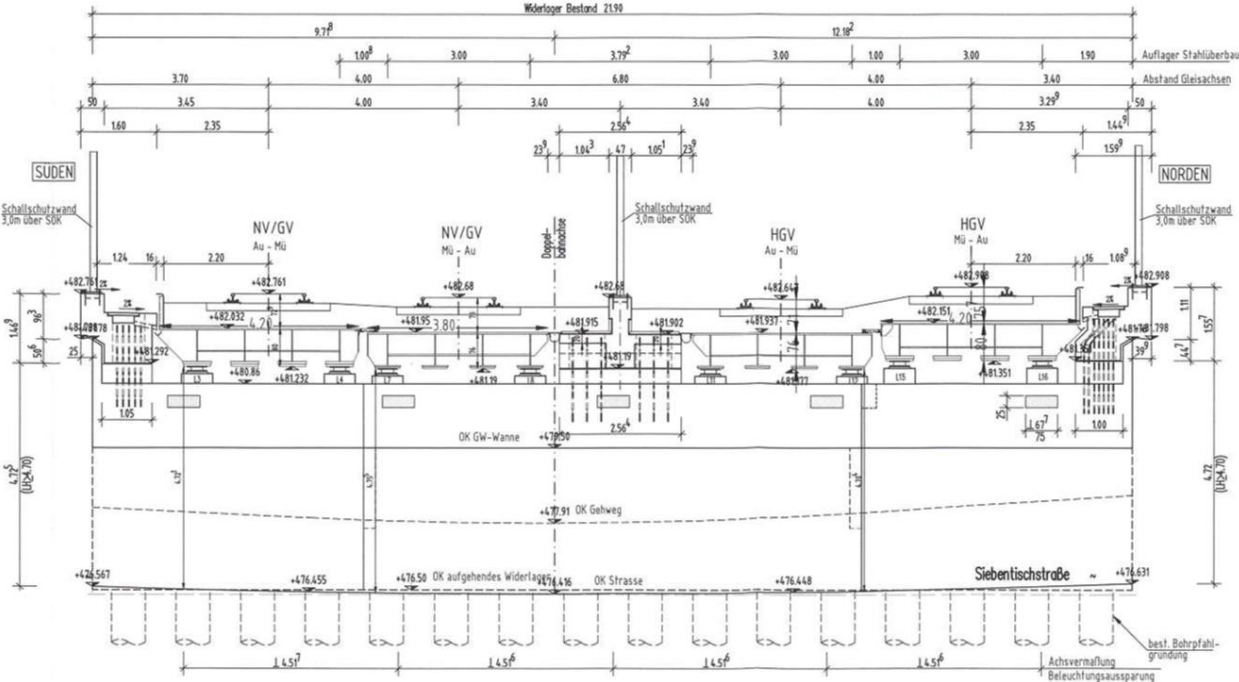
Nuthe Drewitz - ID23194			
Country	**Line designation**	**Maximum speed**	**Infrastructure Manager**
Germany	6118: Berlin-Charlottenburg – Blankenheim GeRiGI	160 km/h	**DB InfraGO**

Structural properties			
Span (m)	17.70	**Type**	Filler beam
Mass (t/m)	17.41	**Configuration**	Simply supported
EI **(N.m^2)**	5.56×10^9	**Normative type**	FB/RC
Dynamic properties			
Test type	Under railway traffic	**Method**	SSI-COV
Range f_1 (Hz)	5.30 – 5.66	**Range ξ_1 (%)**	4.70 – 7.61
Range A_1 (m/s^2)	0.005 – 0.151	**No. valid measurements**	20
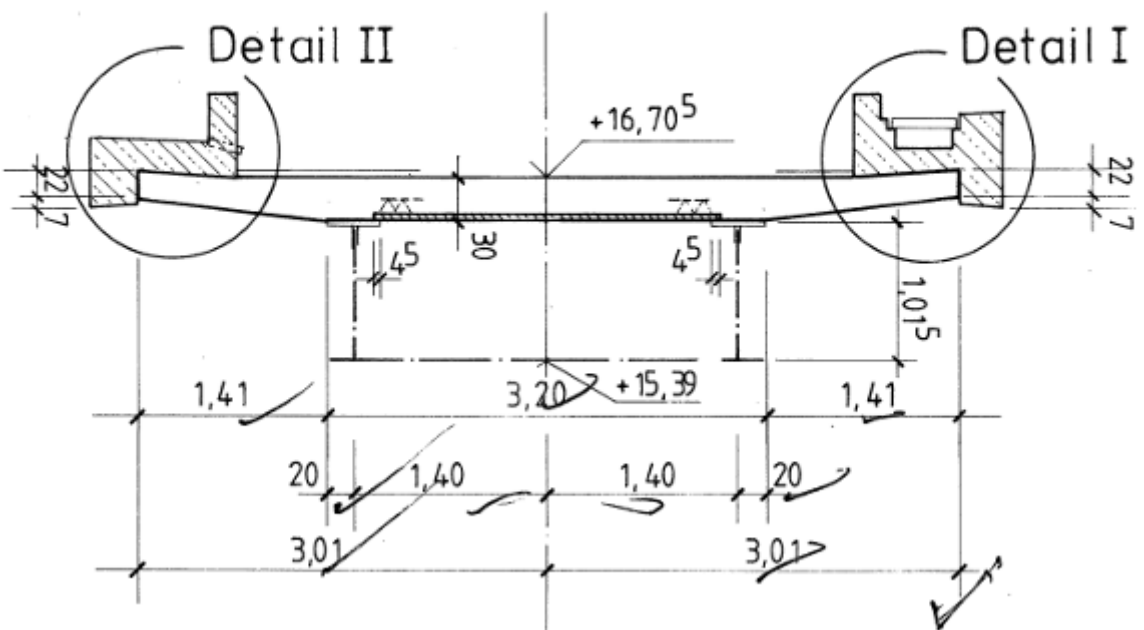
Straßenunterführung - ID12391			
Country	**Line designation**	**Maximum speed**	**Infrastructure Manager**
Germany	6340: Halle – Baunatal-Guntershausen	160 km/h	DB InfraGO

Structural properties			
Span (m)	12.00	**Type**	Filler beam
Mass (t/m)	14.05	**Configuration**	Simply supported
EI (N.m^2)	2.68×10^9	**Normative type**	FB/RC
Dynamic properties			
Test type	Under railway traffic	**Method**	SSI-COV
Range f_1 (Hz)	7.98 – 8.12	**Range ξ_1 (%)**	3.30 – 6.42
Range A_1 (m/s^2)	0.006 – 0.098	**No. valid measurements**	13
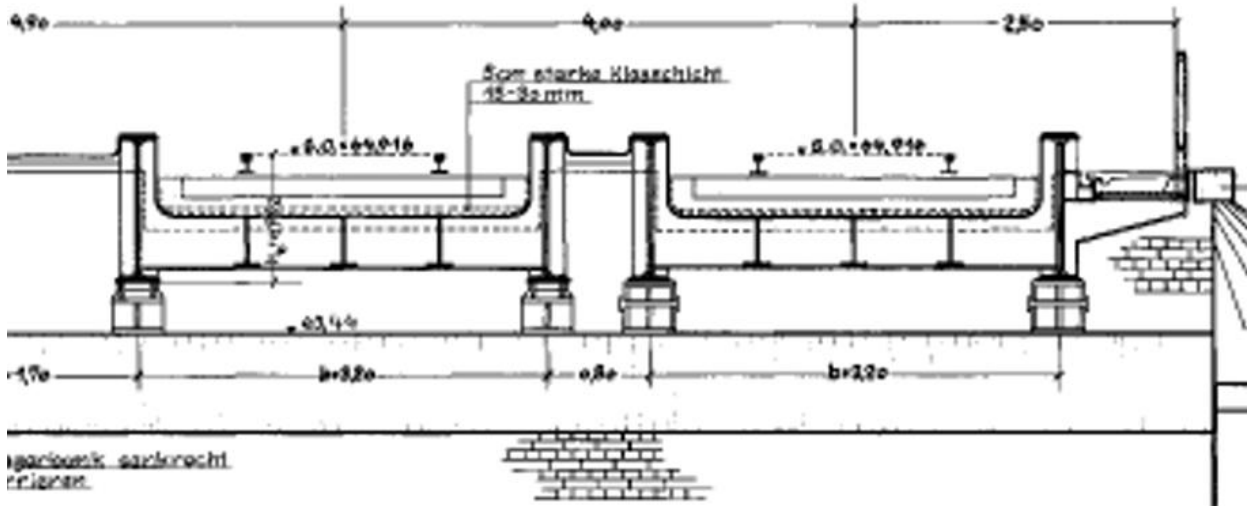
Ebr ü.Wenderterstraße - ID5046

Country	Line designation	Maximum speed	Infrastructure Manager
Germany	1733: Hannover Hbf – Würzburg Hbf GeRiGI	280 km/h	**DB** InfraGO

Structural properties

Span (m)	22.60	**Type**	Slab beam
Mass (t/m)	29.84	**Configuration**	Simply supported
EI (N.m²)	5.61×10^{10}	**Normative type**	PSC

Dynamic properties

Test type	Under railway traffic	**Method**	SSI-COV
Range f_1 (Hz)	5.20 – 5.37	**Range ξ_1 (%)**	4.21 – 6.30
Range A_1 (m/s²)	0.019 – 0.139	**No. valid measurements**	31
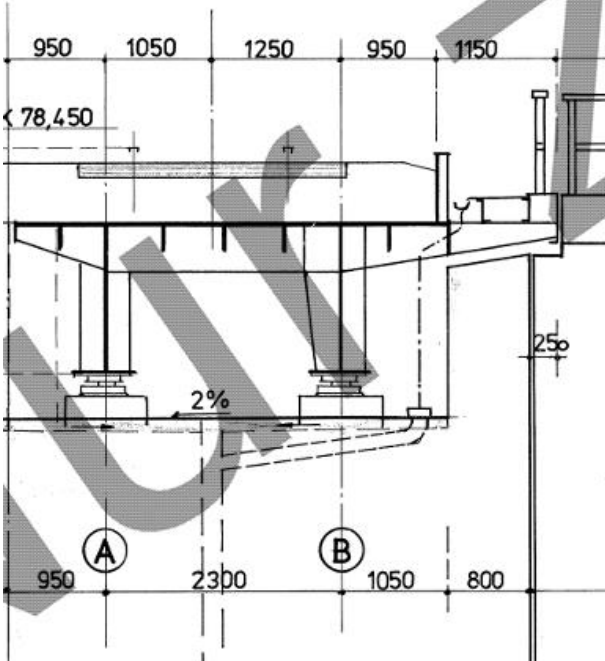
Hamminkelner Landstr - ID34492			
Country	**Line designation**	**Maximum speed**	**Infrastructure Manager**
Germany	2270: Oberhausen Hbf – Emmerich Grenze	160 km/h	**DB InfraGO**

Structural properties			
Span (m)	16.73	**Type**	Slab beam
Mass (t/m)	16.90	**Configuration**	Simply supported
EI (N.m²)	1.00×10^{10}	**Normative type**	PSC
Dynamic properties			
Test type	Under railway traffic	**Method**	SSI-COV
Range f_1 (Hz)	8.62 – 8.82	**Range ξ_1 (%)**	3.25 – 7.22
Range A_1 (m/s²)	0.025 – 0.106	**No. valid measurements**	13

Friedrich Allee - ID7341			
Country	**Line designation**	**Maximum speed**	**Infrastructure Manager**
Germany	2630: Köln Hbf – Bingen Hbf	160 km/h	**DB InfraGO**

Structural properties			
Span (m)	14.71	**Type**	Trough cross-section
Mass (t/m)	6.00	**Configuration**	Simply supported
EI (N.m^2)	4.01×10^9	**Normative type**	STL
Dynamic properties			
Test type	Under railway traffic	**Method**	SSI-COV
Range f_1 (Hz)	8.03 – 8.17	**Range ξ_1 (%)**	1.38 – 2.56
Range A_1 (m/s^2)	0.015 – 0.116	**No. valid measurements**	13
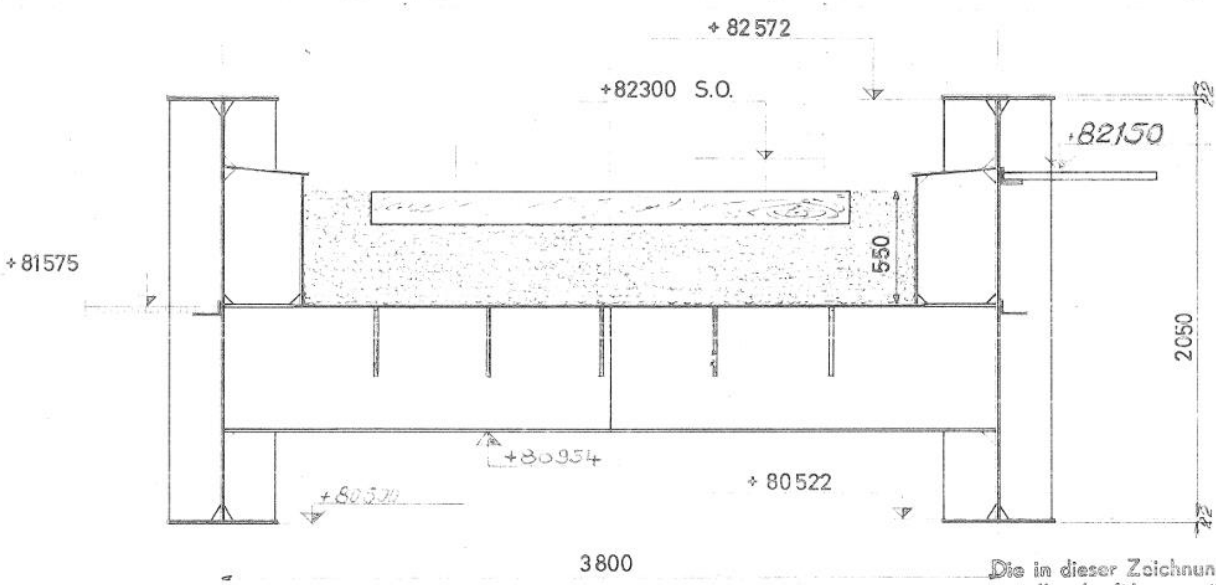
Augsburg - ID31962			
Country	**Line designation**	**Maximum speed**	**Infrastructure Manager**
Germany	5581: München Hbf – Augsburg Hbf	150 km/h	DB InfraGO

Structural properties			
Span (m)	20.08	**Type**	Trough cross-section
Mass (t/m)	6.79	**Configuration**	Simply supported
EI (N.m^2)	7.30×10^9	**Normative type**	STL
Dynamic properties			
Test type	Under railway traffic	**Method**	SSI-COV
Range f_1 (Hz)	4.36 – 4.85	**Range ξ_1 (%)**	3.43 – 7.02
Range A_1 (m/s^2)	0.020 – 0.600	**No. valid measurements**	11
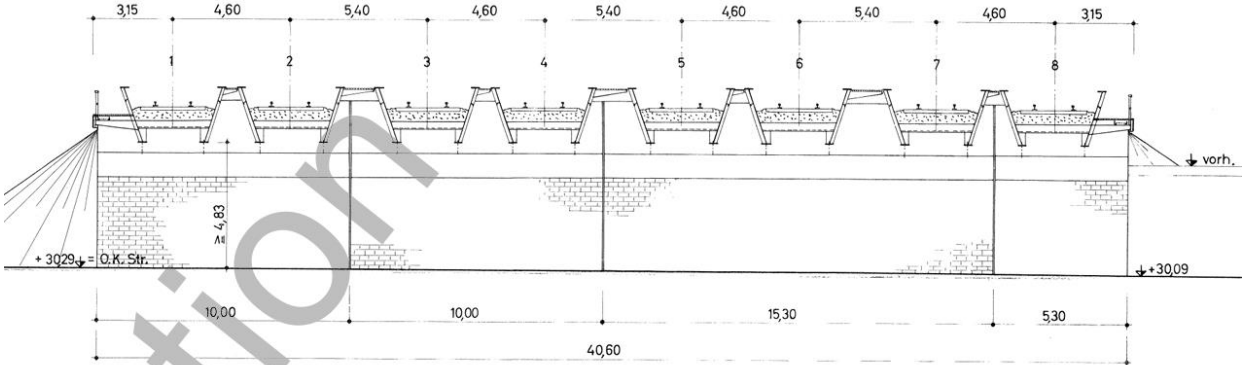
BadOldesloe - ID24517			
Country	**Line designation**	**Maximum speed**	**Infrastructure Manager**
Germany	1120: Lübeck Hbf – Hamburg Hbf GeRiGI	140 km/h	**DB InfraGO**

Structural properties			
Span (m)	30.10	**Type**	Steel hollow box with concrete slab
Mass (t/m)	13.14	**Configuration**	Simply supported
EI (N.m^2)	3.65×10^{10}	**Normative type**	COMP
Dynamic properties			
Test type	Under railway traffic	**Method**	SSI-COV
Range f_1 (Hz)	2.78 – 3.97	**Range ξ_1 (%)**	2.07 – 4.54
Range A_1 (m/s^2)	0.009 – 0.207	**No. valid measurements**	8
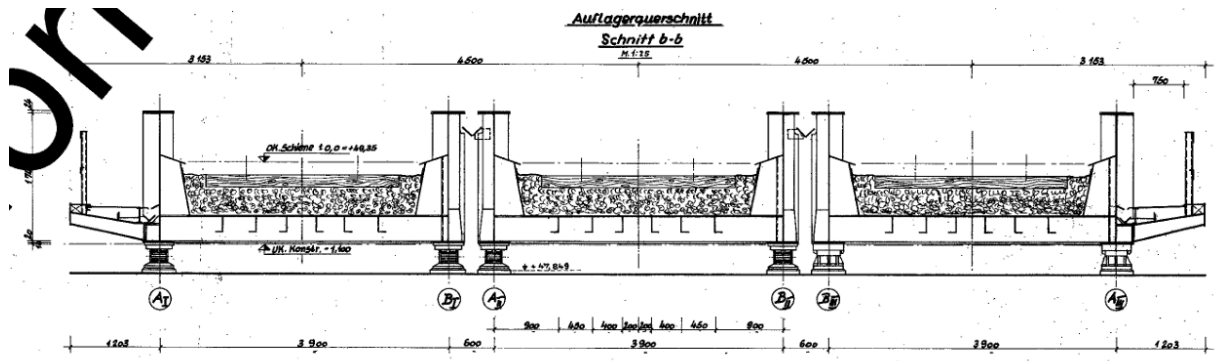
Bonn - ID7342 | 7343			
Country	**Line designation**	**Maximum speed**	**Infrastructure Manager**
Germany	2630: Köln – Bingen	160 km/h	**DB** InfraGO

Structural properties			
Span (m)	14.37	**Type**	Trough cross-section
Mass (t/m)	ID7342: 4.45 ID7343: 6.22	**Configuration**	Simply supported
EI (N.m²)	4.92×10^9	**Normative type**	STL
Dynamic properties			
Test type	Under railway traffic	**Method**	SSI-COV
Range f_1 (Hz)	8.58 – 9.01	**Range ξ_1 (%)**	1.73 – 4.99
Range A_1 (m/s²)	0.035 – 0.170	**No. valid measurements**	10

Boppard - ID7640			
Country	**Line designation**	**Maximum speed**	**Infrastructure Manager**
Germany	2630: Köln – Bingen	120 km/h	**DB InfraGO**

Structural properties			
Span (m)	27.30	**Type**	Trough cross-section
Mass (t/m)	8.93	**Configuration**	Simply supported
EI (N.m²)	1.99×10^{10}	**Normative type**	STL
Dynamic properties			
Test type	Under railway traffic	**Method**	SSI-COV
Range f_1 (Hz)	4.59 – 5.06	**Range ξ_1 (%)**	1.32 – 6.55
Range A_1 (m/s²)	0.035 – 0.700	**No. valid measurements**	12
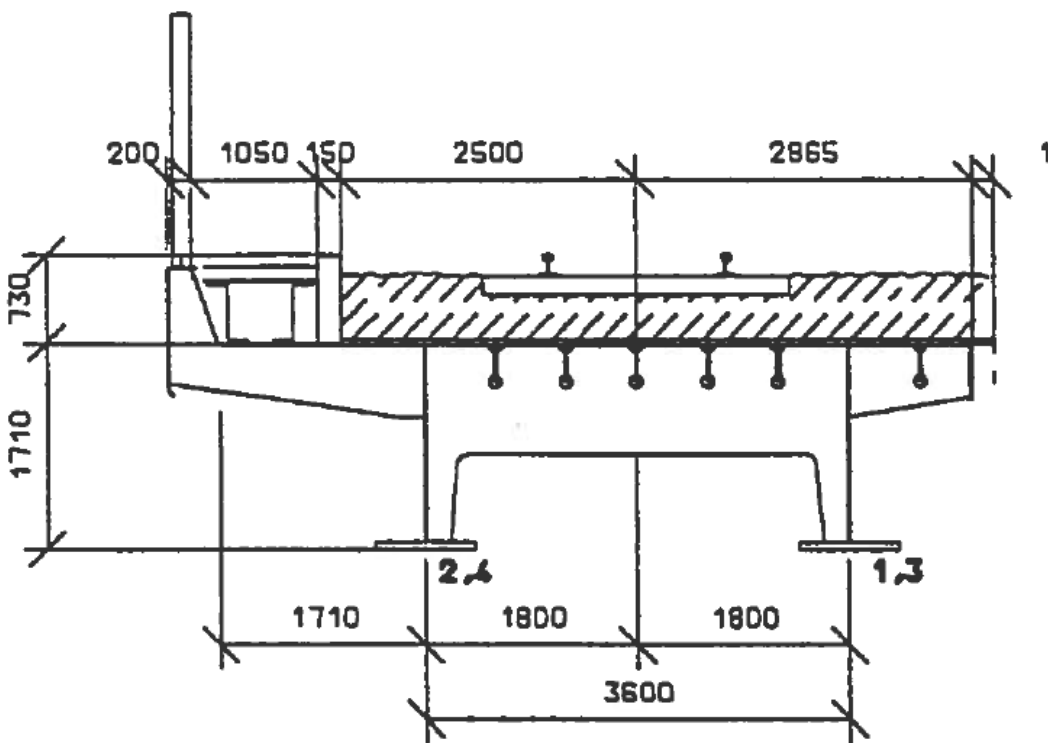
Boppard - ID7641			
Country	**Line designation**	**Maximum speed**	**Infrastructure Manager**
Germany	2630: Köln – Bingen	120 km/h	**DB InfraGO**

Structural properties			
Span (m)	31.80	**Type**	Trough cross-section
Mass (t/m)	8.93	**Configuration**	Simply supported
EI (N.m²)	1.99×10^{10}	**Normative type**	STL
Dynamic properties			
Test type	Under railway traffic	**Method**	SSI-COV
Range f_1 (Hz)	3.55 – 3.73	**Range ξ_1 (%)**	1.43 – 5.33
Range A_1 (m/s²)	0.019 – 0.350	**No. valid measurements**	14
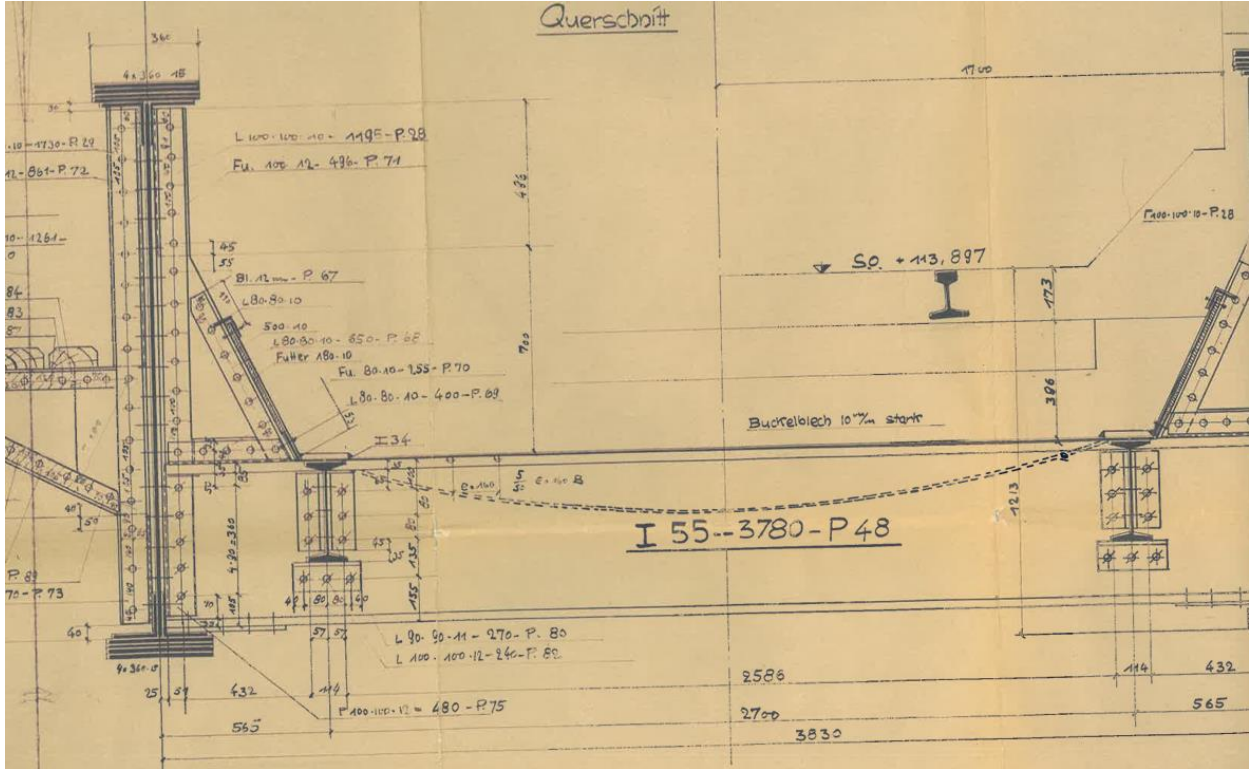
Braunschweig - ID3648

Country	Line designation	Maximum speed	Infrastructure Manager
Germany	1730: Hannover – Braunschweig RiGI	140 km/h	**DB** InfraGO

Structural properties

Span (m)	35.20	**Type**	Trough cross-section
Mass (t/m)	4.09	**Configuration**	Simply supported
EI **(N.m^2)**	3.62×10^{10}	**Normative type**	STL

Dynamic properties

Test type	Under railway traffic	**Method**	SSI-COV
Range f_1 (Hz)	3.35 – 3.45	**Range ξ_1 (%)**	0.83 – 2.81
Range A_1 (m/s^2)	0.050 – 0.500	**No. valid measurements**	17
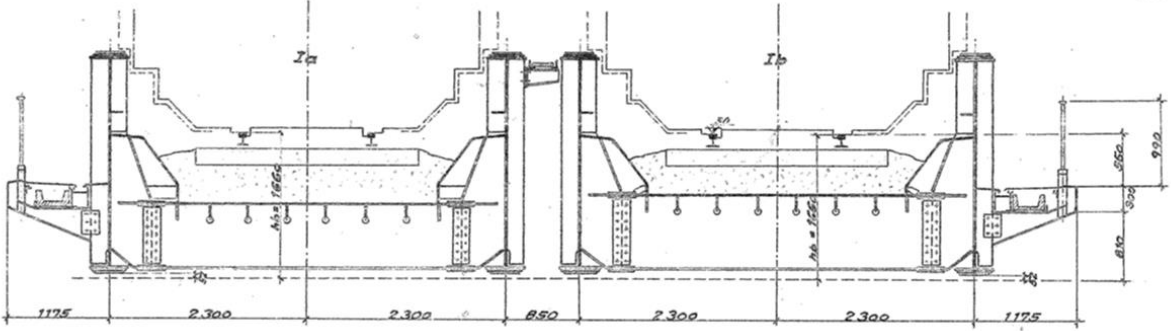
Duisburg - ID15906 | 16955			
Country	**Line designation**	**Maximum speed**	**Infrastructure Manager**
Germany	2650: Köln – Essen	140 km/h	DB InfraGO

Structural properties			
Span (m)	30.20	**Type**	Trough cross-section
Mass (t/m)	5.90	**Configuration**	Simply supported
EI (N.m^2)	2.53×10^{10}	**Normative type**	STL
Dynamic properties			
Test type	Under railway traffic	**Method**	SSI-COV
Range f_1 (Hz)	3.72 – 3.85	**Range ξ_1 (%)**	0.93 – 1.60
Range A_1 (m/s^2)	0.025 – 1.100	**No. valid measurements**	35
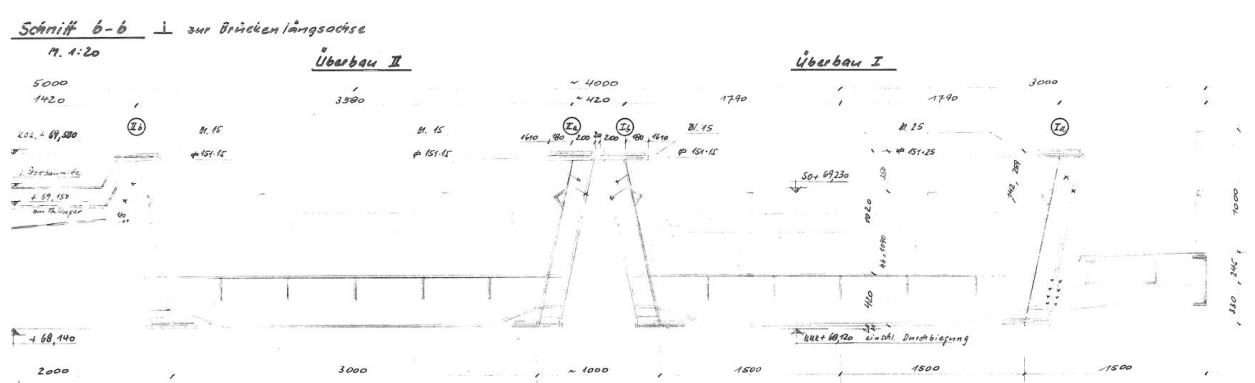
Essen - ID17028 | 17553			
Country	**Line designation**	**Maximum speed**	**Infrastructure Manager**
Germany	2650: Köln – Hamm	160 km/h	**DB** InfraGO

Structural properties			
Span (m)	22.70	**Type**	Trough cross-section
Mass (t/m)	5.06	**Configuration**	Simply supported
EI (N.m²)	1.25×10^{10}	**Normative type**	STL
Dynamic properties			
Test type	Under railway traffic	**Method**	SSI-COV
Range f_1 (Hz)	4.68 – 5.24	**Range ξ_1 (%)**	1.00 – 1.66
Range A_1 (m/s²)	0.017 – 0.420	**No. valid measurements**	33

Halle - ID11874 | 11875			
Country	**Line designation**	**Maximum speed**	**Infrastructure Manager**
Germany	6132: Berlin – Halle	80 km/h	**DB** InfraGO
No Drawings			
Structural properties			
Span (m)	28.00	**Type**	Trough cross-section
Mass (t/m)	9.60	**Configuration**	Simply supported
EI (N.m^2)	2.89×10^{10}	**Normative type**	STL
Dynamic properties			
Test type	Under railway traffic	**Method**	SSI-COV
Range f_1 (Hz)	4.11 – 4.30	**Range ξ_1 (%)**	0.44 – 2.77
Range A_1 (m/s^2)	0.010 – 0.100	**No. valid measurements**	20

HannoverLeinhausen - ID4500			
Country	**Line designation**	**Maximum speed**	**Infrastructure Manager**
Germany	1700: Hannover - Leinhausen	160 km/h	**DB** **InfraGO**

Structural properties			
Span (m)	21.00	**Type**	Girder grid with concrete slab
Mass (t/m)	9.52	**Configuration**	Simply supported
EI (N.m²)	4.22×10^{10}	**Normative type**	COMP

Dynamic properties			
Test type	Under railway traffic	**Method**	SSI-COV
Range f_1 (Hz)	4.16 – 4.26	**Range ξ_1 (%)**	2.81 – 4.40
Range A_1 (m/s²)	0.030 – 0.200	**No. valid measurements**	11
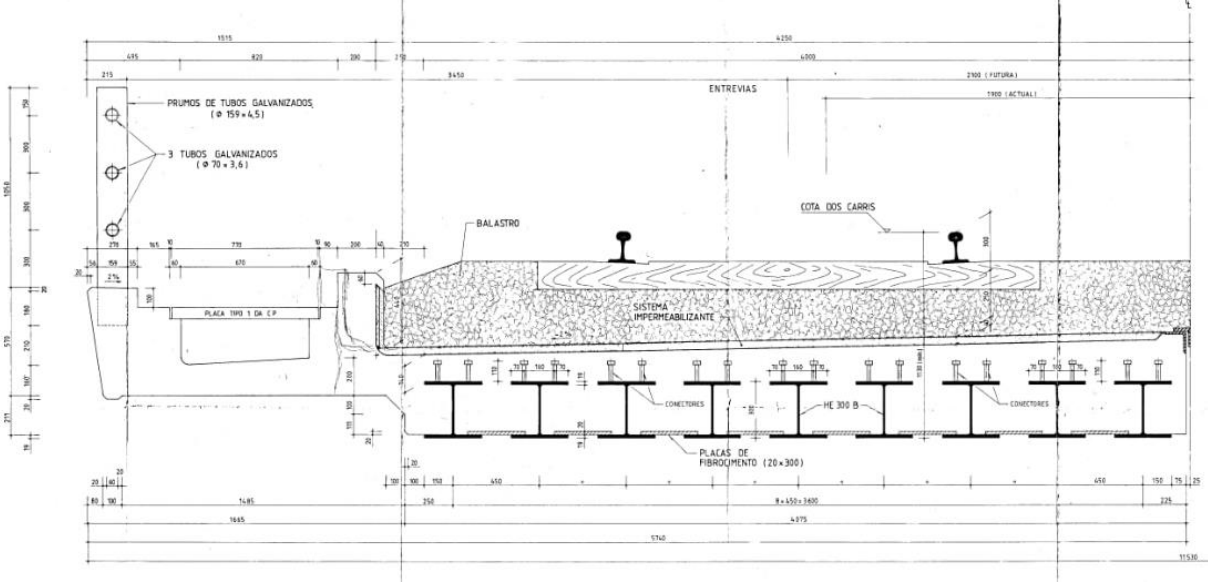
Karlsruhe - ID6007	6008			
Country	**Line designation**	**Maximum speed**	**Infrastructure Manager**
Germany	4020: Mannheim - Rastatt	200 km/h	**DB** InfraGO

Structural properties			
Span (m)	21.00	**Type**	Trough cross-section
Mass (t/m)	5.51	**Configuration**	Simply supported
EI (N.m²)	2.47×10^{10}	**Normative type**	STL
Dynamic properties			
Test type	Under railway traffic	**Method**	SSI-COV
Range f_1 (Hz)	7.00 – 7.46	**Range ξ_1 (%)**	0.97 – 5.44
Range A_1 (m/s²)	0.035 – 0.450	**No. valid measurements**	31
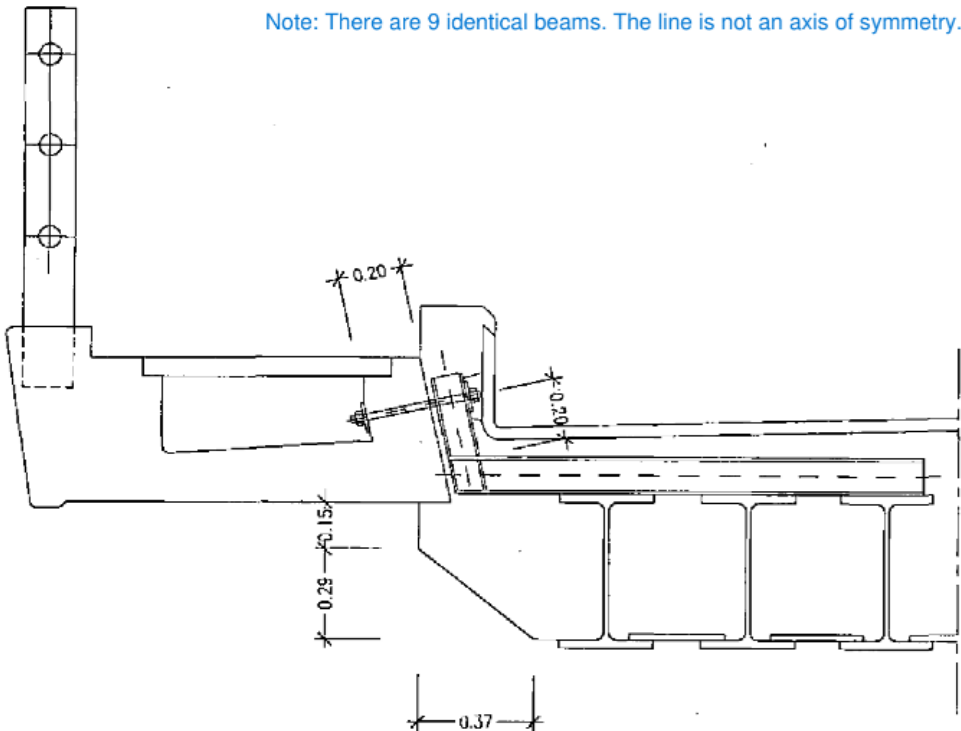
Langenhorn - ID23875			
Country	**Line designation**	**Maximum speed**	**Infrastructure Manager**
Germany	1210: Elmshorn – Westerlang RiGI	140 km/h	**DB** InfraGO

Structural properties			
Span (m)	36.30	**Type**	Trough cross-section
Mass (t/m)	7.73	**Configuration**	Simply supported
EI (N.m^2)	4.81×10^{10}	**Normative type**	STL
Dynamic properties			
Test type	Under railway traffic	**Method**	SSI-COV
Range f_1 (Hz)	4.04 – 4.13	**Range ξ_1 (%)**	1.36 – 1.89
Range A_1 (m/s^2)	0.140 – 0.300	**No. valid measurements**	9
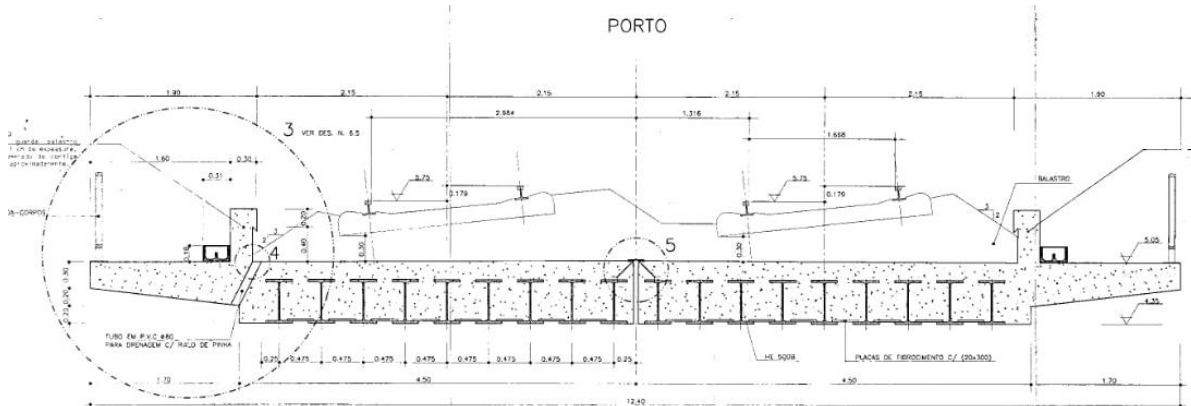
Sehnde - ID15894	18019			
Country	**Line designation**	**Maximum speed**	**Infrastructure Manager**
Germany	1770: Lehrte – Nordstemmen GeRiGI	140 km/h	**DB** InfraGO

Structural properties			
Span (m)	20.10	**Type**	Trough cross-section
Mass (t/m)	ID15894: 5.86 ID18019: 5.23	**Configuration**	Simply supported
EI (N.m²)	1.04×10^{10}	**Normative type**	STL
Dynamic properties			
Test type	Under railway traffic	**Method**	SSI-COV
Range f_1 (Hz)	5.15 – 5.69	**Range ξ_1 (%)**	2.59 – 3.93
Range A_1 (m/s²)	0.004 – 0.650	**No. valid measurements**	7
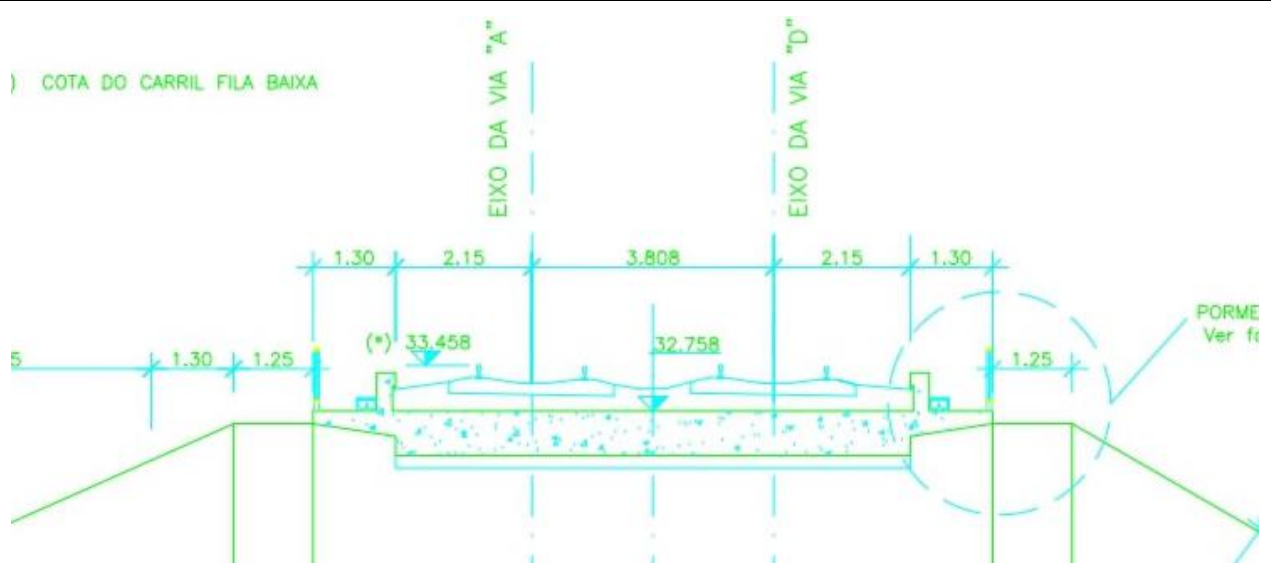
B.3. Bridges from Portugal (Infraestruturas de Portugal)
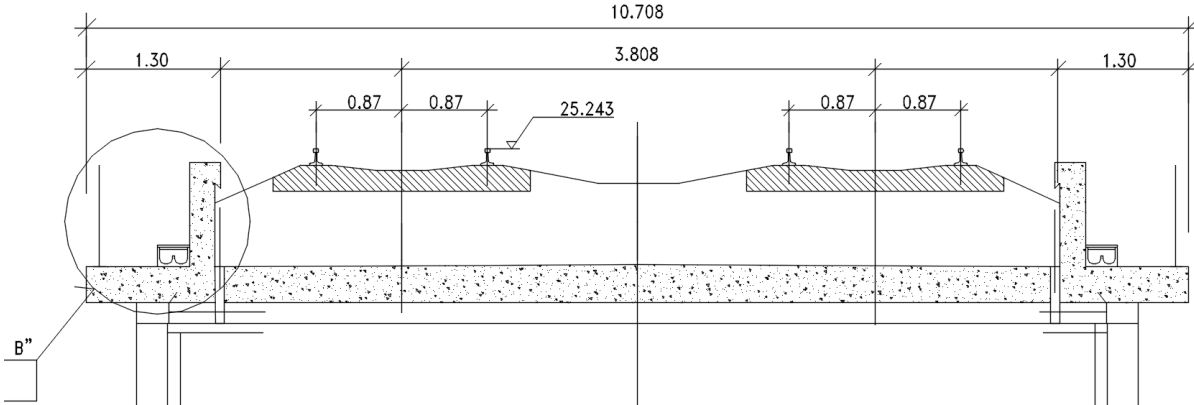
95.965 - PI Braço do Cortiço			
Country	**Line designation**	**Maximum speed**	**Infrastructure Manager**
Portugal	Northern line: Lisboa - Porto	160 km/h	Infraestruturas de Portugal

Structural properties			
Span (m)	7.02	**Type**	Filler beam
Mass (t/m)	10.54	**Configuration**	Simply supported
EI (N.m^2)	2.73×10^9	**Normative type**	FB/RC
Dynamic properties			
Test type	Under railway traffic	**Method**	SSI-COV
Range f_1 (Hz)	15.35 – 16.09	**Range ξ_1 (%)**	3.01 – 7.17
Range A_1 (m/s^2)	0.036 – 0.280	**No. valid measurements**	18

100.629 - PI da Cascalheira			
Country	**Line designation**	**Maximum speed**	**Infrastructure Manager**
Portugal	Northern line: Lisboa - Porto	160 km/h	Infraestruturas de Portugal

CORTE CORRENTE - P.I. DA CASCALHEIRA (ESC. 1/20)

Note: There are 9 identical beams. The line is not an axis of symmetry.

Structural properties			
Span (m)	10.92	**Type**	Filler beam
Mass (t/m)	13.97	**Configuration**	Simply supported
EI (N.m^2)	1.09×10^{10}	**Normative type**	FB/RC

Dynamic properties			
Test type	Under railway traffic	**Method**	SSI-COV
Range f_1 (Hz)	9.06 – 10.14	**Range ξ_1 (%)**	7.78 – 10.30
Range A_1 (m/s^2)	0.010 – 0.150	**No. valid measurements**	7
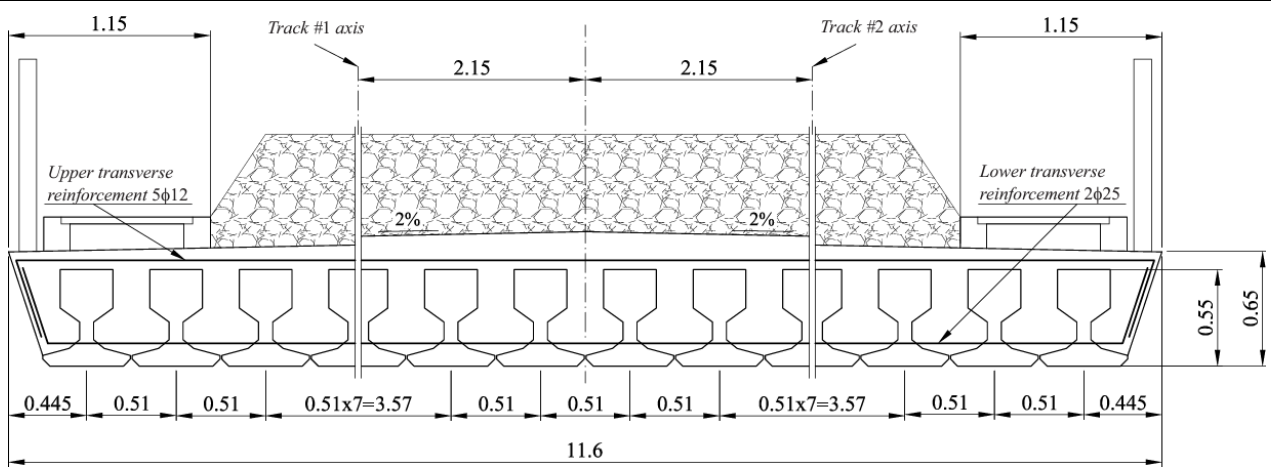
282.943 - Ponte de Canelas

Country	Line designation	Maximum speed	Infrastructure Manager
Portugal	Northern line: Lisboa - Porto	170 km/h	Infraestruturas de Portugal

Structural properties

Span (m)	12.00	**Type**	Filler beam
Mass (t/m)	16.17	**Configuration**	Simply supported
EI (N.m²)	8.91×10^9	**Normative type**	FB/RC

Dynamic properties

Test type	Under railway traffic	**Method**	SSI-COV
Range f_1 (Hz)	7.77 – 8.36	**Range ξ_1 (%)**	1.61 – 5.34
Range A_1 (m/s²)	0.026 – 0.220	**No. valid measurements**	13
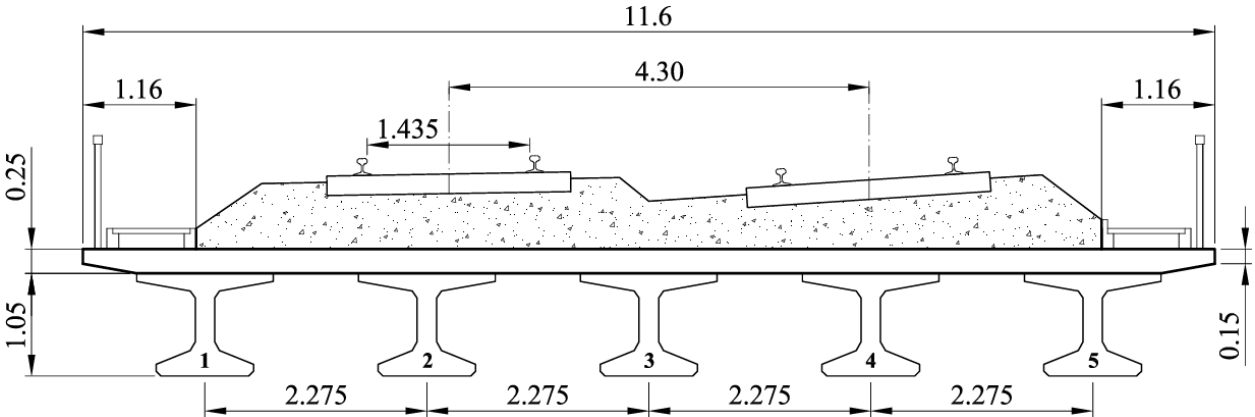
Sangalhos			
Country	**Line designation**	**Maximum speed**	**Infrastructure Manager**
Portugal	Northern line: Lisboa - Porto	220 km/h	Infraestruturas de Portugal

Structural properties			
Span (m)	8.00	**Type**	Portal Frame
Mass (t/m)	24.00	**Configuration**	Portal frame closed
EI (N.m^2)	1.32×10^{10}	**Normative type**	PF
Dynamic properties			
Test type	Under railway traffic	**Method**	SSI-COV
Range f_1 (Hz)	17.46 – 20.16	**Range ξ_1 (%)**	5.02 – 7.47
Range A_1 (m/s^2)	0.048 – 0.262	**No. valid measurements**	6
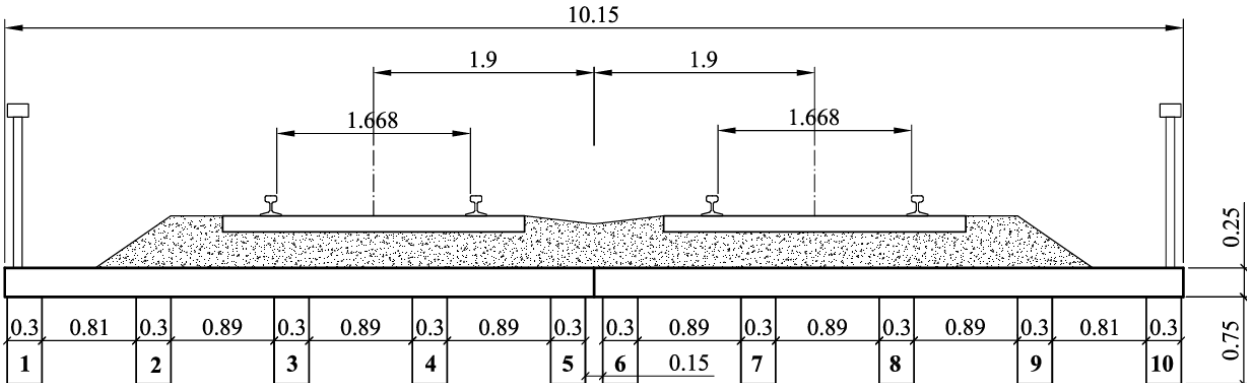
Pausinho			
Country	**Line designation**	**Maximum speed**	**Infrastructure Manager**
Portugal	Northern line: Lisboa - Porto	220 km/h	Infraestruturas de Portugal

Structural properties			
Span (m)	3.25	**Type**	Portal Frame
Mass (t/m)	23.16	**Configuration**	Portal frame closed
EI (N.m²)	$1.03{\times}10^{10}$	**Normative type**	PF
Dynamic properties			
Test type	Under railway traffic	**Method**	SSI-COV
Range f_1 (Hz)	46.56 – 56.41	**Range ξ_1 (%)**	7.88 – 11.18
Range A_1 (m/s²)	0.095 – 0.683	**No. valid measurements**	7
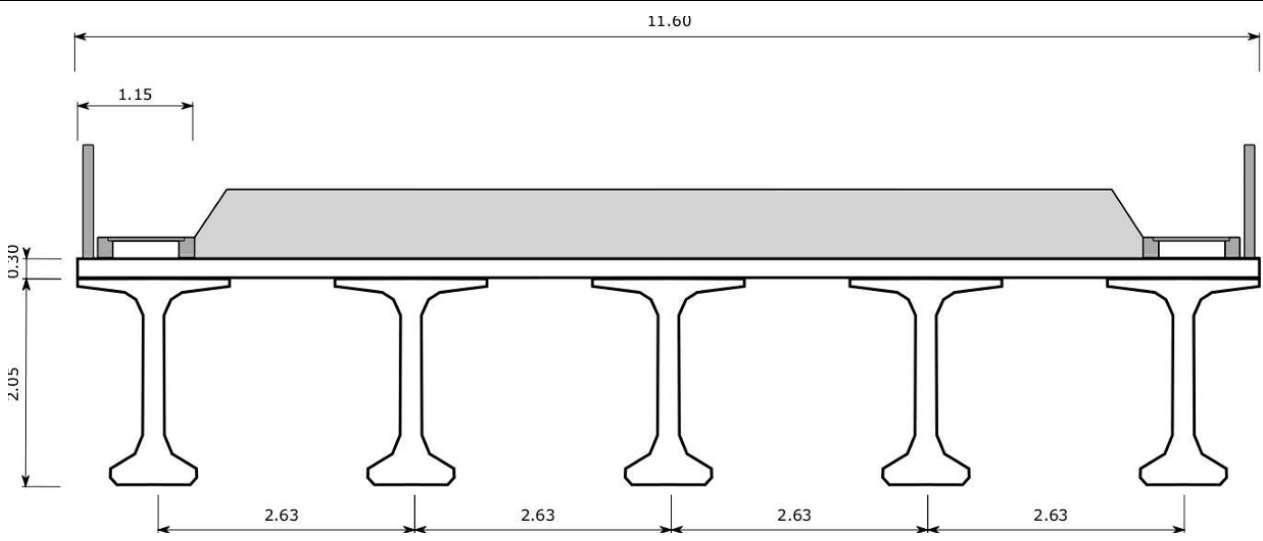
B.4. Bridges from Spain (ADIF)
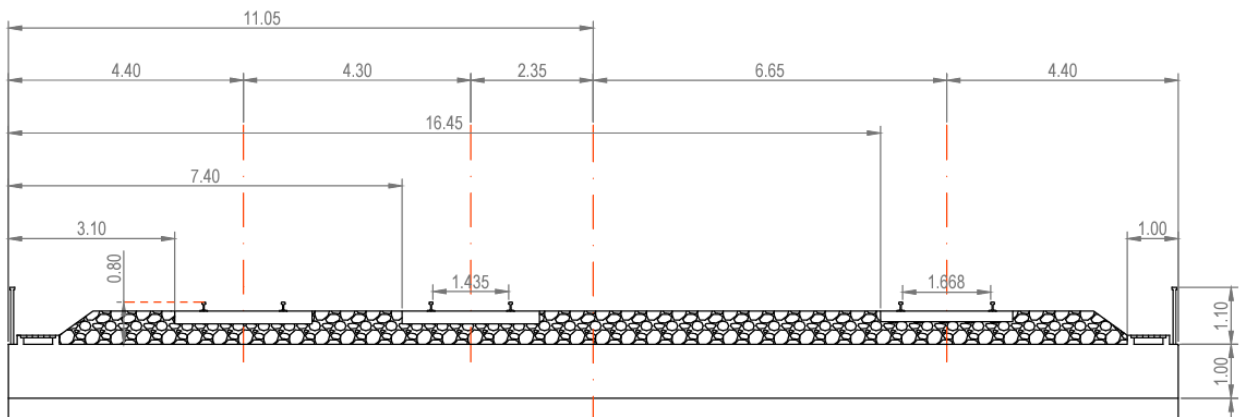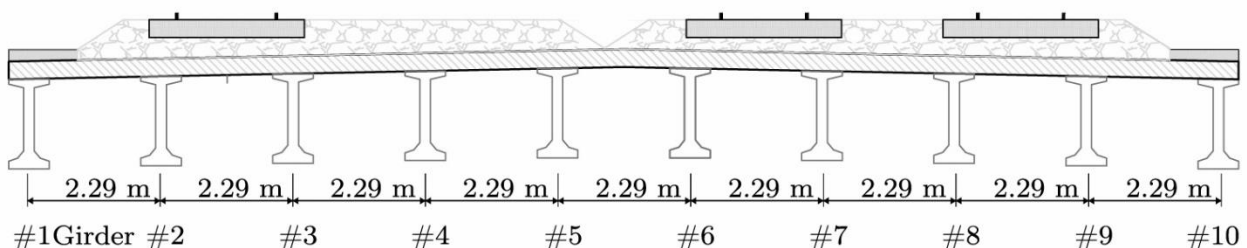
Algodor			
Country	**Line designation**	**Maximum speed**	**Infrastructure Manager**
Spain	Madrid-Seville HSL	300 km/h	adif ADMINISTRADOR DE INFRAESTRUCTURAS FERROVIARIAS

Structural properties			
Span (m)	10.25	**Type**	Filler beam
Mass (t/m)	29.80	**Configuration**	Simply supported
EI (N.m^2)	1.63×10^{10}	**Normative type**	FB/RC
Dynamic properties			
Test type	Under railway traffic	**Method**	MCO
Range f_1 (Hz)	11.40	Range ξ_1 (%)	2.36
Range A_1 (m/s^2)	0.326	**No. valid measurements**	1
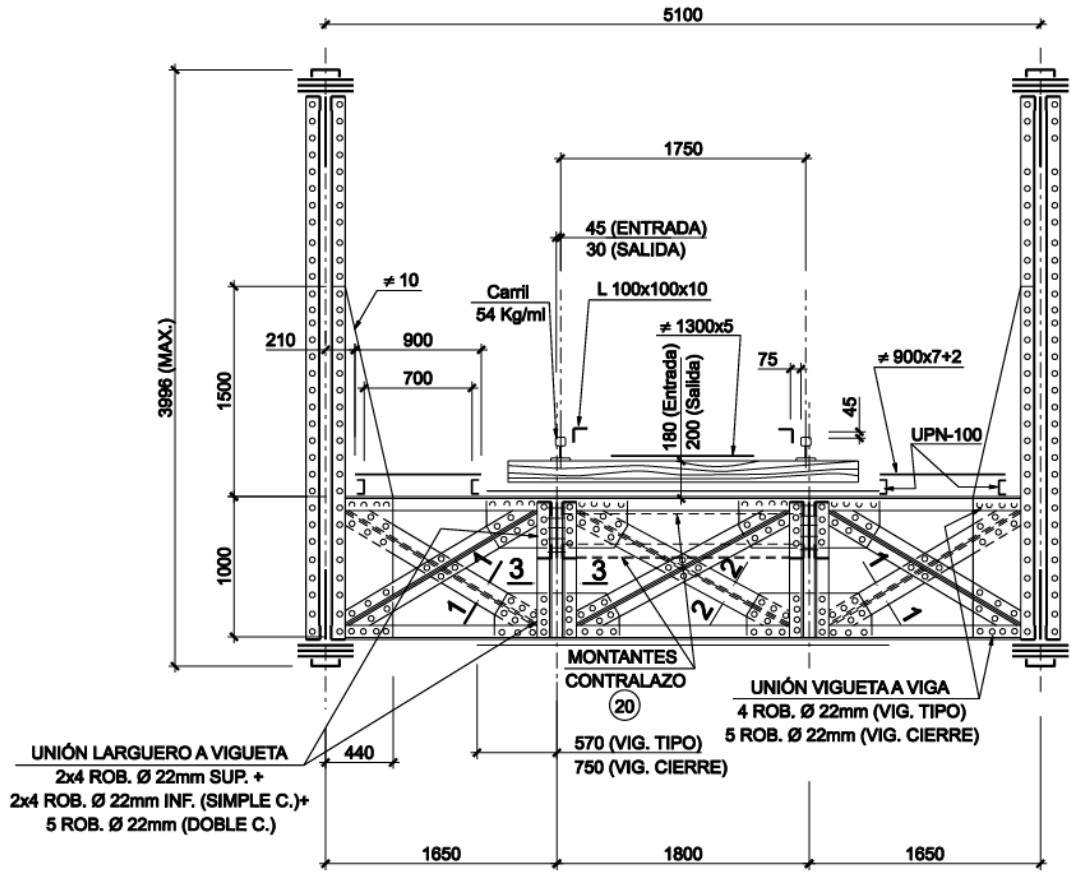
Bracea			
Country	**Line designation**	**Maximum speed**	**Infrastructure Manager**
Spain	Madrid-Seville HSL	300 km/h	adif ADMINISTRADOR DE INFRAESTRUCTURAS FERROVIARIAS

Structural properties			
Span (m)	15.25	**Type**	Girder deck
Mass (t/m)	26.26	**Configuration**	Simply supported
EI (N.m^2)	4.92×10^{10}	**Normative type**	PSC
Dynamic properties			
Test type	Under railway traffic	**Method**	MCO
Range f_1 (Hz)	9.20 – 9.43	**Range ξ_1 (%)**	1.99 – 5.57
Range A_1 (m/s^2)	0.077 – 0.331	**No. valid measurements**	4
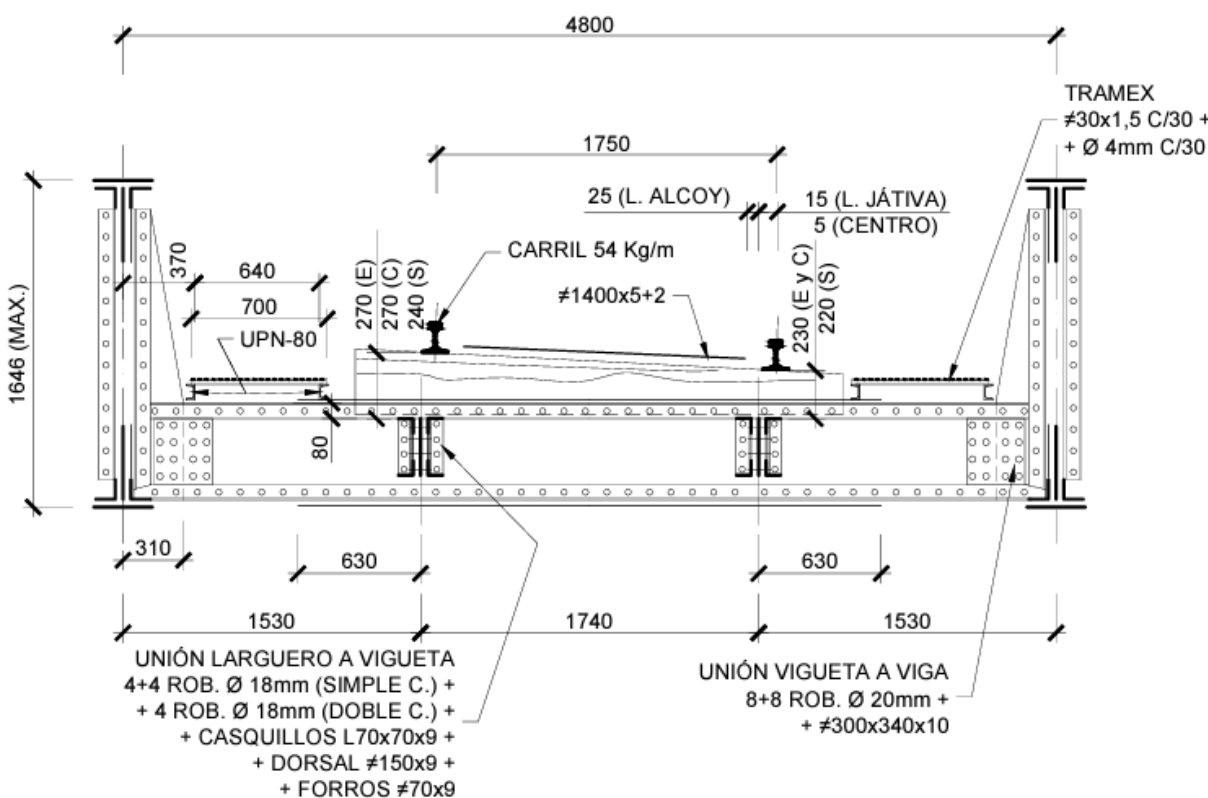
Guadiana			
Country	**Line designation**	**Maximum speed**	**Infrastructure Manager**
Spain	Madrid-Alcázar de San Juan	km/h	

Structural properties			
Span (m)	11.93	**Type**	Girder deck
Mass (t/m)	9.35	**Configuration**	Simply supported
EI (N.m^2)	7.4×10^9	**Normative type**	PSC
Dynamic properties			
Test type	Under railway traffic	**Method**	MCO
Range f_1 (Hz)	9.70 – 9.90	**Range ξ_1 (%)**	4.87 – 5.39
Range A_1 (m/s^2)	0.027 – 0.097	**No. valid measurements**	2

Jabalon			
Country	**Line designation**	**Maximum speed**	**Infrastructure Manager**
Spain	Madrid-Seville HSL	300 km/h	adif ADMINISTRADOR DE INFRAESTRUCTURAS FERROVIARIAS

Structural properties			
Span (m)	24.00	**Type**	Girder deck
Mass (t/m)	29.00	**Configuration**	Simply supported
EI **(N.m^2)**	1.55×10^{11}	**Normative type**	PSC
Dynamic properties			
Test type	Under railway traffic	**Method**	MCO
Range f_1 **(Hz)**	6.17 – 6.19	**Range** ξ_1 **(%)**	2.05 – 3.05
Range A_1 **(m/s^2)**	0.089 – 0.142	**No. valid measurements**	3

Laguna Blanca			
Country	**Line designation**	**Maximum speed**	**Infrastructure Manager**
Spain	Madrid-Seville HSL	300 km/h	adif ADMINISTRADOR DE INFRAESTRUCTURAS FERROVIARIAS

Structural properties			
Span (m)	8.00	**Type**	Prestressed Portal Frame
Mass (t/m)	20.00	**Configuration**	Portal frame closed
EI (N.m^2)	3.2×10^9	**Normative type**	PF / PSC
Dynamic properties			
Test type	Under railway traffic	**Method**	SSI-COV
Range f_1 (Hz)	21.78 – 23.42	**Range ξ_1 (%)**	4.74 – 5.78
Range A_1 (m/s^2)	0.069 – 0.284	**No. valid measurements**	6

Tirteafuera			
Country	**Line designation**	**Maximum speed**	**Infrastructure Manager**
Spain	Madrid-Seville HSL	300 km/h	adif ADMINISTRADOR DE INFRAESTRUCTURAS FERROVIARIAS

Structural properties			
Span (m)	18.00	**Type**	Girder deck
Mass (t/m)	No data	**Configuration**	Simply supported
EI (N.m^2)	No data	**Normative type**	PSC
Dynamic properties			
Test type	Under railway traffic	**Method**	MCO
Range f_1 (Hz)	8.06 – 8.20	**Range ξ_1 (%)**	1.71 – 2.82
Range A_1 (m/s^2)	0.046 – 0.105	**No. valid measurements**	10

Arroyo Corbones: PC029_100017615			
Country	**Line designation**	**Maximum speed**	**Infrastructure Manager**
Spain	Alcazar a Sevilla	km/h	adif ADMINISTRADOR DE INFRAESTRUCTURAS FERROVIARIAS

Structural properties			
Span (m)	30.42	**Type**	Truss
Mass (t/m)	No data	**Configuration**	Simply supported
EI (N.m^2)	No data	**Normative type**	STL
Dynamic properties			
Test type	Under railway traffic	**Method**	MCO
Range f_1 (Hz)	7.62	**Range ξ_1 (%)**	2.45
Range A_1 (m/s^2)	0.050	**No. valid measurements**	1

Barranco Bancal Redo: PC030_100017609			
Country	**Line designation**	**Maximum speed**	**Infrastructure Manager**
Spain	342 - Xátiva - Alcoi	km/h	adif ADMINISTRADOR DE INFRAESTRUCTURAS FERROVIARIAS

SECCIÓN TRANSVERSAL A-A
(E=1:40)

Structural properties			
Span (m)	16.00	**Type**	Truss
Mass (t/m)	No data	**Configuration**	Simply supported
EI (N.m^2)	No data	**Normative type**	STL
Dynamic properties			
Test type	Under railway traffic	**Method**	MCO
Range f_1 (Hz)	10.02	**Range ξ_1 (%)**	1.40
Range A_1 (m/s^2)	0.015	**No. valid measurements**	1

Barranco De Los Corrimientos: PC040_100016018			
Country	**Line designation**	**Maximum speed**	**Infrastructure Manager**
Spain	Frontera La Tour De Carol-Enveigt	km/h	adif ADMINISTRADOR DE INFRAESTRUCTURAS FERROVIARIAS
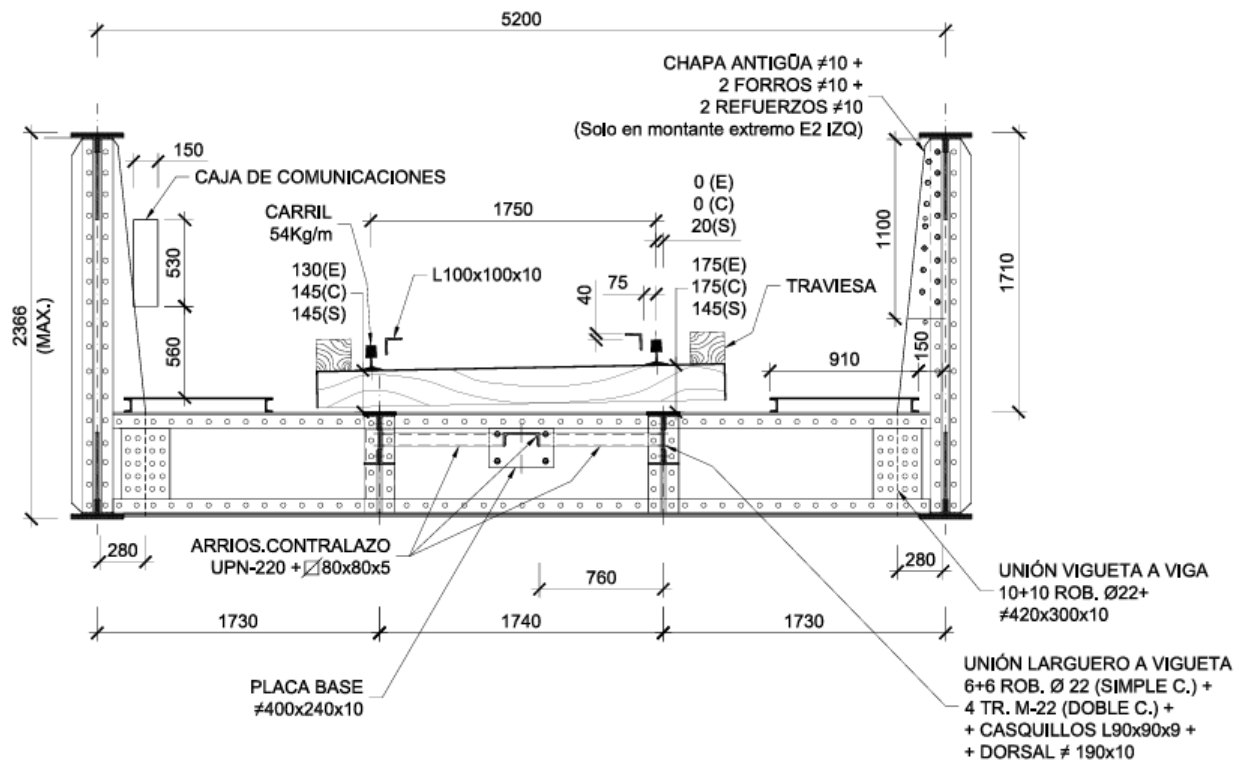
Structural properties			
Span (m)	21.20	**Type**	Truss
Mass (t/m)	No data	**Configuration**	Simply supported
EI (N.m^2)	No data	**Normative type**	STL
Dynamic properties			
Test type	Under railway traffic	**Method**	MCO
Range f_1 (Hz)	8.01	**Range ξ_1 (%)**	0.94
Range A_1 (m/s^2)	0.035	**No. valid measurements**	1
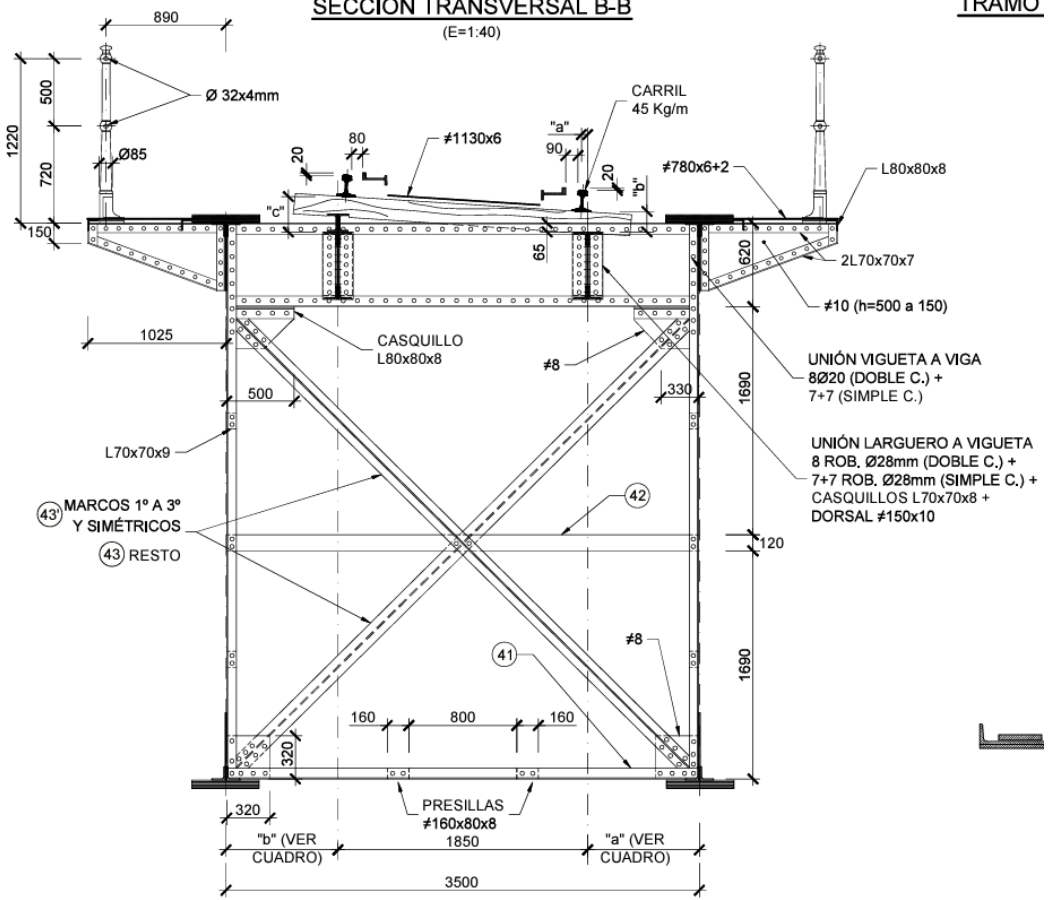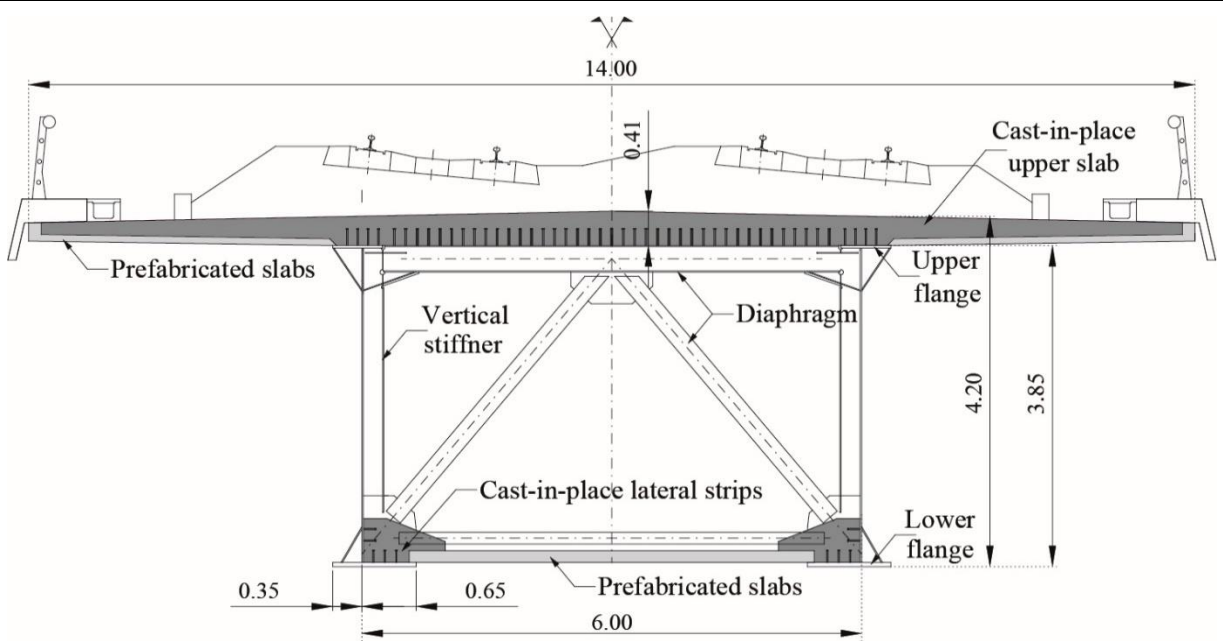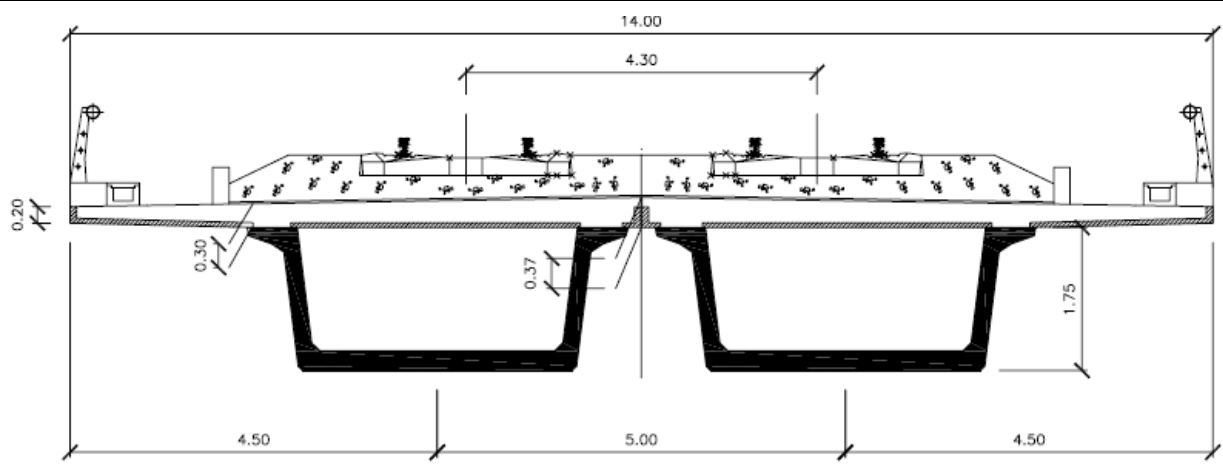
Tejería: PC041_100015418_Lateral			
Country	**Line designation**	**Maximum speed**	**Infrastructure Manager**
Spain	Aranjuez a Valencia - La Font De Sant Lluis	km/h	adif ADMINISTRADOR DE INFRAESTRUCTURAS FERROVIARIAS

SECCIÓN TRANSVERSAL A-A
(E=1:40)

Structural properties			
Span (m)	25.90	**Type**	Truss
Mass (t/m)	No data	**Configuration**	Simply supported
EI (N.m²)	No data	**Normative type**	STL

Dynamic properties			
Test type	Under railway traffic	**Method**	MCO
Range f_1 (Hz)	8.14	**Range ξ_1 (%)**	1.44
Range A_1 (m/s²)	0.036	**No. valid measurements**	1

Tejería: PC041_100015418_Central			
Country	**Line designation**	**Maximum speed**	**Infrastructure Manager**
Spain	Aranjuez a Valencia - La Font De Sant Lluis	km/h	adif ADMINISTRADOR DE INFRAESTRUCTURAS FERROVIARIAS

Structural properties			
Span (m)	41.00	**Type**	Truss
Mass (t/m)	No data	**Configuration**	Simply supported
EI (N.m^2)	No data	**Normative type**	STL
Dynamic properties			
Test type	Under railway traffic	**Method**	MCO
Range f_1 (Hz)	5.08	**Range ξ_1 (%)**	1.19
Range A_1 (m/s^2)	0.036	**No. valid measurements**	1
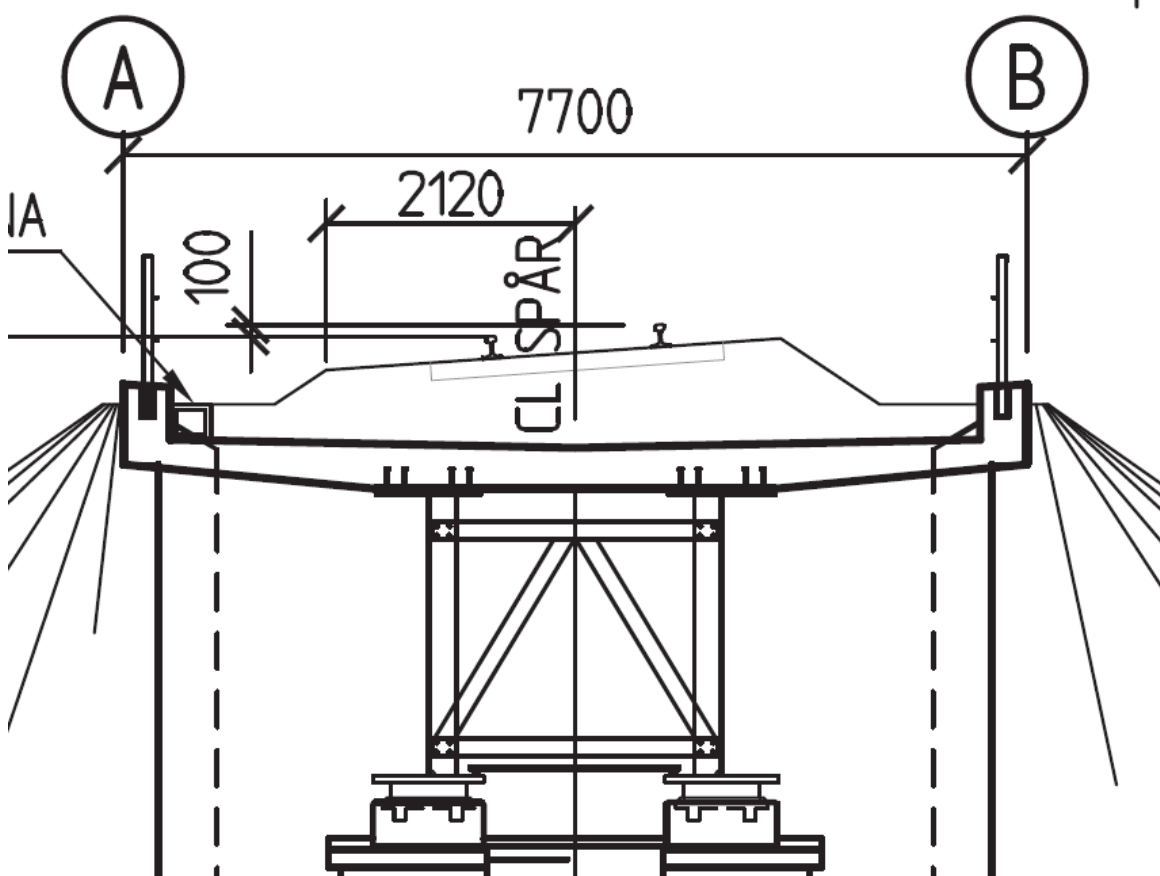
Arroyo de las Piedras			
Country	**Line designation**	**Maximum speed**	**Infrastructure Manager**
Spain	Madrid-Málaga HSL	300 km/h	adif ADMINISTRADOR DE INFRAESTRUCTURAS FERROVIARIAS

Structural properties			
Span (m)	44.00	**Type**	Steel box with concrete slab
Mass (t/m)	31.30	**Configuration**	Simply supported
EI **(N.m^2)**	2.79×10^{11}	**Normative type**	PSC
Dynamic properties			
Test type	Under railway traffic	**Method**	SSI-COV
Range f_1 (Hz)	3.99 – 4.05	**Range ξ_1 (%)**	1.05 – 2.01
Range A_1 (m/s^2)	0.022 – 0.063	**No. valid measurements**	8
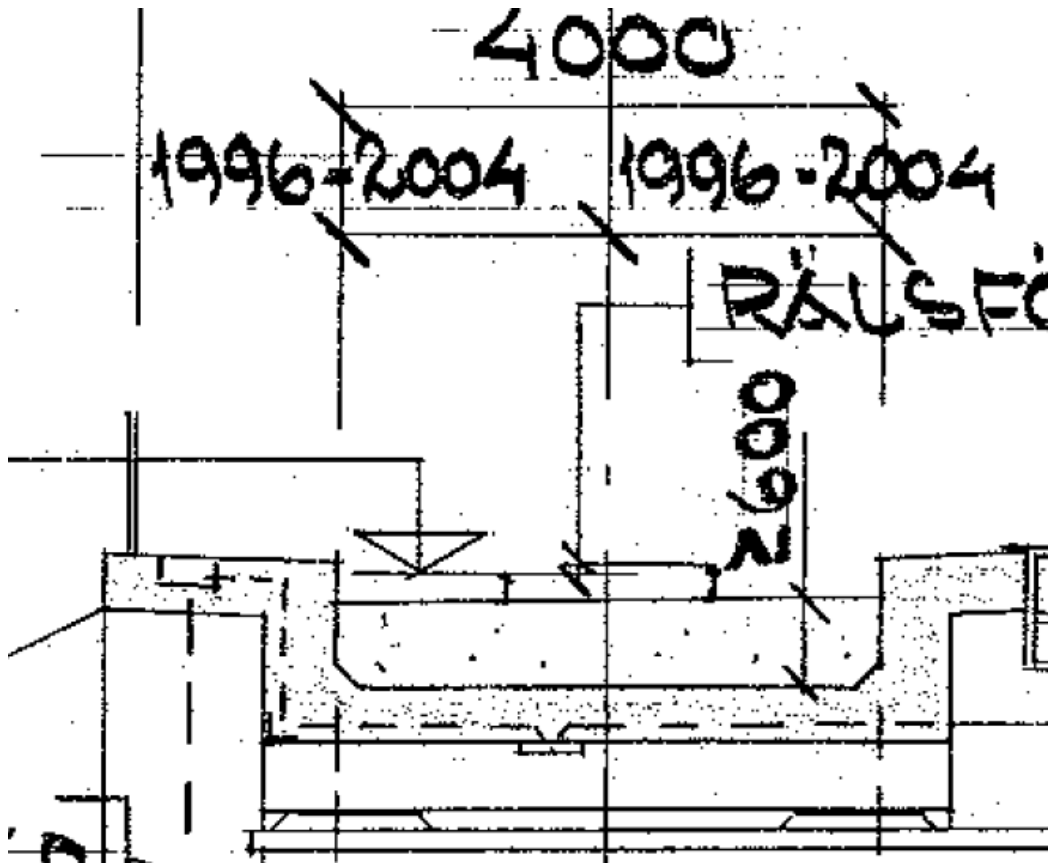
Casamisarro			
Country	**Line designation**	**Maximum speed**	**Infrastructure Manager**
Spain	Madrid-Valencia HSL	300 km/h	adif ADMINISTRADOR DE INFRAESTRUCTURAS FERROVIARIAS

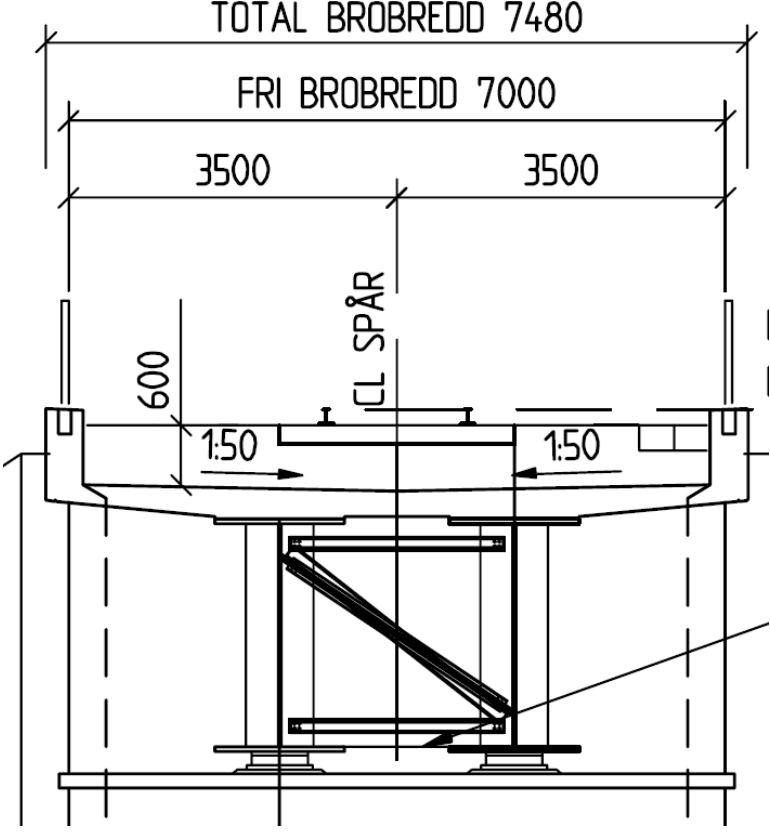| Structural properties			
Span (m)	29.65	**Type**	U-Girder deck
Mass (t/m)	15.55	**Configuration**	Continuous
EI **(N.m^2)**	7.08×10^{10}	**Normative type**	COMP
Dynamic properties			
Test type	Under railway traffic	**Method**	SSI-COV
Range f_1 **(Hz)**	5.05 – 5.45	**Range** ξ_1 **(%)**	2.11 – 6.27
Range A_1 **(m/s^2)**	0.043 – 0.612	**No. valid measurements**	30
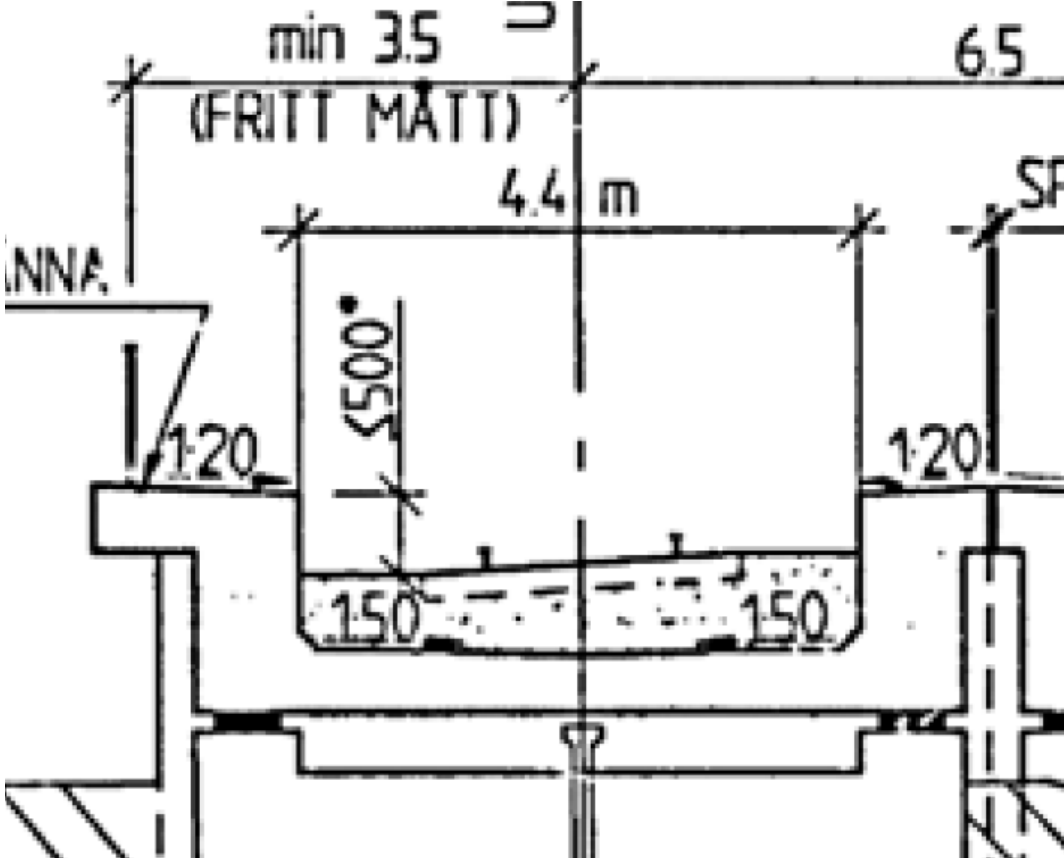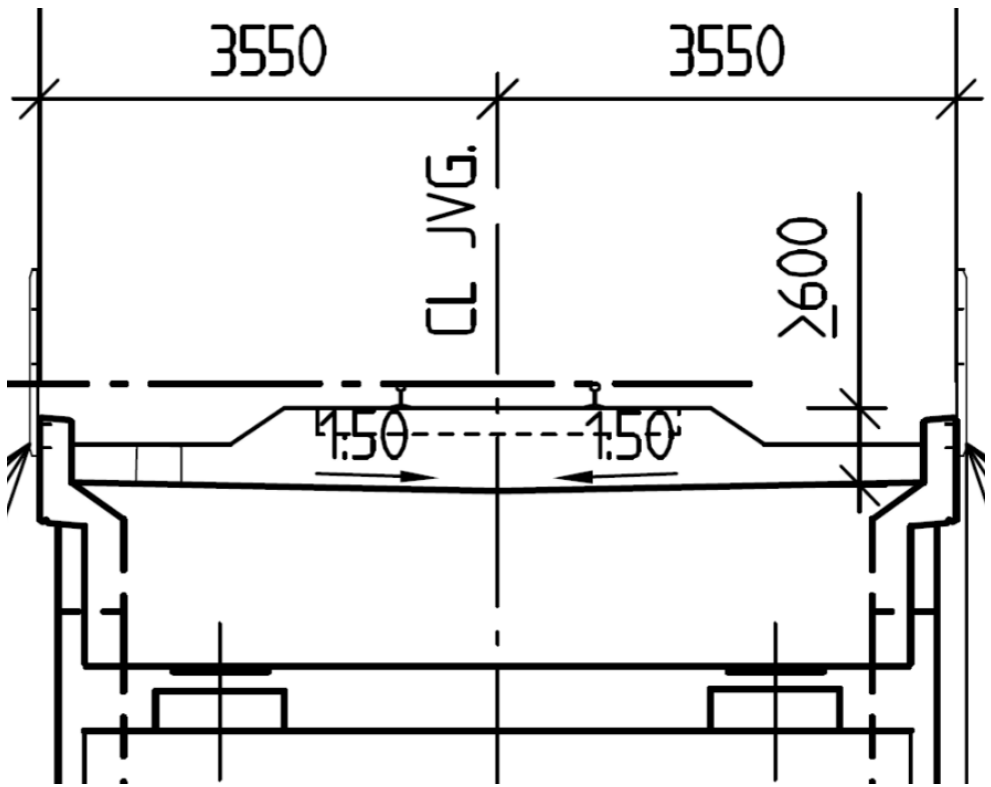
B.5. Bridges from Sweden (Trafikverket)
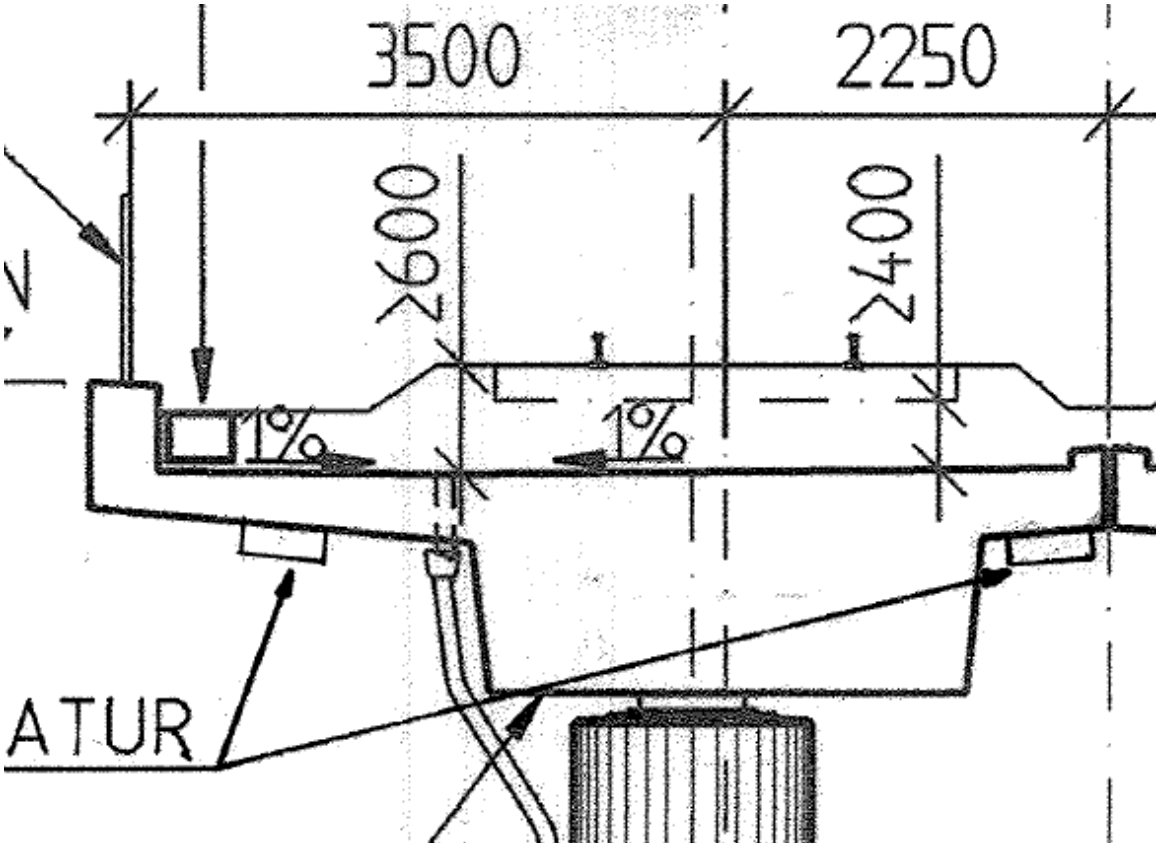
Banafjällsån			
Country	**Line designation**	**Maximum speed**	**Infrastructure Manager**
Sweden	Bothnia line: Örnsköldsvik - Husum	250 km/h	TRAFIKVERKET

Structural properties			
Span (m)	42.00	**Type**	Steel beam with concrete slab
Mass (t/m)	16.93	**Configuration**	Simply supported
EI **(N.m^2)**	$1.29{\times}10^{11}$	**Normative type**	COMP
Dynamic properties			
Test type	Under railway traffic	**Method**	SSI-COV
Range f_1 (Hz)	3.25 – 3.26	**Range ξ_1 (%)**	1.80 – 2.45
Range A_1 (m/s^2)	0.116 – 0.171	**No. valid measurements**	2
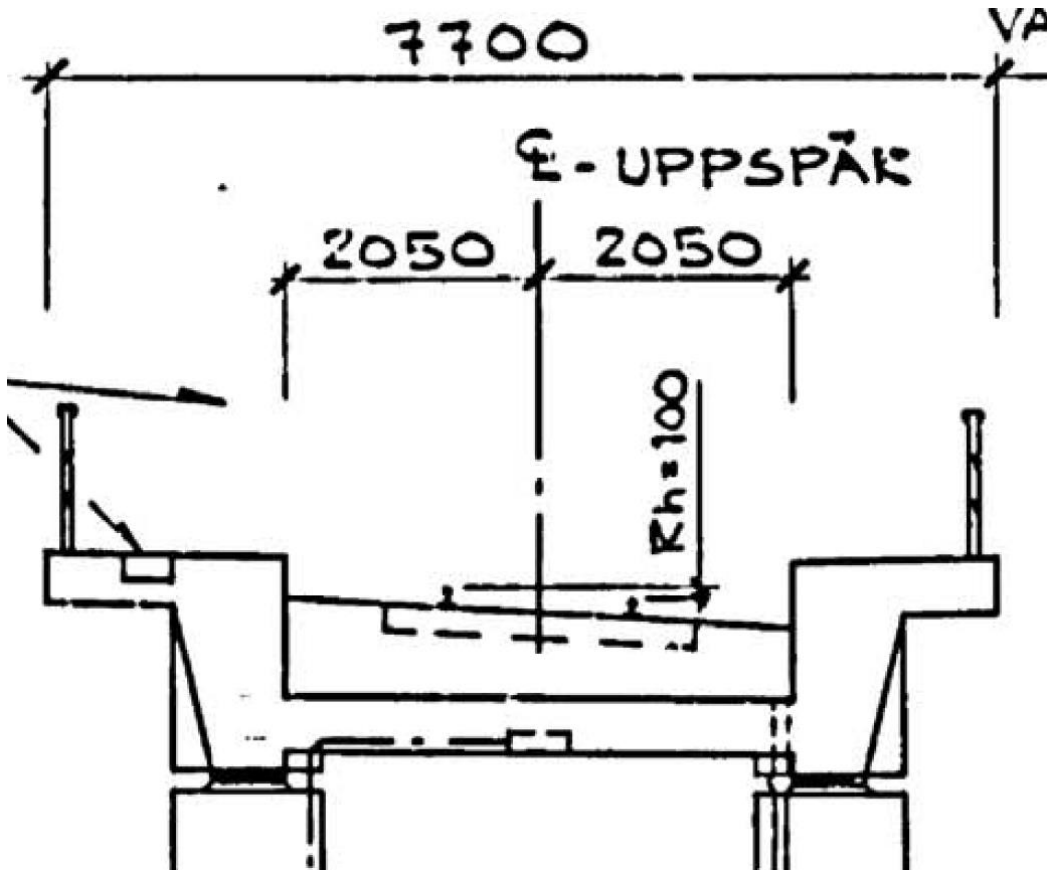
Hästhovsgatan			
Country	**Line designation**	**Maximum speed**	**Infrastructure Manager**
Sweden	Mälarbanan line: Kallhäll - Västerås	200 km/h	TRAFIKVERKET

Structural properties			
Span (m)	14.20	**Type**	Slab full
Mass (t/m)	13.90	**Configuration**	Simply supported
EI (N.m²)	1.98×10^{10}	**Normative type**	FB/RC

Dynamic properties			
Test type	i) Under railway traffic ii) Under forced excitation	**Method**	i) SSI-COV ii) *'modalfit'*
Range f_1 (Hz)	i) 11.87 – 12.45 ii) 11.53 – 11.54	**Range ξ_1 (%)**	i) 2.26 – 3.61 ii) 2.45 – 2.60
Range A_1 (m/s²)	i) 0.015 – 0.131 ii) 2.900	**No. valid measurements**	i) 10 ii) 2
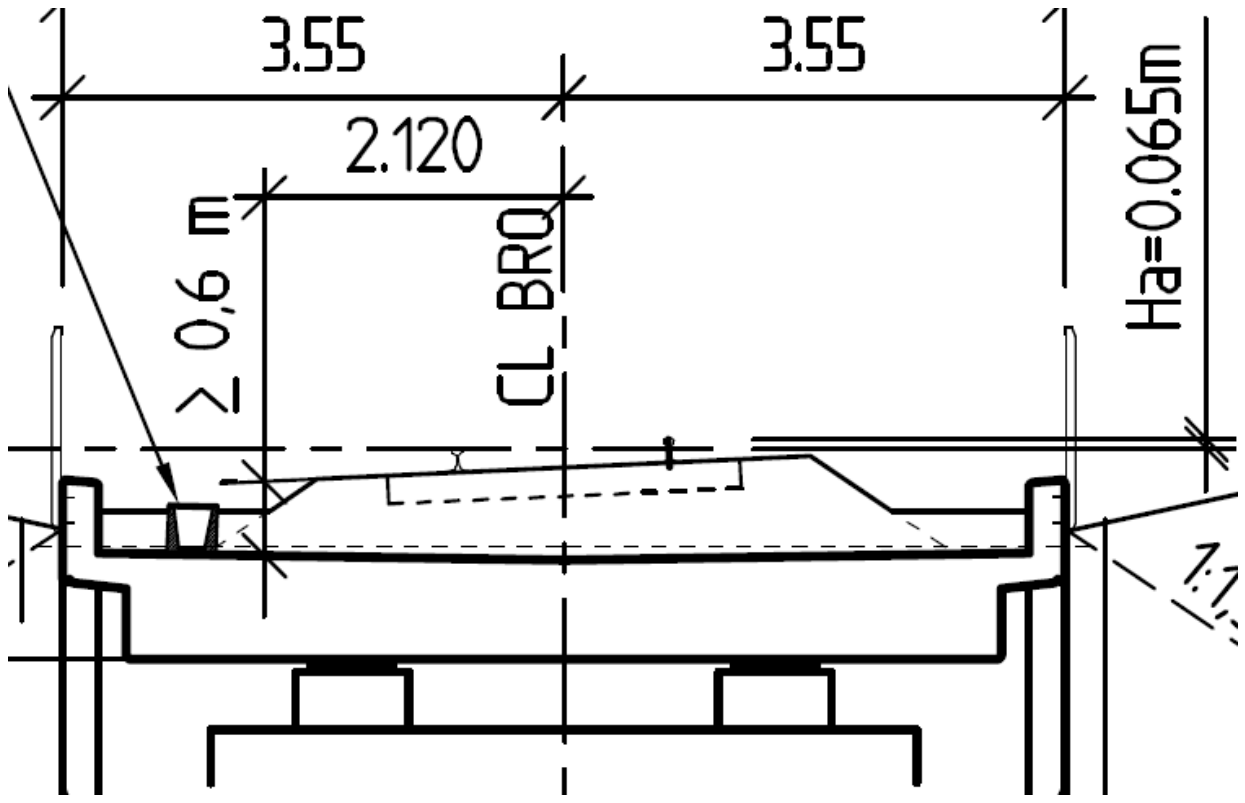
Bryngeån			
Country	**Line designation**	**Maximum speed**	**Infrastructure Manager**
Sweden	Bothnia line: Örnsköldsvik - Husum	250 km/h	TRAFIKVERKET

Structural properties			
Span (m)	48.00	**Type**	Steel beam with concrete slab
Mass (t/m)	17.84	**Configuration**	Simply supported
EI (N.m^2)	2.08×10^{11}	**Normative type**	COMP
Dynamic properties			
Test type	i) Under railway traffic ii) Under forced excitation	**Method**	i) SSI-COV ii) *'modalfit'*
Range f_1 (Hz)	i) 2.49 – 2.60 ii) 2.45	**Range ξ_1 (%)**	i) 1.11 – 1.92 ii) 1.18
Range A_1 (m/s^2)	i) 0.020 – 0.471 ii) 0.450	**No. valid measurements**	i) 7 ii) 1
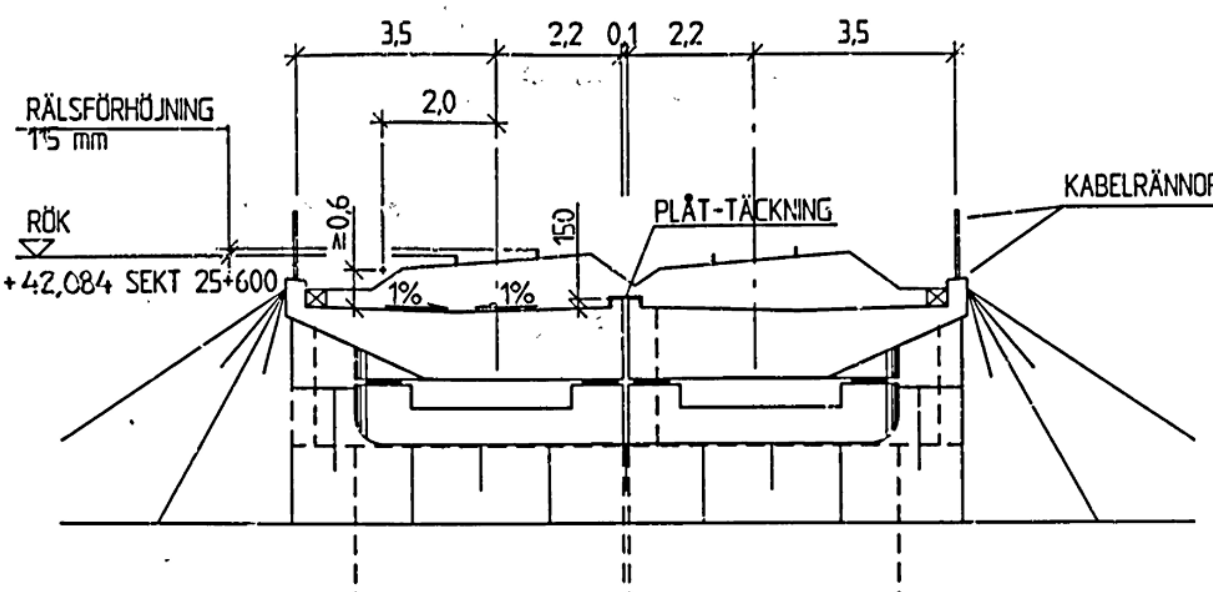
Bodavägen			
Country	**Line designation**	**Maximum speed**	**Infrastructure Manager**
Sweden	Mälarbanan line: Kallhäll - Västerås	200 km/h	TRAFIKVERKET

Structural properties			
Span (m)	22.00	**Type**	Beam
Mass (t/m)	19.05	**Configuration**	Simply supported
EI (N.m²)	4.38×10^{10}	**Normative type**	PSC
Dynamic properties			
Test type	i) Under railway traffic ii) Under forced excitation	**Method**	i) SSI-COV ii) *'modalfit'*
Range f_1 (Hz)	i) 8.16 – 8.38 ii) 7.38 – 7.62	**Range ξ_1 (%)**	i) 1.61 – 1.73 ii) 2.57 – 3.21
Range A_1 (m/s²)	i) 0.021 – 0.024 ii) 0.600 – 1.400	**No. valid measurements**	i) 2 ii) 6
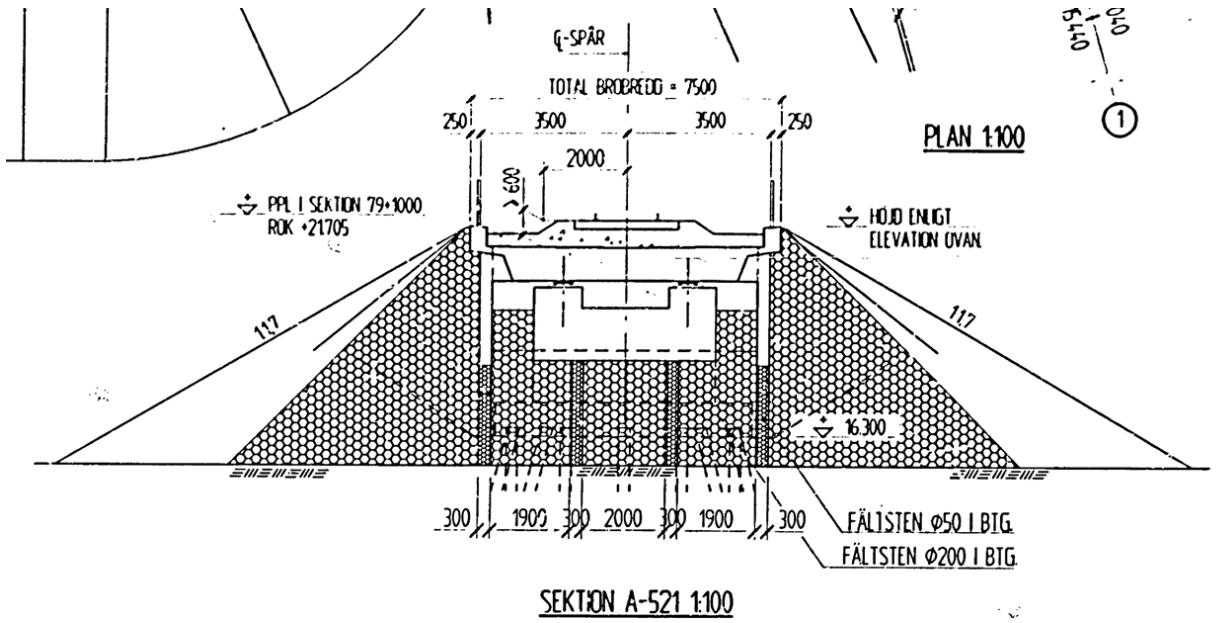
Aspan			
Country	**Line designation**	**Maximum speed**	**Infrastructure Manager**
Sweden	Bothnia line: Husum - Nordmaling	250 km/h	TRAFIKVERKET

Structural properties			
Span (m)	24.00	**Type**	Slab full
Mass (t/m)	28.65	**Configuration**	Simply supported
EI **(N.m^2)**	4.90×10^{10}	**Normative type**	FB/RC

Dynamic properties			
Test type	i) Under railway traffic ii) Under forced excitation	**Method**	i) SSI-COV ii) *'modalfit'*
Range f_1 (Hz)	i) 6.58 – 6.69 ii) 6.39	**Range ξ_1 (%)**	i) 1.07 – 1.57 ii) 2.03
Range A_1 (m/s^2)	i) 0.013 – 0.024 ii) 0.500	**No. valid measurements**	i) 9 ii) 1
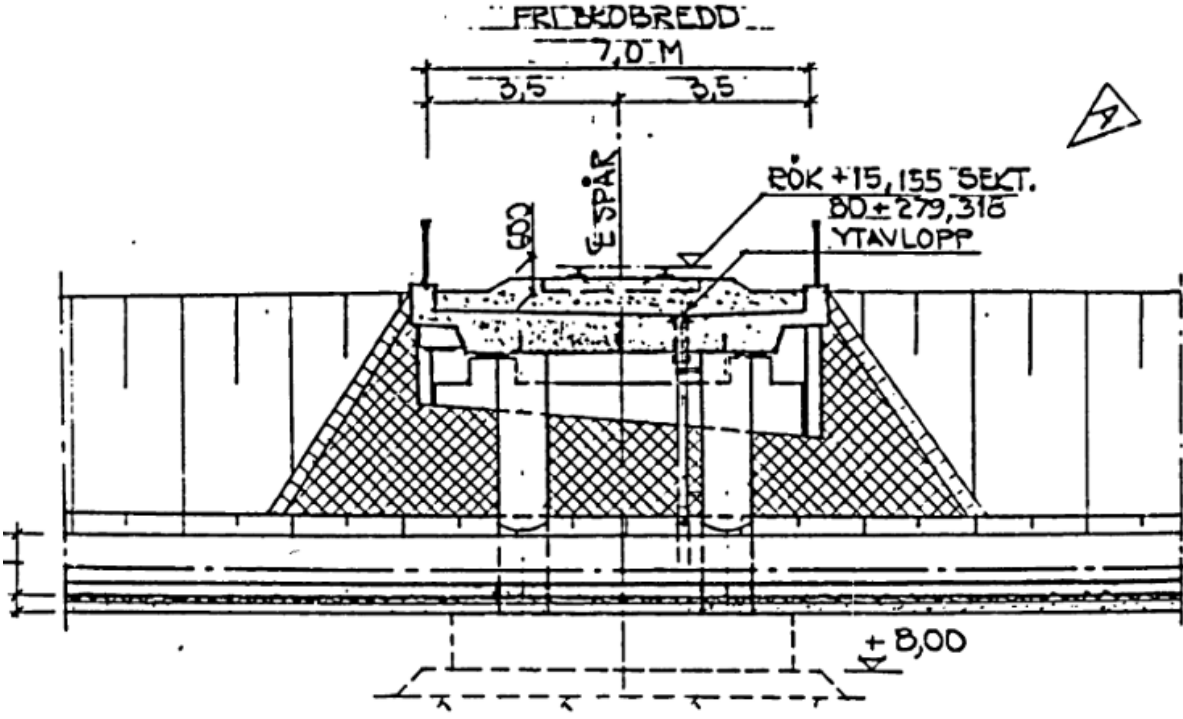
Enköpingsvägen			
Country	**Line designation**	**Maximum speed**	**Infrastructure Manager**
Sweden	Mälarbanan line: Kallhäll - Västerås	200 km/h	TRAFIKVERKET

Structural properties			
Span (m)	20.00	**Type**	Beam
Mass (t/m)	17.70	**Configuration**	Continuous
EI **(N.m²)**	2.96×10^{10}	**Normative type**	PSC
Dynamic properties			
Test type	i) Under railway traffic ii) Under forced excitation	**Method**	i) SSI-COV ii) *'modalfit'*
Range f_1 (Hz)	i) 7.96 – 8.04 ii) 7.74 – 7.83	**Range ξ_1 (%)**	i) 1.79 – 2.52 ii) 1.34 – 1.51
Range A_1 (m/s²)	i) 0.046 – 0.148 ii) 0.250 – 0.700	**No. valid measurements**	i) 2 ii) 6
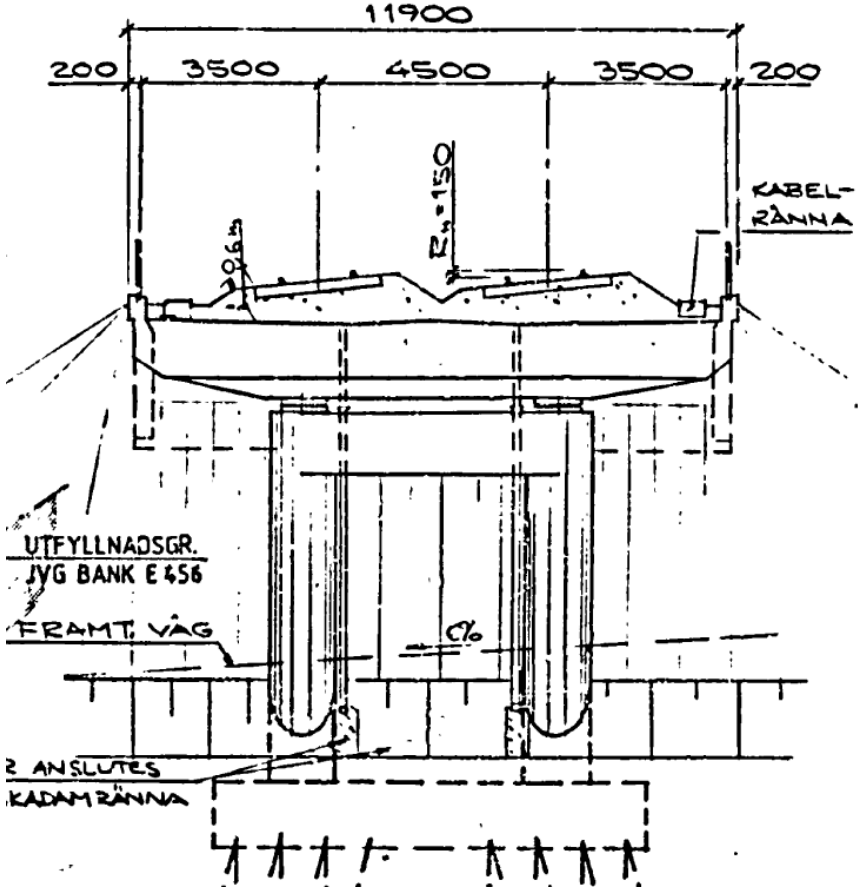
Fanna			
Country	**Line designation**	**Maximum speed**	**Infrastructure Manager**
Sweden	Mälarbanan line: Kallhäll - Västerås	200 km/h	TRAFIKVERKET

Structural properties			
Span (m)	20.30	**Type**	Beam
Mass (t/m)	18.68	**Configuration**	Continuous
EI (N.m^2)	5.14×10^{10}	**Normative type**	PSC
Dynamic properties			
Test type	i) Under railway traffic ii) Under forced excitation	**Method**	i) SSI-COV ii) *'modalfit'*
Range f_1 (Hz)	i) 8.10 – 8.19 ii) 8.02 – 8.06	**Range ξ_1 (%)**	i) 2.57 – 3.06 ii) 3.50 – 4.27
Range A_1 (m/s^2)	i) 0.012 – 0.150 ii) 0.500	**No. valid measurements**	i) 2 ii) 4
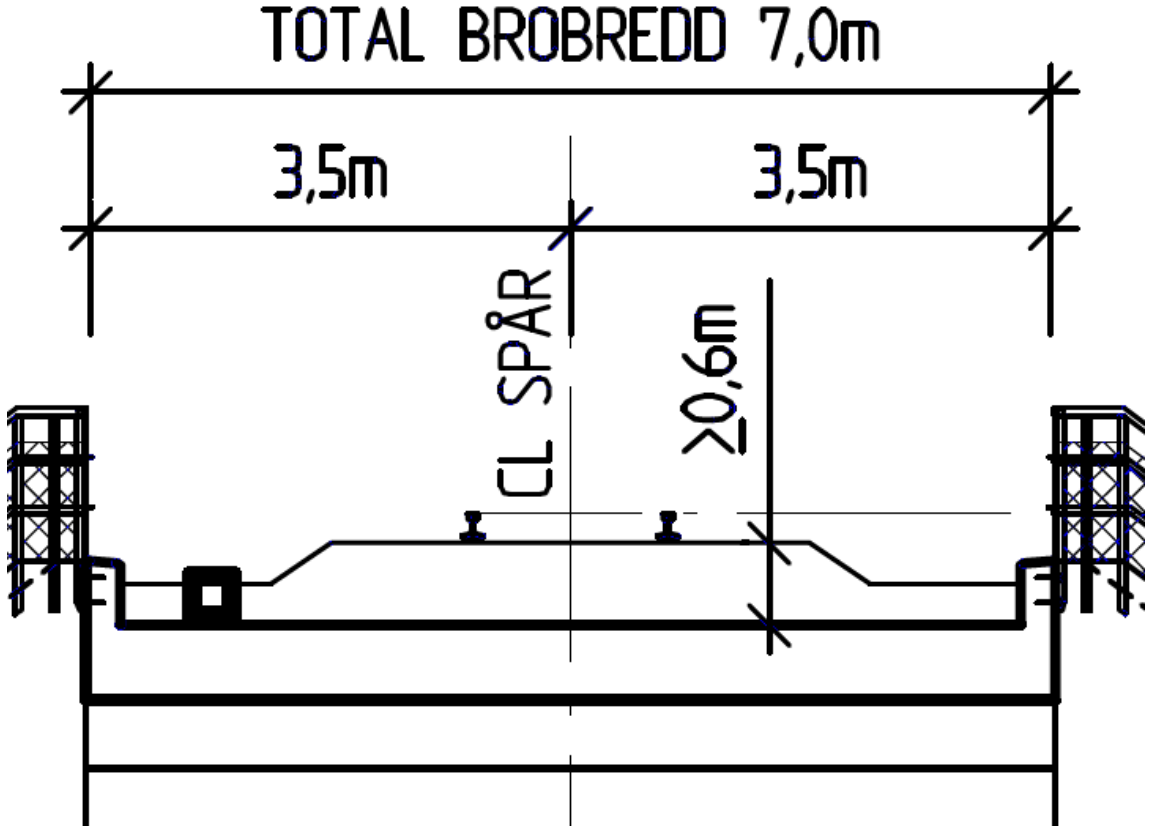
Sidensjövägen			
Country	**Line designation**	**Maximum speed**	**Infrastructure Manager**
Sweden	Bothnia line: Nyland - Örnsköldsvik	250 km/h	TRAFIKVERKET

Structural properties			
Span (m)	17.00	**Type**	Slab full
Mass (t/m)	22.35	**Configuration**	Continuous
EI (N.m^2)	1.90×10^{10}	**Normative type**	FB/RC

Dynamic properties			
Test type	i) Under railway traffic ii) Under forced excitation	**Method**	i) SSI-COV ii) *'modalfit'*
Range f_1 (Hz)	i) 8.50 – 8.52 ii) 8.33	**Range ξ_1 (%)**	i) 0.60 – 0.67 ii) 0.98 – 1.01
Range A_1 (m/s^2)	i) 0.019 – 0.030 ii) 1.800 – 2.000	**No. valid measurements**	i) 4 ii) 2
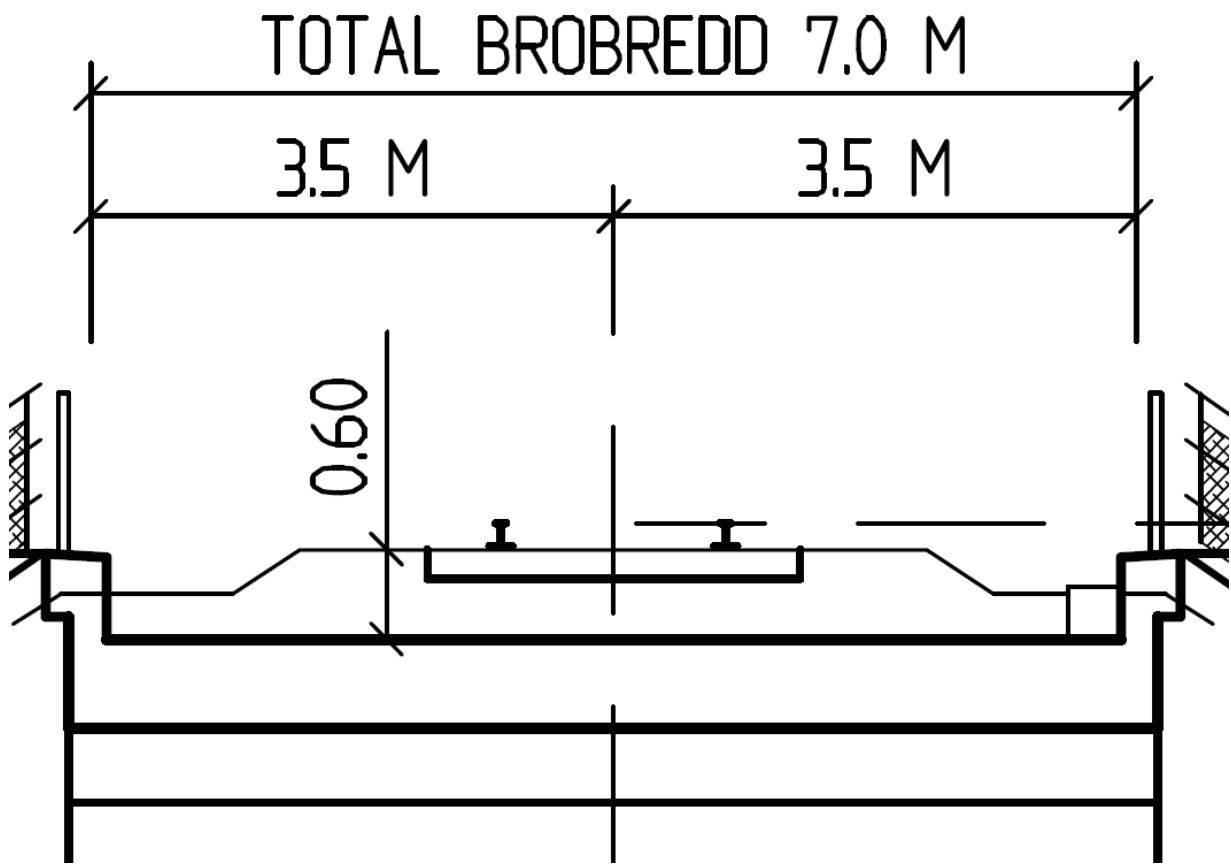
Taxinge			
Country	**Line designation**	**Maximum speed**	**Infrastructure Manager**
Sweden	Svealandsbanan line: Ryssjön - Läggesta	200 km/h	TRAFIKVERKET

Structural properties			
Span (m)	22.90	**Type**	Slab full
Mass (t/m)	21.50	**Configuration**	Continuous
EI (N.m^2)	2.82×10^{10}	**Normative type**	PSC
Dynamic properties			
Test type	i) Under railway traffic ii) Under forced excitation	**Method**	i) SSI-COV ii) *'modalfit'*
Range f_1 (Hz)	i) 5.43 – 5.59 ii) 5.39 – 5.50	**Range ξ_1 (%)**	i) 1.53 – 2.67 ii) 1.50 – 1.76
Range A_1 (m/s^2)	i) 0.139 – 0.485 ii) 0.250 – 0.450	**No. valid measurements**	i) 7 ii) 5
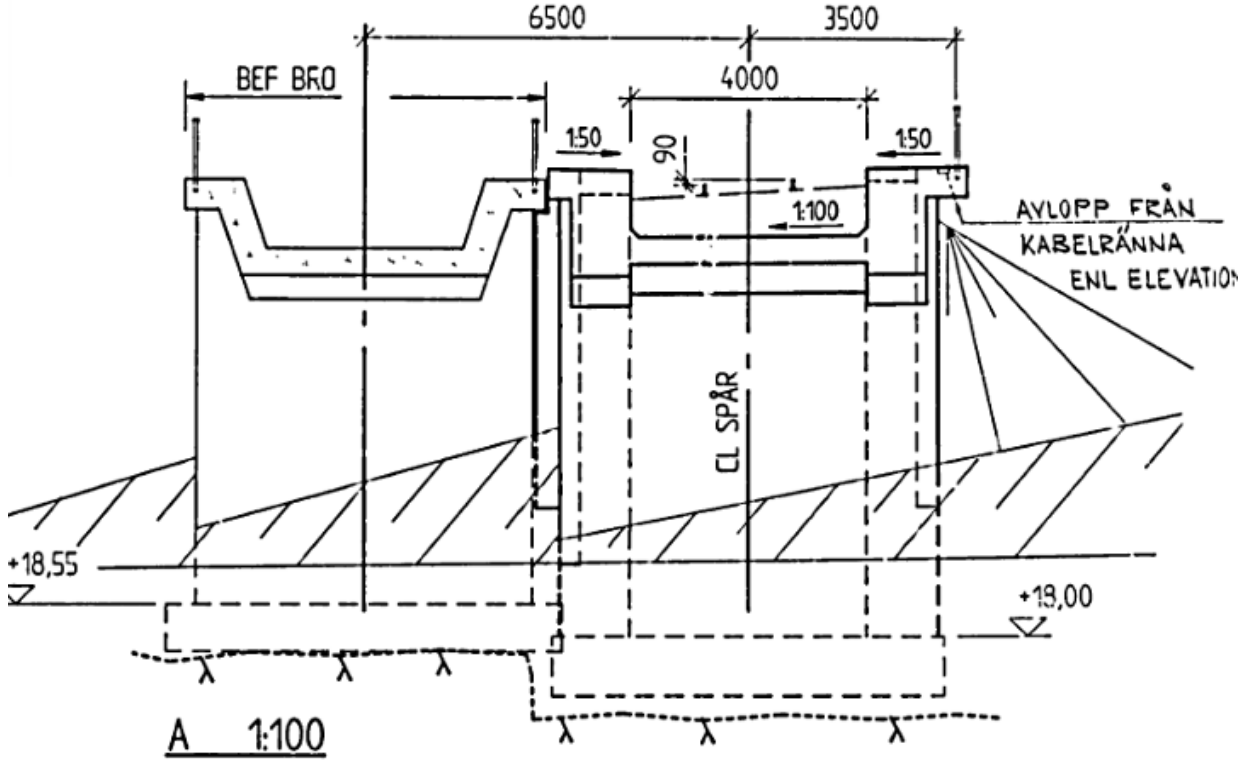
Sveavägen			
Country	**Line designation**	**Maximum speed**	**Infrastructure Manager**
Sweden	Svealandsbanan line: Strängnäs - Eskilstuna	200 km/h	TRAFIKVERKET

Structural properties			
Span (m)	11.60	**Type**	Slab full
Mass (t/m)	18.00	**Configuration**	Continuous
EI (N.m^2)	1.46×10^{10}	**Normative type**	FB/RC
Dynamic properties			
Test type	Under forced excitation	**Method**	*'modalfit'*
Range f_1 (Hz)	13.72 – 13.82	**Range ξ_1 (%)**	2.37 – 2.46
Range A_1 (m/s^2)	0.500 – 0.950	**No. valid measurements**	4
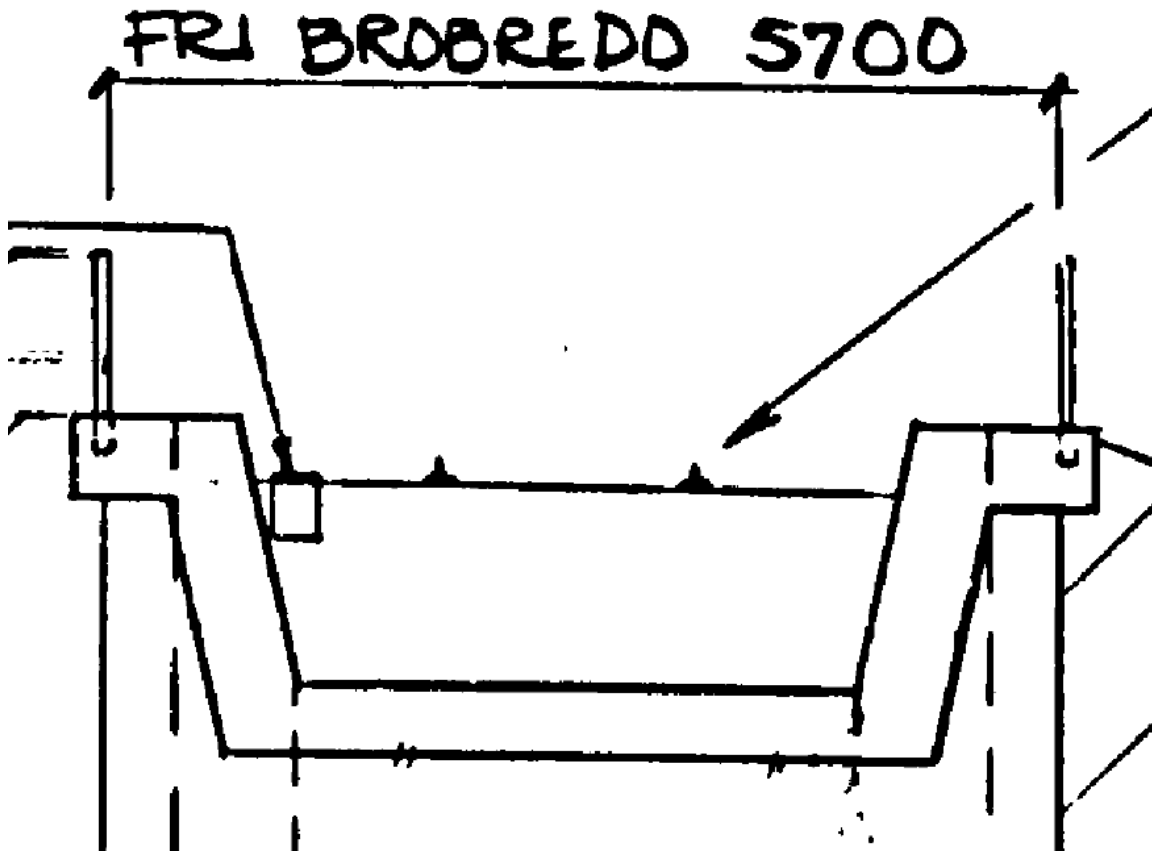
Vasavägen			
Country	**Line designation**	**Maximum speed**	**Infrastructure Manager**
Sweden	Svealandsbanan line: Strängnäs - Eskilstuna	200 km/h	TRAFIKVERKET

Structural properties			
Span (m)	12.50	**Type**	Slab full
Mass (t/m)	19.00	**Configuration**	Continuous
EI (N.m^2)	1.19×10^{10}	**Normative type**	FB/RC
Dynamic properties			
Test type	i) Under railway traffic ii) Under forced excitation	**Method**	i) SSI-COV ii) *'modalfit'*
Range f_1 (Hz)	i) 12.28 – 12.64 ii) 12.19	**Range ξ_1 (%)**	i) 0.98 – 1.43 ii) 1.18
Range A_1 (m/s^2)	i) 0.017 – 0.200 ii) 1.700	**No. valid measurements**	i) 7 ii) 1
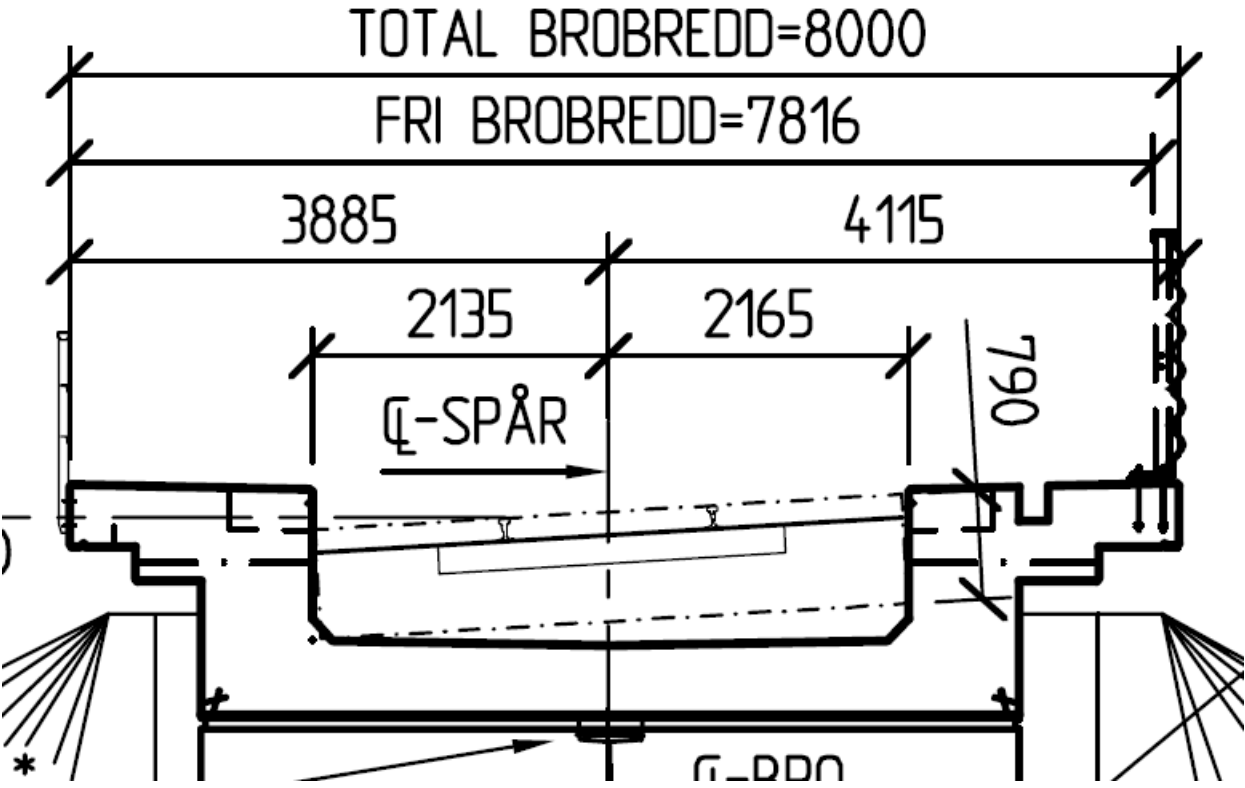
Pershagen			
Country	**Line designation**	**Maximum speed**	**Infrastructure Manager**
Sweden	Västra stambanan line: Flemingsberg - Järna	200 km/h	TRAFIKVERKET

Structural properties			
Span (m)	18.40	**Type**	Slab full
Mass (t/m)	No data	**Configuration**	Continuous
EI (N.m^2)	No data	**Normative type**	FB/RC
Dynamic properties			
Test type	Under forced excitation	**Method**	*'modalfit'*
Range f_1 (Hz)	7.82	**Range ξ_1 (%)**	1.29 – 1.32
Range A_1 (m/s^2)	0.550 – 0.600	**No. valid measurements**	2
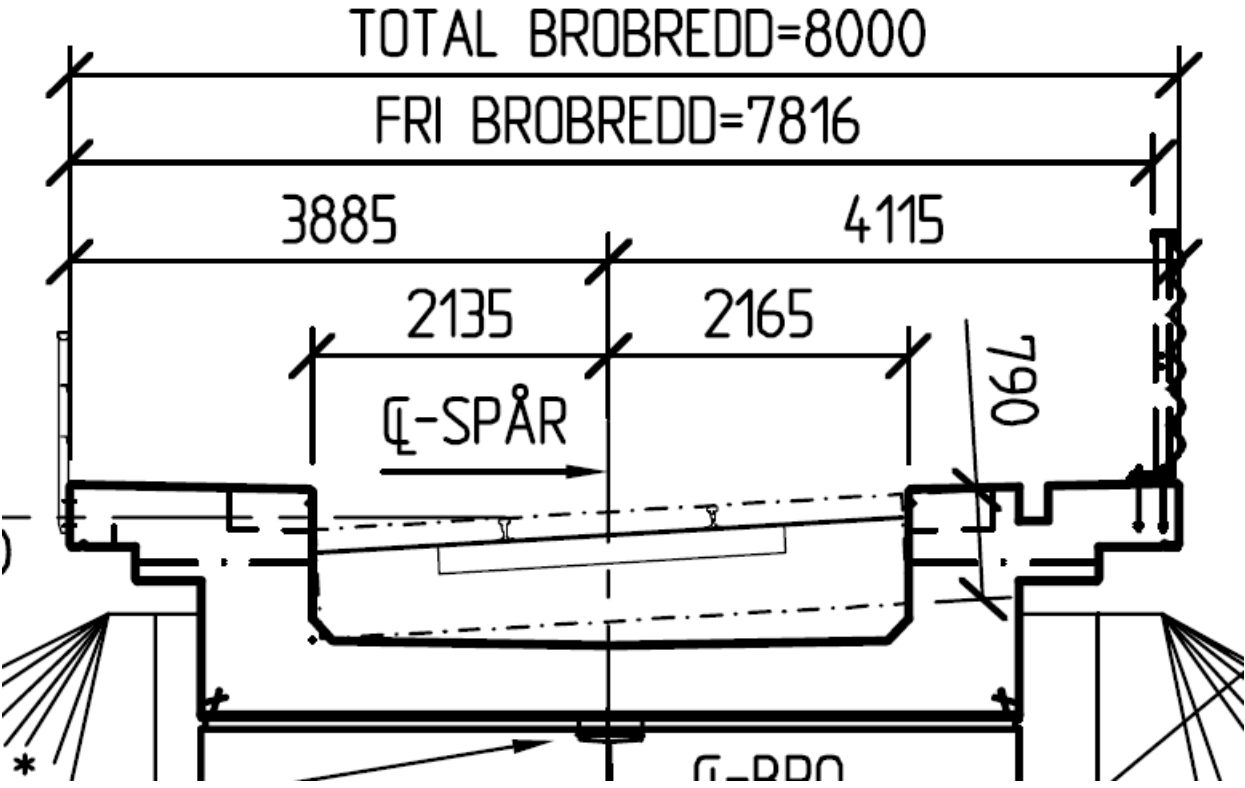
Degermyran			
Country	**Line designation**	**Maximum speed**	**Infrastructure Manager**
Sweden	Bothnia line: Husum - Nordmaling	250 km/h	TRAFIKVERKET

Structural properties			
Span (m)	8.70	**Type**	Portal Frame
Mass (t/m)	15.83	**Configuration**	Portal frame open
EI (N.m^2)	4.08×10^9	**Normative type**	PF
Dynamic properties			
Test type	Under forced excitation	**Method**	*'modalfit'*
Range f_1 (Hz)	30.42 – 31.58	**Range ξ_1 (%)**	9.45 – 12.85
Range A_1 (m/s^2)	0.080	**No. valid measurements**	4

Faresmyren			
Country	**Line designation**	**Maximum speed**	**Infrastructure Manager**
Sweden	Bothnia line: Örnsköldsvik - Husum	250 km/h	TRAFIKVERKET

Structural properties			
Span (m)	8.70	**Type**	Portal Frame
Mass (t/m)	17.76	**Configuration**	Portal frame open
EI (N.m^2)	7.34×10^9	**Normative type**	PF
Dynamic properties			
Test type	Under forced excitation	**Method**	*'modalfit'*
Range f_1 (Hz)	29.10 – 29.17	**Range ξ_1 (%)**	14.45 – 20.03
Range A_1 (m/s^2)	0.150 – 0.600	**No. valid measurements**	5

Gesällgatan North			
Country	**Line designation**	**Maximum speed**	**Infrastructure Manager**
Sweden	Mälarbanan line: Enköping - Lundby	200 km/h	TRAFIKVERKET

Structural properties			
Span (m)	30.60	**Type**	Beam
Mass (t/m)	19.00	**Configuration**	Continuous abutment
EI **(N.m²)**	5.44×10^{10}	**Normative type**	PF / PSC
Dynamic properties			
Test type	Under forced excitation	**Method**	*'modalfit'*
Range f_1 (Hz)	6.54 – 6.55	**Range ξ_1 (%)**	1.38 – 1.43
Range A_1 (m/s²)	0.800 – 1.000	**No. valid measurements**	4

Gesällgatan South			
Country	**Line designation**	**Maximum speed**	**Infrastructure Manager**
Sweden	Mälarbanan line: Kallhäll - Västerås	200 km/h	TRAFIKVERKET

Structural properties			
Span (m)	28.60	**Type**	Beam
Mass (t/m)	18.03	**Configuration**	Continuous abutment
EI **(N.m^2)**	6.22×10^{10}	**Normative type**	PF / PSC
Dynamic properties			
Test type	Under forced excitation	**Method**	*'modalfit'*
Range f_1 (Hz)	5.65 – 5.67	**Range ξ_1 (%)**	1.91 – 2.91
Range A_1 (m/s^2)	2.200	**No. valid measurements**	5

Norra Kungsvägen			
Country	**Line designation**	**Maximum speed**	**Infrastructure Manager**
Sweden	Bothnia line: Hörnefors - Umea	250 km/h	TRAFIKVERKET

Structural properties			
Span (m)	15.70	**Type**	Portal Frame
Mass (t/m)	20.58	**Configuration**	Portal frame open
EI (N.m^2)	4.32×10^{10}	**Normative type**	PF
Dynamic properties			
Test type	Under forced excitation	**Method**	*'modalfit'*
Range f_1 (Hz)	16.36 – 16.43	**Range ξ_1 (%)**	3.86 – 4.13
Range A_1 (m/s^2)	0.030 – 0.550	**No. valid measurements**	7

Sodra Kungsvägen			
Country	**Line designation**	**Maximum speed**	**Infrastructure Manager**
Sweden	Bothnia line: Nordmaling - Hörnefors	250 km/h	TRAFIKVERKET

Structural properties			
Span (m)	15.25	**Type**	Portal Frame
Mass (t/m)	20.68	**Configuration**	Portal frame open
EI (N.m²)	4.35×10^{10}	**Normative type**	PF
Dynamic properties			
Test type	Under forced excitation	**Method**	*'modalfit'*
Range f_1 (Hz)	15.33 – 15.90	**Range ξ_1 (%)**	4.54 – 6.00
Range A_1 (m/s²)	0.080 – 1.200	**No. valid measurements**	7